The Role of NADPH Oxidase-2 in the Development of Cardiac Fibrosis

Richards, Daniel Antonio

Awarding institution:
King's College London

THESIS SUBMITTED FOR THE DEGREE OF:
DOCTOR OF PHILOSOPHY IN CARDIOVASCULAR SCIENCES
CARDIOVASCULAR DIVISION – KING'S COLLEGE LONDON

The Role of NADPH Oxidase-2 in the Development of Cardiac Fibrosis

Daniel Richards

Supervisors: Ajay M. Shah and Fiona M. Watt

October 2016

Abstract

Background: Cardiac fibrosis, a component of pathological remodelling, often arises secondary to hypertension or myocardial infarction. It leads to systolic and diastolic cardiac dysfunction, since the increased collagen deposition increases myocardial stiffness. Reactive oxygen species (ROS) are implicated in this pathology and NADPH oxidase-2 (NOX2), a major producer of ROS, is elevated in heart failure settings. Previous work showed that global NOX2 knockout (KO) mice had reduced generation of cardiac fibrosis, but the cell-type specific role of NOX2 is yet to be investigated in this context.

Aim: This research aimed to determine the role of fibroblast and endothelial cell NOX2 in the development of cardiac fibrosis in mice. In addition, the extent of endothelial-mesenchymal transition (EndoMT) in the development of cardiac fibrosis was to be assessed using a lineage tracing approach.

Methods and Results: Tamoxifen-inducible fibroblast-specific NOX2 KO mice were generated by crossing novel NOX2 floxed mice with Collagen 1α2 (*Col1α2*)-Cre mice. Cardiac NOX2 protein expression was reduced by 60% in these mice. Cardiac fibrosis was induced using chronic angiotensin II (Ang II) infusion (1.1mg/kg/day) and blood pressure was monitored by ambulatory telemetry. Fibroblast NOX2 KO mice had a significantly delayed hypertensive response and less cardiac fibrosis compared to wildtype (WT), as determined by histological analysis of cardiac sections. In contrast, fibroblast NOX2 KO mice were not protected from cardiac fibrosis when subjected to chronic pressure overload by transverse aortic constriction (TAC), nor were they protected from systolic and diastolic dysfunction as determined by serial echocardiography.

Similarly, endothelial cell-specific NOX2 KO mice were generated by crossing floxed NOX2 mice with VE-Cadherin (*Cdh5*)-Cre mice, with a 60% reduction in aortic NOX2 protein levels. These mice were also not protected from developing cardiac fibrosis or cardiac dysfunction when subjected to TAC.

The *Col1α2* and *Cdh5* Cre-recombinase efficiencies were assessed by crossing with a tdTomato "STOP" floxed reporter mouse, showing high tdTomato expression in specific cell types and estimated high efficiency of ≥70% using flow cytometry. The extent of EndoMT was assessed in *Cdh5* tdTomato (EndoTom) mice subjected to TAC using a lineage tracing approach. There was no convincing evidence of EndoMT in cardiac or lung tissue, since the percentage of tdTomato^{+} (*Cdh5* lineage traced) cells expressing the fibroblast marker CD140α was not augmented by TAC (determined by flow cytometry).

Conclusion: Although fibroblast NOX2 contributes to the development of Ang II-induced cardiac fibrosis it is dispensable for TAC-induced fibrosis. Endothelial cell NOX2 is also dispensable for TAC-induced fibrosis. These results suggest that the cell-specific role of NOX2 in cardiac fibrosis is stimulus dependent. The activation of NOX2 in other cell types may be required for the development of cardiac fibrosis in response to chronic pressure overload. Furthermore, EndoMT appears to be at most a minor contributor to the development of cardiac fibrosis after TAC. Taken together, this work provides new insights into the cell-specific roles of NOX2 in the development of cardiac fibrosis.

Acknowledgements

I have been looking forward to this bit and I'm sure it will extend to 2 pages or more!

I would like to thank my primary supervisor Professor Ajay Shah; firstly for responding positively to my request to do a PhD project in his lab and secondly, for his ongoing support and belief in my abilities and the project. I am happy I managed to persuade you to let me present at the ISHR meeting in Argentina, knowing full-well it was an excuse for a holiday! Thank you also to my second supervisor Professor Fiona Watt for providing me with the tomato reporter and adding a new dimension to my PhD project.

The early work completed in this thesis would not have been possible without the help and guidance offered by Dr. Craig Harrison. I am very grateful for the knowledge he has extended to me and his ability to keep spirits high, even in the wake of sometimes disappointing results. I am thankful for his work on characterising the FS mouse and also for him showing me the ropes in the lab. Your trademark golf swing and (often) inappropriate, but hilarious comments in the lab are greatly missed in the lab!

I would also like to thank Dr. Héloïse Mongue-Din for her invaluable discussions regarding life as a scientist and life in general. Heloïse is an amazing mentor and colleague, with an unrivalled aptness for imparting knowledge and reassurance.

Thank you also to my fellow students, firstly Amber Emmerson, who, during her final weeks as a PhD student gave up her time to introduce me to the world of flow cytometry! Secondly, Ally Santu - although you didn't know it, we have been in constant competition, fuelling my desire to complete this thing! Lastly thank you to Moritz Schnelle for being generally unpleasant, but providing me with a lot of laughs along the way!

Finally, I would like to say thank you to the rest of the Shah lab and others, in particular Dr. Greta Sawyer, Dr. Helena Zhang and Norman Catibog for advice, discussion and surgical and technical expertise. A special mention goes to Monica Brennan, Dr. Daniel Martin, Dr. Can Sag, Lauren McLaughlin, Dr. Lynsey Whilding, Caroline Gough and Stephanie Telerman, who have all contributed in a major way.

I must acknowledge the many people who have contributed to my wellbeing and success, despite not being directly related to this project.

Firstly, I would like to thank my two best friends, Davina Chandler and Claire Spearman, who have tirelessly supported me throughout this endeavour, despite often struggling to understand what I have been doing! Davina, I love that I have been a Dr. in your eyes since day 1; this definitely spurred me on to completion!

Grace Jefferies also deserves a special mention for her support and confidence in my abilities over the years. I really appreciate your positive attitude towards my work, even when you said things like, “sounds awful, rather you than me!”

Rakeem Noble has been the greatest training partner I could ask for. Those early morning wake up calls to run up and down hills were much appreciated! Thanks also for helping me join the sub 20 club! A big thanks to the rest of the Philippines family too, in particular Anna Church for being a positive role model.

It wouldn’t be right if I didn’t extend my thankyous to King’s College London Athletics Club. I have really enjoyed being a part of the club and you nearly brought me to tears when you voted me winner of the 2016 “Superstar” award! Thank you for allowing me to pound the track with you and let off some PhD steam! Special mention to James Findon, Harry Browning, K-dot, Amy Mat and the rest of the sprint squad!

On the same theme, thank you to my football group: Festus, Gab, Preet, Thiago and others and in particular Morgan Ereku. Our discussions definitely helped to keep my mind sharp and focussed, although sometimes I did wish I was doing a psychology PhD so I could understand the deeper topics!

Most importantly, there’s family.

Thank you to Roxanne and Lee Merry for always steering me in the right direction and for being the best siblings I could ask for!

I wouldn’t be here without mum (Barbara) and dad (Trevor), so thanks for that! You both taught me to believe in myself and make me feel that I capable of great things.

Finally, thank you to those listed above and those who I may have forgotten. Your support will be immortalised in this thesis!

Declaration

I declare that I am the sole author of this thesis and it contains my own work, except where indicated.

Daniel Richards

Table of Contents

List of Figures

List of Tables

Abbreviations

A wave	-	Late ventricular filling velocity (Doppler-derived)
A’	-	Late mitral valve diastolic annular motion
AAB	-	Abdominal aortic banding
AAC	-	Ascending aortic constriction
ACE	-	Angiotensin converting enzyme
ADH	-	Anti-diuretic hormone
Ang II	-	Angiotensin II
ANOVA	-	Analysis of variance
APC	-	Allophycocyanin
AT1	-	Angiotensin receptor 1
AT1R	-	Angiotensin II receptor type 1
CD140α	-	Cluster of differentiation 140-alpha (PDGFR1α)
CD144	-	Cluster of differentiation 144 (vascular endothelial cadherin)
CD201	-	Cluster of differentiation 201 (endothelial protein C receptor)
CD31	-	Cluster of differentiation 31 (platelet endothelial cell adhesion molecule 1)
CD90	-	Cluster of differentiation 90 (thymocyte antigen 1.2)
Cdh5	-	VE-Cadherin gene
cDNA	-	Complimentary deoxyribonucleic acid
Col1α2	-	Collagen type 1 alpha 2 chain gene
CreER(T)	-	Inducible Cre recombinase
Ct (values)	-	Cycle threshold (values)
CTGF	-	Connective tissue growth factor
CVF	-	Collagen volume fraction
DAPI	-	4',6-diamidino-2-phenylindole
DDR2	-	Discoidin domain receptor 2
DMEM	-	Dulbecco’s Modified Eagle’s Medium

DNA	-	Deoxyribonucleic acid
DPX	-	Distyrene, a plasticizer and xylene (mixture of)
DsRed	-	Discosoma sp. Red
E wave	-	Early ventricular filling velocity (Doppler-derived)
E/A ratio	-	Early/late ventricular filling velocity ratio (Doppler-derived)
E/E'	-	Mitral valve 'E' wave velocity to annular motion ratio
E'	-	Early mitral valve diastolic annular motion
ECM	-	Extracellular matrix
EDTA	-	Ethylenediaminetetraacetic acid
eGFP	-	Enhanced green fluorescent protein
EndoMT	-	Endothelial to mesenchymal transition
EndoTom	-	Endothelial cell reporter mice (*Cdh5*CreER(T2):*ROSA26R*-tdTomato$^{flox/flox}$)
eNOS	-	Endothelial nitric oxide synthase
ERK1/2	-	Extracellular-signal-regulated kinase type 1/2
FBS	-	Foetal bovine serum
FibroTom	-	Fibroblast reporter mice (*Col1α2*CreER(T):ROSA26R-tdTomato$^{flox/flox}$)
FITC	-	Fluorescein isothiocyanate
FSC-A/H	-	Forward scatter area/height
FSP-1	-	Fibroblast-specific protein-1
GDP	-	Guanosine diphosphate
GFP	-	Green fluorescent protein
GTP	-	Guanosine triphosphate
HFpEF	-	Heart failure with preserved ejection fraction
HW	-	Heart weight
HW: BW	-	Heart weight to body weight ratio
IVCT	-	Isovolumic contraction Time
IVRT	-	Isovolumic relaxation time

KO	-	Knockout
LA	-	Left atrium
LacZ	-	Beta-galactosidase (β-galactosidase)
LoxP	-	Locus of X-over P1
LV	-	Left ventricle
MAP	-	Mitogen activated protein
MI	-	Myocardial infarction
MMP(s)	-	Matrix metalloproteinase(s)
mRNA	-	Messenger ribonucleic acid
NADPH	-	Nicotinamide adenine dinucleotide phosphate
NaOH	-	Sodium hydroxide
NOS	-	Nitric oxide synthase
NOX	-	NADPH oxidase
PBS	-	Phosphate buffered saline
PCR	-	Polymerase chain reaction
PDGFR1α	-	Platelet-derived growth factor receptor 1-alpha
PE	-	Phycoerythrin
PFA	-	Paraformaldehyde
PI3Kγ	-	Phosphoinositide 3-kinase gamma
Postn	-	Periostin gene
qPCR	-	Quantitative polymerase chain reaction
RA	-	Right atrium
RAAS	-	Renin angiotensin aldosterone system
RNA	-	Ribonucleic acid
ROS	-	Reactive oxygen species
RV	-	Right ventricle
SDS	-	Sodium dodecyl sulfate
SOD	-	Superoxide dismutase

SPARC	-	Secreted-protein, acidic and rich in cysteine
SSC-A/H	-	Side scatter area/height
TAC	-	Transverse aortic constriction
TAE	-	Buffer containing 40mM Tris, 20mM acetic acid, and 1mM EDTA
Taq	-	DNA polymerize derived from *Thermus Aquaticus*
tdTomato	-	Tandem dimer tomato
TGFβ	-	Transforming growth factor beta
Tie1	-	Tunica intima endothelial kinase 1 gene
Tie2	-	Tunica intima endothelial kinase 2 gene
TIMP(s)	-	Tissue inhibitors of metalloproteinase(s)
TNFα	-	Tumour necrosis factor alpha
VE-Cadherin	-	Vascular endothelial cadherin
WGA	-	Wheat germ agglutinin
WT	-	Wildtype
αSMA	-	Alpha smooth muscle actin

CHAPTER 1: General Introduction

1.1 Cardiovascular Disease, Cardiac Fibrosis and Cardiac Function

The heart is central to the cardiovascular system, operating without rest and with limited regenerative capacity. Pathological stresses on the heart can be either acute or chronic in nature, but both will lead to initially compensatory changes in the geometry, function and composition of the heart, known as cardiac remodelling. Cardiac hypertrophy, for example, is the growth of cardiomyocytes, either concentric (thickening) or eccentric (elongation) and may result in dilated cardiomyopathy.[1] Functional changes will occur as a consequence and may affect overall cardiac pumping efficiency.

Cardiac fibrosis is a component of pathological cardiac remodelling, described as the excessive deposition of collagen and the formation of scar tissue.[2] It is seen in a wide range of cardiovascular pathologies and diseases, including chronic hypertension, aortic stenosis, cardiac valve disease, diabetes and after more acute events such as myocardial infarction (MI) and myocarditis.[3-7] Cardiovascular disease is now a major cause of morbidity and age-related mortality in the developed and increasingly in the developing world,[8, 9] with most leading to some form of cardiac fibrosis.[5, 10] Hypertension, for example, has a high prevalence of 26% and is itself a promoter of ischaemic heart disease and MI events.[11]

One important functional consequence of cardiac fibrosis is diastolic dysfunction, which describes impairment of the filling function of the heart. This occurs in many cardiac conditions but is especially relevant to the relatively new concept of heart failure with preserved ejection fraction (HFpEF). Of all heart failure cases around 50% are thought to be HFpEF, for which there is no proven therapy.[12] In mechanical terms, an increase in interstitial cardiac collagen deposition will lead to myocardial stiffening,[13] thereby reducing ventricular elasticity, or compliance, culminating in compromised ventricular filling.[12, 14, 15] Cardiac fibrosis also involves the deposition of a range of extracellular matrix components, further discussed in chapter 1.2. Impaired relaxation will cause an increase in ventricular and atrial filling pressures and over time may lead to secondary pulmonary hypertension and other symptoms of heart failure, including congestion and lung oedema.[16] Although ventricular

ejection fraction and cardiac output are preserved at rest, patients with HFpEF may have a reduced capacity to augment these indices during exercise, severely impacting quality of life.[12, 17, 18]

Cardiac fibrosis can also directly cause systolic cardiac dysfunction. Electrical conduction during systole follows two paths; conduction along myocardial fibres and conduction across fibres to adjacent fibres. Collagen deposition between adjacent myocardial fibres delays electrical conduction velocities, whereas conduction along an individual bundle will be largely undisturbed.[19] In simple terms, this fibrosis-induced difference in conduction velocities uncouples electrical signalling between cardiomyocytes, causing ventricular dyssynchrony and reduced systolic pumping efficiency.[20, 21] There is also an increased propensity towards cardiac arrhythmias and sudden cardiac death.[19, 22]

Cardiac fibrosis, diastolic dysfunction and HFpEF currently have no specific treatments and together demonstrate an area of high unmet medical need; hence understanding the processes involved in the development of cardiac fibrosis is an important and urgent research goal.

1.2 The Cardiac Extracellular Matrix in Health and Disease

Cardiac fibrosis develops in the extracellular matrix (ECM), a diverse and dynamic network of structural and non-structural proteins responsible for maintaining cell organisation and tissue structure.[23] The ECM provides anchoring points for cardiomyocytes, essential for mechanical force transmission during systole, whilst preventing overstretching during diastole.[7] The ECM also provides support and flexibility for coronary vessels operating under high pressures[10] and further functions as a modulator of electrical signalling between cardiac cells and between atria and ventricles, providing insulation to prevent premature contractions.[5, 10]

A delicate balance of ECM synthesis and degradation exists in a healthy heart, allowing for normal growth and remodelling.[24] During adaptive cardiac hypertrophy, such as in elite athletes in training, proportionate growth, remodelling and expansion of the ECM occurs as a homeostatic mechanism in order to support cardiomyocyte

growth.[25, 26] Key to this process are the matrix metalloproteinases (MMPs) and tissue inhibitors of metalloproteinases (TIMPs) which are discussed later in chapter 1.2.1.

In contrast, during diseases such as chronic hypertension or in experimental models of pressure overload, a disproportionate increase in ECM deposition is observed, upsetting the delicate balance and promoting cardiac fibrosis.[24, 27, 28] The deposition of ECM is excessive and sustained, collagen chains also become cross-linked, leading to progressive detrimental effects on cardiac structure and function.

Cardiac fibrosis can be divided into two broad categories. Replacement fibrosis occurs predominantly after an acute inflammatory event such as MI; the sudden death of cardiomyocytes after infarction causes a spike in inflammatory signalling, leading to the eventual replacement of dead myocytes with collagen.[27, 28] In contrast, reactive fibrosis has mechanical stress origins and is more diffuse throughout the myocardium.[24] Replacement and reactive fibrosis can be easily modelled in animal models using myocardial infarction and chronic angiotensin II or pressure overload surgical models, respectively, where cardiac fibrosis is evident both in the interstitial and perivascular regions.[29-34]

1.2.1 ECM Components

The ECM contains a plethora of different cells, enzymes, structural and non-structural components, as well as growth factors and cytokines.[28] Fibrillar collagen, with its triple helix structure, is the most abundant non-cellular component in the heart, with types I and III providing tensile strength and elasticity, respectively.[24] Collagen I forms thick fibres and accounts for around 85% of total cardiac ECM collagen, with thinner collagen III as the next most abundant.[28] Fibrillar collagen is synthesised as procollagen, before undergoing post-translational processing to form collagen fibrils and eventually thicker collagen fibres.[24] In addition to collagens I and III, there over 20 collagens exist, many of which are expressed in heart. In particular, collagen IV and collagen VI are shown to have increased expression following myocardial infarction or chronic pressure overload. Some collagens, such as collagen XVIII, even play a protective role during cardiac pathology.[24] It is also worth noting that a number of cardiac cells produce collagen and increase production during pathological cardiac stress, including MI and pressure overload.

Another major structural component is fibronectin, a fibril-forming glycoprotein secreted by fibroblasts. Fibronectin forms large, complex, cross-linked networks and interacts with ECM components such as collagen and fibroblasts via integrin receptors, a process important for cell adhesion, migration, growth and proliferation.[28] Similar to collagen, the expression of fibronectin is increased during cardiac pathologies and is a marker of cardiac fibrosis.[32, 35]

Elastin is important in tissues required to stretch and recoil, such as the heart, lungs and aorta. It is a fibrous, elastic polymer, giving rise to flexibility in cardiac tissue during diastole and also plays a role in cell adhesion, migration, differentiation and survival.[36] Elastin has been shown as essential, since elastin knockout (KO) mice die shortly after birth.[37] In pathology, recombinant elastin can prevent cardiac dysfunction and reduce fibrotic scar expansion in a model of rat myocardial infarction.[38] A reduction in cardiac fibrosis following chronic pressure overload was also shown to be associated with increased elastin expression in mice.[39]

Tissue MMPs and TIMPs are groups of non-structural proteins involved in ECM turnover. As with the structural ECM components, MMPs and TIMPs also have altered expression during cardiac stress and remodelling.[40] MMPs are expressed by cardiomyocytes, endothelial cells and fibroblasts and are the major proteolytic enzymes in collagen, fibronectin and other structural ECM component breakdown.[24] Over 20 MMPs have been identified and grouped according to their primary targets, for example MMPs 1, 8 and 13 are regarded as collagenases, involved in the digestion of collagen types I and III amongst others. MMPs are synthesised as pro-MMPs and must first be activated by cleavage of an amino domain, either by another proteolytic enzyme or by auto-proteolysis.

Indiscriminate breakdown of the ECM is avoided by specific inhibitors of MMPs, known as TIMPs. TIMPs are small molecules which essentially act like a plug to block the active proteolytic sites of MMPs. Together, the 4 TIMP subtypes inhibit virtually all MMPs, though there are reported differences in affinity for specific MMPs.[24] TIMPs may also have MMP-independent functions, for example TIMP-2 is believed to be inhibitory to cell proliferation.[41]

Matricellular proteins are non-structural, but bind to structural components and cardiac cells to aid stability.[42] For example, secreted-protein-acidic and rich in cysteine (SPARC) expression is increased after infarction and is particularly important in post infarct cardiac stability, since targeted deletion in mice (SPARC KO) results in increased post infarct mortality by cardiac rupture.[43] The authors also showed a reduction in systolic function in SPARC KO mice accompanied by abnormal and immature collagen deposition. In chronic pressure overload, a model less likely to result in cardiac rupture, it was shown that SPARC KO mice had less cardiac fibrosis, less myocardial passive stiffness and a non-significant improvement in mortality compared to controls.[44] Another key matricellular protein is osteopontin, a secreted protein expressed during cardiac stress and remodelling.[24] In contrast to SPARC KO, mice with deletion of osteopontin (osteopontin KO) did not have reduced cardiac fibrosis in response to chronic pressure overload,[45] but a reduction was observed in a chronic angiotensin II model.[42] Interestingly, similar to SPARC KO, osteopontin KO appears detrimental in infarcted mouse models,[42] suggesting that these matricellular proteins are most important in post-infarct stability and remodelling.

1.3 Cardiac Cells in Cardiac Fibrosis

Multiple cell types and cell-cell interactions are involved in both ECM homeostasis and cardiac fibrosis pathology, notably cardiomyocytes, endothelial cells, inflammatory cells and cardiac fibroblasts.[46]

1.3.1 Cardiac Fibroblasts

The adult human heart is thought to be composed of approximately 70% non-cardiomyocytes, of which fibroblasts are assumed to be the most abundant. Fibroblasts help to maintain ECM structure, function and integrity through autocrine and paracrine signalling, as well as physically through cell-cell and cell-ECM interactions.[46] Resident cardiac fibroblasts are therefore key players in ECM homeostasis (Figure 1-1), since they produce mainly types I and III collagen, in addition to degradative enzymes MMPs for remodelling.[5]

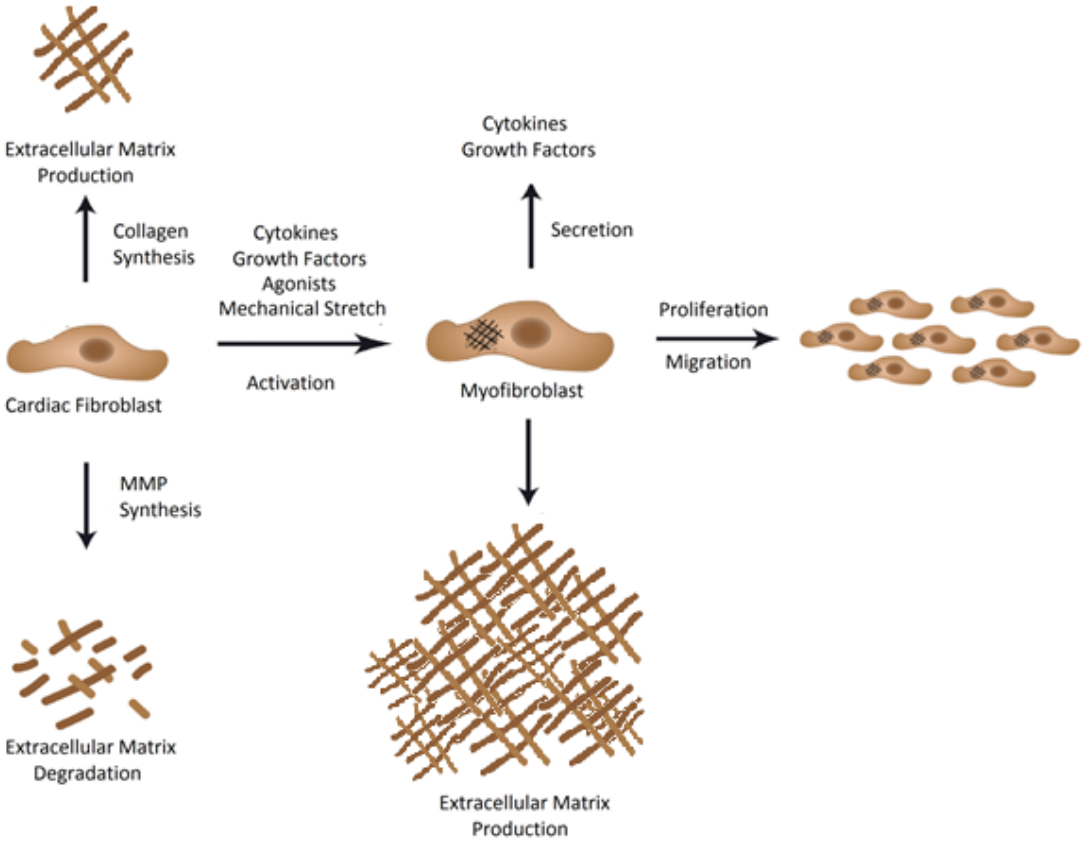

Figure 1-1: The roles of a cardiac fibroblast in the extracellular matrix. Cardiac fibroblasts are central to extracellular matrix (ECM) homeostasis, able to promote both synthesis and degradation of ECM components. Cardiac fibroblasts are able to respond to various activation stimuli, transforming to highly active myofibroblasts with proliferative and migratory tendencies. Image adapted from *Krenning et al., 2010*.[5]

Upon activation by pathological stimuli, fibroblasts transform and take on a slightly different phenotype, displaying stress fibres and markers similar to those of smooth muscle cells, such as smooth muscle actin alpha (αSMA; Figure 1-1).[7] Fibroblasts may become activated by a range of stimuli including, A: growth factors (e.g. transforming growth factor-β (TGFβ), connective tissue growth factor [CTGF], endothelin-1) released by cardiomyocytes or endothelial cells; B: cytokines (e.g. tumour necrosis factor-α [TNFα] and interleukins) released by infiltrating inflammatory cells; C: neurohumoral stimuli such as angiotensin-II (Ang II); or D: mechanical stimuli such as stretch.[5] Activated fibroblasts, known as myofibroblasts, are highly migratory and proliferative and themselves secrete pro-inflammatory growth factors and cytokines,

in addition to increased ECM synthesis such as collagen.[46] The combination of persistent fibroblast activation and increased rates of proliferation and accumulation is the main contributor to pathological ECM deposition and the progression of cardiac fibrosis towards heart failure.[5, 46]

1.3.2 Cardiomyocytes

In addition to inflammatory signalling due to cardiomyocyte death, cardiomyocytes can directly activate interstitial fibroblasts via the release of factors such as TGFβ and Ang II (discussed later in section 1.5). This so-called paracrine signalling from cardiomyocytes to fibroblasts promotes pro-fibrotic signalling and is proving to be a key mechanism in the development of cardiac fibrosis.[47] A number of studies have used gene knockout (KO) mice to successfully disrupt cardiomyocyte signalling and the development of cardiac fibrosis, indicating a major role for this cell type. For example, mice deficient in cardiomyocyte TGFβ-2 receptor had significantly reduced cardiac fibrosis following TAC,[48] with similar results for mice deficient in cardiomyocyte RhoA.[49] In addition, an overexpression approach was used to show that TAK1 in cardiomyocytes, a target for TGFβ, mediates cardiac fibrosis and other deleterious effects.[50]

1.3.3 Endothelial Cells

Endothelial cells may contribute to cardiac fibrosis at least in part due to endothelial-mesenchymal transition (EndoMT).[51] Limited studies have shown that endothelial cells may convert to a fibroblast-like phenotype, synthesize collagen and contribute to cardiac fibrosis.[30, 52, 53] The role of endothelial cells in EndoMT is further discussed in chapter 5.1 and chapter 6.1. Endothelial cells are further implicated due to their signalling through endothelin-1, a pro-fibrotic mediator shown as essential for cardiac fibrosis in a mouse model of chronic Ang II.[54]

1.3.4 Inflammatory Cells

Inflammatory cells are present in low numbers under basal conditions in cardiac tissue. Following an ischaemic event or cardiomyocyte cell death, inflammatory leukocytes, mainly neutrophils, are attracted to sites of damage from the circulation and further release pro-inflammatory mediators such as interleukins and TGFβ.[55] Chronic angiotensin II acting via the angiotensin II type 1 receptor is known to

promote the release of chemoattractant molecules such as MCP-1 by monocyte/macrophages.[56] Various studies have shown a role for mast cells, T-lymphocytes and macrophages in the development of cardiac fibrosis in response to both chronic angiotensin II and pressure overload.[57] It is suggested that signalling from these inflammatory cells causes the activation of cardiac fibroblasts which then secrete ECM. A possible role for inflammatory cells in the development of cardiac fibrosis is exemplified by interleukin-6 KO mice, which develop less inflammation and cardiac fibrosis as a result of chronic Ang II treatment.[58]

1.3.5 Fibrocytes

Fibrocytes are similar in shape to fibroblasts, produce collagen and other structural fibres and are elevated in cardiac fibrosis.[59] They are found in the circulation where they can respond quickly to sites of damage such as skin wounds. Fibrocytes therefor cannot be overlooked with regard to the development of cardiac fibrosis. Furthermore they are capable of differentiating into myofibroblasts allowing it to carry out functions detailed in chapter 1.3.1.[60]

1.4 Mouse Models of Cardiac Fibrosis

Mouse models of cardiovascular disease have made it possible to elucidate mechanisms and a more thorough understanding of cardiac fibrosis and its drivers. As in humans, both reactive and replacement cardiac fibrosis exist in mice, resulting in fibrillar collagen deposition and increased myocardial stiffness.[61] It is worth noting that both chronic renin-angiotensin and chronic pressure overload models will have rapid onset of pathology (<2 weeks) in mouse models, compared to progressive onset (>40 years) in humans. This limitation is further discussed in chapter 7.4.

1.4.1 Experimental Renin-Angiotensin-Aldosterone Chronic Stimulation

Chronic stimulation of the renin-angiotensin-aldosterone system (RAAS) leads to hypertension. Hypertension is a precursor for cardiac fibrosis and experimental mouse models have been designed to chronically target specific aspects, such as chronic infusion with angiotensin II[35, 62], aldosterone[35, 63] or the synthetic mimetic deoxycorticosterone acetate,[64, 65] all of which induce hypertension and cardiac

fibrosis in mice. These models can often lead to systolic and diastolic dysfunction as a result of cardiac fibrosis, depending on the angiotensin II dose and duration.

1.4.2 Experimental Chronic Pressure Overload

In contrast to replacement fibrosis, reactive fibrosis occurs in the absence of major myocyte necrosis and is characterised by diffuse ECM deposition and accumulation of collagens in the interstitial or perivascular space.[61, 66]

The suprarenal abdominal aortic banding (AAB) and transverse aortic constriction (TAC) mouse models mimic vascular stenosis and are both regularly used to generate profound pressure overload-induced cardiac fibrosis and even lung fibrosis.[29, 31, 67-72] Cardiac pressure overload causes fibrosis since fibroblasts can become activated due to mechanical stress, e.g. stretch, leading to fibroblast differentiation, proliferation, pro-fibrotic signalling and excessive collagen deposition.[5] Chronic pressure overload invariably leads to severe systolic and often diastolic dysfunction, particularly after longer durations.

1.4.3 Experimental Myocardial Infarction (MI)

Replacement or reparative fibrosis occurs as a result of cardiomyocyte loss due to necrosis, where dead cells are replaced by fibrotic scar tissue.[73] This can be induced by the MI model in mice, since permanent cardiomyocyte loss occurs, followed by the formation of a discrete scar.[74] The MI surgical mouse model mimics human myocardial infarction by permanently ligating the left anterior descending coronary artery. This results in an ischaemic, infarcted zone and cardiomyocyte death. The ischaemic area will become akinetic and surrounding fibrotic regions may affect border zone contractility.[75]

1.5 Pro-fibrotic Signalling

A range of interconnected, pro-fibrotic signalling pathways and mediators have been described in the heart. Studies have used receptor blockade and various gene modification techniques to show significant reductions in the development of cardiac fibrosis. Key targets are given in Table 1-1.

Table 1-1: Signalling pathways targeted to prevent the development of cardiac fibrosis. *Rho-kinase (ROCK) inhibitor involved in the TGF-β-TAK1 pathway, #traditionally an angiotensin converting enzyme inhibitor.

Target/ Inhibitor	Outcome	Models	Ref.
Ang II (AT1) receptor/ irbesartan, losartan, valsartan	Reduced EndoMT, fibrosis and fibrosis-induced arrhythmias. Improved cardiac function	Diabetic cardiomyopathy, senescence, doxorubicin, autoimmune myocarditis, aldosterone/ nephrectomy	76-79
Mineralocorticoid receptor/ spironolactone, eplerenone	Reduced fibrosis and fibrosis-induced arrhythmias	Chronic aldosterone, senescence, myocardial infarction, chronic Angiotensin II	33, 35, 77, 80
TGFβ signalling or receptor/ Soluble TGFβ competitive inhibitor (adenovirus), neutralising antibody, BMP-7, fasudil*	Reduced fibrosis and improved cardiac function	Myocardial infarction, transverse aortic constriction	30, 67, 81, 82
Endothelin-1 / Endothelin-1 receptor knockdown, siRNA knockdown, converting enzyme inhibitor, Bosentan	Reduced fibrosis, hypertrophy and fibrotic gene expression	Chronic angiotensin II, cultured cell aging, Streptozotocin-induced diabetes	52, 54, 83, 84
ROS signalling/ N-acetylcysteine, apocynin, enalaprilat#	Reduced fibrosis and improved cardiac function	Chronic angiotensin II, transverse aortic constriction	31, 35, 85, 86

1.5.1 Activation of the Renin-Angiotensin-Aldosterone System

The RAAS is a potent hormone system involved in salt regulation and arterial blood pressure homeostasis. Under physiological conditions, a reduction in arterial and therefore renal blood pressure is detected by the juxtaglomerular apparatus in the kidney, leading to the cleavage and secretion of renin.[87] Renin is an enzyme which cleaves circulating hepatic angiotensinogen to angiotensin I, which is further cleaved to angiotensin II by angiotensin-converting enzyme (ACE) in the lungs. Angiotensin II is a potent vasoactive peptide, acting primarily on AT1 receptors to induce

constriction of blood vessels.[88] AT1 receptor activation also promotes the upregulation of the pro-fibrotic cytokine TGFβ.[2]

Release of anti-diuretic hormone (ADH) is also stimulated by angiotensin II, as well as release of aldosterone, a hormone which acts on the distal collecting tubes of the kidney to increase sodium and water reabsorption.[88] The net result of RAAS stimulation is an increase in effective circulating volume, through sodium and water retention, as well as an increase in arterial blood pressure (in part mediated via vasoconstriction). Chronic activation of the RAAS therefore causes hypertension and each RAAS effector such as Ang II and aldosterone, or downstream mediators such as TGFβ, have been shown experimentally to contribute to cardiac fibrosis (Table 1-1).

In addition to the classical circulating RAAS, mounting evidence suggests that the RAAS can be found locally in individual tissues, capable of producing and responding to Ang II, most likely initiated by tissue uptake of circulating renal renin and hepatic angiotensinogen.[87, 89] The so-called local tissue RAAS operates alongside circulating RAAS in the heart, where it is thought to be involved in the inhibition of cell growth and proliferation.[87] The implications of local tissue RAAS are currently unknown, but the classical circulating RAAS is a common target for the clinical and experimental reversal of chronic hypertension, cardiac dysfunction and the management of fibrosis.[24, 88]

It is worth noting that the metabolites of angiotensin II, Ang1-7 and Ang1-9, are thought to oppose the pathological signalling of angiotensin II and Ang1-9 has recently been shown to attenuate cardiac fibrosis in mice.[90]

1.5.2 TGFβ-dependent Signalling

Often at the heart of pro-fibrotic signalling is TGFβ, a pleiotropic cytokine, regarded as a master switch in the initiation of cardiac fibrosis following inflammation.[91] TGFβ has enhanced expression in a range of pathologies, including cardiac fibrosis and its expression can be induced experimentally by Ang II or by the application of mechanical stretch.[66, 91, 92] Following synthesis, TGFβ is secreted in an inactive form and must be proteolytically cleaved for activation. MMP-2, MMP-9, plasmin and thrombospondin have all been recognised as activators, allowing TGFβ to associate

with its type II receptor which dimerises with and activates the type I receptor.[66] TGFβ signalling can be through Smad transcription factors (canonical) or Smad-independent (non-canonical) pathways. Canonical pathways involve Smad3 activation of TGFβ response elements to induce collagen transcription and synthesis, whereas non-canonical pathways involve activation of kinases such as p38 MAP kinase and ERK1/2 kinases.[66] The net result of TGFβ signalling in this context is fibroblast differentiation to myofibroblasts, cardiomyocyte hypertrophy, collagen synthesis and cardiac fibrosis through both autocrine and paracrine mechanisms.[93] Although incompletely understood, a direct link between nicotinamide adenine dinucleotide phosphate (NADPH) oxidase (NOX)-derived reactive oxygen species (ROS) signalling and TGFβ activation has been described, a mechanism in which ROS and TGFβ induce the production and activation of each other.[86] In addition, TGFβ has been shown to play a role in EndoMT.[30, 86, 94]

The diversity of signalling by TGFβ highlights its importance and appears to link together the variety of studies listed in table 1.

1.5.3 Endothelin-1

Endothelin-1 is a protein secreted predominantly by endothelial cells, but also by fibroblasts and other cardiac cell types.[95] It is downstream of TGFβ signalling and can be induced by Ang II and ROS; with evidence of reciprocal activation.[52, 95-97] Acting through its endothelin-A and –B receptor subtypes, endothelin-1 is a potent vasoactive peptide, elevated in hypertension and is able to induce fibroblast differentiation to myofibroblasts as well as collagen synthesis and ECM deposition.[95]

Mice with vascular endothelial cell-specific deletion of endothelin-1 were shown to be resistant to developing both perivascular and interstitial cardiac fibrosis in response to chronic Ang II[54] and streptozotocin-induced diabetes.[52] Endothelin-1 is upregulated in diabetic cardiomyopathy and may promote EndoMT, since endothelin-1 KO mice did not show co-localisation of endothelial and mesenchymal markers in hearts of diabetic mouse hearts.[52] Endothelin-1 upregulation is also associated with aging and age-related cardiac fibrosis; histological analysis of aged human cardiac tissue showed profound upregulation with accompanying fibrosis compared to

young.[83] Similar results were obtained in aged mice and senescent cultured fibroblast studies.[83]

These studies indicate an important role for endothelin-1 and highlight a viable therapeutic target for receptor blockade.

1.5.4 Reactive Oxygen Species

Reactive oxygen species (ROS) were originally thought only to cause oxidative damage to cell membranes, proteins and DNA, leading to cellular dysfunction and death via apoptosis and necrosis.[98] It is now accepted that ROS such as superoxide and hydrogen peroxide are also involved in cell signalling and recent evidence points towards ROS signalling in the generation of cardiovascular pathologies, including cardiac fibrosis.[99] Indeed, the redox-sensitive activation of p38 mitogen-activated protein (MAP) kinase and extracellular-signal-regulated kinase-1/2 (ERK1/2) in fibroblasts, ROS-dependent generation of TGFβ and CTGF, and redox-dependent enhancement of TGFβ signalling have all been experimentally demonstrated to be involved in fibroblast proliferation or ECM synthesis, key processes in the initiation of cardiac fibrosis.[100-103]

Under physiological conditions, ROS are maintained at very low levels via antioxidant systems, including glutathione, superoxide dismutase (SOD), catalase and peroxiredoxins.[104, 105] For example, SOD, which comprises a family of three isoforms, is primarily responsible for the dismutation of superoxide into hydrogen peroxide and molecular oxygen in cells and tissues.[106] Glutathione, catalyses the reduction of hydrogen peroxide into water at high peroxide concentrations, whereas catalase appears more important at low peroxide levels.[98, 107] In addition, the body controls ROS levels using non-enzymatic methods with vitamin C and vitamin E, which are ROS scavengers.[106] Despite this, some pathological states are characterised by a combination of increased ROS production and decreased antioxidant systems, contributing to oxidative stress. Oxidative stress is defined as a localised imbalance in ROS production and anti-oxidant capacity and the imbalance has been described as pro-fibrotic in a number of tissues including the heart, likely through promotion of pro-fibrotic signalling pathways.[102, 108]

The importance of ROS signalling in oxidative stress has been highlighted by a number of animal studies in which antioxidants or endogenous antioxidant overexpression were used to reduce cardiac fibrosis and/or pathological cardiac remodelling and to improve cardiac function.[31, 33, 35, 109-111] Whilst antioxidants such as N-acetylcysteine[112] and resveratrol[65] have often been used successfully in animals, these effects rarely translate to human clinical studies, or do so with conflicting results.[113] This not only indicates possible species differences, but also a need for greater mechanistic understanding, especially concerning the nature and source of ROS generation.

1.6 NADPH Oxidases as ROS Sources

Different sources of ROS exist within the cardiovascular system, including xanthine oxidases, mitochondria, uncoupled nitric oxide synthases and NOX enzymes.[99] NOXs are of particular importance in cardiovascular disease, being described as a major source of ROS, and especially important in redox signalling.[102]

NOXs are a family of multi-subunit enzymes, each containing a catalytic core which gives rise to the name. There are 7 isoforms, NOX1-5 and Duox1 and 2, each based on a distinct catalytic subunit.[114] Of the 5 known NOX isoforms, NOX2, NOX4 and NOX5 are expressed in the human heart, however only NOX2 and NOX4 exist in mice. NOX2 and NOX4 are expressed in endothelium, cardiomyocytes and cardiac fibroblasts, but appear to have distinct roles due to differences in their activation mechanism, subcellular location and nature of ROS species generated.[103, 115] Both NOX2 and NOX4 form a membrane-bound heterodimer with a $p22^{phox}$ subunit, but NOX2 is normally quiescent whereas NOX4 is constitutively active.[114] The catalytic subunit of NOX2 is $gp91^{phox}$, which contains a flavoprotein domain essential for complex assembly and activation. NOX2 is activated upon cell stimulation by agonists such as Ang II or TNFα in a process that involves the translocation and binding of cytosolic regulatory subunits ($p47^{phox}$, $p67^{phox}$, $p40^{phox}$, Rac1/2; Figure 1-2A and B).[114] Once assembled at the cell membrane, these subunits support full activation of NOX2 and the catalytic transfer of electrons from NADPH to molecular oxygen to generate superoxide (Figure 1-2C).[102] In contrast, NOX4 does not require the binding of regulatory subunits and when expressed is constitutively active to produce hydrogen peroxide.[116]

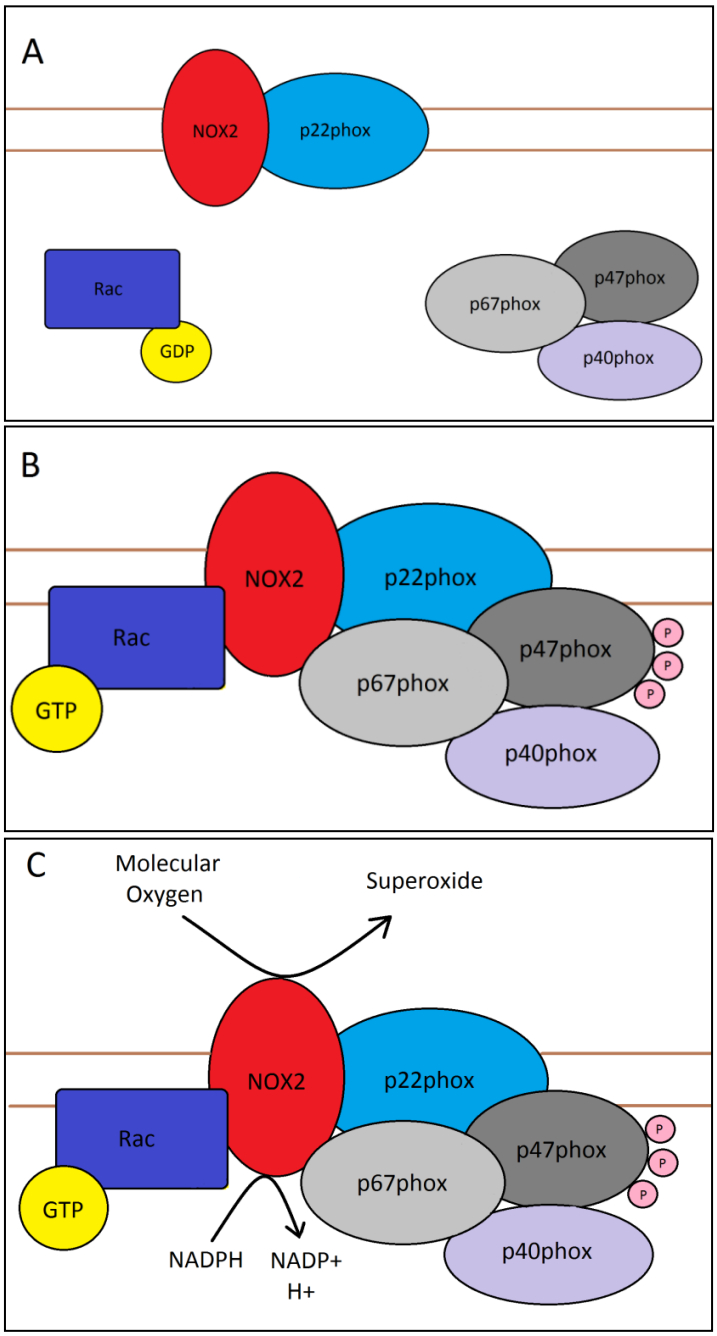

Figure 1-2: Subunit assembly of NOX2. **A:** The gp91^{phox} subunit of NOX2 (red) is found associated with p22^{phox} where they co-stabilise each other in cell membranes. Upon activation, **B:** the GDP bound to Rac is exchanged for GTP causing Rac activation. The p47^{phox} subunit becomes phosphorylated in the cytosol, causing conformational changes which facilitate binding to p22^{phox} and association of the entire NOX2 enzyme complex. **C:** this marks full activation of the NOX2 enzyme and allows the transfer of electrons from NADPH to molecular oxygen to form the superoxide anion.

The involvement of NOX in the activation of cardiac fibroblasts can be studied *in vitro* using TGFβ or other applied stimuli. Whilst this is useful in determining changes in

activity and superoxide generation, as well as downstream signalling, the complexity of cardiac fibrosis development demands that the role of NOX is studied *in vivo* to better understand the processes at play. In addition, functional consequences such as cardiac contractility and relaxation properties are ultimately important when considering the clinical relevance of these studies and unfortunately cannot be determined in culture.

1.6.1 NOX2 in the Development of Cardiac Fibrosis

In recent years, a key finding was that NOX2 seemed to be essential for the development of cardiac fibrosis in an Ang II infusion model.[62] Global NOX2 KO mice were subjected to chronic Ang II infusion for two weeks at a subpressor (non-hypertensive) dose. Interstitial cardiac fibrosis developed in wildtype (WT) littermates as expected, but fibrosis was significantly attenuated in NOX2 KO mice.[62] Subsequent studies from our group and others found a similar inhibition of fibrosis in several different mouse models, including pressor (hypertension-inducing) Ang II infusion,[35, 117] TAC-induced pressure overload,[31, 118] chronic aldosterone treatment,[35] MI[32, 119] and chronic genetic renin-angiotensin activation.[117] This supported the early finding that expression of $gp91^{phox}$, the catalytic subunit for NOX2, was elevated in failing human hearts and accompanied by increased oxidase activity.[118, 120]

Whilst both NOX2 and NOX4 increase their expression in response to stress, it was found that NOX4 mediates beneficial adaptive effects during chronic pressure overload induced by TAC.[34] This study used both loss and gain of function gene-modified mice, showing that NOX4 KO mice experienced exaggerated cardiac hypertrophy and fibrosis in response to TAC compared to WT controls, whereas NOX4 overexpressing mice appeared to be partially protected.[34] Taken together, these results strongly suggest a pivotal, detrimental role for NOX2 in the development of cardiac fibrosis and shift the focus away from non-selective antioxidant therapy. Indeed, the beneficial effects of NOX4 in chronic pressure overload may provide an explanation for why antioxidant therapies have been less than successful in the clinic, since although pathological NOX2 effects would be blocked, so would the beneficial NOX4 effects.

1.6.2 Cellular Sources of NOX2

NOX2 is present in a range of cardiovascular cell types such as cardiac fibroblasts, inflammatory cells, endothelial cells and cardiomyocytes, any of which could be drivers of cardiac fibrosis. Previous studies used global NOX2 KO mice and therefore could not identify the important cell type responsible for the pro-fibrotic effects of NOX2. Given the importance of fibroblasts in the development of fibrosis, NOX2 in these cells would be expected to be important, but this has not previously been investigated *in vivo*.

NOX2 is basally present in cardiomyocytes, with increased expression in patients with MI.[121] A series of *in vitro* experiments on H9c2 (rat cardiomyocyte) cells show nuclear expression of NOX2 during ischaemic stress, activating apoptosis via caspase-3.[122] The non-specific NOX inhibitors apocynin (an antioxidant) and diphenyleneiodonium (a general flavoprotein enzyme inhibitor) were used to show a reduction in apoptosis, highlighting a role for NOX2 in cardiomyocyte cell death.[122] Since reactive fibrosis occurs largely as a consequence of cardiomyocyte cell death, it is possible that NOX2 in cardiomyocytes indirectly contributes to the development of cardiac fibrosis. Indeed, it has recently been shown that overexpression of cardiomyocyte NOX2 induced more severe cardiac fibrosis in response to myocardial infarction *in vivo*.[123]

Inflammatory cells are high expressers of NOX2 and invade myocardial tissue during cardiac stress. To study the effect of NOX2 in inflammatory cells, bone marrow chimeric mice were generated, in which WT mice were irradiated and the bone marrow was reconstituted with either NOX2 KO or WT cells.[53] The fibrotic response to chronic Ang II infusion was then investigated, showing similar levels of cardiac fibrosis in WT mice with either (a) NOX2-deficient or (b) NOX2-intact bone marrow cells (Figure 1-3)[53]. These data indicated that NOX2 in inflammatory cells may be dispensable in Ang II-induced cardiac fibrosis.

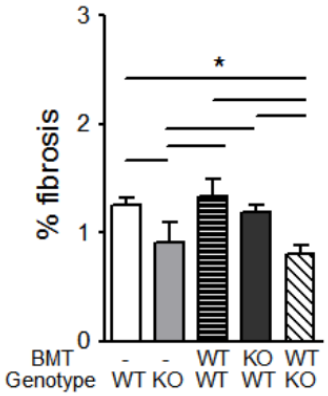

Figure 1-3: Quantification of Ang II-induced cardiac fibrosis in chimeric mice. WT or global NOX2 KO mice were irradiated, then bone marrow reconstituted with either WT or NOX2 KO cells. Cardiac fibrosis is the same, independent of bone marrow type (BMT). Horizontal lines above bars indicate a significant difference (*$P<0.05$) by 1-way ANOVA; n≥5/group. Reproduced from Murdoch et al., 2014.[53]

By contrast, endothelial cell NOX2 appears to play an important role in cardiac fibrosis development. A novel transgenic mouse overexpressing NOX2 specifically in endothelial cells was developed[124] and, when subjected to chronic Ang II infusion, displayed significantly more interstitial cardiac fibrosis than WT mice (Figure 1-4).[53] This was shown to be due in part to enhanced EndoMT in transgenic mice. The enhancement of cardiac fibrosis was confirmed as ROS-dependent, since treatment of transgenic mice with *N*-acetylcysteine abolished the enhancement. Unfortunately however, the effect of *N*-acetylcysteine treatment was not investigated in the context of EndoMT, which could feasibly also be ROS-dependent.

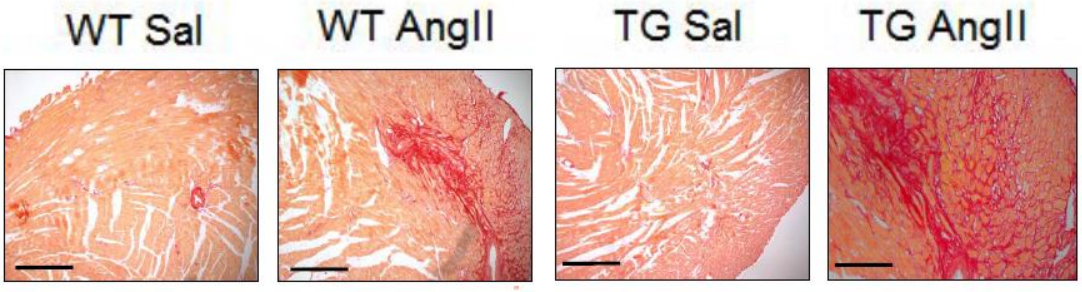

Figure 1-4: Quantification of Ang II-induced cardiac fibrosis in endothelial cell NOX2 transgenic mice. Picrosirius Red-stained sections from mice infused with saline (Sal) or Ang II. Scale bars 100µm. Sal: saline infused controls; TG: transgenic endothelial NOX2 overexpressing mice. Reproduced from Murdoch et al., 2014.[53]

1.7 Summary

Cardiac fibrosis is seen in a variety of cardiovascular pathologies, leading to cardiac dysfunction and increased mortality. Cardiac fibrosis is multifactorial, with many contributing pro-fibrotic pathways, many of which are stimulated by ROS. The current literature suggests a key role for NOX2 in the development of cardiac fibrosis and in particular, NOX2 in fibroblasts and endothelial cells. This is owing to the central role in ECM homeostasis and EndoMT for fibroblasts and endothelial cells, respectively.

Identification of a crucial cellular ROS source in the development of cardiac fibrosis could yield more specific and targeted ROS-directed therapies.

1.8 Research Aims and Objectives

The aim of this thesis is to determine the role of fibroblast and endothelial cell NOX2 activation in the generation of cardiac fibrosis in mice.

To address this aim, the following specific objectives were set out:

1. Establish a suitable and reproducible mouse model of cardiac fibrosis.
2. Generate tamoxifen-inducible fibroblast and endothelial cell-specific NOX2 knockout mice and induce cardiac fibrosis via surgical intervention.
3. Determine the effects of fibroblast and endothelial cell NOX2 deletion on the generation of cardiac fibrosis by assessing cardiac function by echocardiography, cardiac fibrosis by histological analysis and the biochemical profile of these knockout mice in the disease setting.
4. Investigate the contribution of EndoMT to the development of cardiac fibrosis using a novel reporter mouse and lineage tracing techniques.

It was hypothesised that specific deletion of NOX2 in fibroblasts and endothelial cells would reduce the development of cardiac fibrosis.

CHAPTER 2: General Methods

2.1 Introduction to Genetic Alteration in Mice

Specific signalling pathways in experimental models of heart failure and fibrosis can be investigated by using gene-modified mice. Commonly, loss-of-function, i.e. gene knockout (KO),[34] or gain-of-function, i.e. gene overexpression,[53] approaches are used, providing an insight into the roles of proteins and pathways of interest.

The Cre-LoxP system for gene KO allows for conditional cell type-specific and temporal-specific analysis of genes of interest.[125] For example, two distinct gene-modified mouse lines can be crossed to generate temporal KO in fibroblast or endothelial cell gene "X". In the first mouse line, mice are generated harbouring two small DNA recognition sites flanking critical components of gene "X" for gene function.[125] These recognition sites are known as Locus of X-over P1 or simply LoxP. This involves gene targeting and recombination and the resulting mice are so-called "floxed" mice (Figure 2-1A). In the second transgenic mouse line, the tamoxifen-inducible Cre-recombinase is placed under the control of the *Col1a2* or *CD144* gene promoter in a transgene construct, conferring fibroblast or endothelial cell specificity (Figure 2-1B). The transgene construct is integrated into the mouse genome either by simple microinjection (random transgenesis) or by targeting to a specific locus (e.g. the ROSA26 locus). The advantage of the latter approach is that a single copy of the transgene is integrated at a specific site but it involves gene targeting. In contrast, the random approach, while simpler, could result in more than one copy of the transgene being integrated, while the site of integration is unpredictable and could in principle disrupt other genes and their function.[126]

Cre-recombinase is a tyrosine kinase which performs site-specific recombination between DNA recognition sites. Upon crossing the two mouse lines, Cre recombinase will recognise and excise any gene region between the two LoxP sites.[125] Cre recombinase will only be expressed in fibroblasts or endothelial cells, hence only fibroblast or endothelial cell gene "X" will be disrupted or "knocked out" (Figure 2-1C).

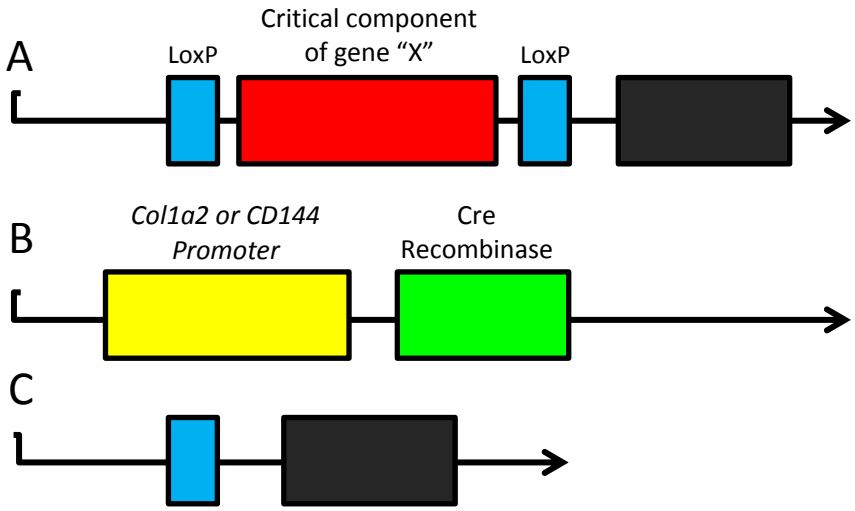

Figure 2-1: Cre-LoxP system for generating knockout mice. **A:** Component of gene "X" critical to gene function (red) is "floxed" by two LoxP sites (blue). The expression of gene "X" is ideally unaffected. **B:** Cre recombinase gene (green) under the control of the fibroblast- or endothelial cell-specific (*Col1a2* or *CD144*) promoter (yellow). **C:** When mice A and B are crossed, the floxed gene will be disrupted and therefore "knocked out" in *Col1a2*$^{+}$ or *CD144*$^{+}$ cells.

Inducible Cre-recombinase (CreER(T/2)) allows for spatial *and* temporal control of target gene excision, with high specificity. In brief, CreER(T/2) is a tyrosine recombinase fused to a modified oestrogen receptor.[127] Under basal conditions the recombinase associates with cytoplasmic chaperone proteins, e.g. heat shock protein-90, rendering it inactive.[125, 128] Upon binding of 4-hydroxytamoxifen, these associations are broken, such that Cre can relocate to the nucleus and bind to LoxP sites which flank genes of interest.[125, 127] Modified tamoxifen (4-hydroxytamoxifen) can be given in the diet,[129] or as a course of intraperitoneal injections.[130]

Successful recombination in mouse progeny can then be confirmed by polymerase chain reaction (PCR) methods, as well as western blotting, quantitative real-time PCR in tissue samples or crossing to a fluorescent reporter strain.[130-132]

2.2 Generation of Experimental Mice

All animal experiments were performed according to the Home Office Guidance on the care and use of animals in science (Scientific Procedures Act, 1986, UK). All mice were on a C57BL/6J background and bred under licence at King's College London,

with *ad libitum* access to food and water. All mouse lines were maintained in house and appeared to breed normally without obvious basal phenotype.

Experimental mice in these studies were generated by taking advantage of the inducible Cre-recombinase transgenic mouse breeding strategy as outlined above. Four distinct transgenic mouse lines were established before being specifically crossed to generate experimental mice, details of which are given in individual chapters.

Line 1 (*NOX2* flox) have LoxP insertions flanking exons 1 and 2 on the NOX2 locus (Figure 2-2A). Crossing with a Cre recombinase-expressing mouse results in disruption of NOX2 function in the specific cell type.

Line 2 (*ROSA26*-CAG-LoxP-STOP-LoxP-tdTomato or simply ROSA26-tdTomato$^{flox/flox}$) mice are prevented from ubiquitously expressing tandem dimer tomato (tdTomato) fluorescent protein (which is targeted to the ROSA26 locus) by an upstream STOP codon (Figure 2-2B). The STOP codon is flanked by LoxP sites so that Cre-mediated excision of the STOP codon allows permanent expression of tdTomato fluorescence. This mouse line has been used extensively owing to its favourable bright fluorescence.[133-136]

Line 3 (*Col1α2*-CreER(T)) harbour a transgenic DNA construct containing a subcloned 6kb transcriptional enhancer from the far upstream regulatory element of the mouse *Col1α2* gene, which drives the expression of CreER(T) (Figure 2-2C).[132] Importantly, this enhancer region is reported to confer specificity to fibroblasts rather than to other collagen 1-expressing lineages.[132, 137] This *Col1α2*-CreER(T) line has been used in previous studies, including a cardiac study.[136, 138] Daily treatment with intraperitoneal injections of 1mg tamoxifen for 10 consecutive days induces Cre activity in this mouse line.[136]

Line 4 (*Cdh5*-CreER(T2)) harbour a transgenic DNA construct containing CreER(T2) subcloned downstream of the 2.5kb mouse *Cdh5* promoter (Figure 2-2D).[130] This *Cdh5*-CreER(T2) mouse line expresses Cre-recombinase in endothelial cells and has been fully characterized and reported in cardiac endothelial cell lineage tracing

experiments.[130, 131, 139] Daily treatment with intraperitoneal injections of 1mg tamoxifen for 3 consecutive days induces Cre activity in this mouse line.[130]

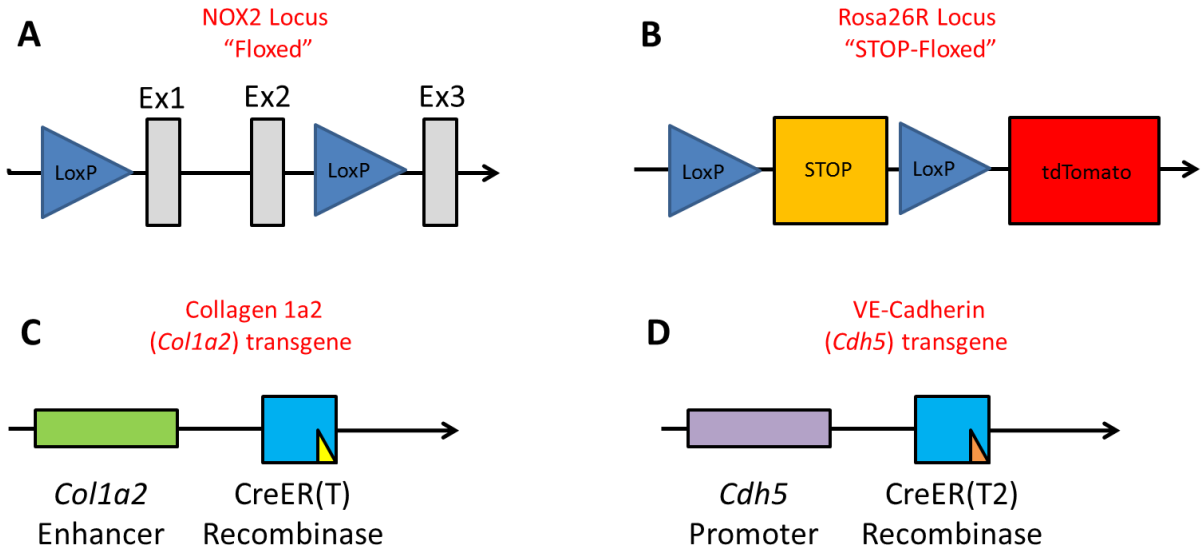

Figure 2-2: Transgenic mouse lines used to generate experimental mice. A: NOX2 floxed mice have LoxP sites flanking critical exons 1 and 2. **B:** ROSA26-tdTomato mice have LoxP sites flanking a STOP codon, preventing tdTomato expression in the absence of Cre recombinase. **C:** *Col1α2*-CreER(T) mice express tamoxifen-inducible Cre recombinase driven by an enhancer region of the *Col1α2* gene. **D:** *Cdh5*-CreER(T2) mice express tamoxifen-inducible Cre recombinase driven by a promoter region of the *Cdh5* gene.

In addition, wildtype (WT) C57Bl/6 mice (Harlan, UK or Charles River, UK) were used in some experiments where stated.

2.3 Surgical Procedures

All mice were given 10µL Vetergesic (buprenorphine hydrochloride) *i.m.* from 0.03mg/mL stock and 50µL finadyne (flunixin meglumine) *s.c.* from 1mg/mL stock as prophylactic pain relief prior to any surgical procedure. Full surgical plane was ensured by toe pinch reflex. Any incision sites were first shaved and swabbed with iodine then chlorhexidine.

2.3.1 Transverse Aortic Constriction (TAC) Surgery

Minimally invasive TAC surgery without intubation was used to induce cardiac fibrosis and hypertrophy over 14 days, based on methods previously described.[140, 141] All TAC operations were performed by Dr. Greta Sawyer, a highly experienced and consistent microsurgeon at King's College London. Briefly, mice were anaesthetised with isoflurane and maintained at 1.5% at 1.5L/min. A small suprasternal incision was made through which the thymus was retracted and the strap muscles were bluntly dissected to expose the aortic arch. A mini proximal sternotomy was made to assist passing a small, hook-shaped needle with 6-0 silk suture under the aorta between the brachiocephalic and left common carotid arteries. The needle was then removed. An angled 27-gauge needle was placed alongside the aorta and the 6-0 silk suture tied snugly around the 27-gauge needle to constrict the aorta. The needle was then promptly removed and the incision closed by suturing. Sham operated mice underwent the same procedure without constriction. Mice were then placed in a heated recovery chamber.

2.4 Physiological Measurements

2.4.1 Echocardiography

Echocardiography was performed as previously described[142] both prior to surgical intervention for baseline cardiac function and again on a weekly basis following mini-osmotic pump implantation or TAC surgery. Briefly, mice were weighed and anaesthetized with 5% isoflurane in medical oxygen at 1L/minute, then maintained on a nose cone at 1-2% isoflurane on a heated stage in the supine position. Heart and respiration rates were continuously monitored throughout via the stage. Hair was removed on the abdomen using hair removal cream (Veet, UK), ensuring that any residual cream was removed fully with water. Ultrasonic gel (Skintact, DE) was applied to the 22-55MHz echocardiography transducer (MS550D; Vevo 2100, FUJIFILM VisualSonics, Canada) and scanning initiated with long and short axis views in B-Mode and M-Mode, according to a standard protocol, with a target heart rate of >400bpm for systolic cardiac function. Pulsed-wave Doppler and tissue Doppler imaging were also used to determine diastolic function, using mitral valve flow for the following indices: early and late filling velocities (E and A wave), E/A ratio, E wave

deceleration time, isovolumic relaxation time (IVRT), isovolumic contraction time (IVCT) and total ejection time (Figure 2-3). E' and A' indices were obtained by tissue Doppler imaging at the mitral annulus (Figure 2-4).

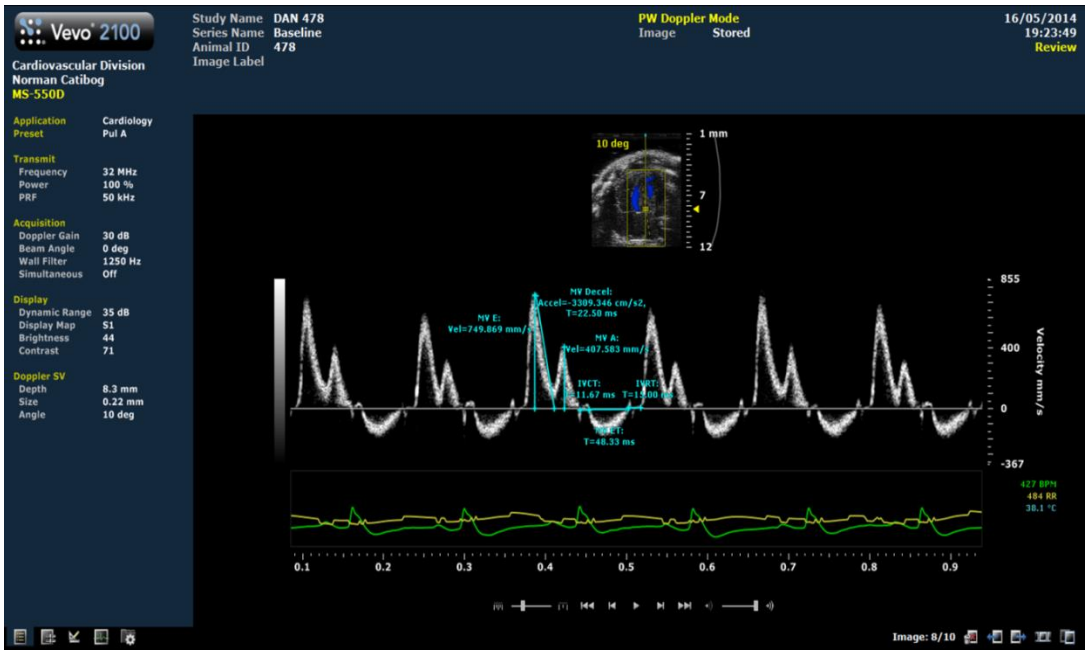

Figure 2-3: Pulsed-wave Doppler imaging by echocardiography for Doppler-derived indices.

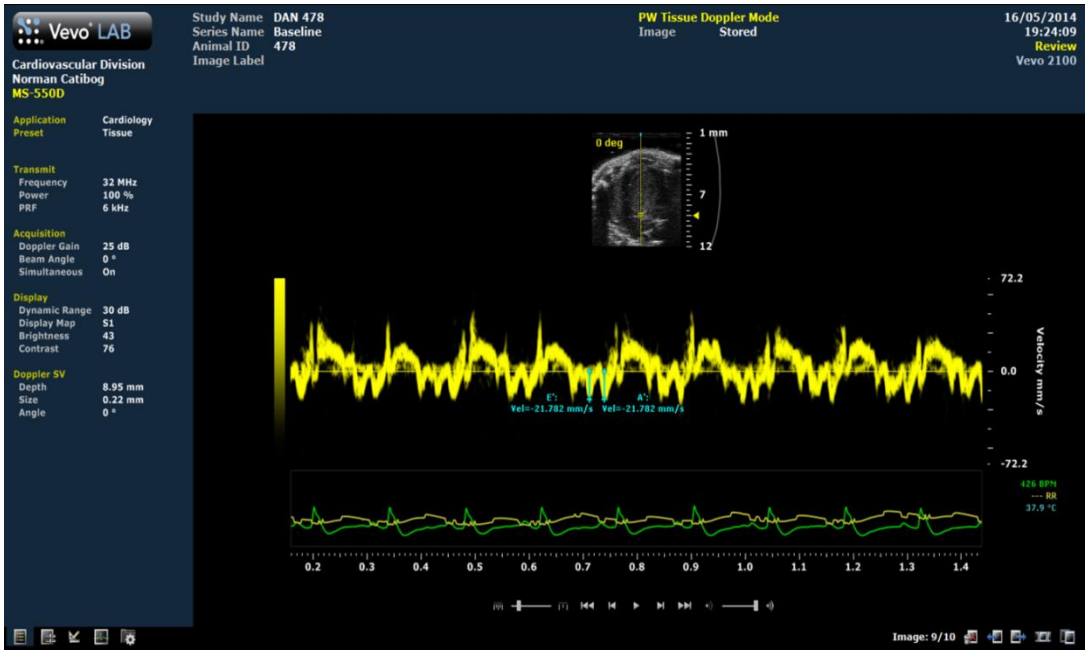

Figure 2-4: Tissue Doppler imaging by echocardiography for mitral annular displacement during early and late diastole (E' and A', respectively). The simultaneous recording of mouse electrocardiogram (green trace) aids interpretation.

TAC pressure gradients were estimated using trans-TAC aortic pulsed-wave Doppler imaging (Figure 2-5). The MS550D transducer was used to visualise the TAC site in standard B-Mode (yellow arrow; Figure 2-5). Colour Doppler was then used, showing either laminar blood flow (sham) or disrupted, turbulent blood flow (TAC). Lastly, a 9-18MHz transducer (MS200) was used to detect higher blood velocities through the TAC constriction using pulsed-wave Doppler. The peaks could then be measured and a peak pressure TAC gradient could be calculated using the modified Bernoulli equation (Pressure gradient = 4*velocity^2).[141]

Strain and strain rate measurements were completed using a semi-automated border tracking technique as previously described.[142] Briefly, tracking points were added to the endocardial and epicardial borders of the left ventricle from a parasternal long axis view in B-Mode. These points are described as a guide for the automated software (VevoStrain) to provide frame-to-frame tracking of ventricular walls throughout the cardiac cycle.[142] Six cardiac 'segments' are assigned to regions of the ventricular wall (e.g. anterior apex) and their delineation during the cardiac cycle is converted to a data curve with positive and negative values for peak radial and longitudinal strain and strain rate, in addition to calculated ventricular volumes and ejection fraction.[142]

All images were analysed using Vevo 2100 software (v1.5.0, FUJIFILM VisualSonics, Canada), taking an average of 3 measurements per variable per animal.

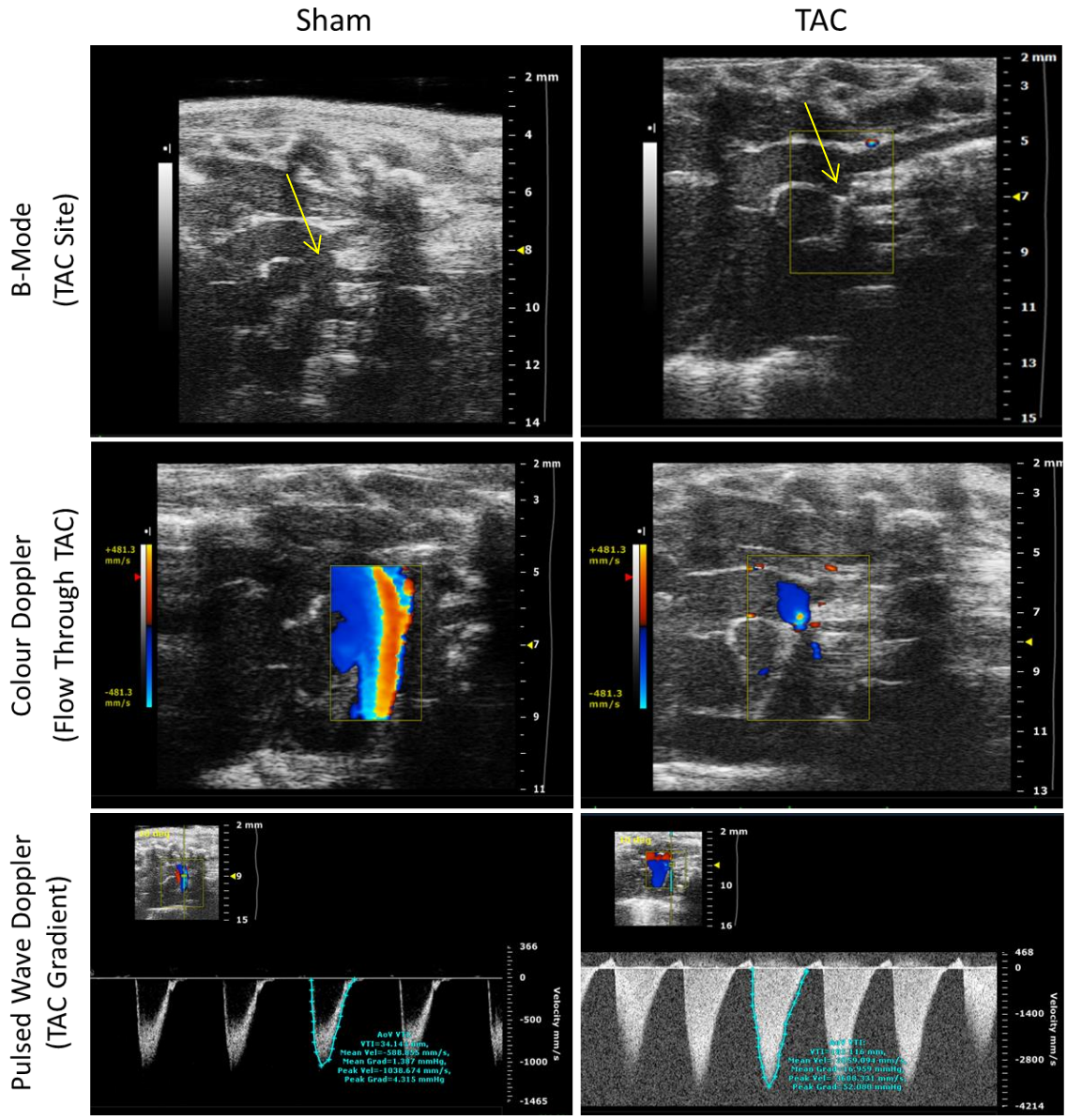

Figure 2-5: Strategy for TAC gradient assessment at 1 day post TAC surgery by echocardiography. First, B-Mode is used to confirm TAC (upper panel), followed by colour Doppler to visualise blood flow through the TAC site (middle panel). Lastly, pulsed wave Doppler is used to determine the maximal blood velocity through the TAC site (lower panel). Measurement of the pulse profile provides an estimate for trans-TAC gradient using the Bernoulli Equation.

2.5 Tissue Harvest and Processing

Mice were weighed then killed according to a schedule 1 method. An abdominal incision was made and continued up to the thorax to expose the heart. The heart was arrested in diastole by injecting approximately 200µL of 5% potassium chloride/ 0.9%

sodium chloride directly into the apex. The whole heart was quickly excised and gently palpated in ice cold phosphate buffered saline (PBS) to remove blood prior to weighing. All four chambers (left and right ventricles and atria) were separated and weighed individually. The left ventricle was divided transversely into apical, mid and basal sections, before being either snap frozen in liquid nitrogen or placed into 4% paraformaldehyde (PFA) for biochemical or histological analysis respectively (Figure 2-6).

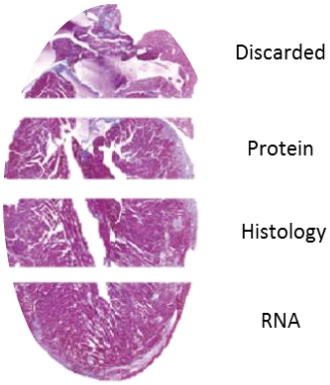

Figure 2-6: Division of the left ventricle for biochemical and histological analysis. Apical, mid and basal sections were used for RNA extraction, histology and protein extraction respectively.

Total liver and lung weights were also recorded, as well as left tibia length for normalization. Lastly, a small ear biopsy was taken for genotype confirmation.

2.5.1 Histology

After 24 hours fixation in 4% PFA, hearts (histology portion; Figure 2-6) were washed in PBS then placed in 70% ethanol. Tissues were prepared for embedding using an automated tissue processor (Shandon Hypercentre XP; Thermo Scientific, UK), then embedded in molten paraffin wax. 6µm tissue sections were cut onto glass slides using a microtome (≥3 sections/slide). After 24 hours drying, slides were de-waxed in xylene and rehydrated through a series of decreasing ethanol concentrations followed by distilled water.

2.5.2 Cardiac Fibrosis Assessment

For the assessment of fibrosis, slides were submerged in 0.1% phosphomolybdic acid for 2 minutes, rinsed in distilled water then stained with Picrosirius red for 2 hours.

Slides were washed in acidified water then dehydrated by successive baths of increasing ethanol. Slides were cleared with xylene before a cover slip was mounted with DPX mounting medium (a mixture of Distyrene, a Plasticizer and Xylene).

Picrosirius red-stained hearts were imaged with both bright field and circularly polarised light on a light microscope (Axioskop 2, Carl Zeiss or DM2000, Leica). Interstitial cardiac fibrosis was determined by taking images of four distinct regions of each cardiac section, imaged at 5x magnification. To determine perivascular fibrosis, four individual coronary vessels per section were identified and imaged such that they occupied the central field of view at 20x magnification. Picrosirius red is used to determine fibrosis as it enhances the birefringency of collagen.[143] Standard bright field images report total collagen content, whereas polarised light is said to increase the stain specificity by showing mainly abnormally cross-linked collagen, therefore naturally reducing false positives.[143] Images were analysed using 'Red-Green-Blue-based' detection for total tissue area and fibrosis, and region of interest tracing for vessel lumen size (Volocity v6.3, PerkinElmer). Images were acquired and analysed in a blinded fashion. Interstitial fibrosis is expressed as a percentage of total tissue and perivascular fibrosis is expressed as percentage of tissue in the perivascular region (up to 450µm from the vessel wall). For perivascular fibrosis attempts were made to analyse similarly-sized vessels.

2.5.3 Cardiomyocyte Hypertrophy Assessment

To determine cardiomyocyte area, rhodamine-conjugated wheat germ agglutinin (WGA) was used to outline cardiomyocytes. Briefly, the antigen was unmasked by heating slides in a steamer of unmasking solution (H3300; Vector Labs, UK) for 10 minutes and left to cool for a further 20 minutes. Slides were washed in PBS, then sections blocked for 45 minutes in 10% goat serum, before being incubated for 2 hours with 2% WGA-rhodamine in 10% goat serum in a humidity chamber at room temperature. Slides were washed with PBS, stained with 4',6-diamino-2-phenylindole (DAPI), then cover slips mounted with mowial.

WGA-stained hearts were imaged using a fluorescence microscope (IX81-2, Olympus) at 40x objective. The average cross-sectional area was determined by tracing the area congruent to the WGA stain in ≥100 cells per slide. Cell exclusion criteria included a

non-transverse orientation and/or an absence of a DAPI-stained nucleus. Images were analysed using Volocity software (v6.3, PerkinElmer).

2.5.4 Protein Preparation and Western Blotting

Tissue samples were placed in liquid nitrogen and crushed using a cryogenic pestle and mortar. The resulting powder was collected and placed directly into an eppendorf containing lysis buffer with 1% proteinase inhibitors (roughly 10µL/µg tissue). Samples were sonicated briefly before being centrifuged at maximum speed for 5 minutes. The supernatant was transferred to a fresh eppendorf. Total protein concentration was determined using the Bicinchoninic acid Protein Assay Reagent kit (Thermo Fisher Scientific, IL, USA). Two dilutions of each sample was made with lysis buffer (1:10 and 1:20), then 25µL of each sample was pipetted into a microplate well (Thermo Fisher Scientific, UK). Concentration standards were prepared according to manufacturer's protocol and a working reagent was made (50 parts Reagent A, 1 part Reagent B). 200µL of working reagent was added to each diluted sample on the microplate. The microplate was then covered and incubated at 37°C for 30 minutes, before being cooled to room temperature and absorbance measured at 562nm on a spectrophotometric plate reader. The absorbance of each standard was blank-corrected by subtraction and a standard curve constructed to determine experimental sample concentrations in µg/mL. Proteins were diluted appropriately into Laemmli sample buffer to yield 30µg/mL.

Sodium dodecyl sulfate (SDS) polyacrylamide gel electrophoresis was carried out using the Bio-Rad Mini-PROTEAN system (Bio-Rad Laboratories, Hertfordshire, UK) using 8% resolving gels. For electrophoresis, gels were loaded into the Bio-Rad Mini-PROTEAN system (Bio-Rad Laboratories, Hertfordshire, UK) and the electrophoresis chamber filled with running buffer solution (100mL 10x running buffer stock [30g Tris Base and 144g Glycine in 1L deionized water] and 10mL 10% SDS made up to 1L with deionized water) to fully submerge gels. A protein standard (PageRuler, Thermo Scientific, UK) was first loaded and run alongside up to 9 protein samples simultaneously. Electrophoresis was started at 120V initially and run until the dye front had just run off.

Gels were transferred to a nitrocellulose membrane using wet transfer (BioRad, UK) at 70V for 45 minutes, followed by membrane blocking in 5% milk-PBS-Tween (0.001%) solution (w/v; Marvel, Chivers Ireland LTD, Ireland) for 1 hour. NOX2 (mouse; anti-gp91phox; 1:1000 dilution; BD Biosciences) and β-actin (rabbit; 1:1000 dilution; Sigma) primary antibodies were applied in 5% milk solution overnight. Anti-mouse and anti-rabbit secondary antibodies (1:15,000; LI-COR Biosciences) were applied for 45 minutes. Membranes were washed with PBS-Tween for 1 hour on a shaker after each antibody to remove non-specific binding. Detection of protein was completed using the Odyssey CLx detection system and quantified using Image Studio Software (LI-COR Biosciences, UK).

2.5.5 RNA Isolation and Reverse Transcription Polymerase Chain Reaction

Approximately 20mg of apical left ventricle tissue was first homogenised with metal beads in 300µL of RLT lysis buffer containing 1% β-mercaptoethanol (Qiagen; GmbH, DE), using a tissue homogeniser (Precellys 24; Bertin Technologies). Ribonucleic acid (RNA) was extracted using the Qiagen RNeasy Fibrous Tissue Mini Kit (Qiagen, UK) according to manufacturer's protocol. After the final centrifugation step, 30µL of RNase-free water was added directly to the spin column membrane and RNA was eluted by centrifuging at maximum speed for 1 minute. The concentration of extracted RNA was determined using a spectrophotometer (NanoDrop ND-1000; Thermo Scientific, UK).

1µg of RNA was reverse transcribed by PCR in 20µL final volume. The volume of RNA required for 1µg/20µL was added to a PCR tube, made up to 11µL with water and 1.5µL of 100µg/mL oligodeoxythymine primers added to each tube. Tubes were heated to 70°C for 5 minutes, then immediately placed on ice. 7.5µL of mastermix (4µL 5x reaction buffer, 1µL deoxyribose nucleoside triphosphate, 0.5µL RNasin, 1µL water and 1µL reverse transcriptase) was added to each tube and the solution incubated at 42°C for 90 minutes for reverse transcription. A negative control was included, lacking reverse transcriptase. Resultant complimentary deoxyribonucleic (cDNA) was diluted with 80µL of water and stored at 4°C.

2.5.6 Quantitative real-time Polymerase Chain Reaction (qPCR)

Relative expression of messenger RNA (mRNA) was determined by quantitative PCR (qPCR) using a SYBR green detection system, with β-actin mRNA for normalization as previously described,[32] performed in duplicate. All qPCR primers are detailed in Table 2-1 and were used at a working concentration of 10µM (Sigma, UK or IDT DNA, UK).

Table 2-1: Primer sequences for qPCR. All sequences are shown as 5'-3'.

Gene of interest	Forward primer sequence	Reverse primer sequence
NOX2 (gp91phox)	ACTCCTTGGGTCAGCACTGG	GTTCCTGTCCAGTTGTCTTCG
p47phox	GGACACCTTCATTCGCCATA	CTGCCACTTAACCAGGAAC
Collagen 1α1	CCTCAGGGTATTGCTGGACAAC	TTGATCCAGAAGGACCTTGTTTG
Collagen 3α1	CCTGGTGGAAAGGGTGAAAT	CGTGTTCCGGGTATACCATTAG
CTGF	TGACCCCTGCGACCCACA	TACACCGACCCACCGAAGACACAG
Fibronectin	CCGGTGGCTGTCAGTCAGA	CCGTTCCCACTGCTGATTTATC
CD31	CAAACAGAAACCCGTGGAGAT	ACCGTAATGGCTGTTGGCTTC
β-actin	CTGTCGAGTCGCGTCCACCC	ATGCCGGAGCCGTTGTCGAC

A separate mastermix for each gene of interest was made (per well: 10µL SYBR Green, 6µL RNase/DNase-free water and 1µL of both forward and reverse primer) before being loaded into an appropriate well on the 96-well plate (ABI Prism, Life Technologies, UK). 2µL of each sample cDNA was added to an appropriate well and finally a plastic film placed on top to seal all wells. The plate was centrifuged briefly at 1000rpm, then loaded into the qPCR machine (Mastercycler ep Realplex2, Eppendorf or StepOnePlus, Applied Biosystems) and run according to the protocol given in Figure 2-7.

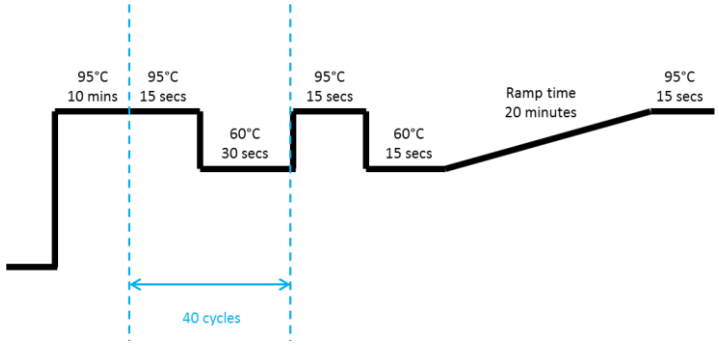

Figure 2-7: Programme to determine gene expression by qPCR using detection of SYBR Green. Samples were heated to 95°C for 10 minutes, then 40 cycles of 95°C for

15 seconds, followed by 60°C for 30 seconds, then 95°C for 15 seconds, 60°C for 15 seconds, then increased slowly to 95°C over 20 minutes and lastly held for 15 seconds at 95°C.

Data was converted to log scale and cycle threshold (Ct) values were obtained after thresholding and drift correction. Ct values were normalised to their respective β-actin Ct values, then expressed in relative terms to percentage of control (vehicle or sham) samples.

2.6 Mouse Genotyping and Polymerase Chain Reaction (PCR)

DNA isolation was performed using small ear punch samples taken from each mouse. Samples were placed into eppendorf tubes, to which 300µL of 50mM sodium hydroxide (NaOH) was added and heated to 95°C for 10-15 minutes. The sample was vortexed and 25µL of 1M Tris HCl (pH8) was added. The final sample (purified DNA) was left to stand for 10 minutes at room temperature, and then stored at 4°C. For PCR, a mastermix was prepared to detect flox insertions (for NOX2 or tdTomato), Cre recombinase or recombined NOX2 (to indicate cell-specific KO mice) given in Tables 2-2, 2-3, 2-4 and 2-5, respectively.

Table 2-2: PCR mastermix used to detect flox insertions in mouse tissue. Red *Thermus Aquaticus* (*Taq*) and nuclease-free water are from Readymix Kit (Red *Taq* PCR reaction mix, Sigma-Aldrich, UK), ASHL1 and ASHL2 are primers designed to recognise flox insertions (Sigma- Aldrich, UK).

Reagent	Volume per sample
Red *Taq*	12.5µL
ASHL1 **5'-GTAAATTCACTGTTCTGGGTCTCAGC-3'**	0.5µL
ASHL2 **5'-ACATGTTCTTCTCACAGGCTCTTCC-3'**	0.5µL
Nuclease-free H_2O	10.5µL

Table 2-3: PCR mastermix used to detect tdTomato 'STOP' flox insertions in mouse tissue. Red *Taq* and nuclease-free water are from Readymix Kit (Red *Taq* PCR reaction mix, Sigma-Aldrich, UK), wildtype and mutant forward and reverse are primers designed to recognise 'STOP' flox insertions (IDT DNA, UK).

Reagent	Volume per sample
Red *Taq*	12.5µL
Wildtype Forward **5'-AAG GGA GCT GCA GTG GAG TA-3'**	1µL
Wildtype Reverse **5'-CCG AAA ATC TGT GGG AAG TC-3'**	1µL
Mutant Forward **5'-CTG TTC CTG TAC GGC ATG G-3'**	1µL
Mutant Reverse **5'-GGC ATT AAA GCA GCG TAT CC-3'**	1µL
Nuclease-free H_2O	6.5µL

Table 2-4: PCR mastermix used to detect Cre recombinase in mouse tissue. MerCreMer and GAPDH are DNA primers (Sigma-Aldrich, UK).

Reagent	Volume per sample
Red *Taq*	12.5µL
MerCreMer (FWD) **5'-TGCCAGGATCAGGGTTAAAC-3'**	0.5µL
MerCreMer (REV) **5'- CCCGGCAAAACAGGTAGTTA-3'**	0.5µL
GAPDH (FWD) **5'-CCTAGACAAAATGGTGAAG-3'**	0.5µL
GAPDH (REV) **5'-GACTCCACGACATACTCAGC-3'**	0.5µL
Nuclease-free H_2O	9µL

Table 2-5: PCR mastermix used to detect the presence of recombined NOX2 in mouse tissue after tamoxifen treatment.

Reagent	Volume per sample
Red *Taq*	12.5µL
NOX2 Cre Forward **5'-GGAATTGAGTTGTAAGAATCAAATGAC-3'**	0.5µL
NOX2 Cre Reverse **5'- ATGATGTGTCCCAAATGTGC-3'**	0.5µL
NOX2 Cre [Wildtype] Forward **5'-GGGGCTGAATGTCTTCCTCT-3'**	0.5µL
Nuclease-free H_2O	9.5µL

After mixing, a 23-24µL aliquot of mastermix was added to appropriately labelled PCR tubes, followed by sample DNA for a total reaction volume of 25µL. PCR was then performed as detailed in Table 2-6.

Table 2-6: Detailed PCR cycle protocols for genotyping mice.

Primer Set	Initialisation	Denaturation/Annealing/Extension (35 cycles)			Final Extension	hold
NOX2 flox	94°C; 2 minutes	94°C; 30 seconds	65°C; 1 minute	68°C; 3 minutes	72°C; 4 minutes	4°C
tdTomato "STOP" flox	94°C; 3 minutes	94°C; 20 seconds	61°C; 30 seconds	72°C; 30 seconds	72°C; 2 minutes	4°C
Cre Recombinase	94°C; 5 minutes	94°C; 30 seconds	60°C; 45 seconds	72°C; 1 minute	72°C; 7 minutes	4°C
Recombined NOX2	94°C; 5 minutes	94°C; 30 seconds	58°C; 45 seconds	72°C; 1 minute	72°C; 7 minutes	4°C

DNA gels were made by heating agarose solution [3g of Agarose in 200mL TAE buffer (40mM Tris, 20mM acetic acid, and 1mM ethylenediaminetetracetic acid (EDTA)] in a microwave for 2-3 minutes. 10µL ethidium bromide or Nancy-520 (Cat# 01494, Sigma, UK) was added and the solution was poured into the gel tank with well combs already inserted. The gel took approximately 20 minutes to set. Well combs were then removed and the gel transferred to a running tank, ensuring full submersion in TAE buffer. 15µL of each DNA sample was run alongside a 7.5µL aliquot of 1Kb DNA ladder (Promega, WI, USA) at 150-170V for 20-25 minutes, ensuring the samples did not run out of the gel. Lastly, gels were exposed under UV light and images saved and/or printed for analysis.

2.7 Statistical Analysis

Data are presented as mean ± S.E.M where applicable. Data are presented and analysed using GraphPad Prism (v6.0, La Jolla, CA, USA), with the statistical test and replicate number (*n*=) detailed in individual figure legends. In general, 2way analysis of variance (ANOVA) was used for data involving two variables (genotype and surgical

intervention) and 2way ANOVA with repeated measures was used for data also including time as an additional variable e.g. echocardiography. *P<0.05* was considered as statistically significant.

CHAPTER 3: Angiotensin II-induced Cardiac Fibrosis

3.1 Introduction

As discussed in chapter 1, Ang II plays a major physiological role in cardiovascular homeostasis. Once cleaved by angiotensin converting enzyme, circulating Ang II acts as a potent vasoconstrictor and signals to increase water and sodium retention, with a net effect of increasing arterial blood pressure.[88] Ang II signalling is a homeostatic response; however the chronic presence of Ang II disrupts this balance and quickly increases blood pressure and haemodynamic load on the heart and other organs.

3.1.1 Chronic Angiotensin II as a Mouse Model

Chronic stimulation with Ang II in mice is amongst the most common models in cardiovascular research. One approach is to use surgically implanted subcutaneous mini-osmotic pumps to administer Ang II over 2 to 4 weeks. A dose of 1.1mg/kg/day has been reported in a number of cardiovascular research studies,[35, 53] causing varying degrees of hypertension, cardiac hypertrophy, fibrosis and dysfunction. In addition to pressor doses of Ang II (hypertension-inducing), subpressor doses in the absence of hypertension can also drive cardiac pathologies including fibrosis, oxidative stress and hypertrophy. This has been reported in a number of studies[62, 144, 145] and most likely reflects direct effects of Ang II-receptor-mediated signalling.

3.1.2 Fibroblast-Myofibroblast Conversion, NADPH Oxidases and Fibrosis

As discussed in chapter 1, the conversion of fibroblasts to active myofibroblasts is a primary step in the development of fibrosis. This conversion involves Ang II/TGFβ-signalling, but importantly also involves reactive oxygen species generated by NOXs.[146] Studies have highlighted the importance of NOX2- and NOX4-mediated fibroblast-myofibroblast conversion in subsequent fibrosis, including in renal fibrosis[147, 148] and hepatic fibrosis, where p47phox KO mice had reduced liver injury and fibrosis following a model of experimental liver fibrosis.[149]

Interestingly, NOX4 activity specifically in lung fibroblasts was increased in cells isolated from patients with idiopathic pulmonary fibrosis.[150] Furthermore, the TGFβ-induced increase in collagen 1α1 expression (indicative of fibroblast-myofibroblast conversion) was reduced in isolated fibroblasts pre-treated with the antioxidant *N*-acetylcysteine, showing the importance of ROS-mediated signalling.[150]

In general, the majority of evidence shows NOX2 activation to be detrimental in the context of cardiac remodelling and fibrosis, whereas the role of NOX4 is disputed. As previously discussed, the global NOX2 KO mouse was shown to be resistant to developing cardiac fibrosis in response to chronic Ang II,[35, 62, 117] pressure overload[31, 118] and myocardial infarction.[32] In addition, NOX2 overexpression led to increased cardiac fibrosis in response to chronic Ang II.[53] In contrast, global NOX4 KO mice were shown to have exacerbated cardiac fibrosis and hypertrophy in response to pressure overload, indicating a protective role for NOX4.[34] Furthermore, mice with cardiomyocyte-specific NOX4 overexpression were resistant to pressure overload-induced cardiac dysfunction and fibrosis. However, work from another group shows almost the exact opposite, with cardiomyocyte NOX4 deletion improving pressure overload-induced cardiac dysfunction and reducing fibrosis. The authors then went on to show NOX4 overexpression as detrimental.[151]

Taken together, fibroblast NOX2 activity is likely to be involved and possibly detrimental in the development of cardiac fibrosis, warranting further investigation.

3.1.3 Chapter Aim

The aim of this chapter was to investigate the contribution of fibroblast NOX2 in the development of Ang II-induced cardiac fibrosis. Owing to the central role of fibroblasts in extracellular matrix homeostasis and the involvement of NOX2, it was hypothesised that specific deletion of NOX2 would reduce subsequent cardiac fibrosis.

3.2 Methods

3.2.1 Generation of Experimental Mice

Male *Col1α2*CreER(T) Cre-positive mice were crossed with Cre-negative female NOX2$^{flox/flox}$ mice to generate experimental *Col1α2*CreER(T)/NOX2$^{flox/y}$ or *Col1α2*CreER(T)/NOX2$^{flox/flox}$ male or female mice respectively, or Cre-negative littermates. Cre-positive progeny are deficient in fibroblast NOX2 following daily *i.p.* injection with 1mg tamoxifen in peanut oil for 10 days.[136]

All experimental mice were NOX2 floxed (Figure 3-1A). Cre-negative male littermates were used as flox controls. Cre recombinase expression is indicated by the presence of a lower band in Figure 3-1B. Figure 3-1C shows recombination of disrupted NOX2 in heart tissue, (following 10-day 1mg *i.p.* tamoxifen injections), indicated by the presence of a lower band. Mice with recombined NOX2 are referred to as "knockout (KO)" and those without are referred to as "flox".

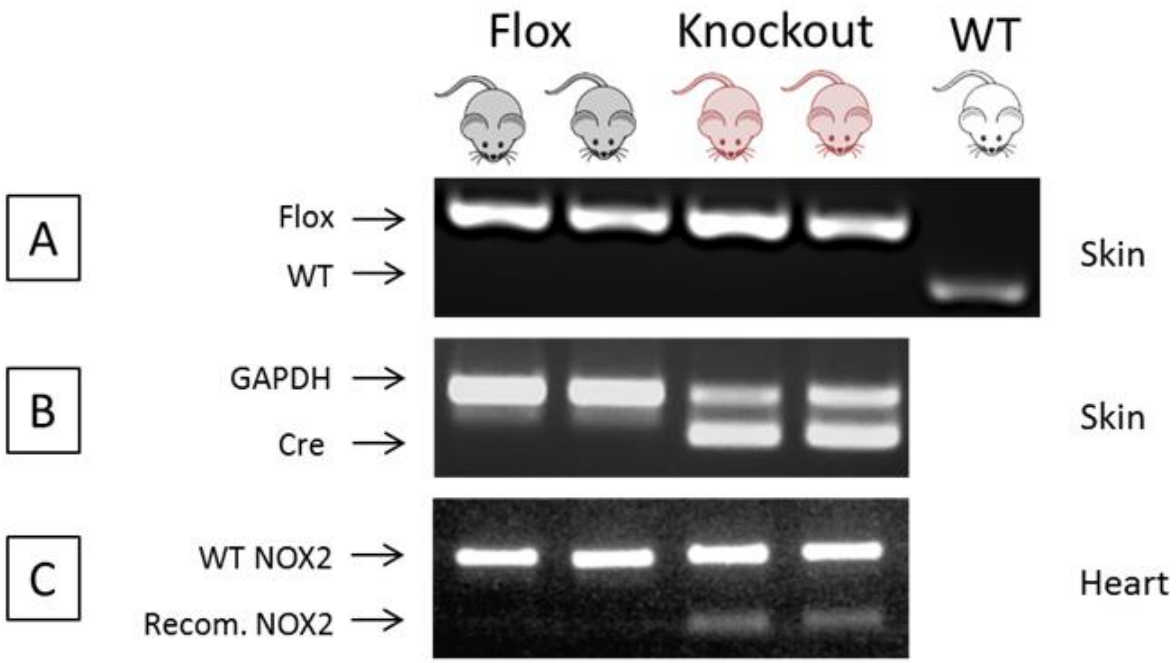

Figure 3-1: PCR-based genotyping of mice using DNA gel analysis. **A:** Primers to recognise floxed and wildtype (WT) NOX2 in ear tissue. **B:** Primers to recognise GAPDH (upper band) and Cre recombinase (lower band) in ear tissue. The presence of the lower band indicated that mice are Cre expressers and that genetic recombination is likely following tamoxifen treatment. **C:** Primers to recognise WT

NOX2 or recombined NOX2 in heart tissue following tamoxifen treatment. The upper band indicated WT NOX2, whereas the lower band indicated the presence of a disrupted (non-functional) NOX2 gene, so-called knockout.

Flox and KO mice were viable, had a normal life expectancy, bred normally and did not show any obvious basal phenotype. Earlier investigations showed that cultured primary cardiac fibroblasts from KO mice are difficult to maintain, making it difficult to determine the extent of fibroblast specific deletion of NOX2 by western blot or qPCR, however whole heart western blotting showed a 50-60% reduction in NOX2 protein levels in mice aged 10+ weeks, a time point commensurate with fibrosis study mice (Figure 3-2).

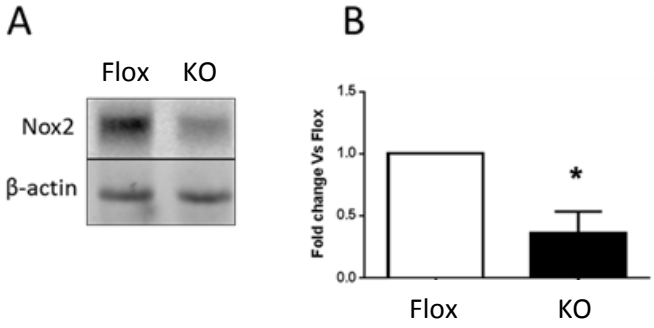

Figure 3-2: NOX2 protein expression in whole heart following mouse treatment with tamoxifen. A: Western blot for NOX2, with β-actin for normalisation, representative image. **B:** Quantification of western blot expressed as fold change compared to flox controls. *n=3; P<0.05; student's t-test*. Reproduced from Harrison et al., 2017; manuscript in preparation.

3.2.2 Blood Pressure Measurement by Telemetry

For the on-going measurement of blood pressure in conscious, unrestrained mice, telemetry units were implanted subcutaneously. Here, surgery was performed by Greta Sawyer and Helena Zhang. Key aspects of the surgical procedure are shown in Figure 3-3. Mice were weighed then anaesthetised with 4% isoflurane in oxygen and air at 4L/min. The neck and chest area was shaved and the mouse moved to an operating table on a heated pad, maintained with 1-2% isoflurane in 1L/min medical oxygen via nose cone in the supine position. An incision into the suprasternal region was made, followed by blunt dissection to form a pocket down towards the lower

abdomen (right side). Approximately 200µL of saline was used to maintain the pocket, delivered by a 1mL syringe. Blunt dissection was again used to separate tissue and locate and isolate the left carotid artery. Two 6-0 silk ligatures were used to obstruct blood flow, followed by the application of a surgical clamp. A small incision was made to the left carotid artery and the area flushed with saline to remove blood from the vessel. The telemeter (placed in saline for 15 minutes prior to implantation) was then inserted into the artery, down to the aortic arch. The telemeter probe was tied in place with 3-4 braided silk ligatures (6-0), followed by removal of the surgical clamp. Lastly, the telemeter unit was inserted into the previously created subcutaneous pocket in the lower right abdomen and the incision closed by suturing. Mice were then placed in a heated (26-28°C) recovery chamber.

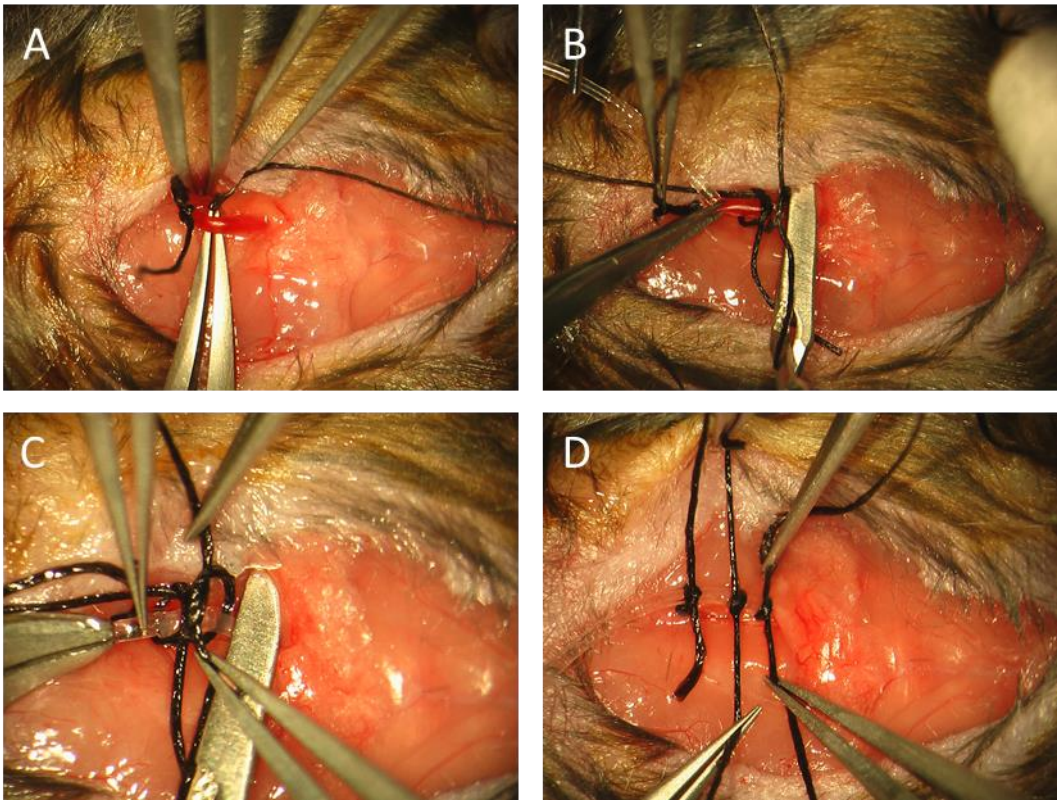

Figure 3-3: Surgical implantation of telemetry devices. **A:** after an initial incision, the left carotid is isolated and tied off. **B:** with a 1cm segment of the vessel completely tied off and clamped, a small incision is made in the left carotid. **C:** the telemeter probe is inserted down to the aortic arch via the small incision. **D:** lastly the telemeter probe is secured in place using 6-0 braided silk ligatures.

Following recovery from anaesthesia, telemetry units were tested using static detection on an amplitude modulation (AM) radio. The telemeter was activated by magnet and the telemeter amplitude tested using a plate reader (usually approximately 20mmHg). Telemeters were then deactivated by magnet until needed.

Blood pressure was recorded and analysed using Dataquest A.R.T.™ System acquisition and analysis software respectively (DSI, Data Sciences International), acquiring at 1000Hz for 10 second durations at 5 minute intervals over 24 hours.

3.2.3 Angiotensin II Infusion by Mini-Osmotic Pump

Mice were infused *s.c.* with subpressor Ang II (0.3mg/kg/day[62]; Human, Cat# A9525, Sigma-Aldrich, MO) for 28 days or pressor Ang II (1.1mg/kg/day)[152] for 14 days or vehicle control via mini-osmotic pumps (model 1002/1004, Alzet Durect, CA). Using 1-3% isoflurane anaesthesia, an incision was made on the mouse dorsum proximal to the scapula. Blunt dissection was used to create a subcutaneous mini-osmotic pump pocket. The pump was inserted according to manufacturer's instructions and the incision closed using 6-0 silk suture. Mice were placed in a recovery chamber and further perioperative care was rarely required.

3.2.4 Blood Pressure Cuff Plethysmography

Blood pressure was acutely measured in conscious mice receiving subpressor Ang II using tail cuff plethysmography (MK-2000ST, Muromachi Kikai, Japan). A 3-day acclimatisation period was used to reduce future stress artefacts, in which mice were placed into the restraint for at least 10 minutes each day followed by 10 blood pressure measurements. Systolic, mean and diastolic blood pressures and heart rate were recorded from an average of 5-10 readings per mouse at baseline and 3-times per week following Ang II treatment.

3.2.5 Echocardiography

Basic echocardiography was performed to include B- and M-Mode systolic function in mice at before and 14 days following treatment with pressor Ang II, performed by Dr. Craig Harrison. As described in chapter 2, full echocardiographic assessment was used for mice receiving subpressor Ang II, measured at baseline and every 7 days up to 28 days following Ang II pump implantation.

3.2.6 Histology

Histological analysis of cardiac tissue was performed as described in chapter 2. Additionally, Masson's Trichrome was also used for the assessment of cardiac fibrosis in mice treated with subpressor Ang II, using the Masson's Trichrome Light Green Variant Kit (RAL Diagnostics, France). Briefly, following treatment and rehydration of tissues as described in chapter 2, sections were stained with Mayer's Haematoxylin for 10 minutes, rinsed in distilled water, stained with Ponceau Fuchsin solution for 5 minutes and rinsed again in distilled water. Sections were then stained with Phosphomolybdic acid for 3 minutes and transferred to Light Green Solution for 5 minutes. Slides were then rinsed in two changes of 1% acetic acid solution, before being dehydrated rapidly through increasing concentrations of ethanol. Finally, cover slips were mounted with DPX.

3.3 Results – Pressor Angiotensin II (1.1mg/kg/day)

To investigate the role of fibroblast NOX2 in the generation of cardiac fibrosis, chronic Ang II infusion, a well-established model of blood pressure driven cardiac fibrosis, was used at a dose of 1.1mg/kg/day for 14 days. This dose has been previously reported to cause hypertension, leading to cardiac fibrosis and variable cardiac hypertrophy in WT mice.[35, 53]

3.3.1 Cardiac Fibrosis

Treatment with 1.1mg/kg/day Ang II led to a significant increase in interstitial cardiac fibrosis in flox mice (1.2 ± 0.1% with vehicle, up to 2.6 ± 0.2% after 14 days Ang II treatment; *P<0.001*; Figure 3-4). In contrast, fibroblast NOX2 KO mice treated with Ang II did not develop significant cardiac fibrosis (1.2 ± 0.2% with vehicle vs. 1.6 ± 0.2% after 14 days Ang II treatment; *P=0.28*). As such, there was a significant interaction between flox and fibroblast NOX2 KO mice receiving Ang II (*$^{\#}$P<0.05*). These data support the hypothesis that NOX2 activation in fibroblasts contributes to cardiac fibrosis, and that deletion of fibroblast NOX2 is beneficial in this disease model.

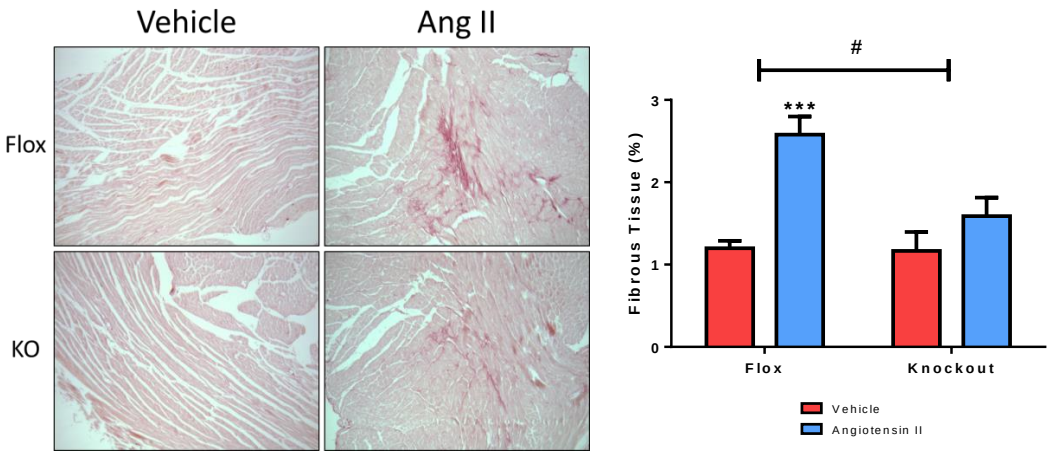

Figure 3-4: Interstitial cardiac fibrosis following 2 week treatment with Ang II. Upper tiles: representative Picrosirius red stained heart sections visualised in brightfield light. **Lower graph:** quantification of fibrous tissue determined by polarised light analysis. Images are representative from n=6, 4, 4, 5, mice respectively per group with a minimum of 4 sample frames/mouse. Scale 200µm. *$^{\#}$P<0.01; significant interaction between angiotensin II-treated flox and knockout mice, ***P<0.001 compared to vehicle*; *2way ANOVA with Bonferroni's multiple comparison post-test*.

3.3.2 Gene Expression

The expression of fibronectin, CTGF, collagen 1α1 and collagen 3α1 mRNA in myocardial tissue was significantly increased in all mice receiving Ang II (Figure 3-5). Bonferroni post-tests revealed significant increases in fibronectin and collagen 3α1 in flox mice, but not in fibroblast NOX2 KO mice receiving Ang II (Figure 3-5A and D) which goes some way towards supporting the cardiac fibrosis data shown in Figure 3-4. It must be noted however, that the usefulness of a post-test is limited in the absence of a significant interaction.

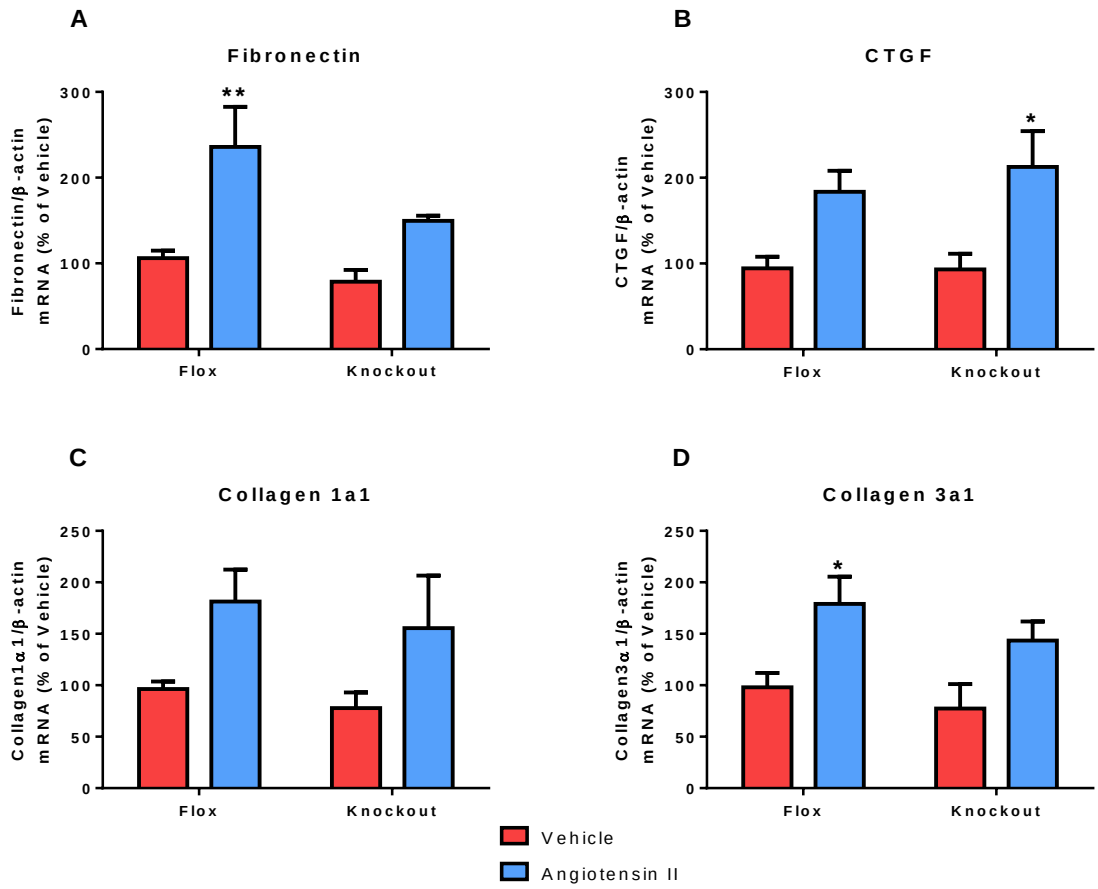

Figure 3-5: Angiotensin II-induced fibrotic gene expression. **A:** fibronectin, **B:** CTGF, **C:** collagen 1α1 and **D:** collagen 3α1 in hearts following Ang II treatment. Each sample is normalised to its own β-actin mRNA control and then expressed as a percentage of vehicle controls. 2way ANOVA shows significant increase vs. vehicle for both groups. **P<0.05, **P<0.01;* 2way ANOVA with Bonferroni's multiple comparison post-test; n=5, 4, 4, 4, respectively for groups.

Interestingly, the expression of NOX2 in myocardial tissue was significantly increased in KO mice following Ang II treatment, with p47phox following a similar, although non-significant trend (Figure 3-6). This could suggest a significant contribution of NOX2 from other cell types, for example infiltrating leukocytes. The expression of NOX4, the other major cardiac isoform, was not investigated, but was believed to be unchanged owing to data from previous studies, discussed further in chapter 7.2. In support of this, expression of p22phox, required for NOX4 activity, was similar in flox and fibroblast NOX2 KO mice (Figure 3-6C).

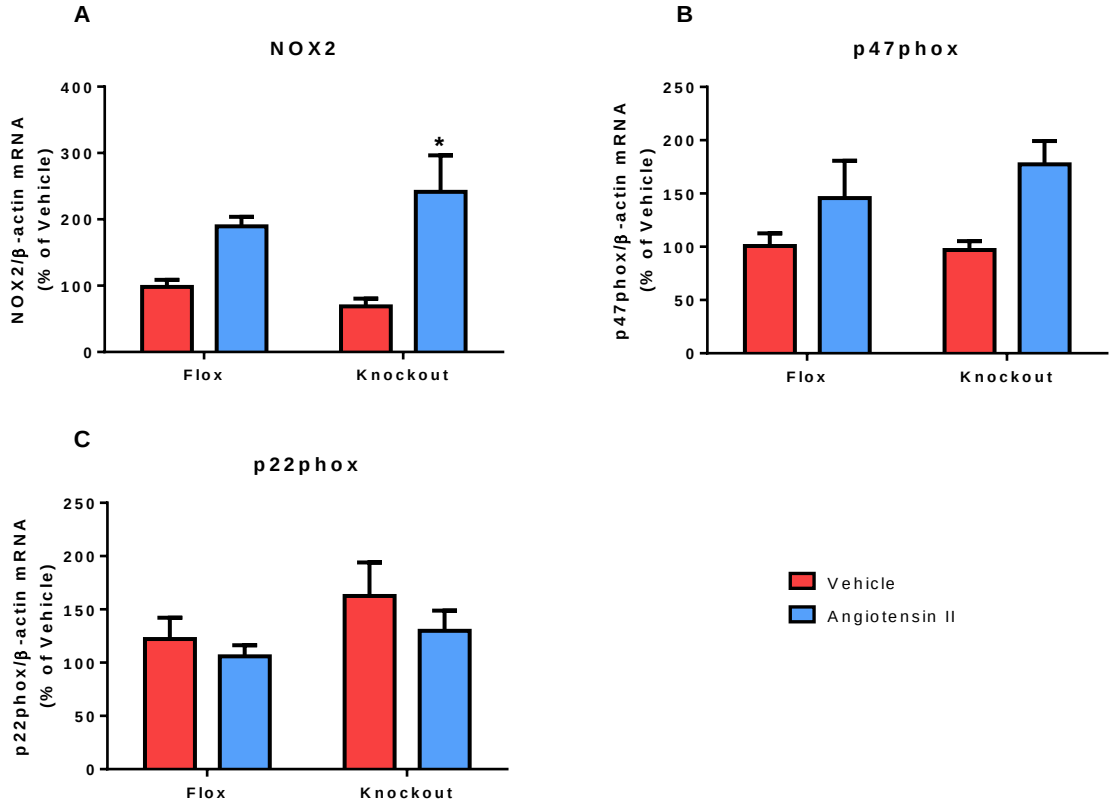

Figure 3-6: Angiotensin II-induced changes in NOX2 and p47phox gene expression. **A:** NOX2, **B:** p47phox and **C:** p22phox gene expression in hearts following Ang II treatment. Each sample is normalised to its own β-actin mRNA control and then expressed as a percentage of vehicle controls. *n=5, 4, 4, 4 respectively for groups; *P<0.05; 2way ANOVA with Bonferroni's multiple comparison post-test*.

3.3.3 Cardiac Function

Echocardiography was used to determine the effects of Ang II on cardiac function. The left ventricular ejection fraction and fractional shortening did not significantly differ after treatment with Ang II for 14 days or between genotypes (Figure 3-7). This is somewhat unexpected, since the majority of reports suggest a reduction in cardiac function following chronic Ang II. This is discussed further in chapter 3.5.1.

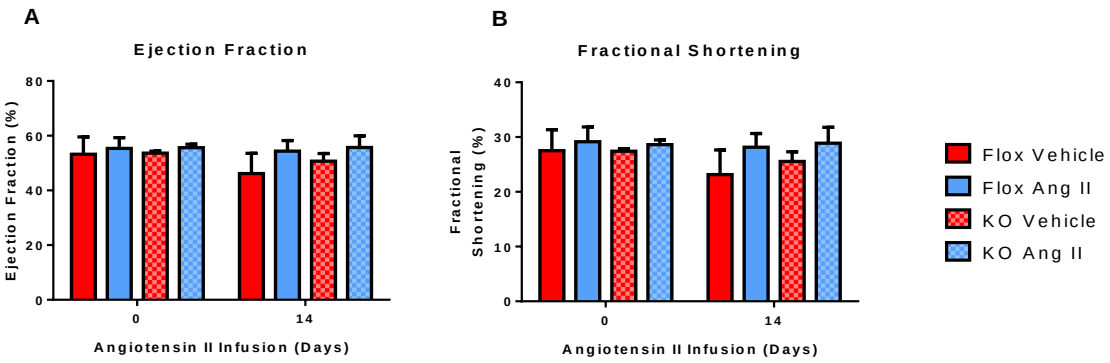

Figure 3-7: Systolic cardiac function determined by echocardiography. A: Left ventricular ejection fraction and **B:** Left ventricular fractional shortening were calculated over at least 3 cardiac cycles. *n=3, 6, 4, 5, respectively; P>0.05; 2way ANOVA with repeated measures*.

3.3.4 Cardiac Hypertrophy and Remodelling

Morphological analysis of the left ventricle by echocardiography showed that septal and posterior wall thicknesses did not increase in Ang II treated hearts, and there was no significant difference between genotypes (Figure 3-8A-B). In addition, left ventricular end systolic and diastolic volumes did not change in either genotype following Ang II treatment (Figure 3-8C-D).

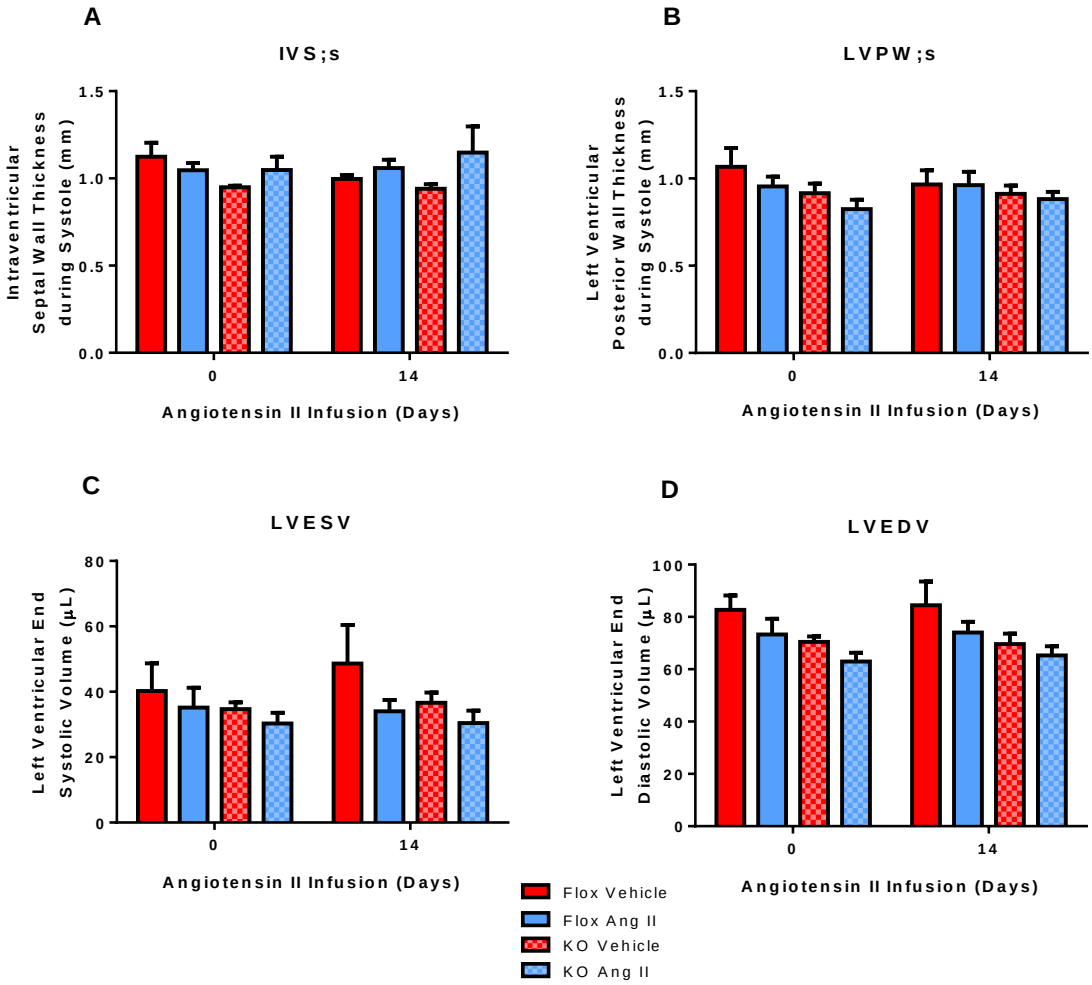

Figure 3-8: Left ventricular wall thicknesses and chamber volumes determined by echocardiography. **A:** Intraventricular septal wall thickness during systole (IVS;s), **B:** Left Posterior wall thickness during systole (LVPWT), **C:** end systolic volume (LVESV) and **D:** end diastolic volume (LVEDV). *n=3, 6, 4, 5 respectively; P>0.05; 2way ANOVA with repeated measures*.

These data suggest that there is no evidence of systolic dysfunction in flox or fibroblast NOX2 KO mice after receiving Ang II for 14 days. Wall thicknesses were also similar amongst all groups, suggesting an absence of significant cardiac hypertrophy. This was confirmed by assessing heart weight and with histological analysis of cardiomyocyte cross sectional area (Figure 3-9).

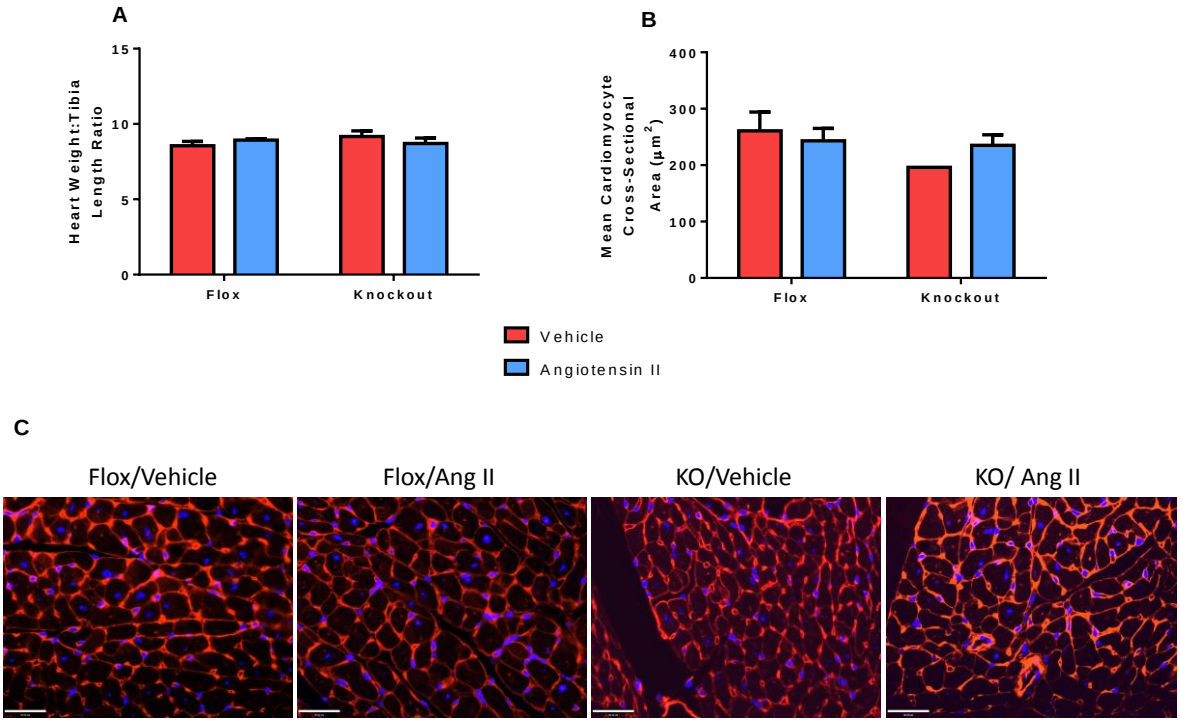

Figure 3-9: Assessment of cardiac hypertrophy following Angiotensin II treatment. **A:** Total heart weight normalised to body weight, **B:** Mean cardiomyocyte cross sectional area in WGA-stained heart sections and **C:** Representative WGA-stained heart sections; scale 30μm. *n=3, 4, 2, 5, respectively*.

3.3.5 Blood Pressure

Ang II (1.1mg/kg/day) caused a significant increase in systolic, diastolic and mean blood pressures in both flox and fibroblast NOX2 KO mice after 14 days (Figure 3-10A-C). This increase however, was significantly blunted in fibroblast NOX2 KO mice, occurring only on day 14, compared to as early as day 2 as seen in flox controls. The mean increase in systolic blood pressure in Ang II treated flox controls was from 108.7 ± 0.5mmHg to 163.8 ± 2.1mmHg, compared to 108.2 ± 1.8mmHg up to only 140.7 ± 11.6mmHg in fibroblast NOX2 KO mice (*P<0.05*). Differences in blood pressure were not accounted for by compensatory heart rate changes (Figure 3-10D).

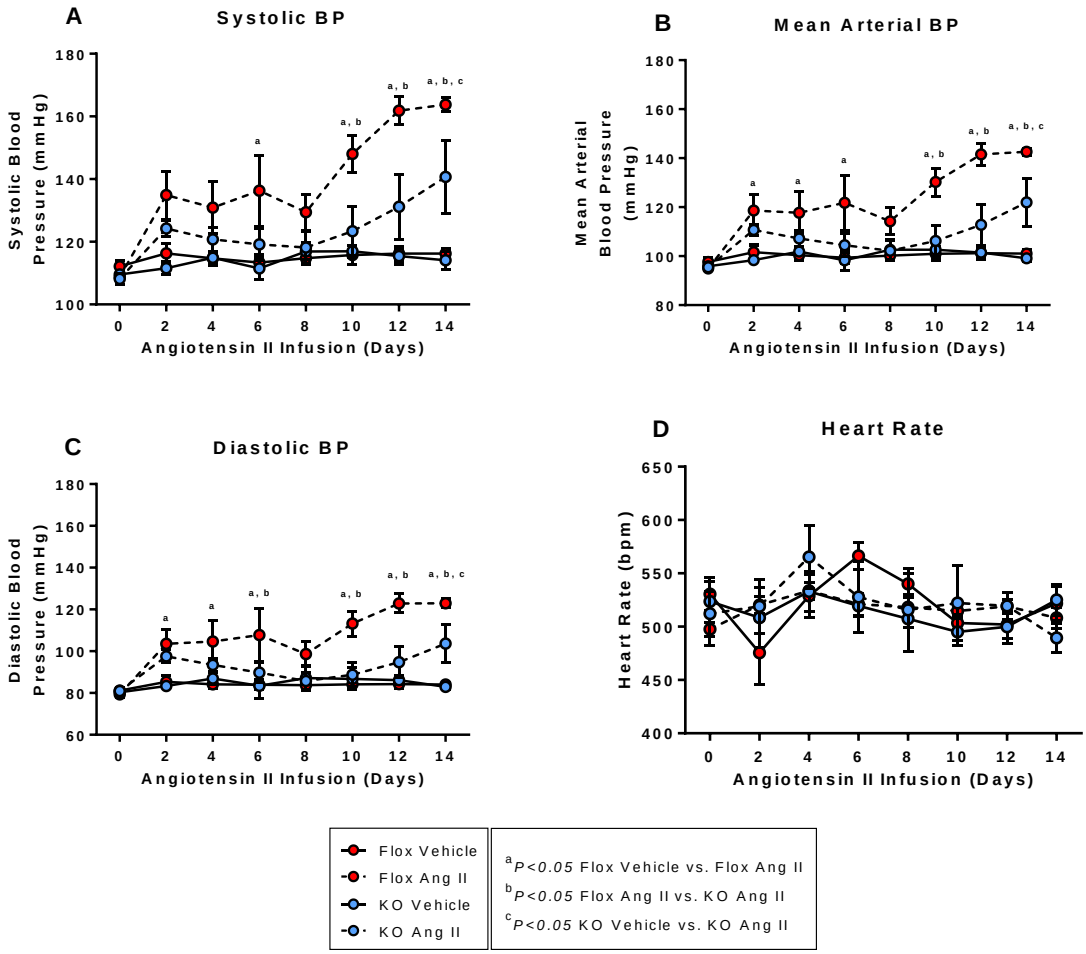

Figure 3-10: Angiotensin II-induced changes in blood pressure. **A:** Daytime ambulatory systolic **B:** diastolic and **C:** mean arterial blood pressures and **D:** heart rate in mice fitted with telemeters during treatment with 1.1mg/kg/day Ang II. Telemetry devices were fitted one week prior to mini-osmotic pump implantation. Data was acquired from each mouse every 5 minutes during each 24 hour sample period, with the group average being used for each data point. Mice were not restrained or disturbed during the acquisition of data. *n=7, 4, 3, 6, respectively;* $^{a, b, c}$ *P<0.05 as indicated; 2way ANOVA with repeated measures with Tukey's multiple comparison test.*

The data presented in part 1 indicate an important role for fibroblast NOX2 in the development of cardiac fibrosis. Differences in flox and KO blood pressure responses to Ang II may in part be an important contributor and suggest a possible indirect, pressor-dependent effect. This is discussed further in chapters 3.5.1, 4 and 7.

3.4 Results – Subpressor Angiotensin II (0.3mg/kg/day)

To assess the blood pressure-independent effects of Ang II, experiments were performed using a chronic *subpressor* dose of Ang II for 28 days.[62] Here, wildtype mice (C57/BL6) were used to verify the model.

3.4.1 Blood Pressure

To verify the model of subpressor Ang II, it was essential to ensure an absence of blood pressure effects during treatment. Serial tail cuff plethysmography revealed that 0.3mg/kg/day Ang II did not alter systolic, diastolic or mean blood pressures in mice compared to vehicle treated control mice over 28 days (Figure 3-11).

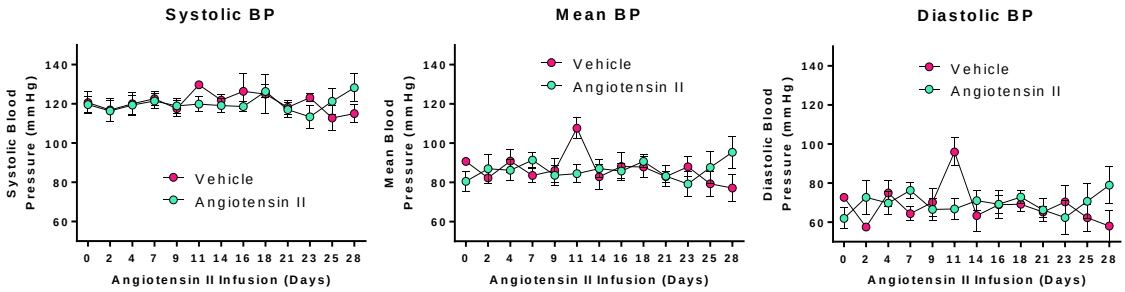

Figure 3-11: Subpressor angiotensin II-induced changes in blood pressure. Systolic, mean and diastolic blood pressures in mice treated with subpressor Ang II. Blood pressure (BP) was measured by tail cuff plethysmography in trained mice before and during subpressor Ang II treatment via implanted mini-osmotic pump. *n=4 and 9, respectively; P>0.05*; 2way ANOVA.

In addition, heart rate, also measured by tail cuff plethysmography, and body weights did not differ between vehicle and Ang II-treated mice at any time point (Figure 3-12).

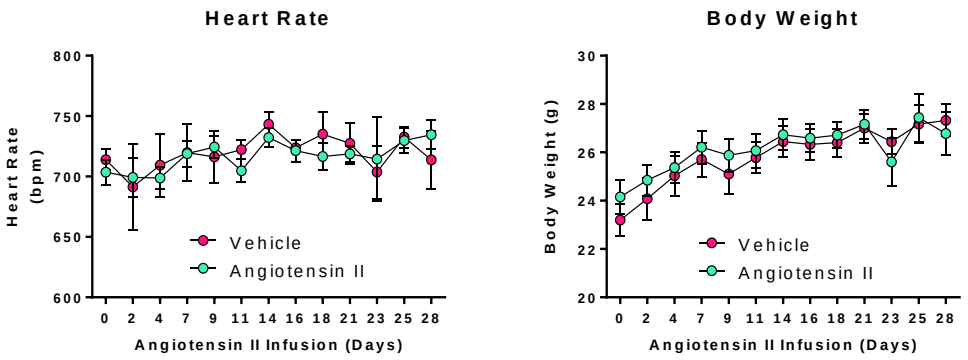

Figure 3-12: Subpressor angiotensin II had no effect on heart rate or body weight. Heart rate (left) and body weight (right) in mice treated with subpressor Ang II. Heart rate was measured by tail cuff plethysmography in trained mice before and during Ang II treatment via implanted mini-osmotic pump. *n=4 and 9, respectively; P>0.05*; 2way ANOVA.

3.4.2 Cardiac Fibrosis

The level of interstitial cardiac fibrosis was determined by staining with Picrosirius red, with analysis of both bright field and circularly polarized light images. Unexpectedly, subpressor Ang II did not lead to a significant increase in cardiac fibrosis after 28 days (Figure 3-13). Mean collagen content was 1.02 ± 0.06% and 0.98 ± 0.09% for vehicle and subpressor Ang II treated hearts respectively (*P>0.05*).

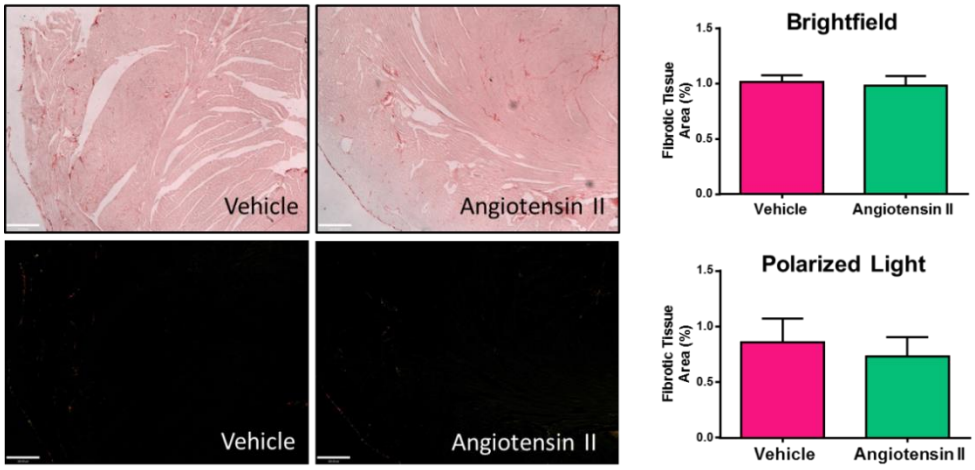

Figure 3-13: Subpressor angiotensin II did not induce cardiac fibrosis. Interstitial cardiac fibrosis visualised with Picrosirius red staining under bright field (upper panel) and circularly polarised light (lower panel). Scale 200µm; *n=4 and 5, respectively; P>0.05; Student's t-test*.

Masson's trichrome staining was also used qualitatively, confirming these findings, using a sample from a 14-day chronic pressure overloaded heart by transverse aortic constriction (Figure 3-14).

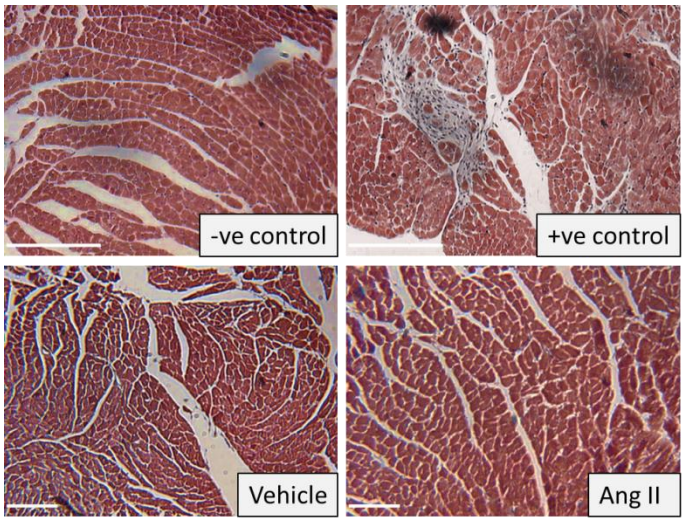

Figure 3-14: Representative images of Masson's Trichrome-stained left ventricle sections. Upper tiles: Negative (-ve) sham-operated and positive (+ve) transverse aortic constriction control images. **Lower tiles:** Vehicle and Ang II treated heart sections. Scale bar 200µm.

3.4.3 Gene Expression

The expression of fibrotic gene markers was determined by qPCR, showing that there was no significant induction of collagen 1α1, collagen 3α1, CTGF or fibronectin following treatment with subpressor Ang II for 28 days (Figure 3-15). This is in stark contrast to gene expression following pressor Ang II.

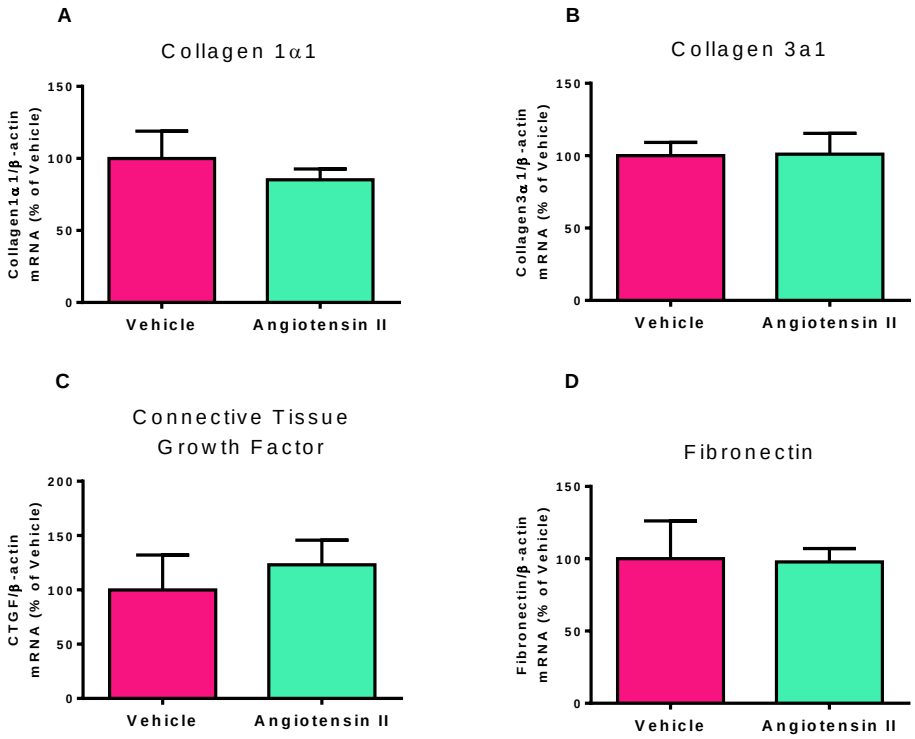

Figure 3-15: Subpressor angiotensin II did not induce the expression of fibrotic gene markers. A: Collagen 1α1, **B:** collagen 3α1, **C:** CTGF and **D:** fibronectin. *n=4 and 5, respectively; P>0.05; Student's t-test*.

3.4.4 Cardiac Function

Cardiac fibrosis can lead to deleterious effects on cardiac function over time, notably diastolic and eventually systolic dysfunction before progressing to heart failure,[28] therefore serial echocardiography was used to assess *in vivo* cardiac function in mice.

Subpressor Ang II did not lead to a reduction in left ventricular ejection fraction or fractional shortening compared to vehicle treated mice, suggesting an absence of systolic dysfunction (Figure 3-16).

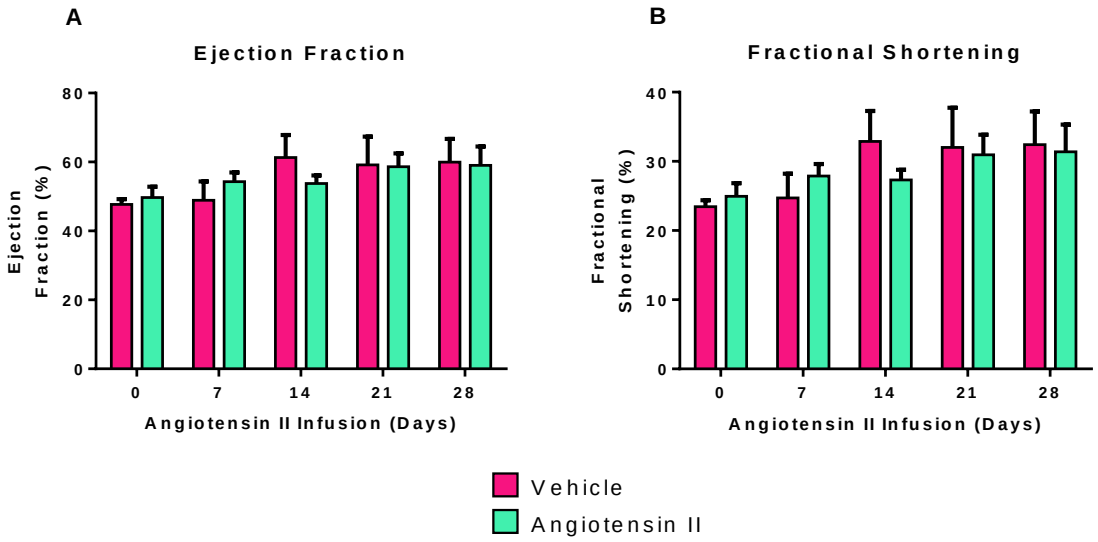

Figure 3-16: Subpressor angiotensin II did not cause systolic dysfunction. **A:** Left ventricular ejection fraction and **B:** fractional shortening following subpressor Ang II infusion. Subpressor Ang II did not lead to a significant difference between groups over the 28 day period. *n=4 and 5, respectively; P>0.05; 2way* ANOVA.

Left ventricular filling indices such as mitral A wave velocity, E/A ratio and mitral valve E', A' and E/E' ratio were not significantly different between treatment groups (Figure 3-17A-E). These indices are reported to correlate with ventricular filling pressures, with an increase indicating potential myocardial stiffening due to fibrosis and diastolic dysfunction.[153] Since increased left ventricular filling pressures often feeds back to the left atrium, leading to atrial enlargement, left atrial area was also measured by echocardiography, however no evidence of left atrial enlargement was found (Figure 3-17F).

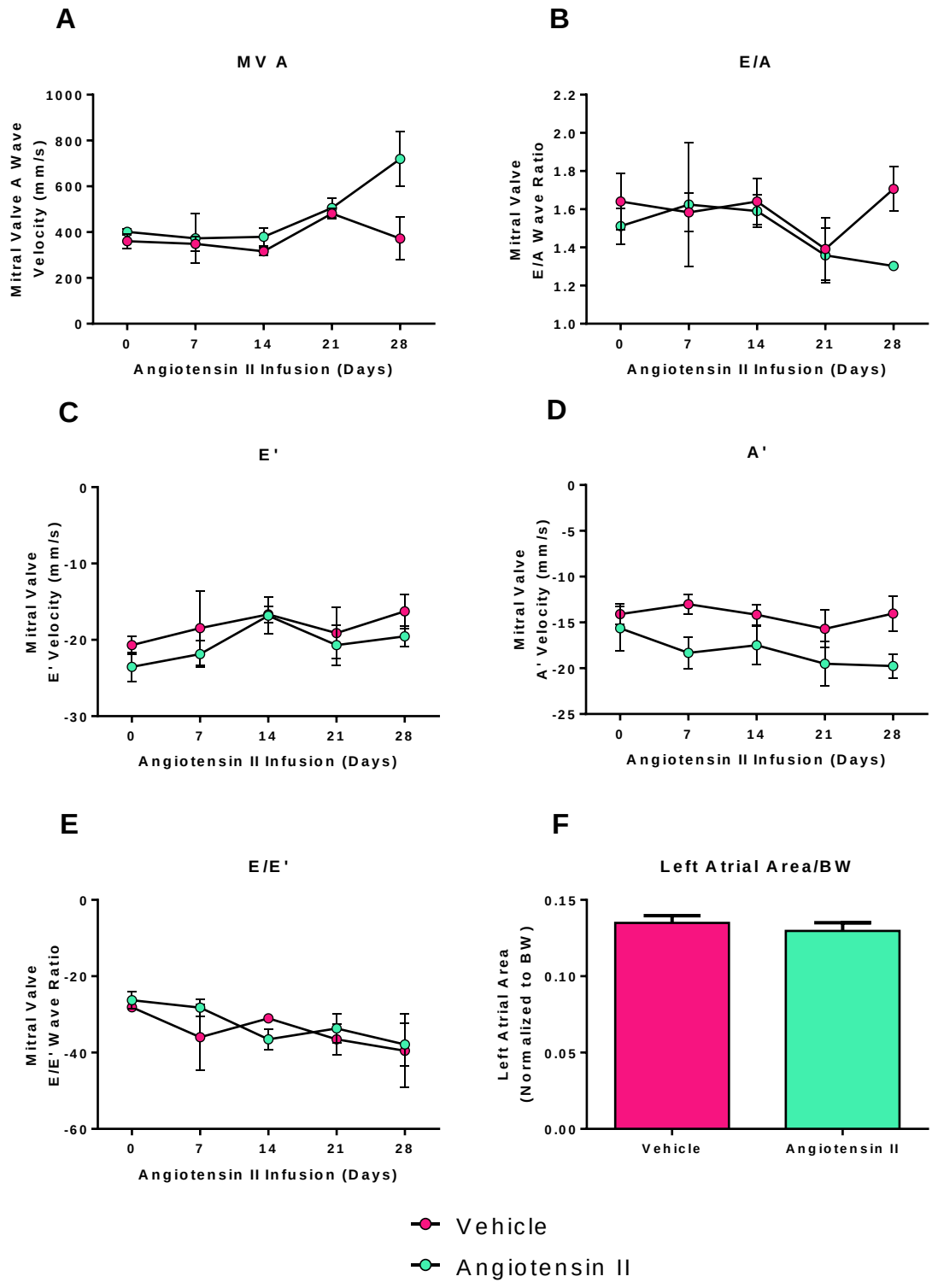

Figure 3-17: Subpressor angiotensin II did not alter left ventricular filling indices or left atrial area. Indices measured by echocardiography following Ang II treatment. *n=4 and 5, respectively*; P>0.05; 2way ANOVA.

Furthermore, other mitral Doppler indices including mitral valve E wave deceleration time, IVCT, IVRT and overall ejection time were similar between Ang II and vehicle treated mice at each time point, indicating an absence of diastolic dysfunction (Figure 3-18A-D).

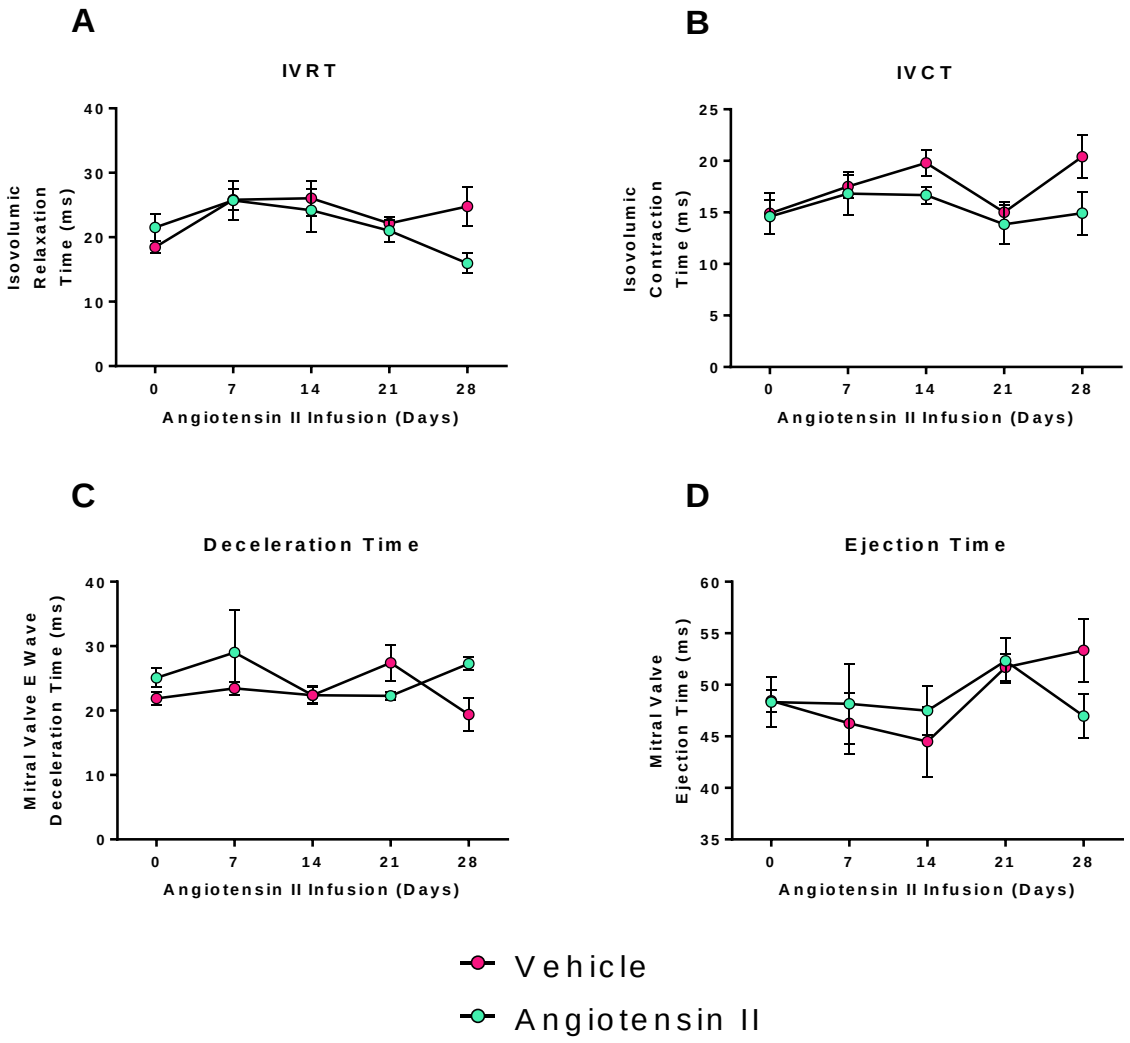

Figure 3-18: Subpressor angiotensin II did not alter cardiac mitral valve Doppler indices. Indices measured by echocardiography following Ang II treatment. *n=4 and 5, respectively; P>0.05; 2way* ANOVA.

Subpressor doses of Ang II have previously been reported to cause cardiac hypertrophy in mice. In the current experiments, however, subpressor Ang II treated mice did not show any increase in echo-derived left ventricular posterior wall or septal wall thickness compared to vehicle controls, during systole or diastole (Figure

3-19A-B). There was also an absence of cardiac remodelling in Ang II-treated mice, shown by end systolic and diastolic left ventricular chamber volumes (Figure 3-19C-D).

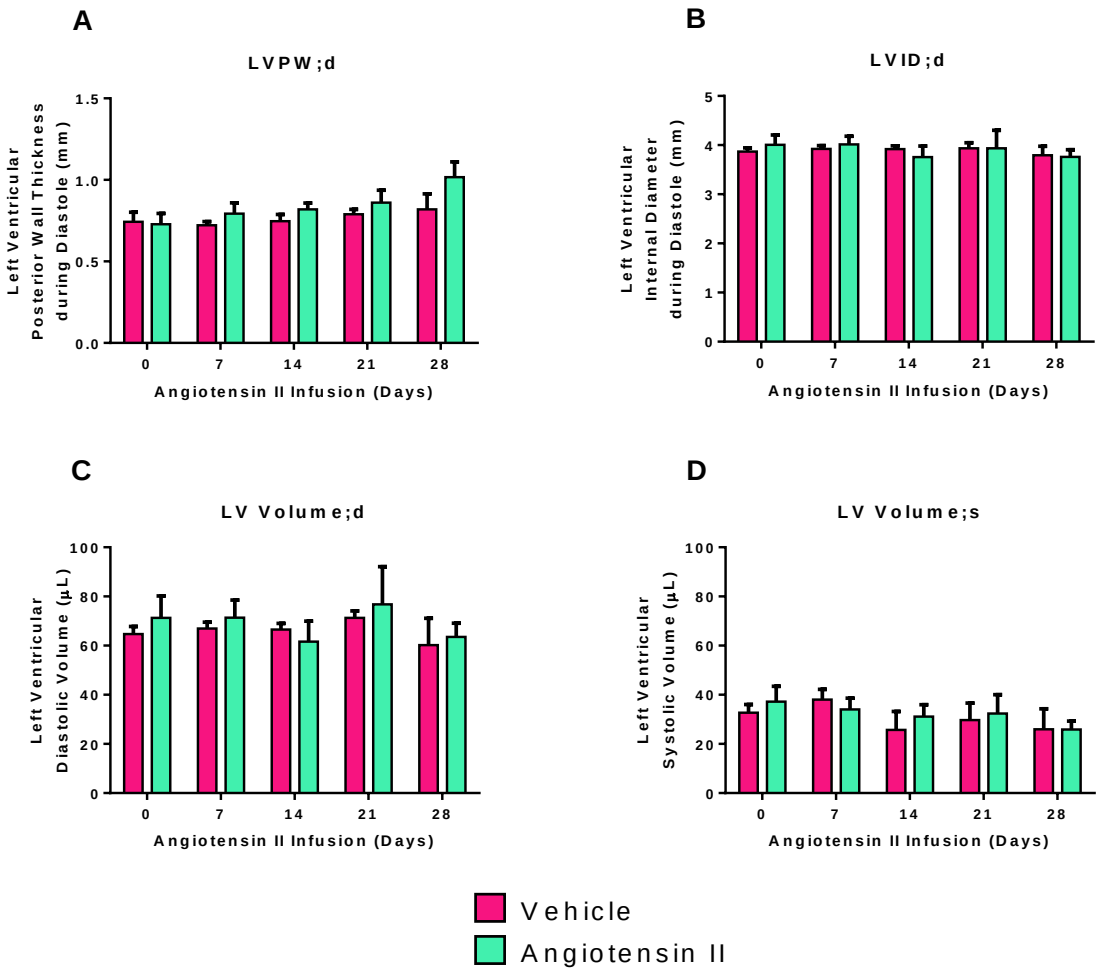

Figure 3-19: Subpressor angiotensin II did not alter left ventricular wall thickness and chamber volumes. Indices measured by echocardiography. **A:** Posterior wall thickness, **B:** internal diameter, **C:** end diastolic volume and **D:** end systolic volume. *n=4 and 5, respectively; P>0.05; 2way ANOVA with repeated measures*.

Strain and strain rate analyses take into account regional stresses experienced by the ventricular wall (wall motion/displacement) during systole and diastole.[142] Both radial and longitudinal peak % and time to peak strain were comparable between vehicle and Ang II treated mice (Figure 3-20A-D). In addition, radial and longitudinal strain rate indices did not significantly differ between treatment groups (Figure 3-20E-H).

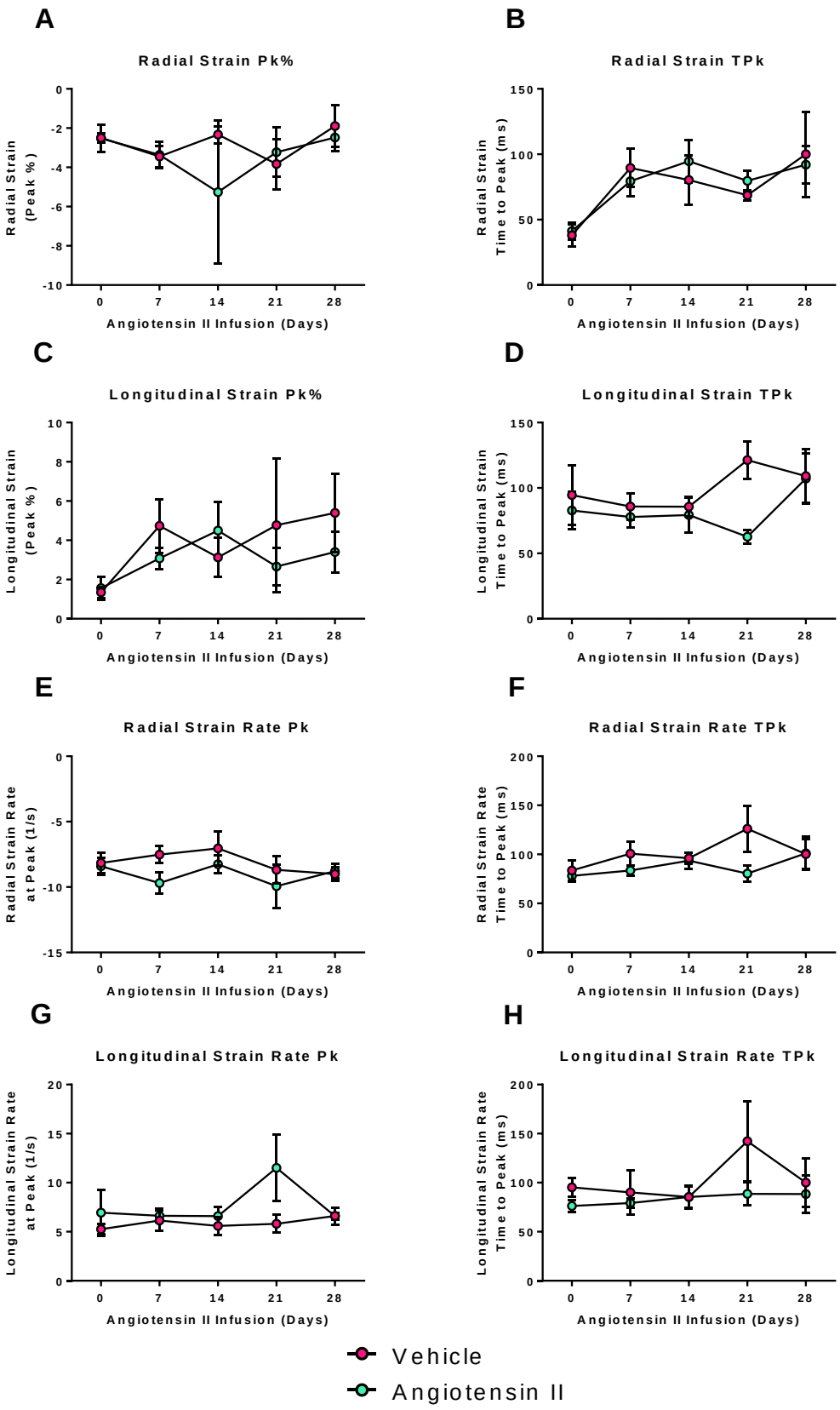

Figure 3-20: Subpressor angiotensin II did not alter left ventricular strain and strain rate indices. Analysis of B-Mode, parasternal long axis images by echocardiography. *n=4 and 5, respectively; P>0.05; 2way ANOVA with repeated measures*.

Taken together, these results indicate that 0.3mg/kg/day Ang II for 28 days did not have any deleterious effects on systolic or diastolic cardiac function in these mice, with no evidence for adverse cardiac remodelling.

3.4.5 Cardiac Hypertrophy

In support of the echocardiographic data, subpressor Ang II did not lead to cardiac hypertrophy vs. vehicle control (*P=0.177*) as determined by normalized heart weight (Figure 3-21A). This was further supported by histological analysis of cardiomyocyte cross-sectional area, revealing similar mean cross-sectional areas of 334.2 ± 37.45µm^2 and 342.0 ± 41.71µm^2 for vehicle and Ang II treated hearts respectively (Figure 3-21B-C). Suitable cross-sections were defined as having a near circular profile, with nuclear staining (blue, DAPI).[154]

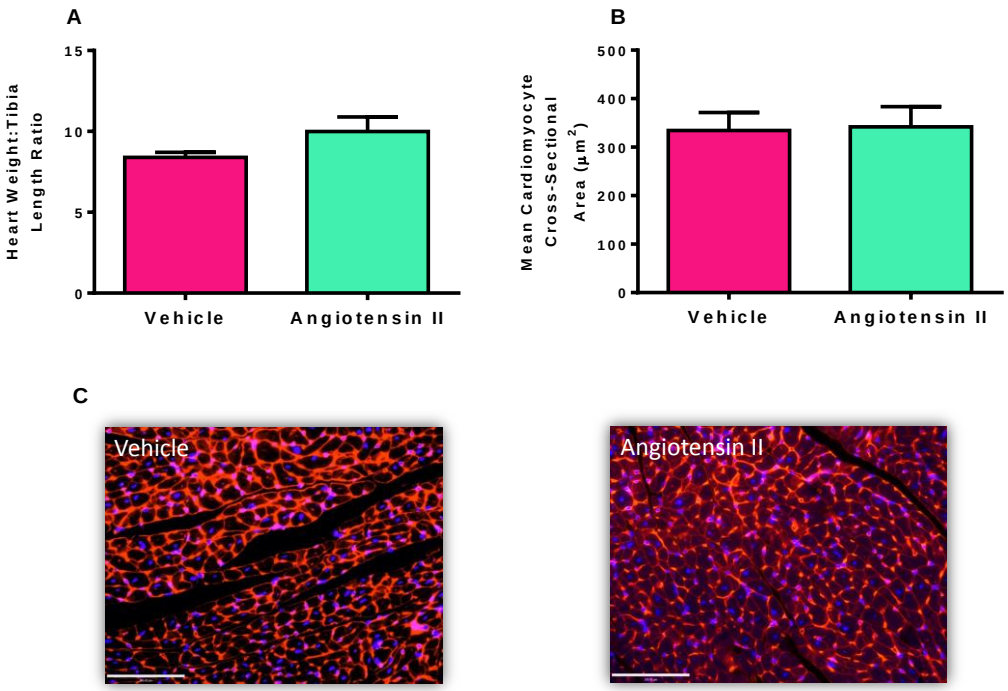

Figure 3-21: Subpressor angiotensin II did not induce cardiac hypertrophy. A: Total heart weight normalised to tibia length, **B:** mean cardiomyocyte cross-sectional area in WGA-stained heart sections and **C:** representative WGA-stained heart sections; scale 30µm. *n=4 and 5, respectively; P>0.05; Student's t-test*.

Taken together, subpressor Ang II treatment in the current study did not cause any functional, morphological or histological changes in wildtype mice.

3.5 Discussion

Chronic administration of Ang II is a well-established model for the induction of cardiac fibrosis in mice.[35, 43, 53, 62] Ang II (1.1mg/kg/day) induces significant hypertension and in the current study we were able to show consistent hypertension in floxed mice from 10 days onwards. In agreement with published reports, we were also able to show significant interstitial cardiac fibrosis and an elevation in supporting gene expression markers, including collagen 1α1,[53] collagen 3α1 and fibronectin after 14 days of chronic Ang II at 1.1mg/kg/day.[35]

This study aimed to build on the landmark study by Bendall et al,[62] by deleting NOX2 in a cell specific manner, namely fibroblasts. It was hypothesised that NOX2 deletion in fibroblasts would mitigate the generation of cardiac fibrosis. By taking advantage of a collagen 1α2-promoted CreER system, the current study has shown successful NOX2 recombination in hearts of 10-day tamoxifen-treated mice, as well as a 50-60% reduction in whole heart NOX2 protein levels. Importantly, we observed that fibroblast NOX2 KO mice were protected from a significant increase in interstitial cardiac fibrosis following chronic pressor Ang II, as determined by Picrosirius red histological analysis. This result was strengthened by fibrotic gene expression analysis, in particular fibronectin and collagen 3α1.

Whilst this result supports the original hypothesis, mice in the KO group did not become hypertensive until approximately day 14 of Ang II, the final day of the study. Since Ang II-induced cardiac fibrosis is reported to be largely dependent on hypertension,[155] it is possible that the reduced tendency towards cardiac fibrosis in KO mice is explained, at least in part, by the delayed development of hypertension. This concept is supported by studies showing a reduction in cardiac fibrosis after treatment to reduce angiotensin II-induced hypertension in mice, for example using resveratrol.[156]

Owing to the observed blood pressure phenotype, it is therefore difficult to definitively determine the role of fibroblast NOX2 deletion in isolation on the development of cardiac fibrosis using the chronic pressor angiotensin II model. It is for this reason that we sought to use a blood pressure-independent model of cardiac fibrosis.

3.5.1 Angiotensin II-based mouse models

In addition to its well-known effects on blood pressure, Ang II has been reported to induce cardiac fibrosis and hypertrophy, independent of hypertension, when used at a lower dose.[62] A subpressor dose of Ang II (0.3mg/kg/day) has previously been shown not to alter blood pressure in WT mice up to 14 days.[62, 124] We opted to use this dose for 14 and 28 days in WT mice to first determine the maximum achievable level of cardiac fibrosis. The results of the current study however, showed that this subpressor dose of Ang II did not cause significant interstitial cardiac fibrosis after 14 (data not shown) or 28 days of chronic treatment.

Cardiac hypertrophy (both increased heart: body weight (HW: BW) ratio and increased cardiomyocyte cross-sectional area) and cardiac fibrosis has been previously reported following 0.3mg/kg/day Ang II for 14 days, independent of blood pressure.[62] A thorough search of the literature reveals conflicting data regarding the effects of low dose Ang II in mice. In another study using a similar dose (0.28mg/kg/day for 28 days), the authors reported an absence of hypertrophy in terms of both HW: BW ratio and cardiomyocyte cross-sectional area.[144] They went on to use echocardiography, showing normal systolic function and no increases in left ventricular wall thicknesses.[144] Another group reported 0.28mg/kg/day to in fact be a pressor dose of Ang II, showing a 14% increase in systolic blood pressure after 13 days chronic treatment.[157] Interestingly, a lower dose of subpressor Ang II (0.144mg/kg/day) was shown to cause cardiac hypertrophy without detectable fibrosis[158] and an even lower dose (0.006mg/kg/day for 3 weeks) reported increases in systolic blood pressure, left ventricular wall thicknesses, cardiac hypertrophy and interstitial and perivascular fibrosis, with complementary gene expression data showing elevated collagen 1, collagen 3 and fibronectin expression.[145] The reasons for these differences are difficult to be certain about, but may reflect mouse diet and housing, gender[159] and possibly age and starting weight differences,[145] as well as method of drug administration e.g. impregnated pellet vs. mini-osmotic pump. Indeed, the study by Bendall and colleagues[62] from our lab was performed many years ago, since which mouse diet formula and housing conditions have changed. These variables offer some explanation. Regardless, based on the current methods

and results, the subpressor Ang II infusion model would not be very useful to investigate our hypothesis.

A reduction in cardiac function following chronic pressor Ang II in mice is a commonly held view. Whilst the variables listed above may also explain the absence of cardiac dysfunction, it has been suggested that in the absence of another stimulus, such as simultaneous aldosterone infusion or prolonged hypertension, Ang II may be incapable of causing morphological or functional changes.[160, 161]

3.5.2 Collagen1α2 Cre and Fibroblasts

Here, we describe a novel mouse model of NOX2 deletion specifically in fibroblasts, allowing insights into the cell-specific role of NOX2 *in vivo* for the first time.

The *Col1α2*-promoted Cre-recombinase transgenic mouse has been extensively characterised in a few studies. Inducible control with tamoxifen has been previously described by Zheng and colleagues, showing β-galactosidase (LacZ) reporter expression in tamoxifen-treated, but not oil/vehicle-treated or wildtype mouse embryos.[132] The authors went on to show that postnatal administration of tamoxifen produced LacZ expression in skin, lung and pericardial tissue, as expected, as well as sustained expression in older mice.[132] Similar results were obtained from Florin and colleagues.[162]

This *Col1α2* Cre mouse was used to identify fibroblasts following cardiac injury using a LacZ reporter cross and a discoidin domain receptor 2 (DDR2) antibody.[136] In addition it has been used to show accelerated wound healing and skin fibrosis in a dermal injury model when a protein, glycogen synthase kinase 3 beta, was deleted specifically in fibroblasts.[138] Importantly, the authors first characterized the extent of knockout, showing an approximate 90% reduction in isolated fibroblast protein levels following 10 days of tamoxifen treatment. Replicating such an experiment in fibroblast NOX2 KO mice proved difficult, since fibroblasts from KO mice did not adhere and grow well *in vitro* following isolation, however the studies discussed, in addition to our own characterization, provides confidence in the ability of *Col1α2*-promoted Cre-recombinase to delete NOX2 in fibroblasts.

3.5.3 Detection of Cardiac Fibrosis

Of the many methods available for the determination of fibrosis, histological analysis of tissue sections stained with Picrosirius red is one of the most simple, reliable and accurate techniques.[163] Picrosirius red is linear and a mix of Sirius red dye and picric acid. Collagen contains basic amino groups with which Sirius red sulphonic acid groups will react and align in a parallel orientation.[163] The result is a highly visible red stain (fibrosis), on a pale yellow non-fibrotic background. A great advantage of Picrosirius red is how it responds to circularly polarised light. The parallel arrangement of dye and collagen, combined with polarised light enhances the birefringency and emitted light intensity of collagen by about 700%, providing a highly collagen-specific stain.[163, 164] Picrosirius red-stained tissue sections viewed under polarised light range from green-yellow to orange-red, thought to correspond to collagen fibre thickness or collagen type, although these reports are disputed.[165, 166] This method also allows for the detection of very thin collagen fibres, missed with traditional bright-field analysis, due to the high contrast against the black background.[163, 164]

Other methods include Masson's Trichrome, an Aniline blue or light-green fibrosis stain on a red, non-fibrous background. This method gives high contrast (red vs. blue) and should in theory give very similar results to non-polarized analysis with Picrosirius red. Masson's Trichrome is however, based solely on acid-base interactions and therefore not exclusively selective for collagen, a problem Picrosirius red staining can overcome by polarization.[143]

Hydroxyproline is a modified amino acid, found largely in collagen, and can be used to give an estimation of total collagen content in tissues. The hydroxyproline assay can be performed using a kit, in which a reaction gives rise to a product quantifiable by calorimetry.[143] The hydroxyproline assay is commonly used, but tissue must be homogenised, removing information on tissue distribution or maturity of collagen. In addition to kit costs, it also requires more expensive apparatus.

Antibody-based staining is also used, but is more costly, requires antibody titration and may have problems with tissue autofluorescence.[143]

Picrosirius red is therefore a sensitive, cheap, easy and reliable method, published to be able to pick up differences in a range of human and animal models.[32, 53, 163-166] We opted to use this method based on the relative ease, sensitivity and cost compared to other methods.

3.5.4 The use of Echocardiography - Diastolic function

Despite the failure of the subpressor Ang II model, this study provided an invaluable opportunity to explore the range of measurable indices by non-invasive echocardiography.[153] Current literature and in house preliminary studies show that subtle functional changes can be detected in more severe heart failure models, such as chronic pressor angiotensin II[31, 33] or chronic pressure overload.[167] In particular, a number of new and emerging techniques in mouse echocardiography are aimed towards assessing diastolic function (further discussed in chapter 4).

Trans-mitral Doppler flow can provide values for mitral valve E and A wave velocities, reflecting diastolic early filling driven by left ventricular suction and late filling driven by atrial contraction, respectively.[153] Impaired left ventricular relaxation is indicated by firstly a reduction in E wave magnitude, followed by an increased reliance on the atrial A wave component. As such, the E/A ratio decreases and indicates stiff or fibrotic cardiac tissue and overall diastolic dysfunction.[153]

Isovolumic relaxation time (IVRT) describes the interval between aortic valve closure and mitral valve opening, that is, the time between end systole and the start of left ventricular diastolic filling. A prolonged IVRT indicates impaired left ventricular isovolumic relaxation,[168] and this finding has also been described in mice following chronic pressor Ang II (2.8mg/kg/day), which showed a 62% prolongation.[33]

3.5.5 The use of Echocardiography - Systolic function

Ejection fraction and fractional shortening are commonly used global measures of myocardial performance. We also used speckle tracking based strain analysis, which may be more sensitive in detecting subtle differences,[142] especially in regional function, to determine if any differences existed following Ang II treatment. Speckle tracking echocardiography has recently been applied to mouse studies and is shown as an efficient, reproducible method for regional and global assessment of left

ventricular function and is also directly comparable to magnetic resonance imaging, regarded as the gold standard.[142] The current study was unable to detect differences in systolic strain or strain rate indices after treatment with subpressor Ang II, indicating a lack of even minor regional changes in systolic function in this model.

Despite a lack of cardiac dysfunction in the subpressor Ang II study, it is anticipated that these recent advances in systolic and especially diastolic echocardiography will provide sensitive endpoints for subsequent mouse models of cardiac fibrosis and aid us in relating findings to the clinical setting.

Taken together, the data in this chapter indicate a role for fibroblast NOX2 in the development of hypertension and interstitial cardiac fibrosis in response to chronic pressor doses of Ang II. The delayed onset of hypertension in fibroblast NOX2 KO mice could in part account for the reduction in fibrosis, requiring the use of a blood pressure-independent model of cardiac fibrosis. The chronic subpressor Ang II model was unable to show the development of cardiac fibrosis in wildtype mice, therefore other mouse models of cardiac fibrosis are required.

CHAPTER 4: Contribution of Fibroblast NOX2 to Pressure Overload Remodelling induced by Transverse Aortic Constriction.

4.1 Introduction

4.1.1 Models of Pressure Overload

The aortic constriction model consists of a permanent ligature placed on the aorta either prior to the brachiocephalic branch (ascending aortic constriction – AAC),[169] or between the brachiocephalic and left common carotid branches of the aortic arch (transverse aortic constriction – TAC; Figure 4-1), leading to chronic pressure overload, cardiac hypertrophy, remodelling and fibrosis.[170] It is a crude model of aortic stenosis, where the chronic elevation of cardiac afterload causes mechanically-induced stress.[141, 171] An increase in cardiac fibroblast cell numbers has been reported,[172] followed by severe cardiac fibrosis in as little as 1-week post-TAC, in addition to systolic and diastolic cardiac dysfunction.[29, 31, 34, 170, 172]

Alternatively, the abdominal aortic banding/constriction (AAB) model places a permanent ligature on the abdominal aorta, often at the level of the suprarenal artery.[152, 173] AAB is technically easier to perform and generally has a lower mortality rate, possible owing to avoidance of thoracic microsurgery. RAAS activation is apparent in pressure overload models, since RAAS inhibitors reduce the deleterious effects, such as the ACE inhibitor captopril.[167] This is more pronounced in AAB, since constriction at the level of the suprarenal artery also creates a degree of renal ischaemia, an additional stimulus for renin release and full RAAS activation involving Ang II and an elevation in blood pressure.[173]

Regardless of the model used, an important consideration in terms of pathological severity and speed of onset is the tightness of the ligature, often reported in reference to a needle gauge.

4.1.2 NOX2 Activation after Pressure Overload

Similar to chronic Ang II, pressure overload has been shown to induce the activation of NOX2 in cardiac tissue.[118] Importantly, global NOX2 KO mice were shown to be protected from developing cardiac fibrosis using the AAB[31, 152] and TAC[118] models, indicating that this would be a suitable alternate model with which to address the hypothesis.

Grieve and colleagues showed profound systolic dysfunction in WT AAB mice by echocardiography, which was absent in global NOX2 KO AAB mice.[31] Additionally, left ventricular pressure-volume analysis was used to show similar results for diastolic dysfunction.[31] These differences in function (between WT and global NOX2 KO AAB mice) potentially provide a window through which to determine the functional role of fibroblast NOX2 specifically.[118]

Recent work by Parajuli in 2014 showed an upregulation of NOX2 and oxidative stress in left ventricular tissue from failing human hearts, alongside evidence of adverse cardiac remodelling such as cardiac fibrosis and cardiomyocyte hypertrophy.[118] These findings were recapitulated in TAC mice and, in agreement with Grieve and colleagues, global NOX2 KO mice were protected from adverse cardiac dysfunction and remodelling.[118] Interestingly however, the majority of studies using global NOX2 KO mice suggest that NOX2 is dispensable in the development of pressure overload-induced cardiac hypertrophy.[31, 152, 174]

Taken together, NOX2 is important for the development of cardiac fibrosis in both TAC and AAB pressure overload models, in addition to the Ang II models discussed in chapter 3. This suggested that a pressure overload model would be suitable for the investigation of cardiac fibrosis development in fibroblast NOX2 KO mice.

4.1.3 Aims

NOX2 activation in fibroblasts plays a significant role in Ang II-induced hypertension and is indicated to have a role in the development of Ang II-induced cardiac fibrosis. It is, however, difficult to separate these two roles using a pressor Ang II model. We therefore aimed to clarify the role of fibroblast NOX2 in the development of cardiac fibrosis by using an alternative model, namely TAC.

4.2 Methods

4.2.1 Generation of Experimental Mice

Male fibroblast NOX2 KO mice and their Cre-negative littermate controls were generated as described in chapter 3.

4.2.2 Transverse Aortic Constriction (TAC) Surgery

Minimally invasive TAC surgery without intubation was used to induce cardiac hypertrophy and fibrosis over 14 days, based on methods previously described (Figure 4-1).[140] Briefly, mice were anaesthetised with isoflurane and maintained via nosecone at 1.5% at 1.5L/min. A small suprasternal incision was made, through which the thymus was retracted and the strap muscles were bluntly dissected to expose the aortic arch. A small, hook-shaped needle was used to pass a 6-0 silk suture under the aorta between the brachiocephalic (right common carotid) and left common carotid arteries. The needle was then removed. An angled 27-gauge needle was placed alongside the aorta and the 6-0 silk suture tied snugly around the 27-gauge needle to constrict the aorta. The needle was then promptly removed and the incision closed by suturing. Sham operated mice underwent the same procedure without constriction.

4.2.3 Estimation of TAC Gradient by Forepaw Blood Pressure Assessment

Successful aortic constriction was confirmed immediately after TAC surgery by estimation of trans-TAC gradient using measured blood pressure differential by plethysmography. Essentially, TAC leads to an increase in right carotid artery blood pressure relative to the left carotid and this will be reflected in peripheral blood pressure (Figure 4-1). Assessing systolic blood pressure in right and left forepaws would therefore give an indication of TAC gradient and the level of TAC. The average systolic blood pressure was measured from both the right and left forepaws of anaesthetised mice maintained with 1.5% isoflurane (5 measurements per forepaw), before mice were placed in a heated recovery chamber. The difference between right and left forepaw systolic blood pressures was calculated, thereby estimating the trans-TAC gradient.

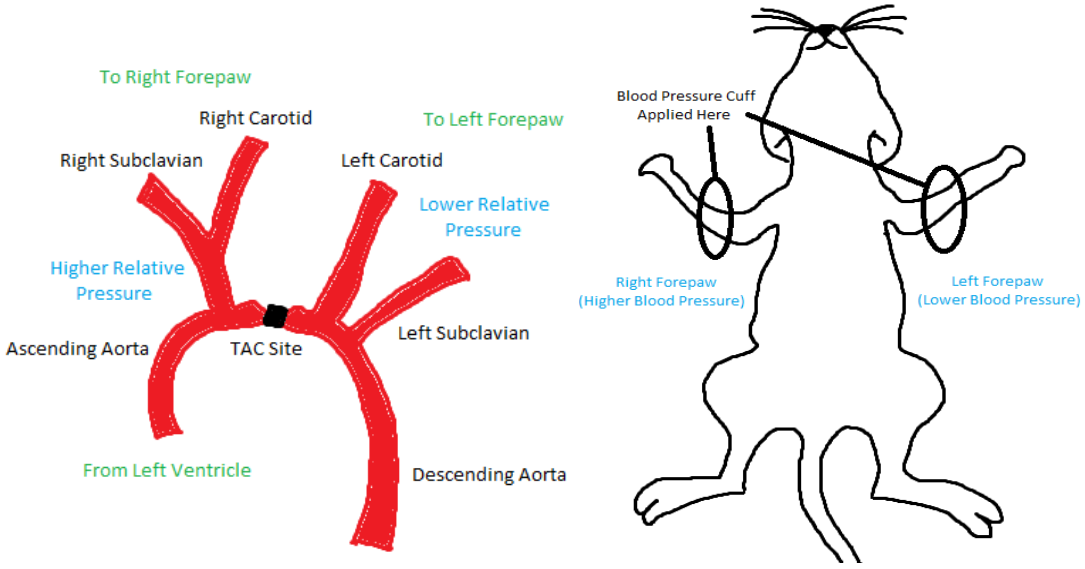

Figure 4-1: Transverse aortic constriction (TAC) model. Constriction of the aorta between the right and left carotid arteries causes an increase in right carotid and right peripheral blood pressure relative to left. The right and left forepaw blood pressure differential gives an estimate of TAC gradient.

4.2.4 Echocardiography

Full echocardiographic assessment was performed for mice before (baseline) and after (7 and 14 days) TAC surgery, as described in chapter 2, to include systolic, diastolic, morphological, strain and strain rate indices. The trans-TAC pressure gradient was also estimated 1 day after TAC surgery (as described in chapter 2) and at 7 and 14 days after.

4.2.5 Tissue Harvest and Processing

14 days following TAC surgery, mice were killed and organs harvested as described in chapter 2. Cardiac tissue was processed for histological and biochemical analysis as described.

4.3 Results

Successful TAC surgery was confirmed by assessment of TAC blood pressure gradients using an immediate, indirect measure (peripheral blood pressure plethysmography) and later the trans-TAC Doppler imaging (echocardiography) up to 24 hours after surgery.

The difference in right and left forepaw systolic blood pressure was significantly higher in mice receiving TAC compared to sham, with comparable values between flox and KO mice (Figure 4-2A). These data were supported by Doppler imaging echocardiography, showing significant TAC gradients of approximately 42-45mmHg for flox and KO TAC mice, respectively (Figure 4-2B) compared to sham. Taken together, data indicate that successful TAC was achieved and TAC surgery had comparable effects between genotypes.

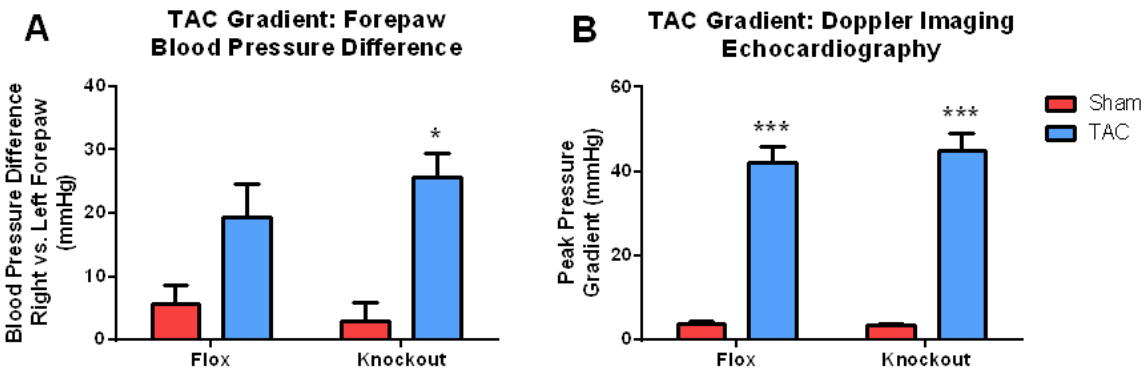

Figure 4-2: Assessment of TAC gradient by forepaw blood pressure plethysmography immediately after TAC surgery. A: Gradients are significantly increased after TAC surgery compared to sham for both groups. * indicates *P<0.05 with Bonferroni post-test*; n=4, 11, 4, 10, respectively; 2-way ANOVA with Tukey post-test. **B:** Central assessment of TAC gradient by Doppler echocardiography performed 24 hours after surgery. Gradients are significantly increased after TAC surgery compared to sham ****P<0.001*; n=8, 10, 8, 8, respectively; 2-way ANOVA with Tukey post-test.

4.3.1 Survival

Deletion of NOX2 in fibroblasts had no effect on survival following TAC surgery (Figure 4-3).

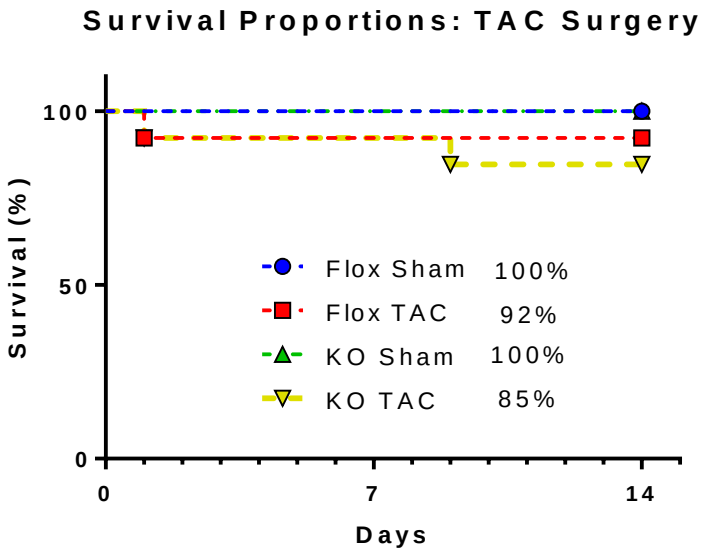

Figure 4-3: Kaplan Meier survival curves for mice from 24 hours after surgery. Survival proportions are listed within, with no significant differences between surgery and genotype groups; *P>0.05*; n=10, 13, 11, 13, respectively.

4.3.2 Cardiac Fibrosis and Hypertrophy

Cardiac sections stained with Picrosirius red revealed profound interstitial and perivascular fibrosis in mice after 2 weeks of TAC, as compared to sham (Figure 4-4). Bright field analysis of Picrosirius red showed a significant total collagen proportion of 5.57% and 5.52% for flox and KO TAC mice, respectively, representing a 360-440% increase vs. sham (Figure 4-4A). Circularly polarised light was also used as it is thought to be more specific for collagen, providing information about collagen fibre thickness, maturity and cross-linking and potentially capable of distinguishing types I and III.[163-165] Analysis indicated a more modest but nonetheless significant increase of 210-220% in collagen (Figure 4-4B). Similar results are observed for perivascular fibrosis analysis (Figure 4-4C and D). Importantly, there appears to be no difference in the extent of cardiac interstitial or perivascular fibrosis between flox and fibroblast NOX2 KO mice following 2 weeks of TAC.

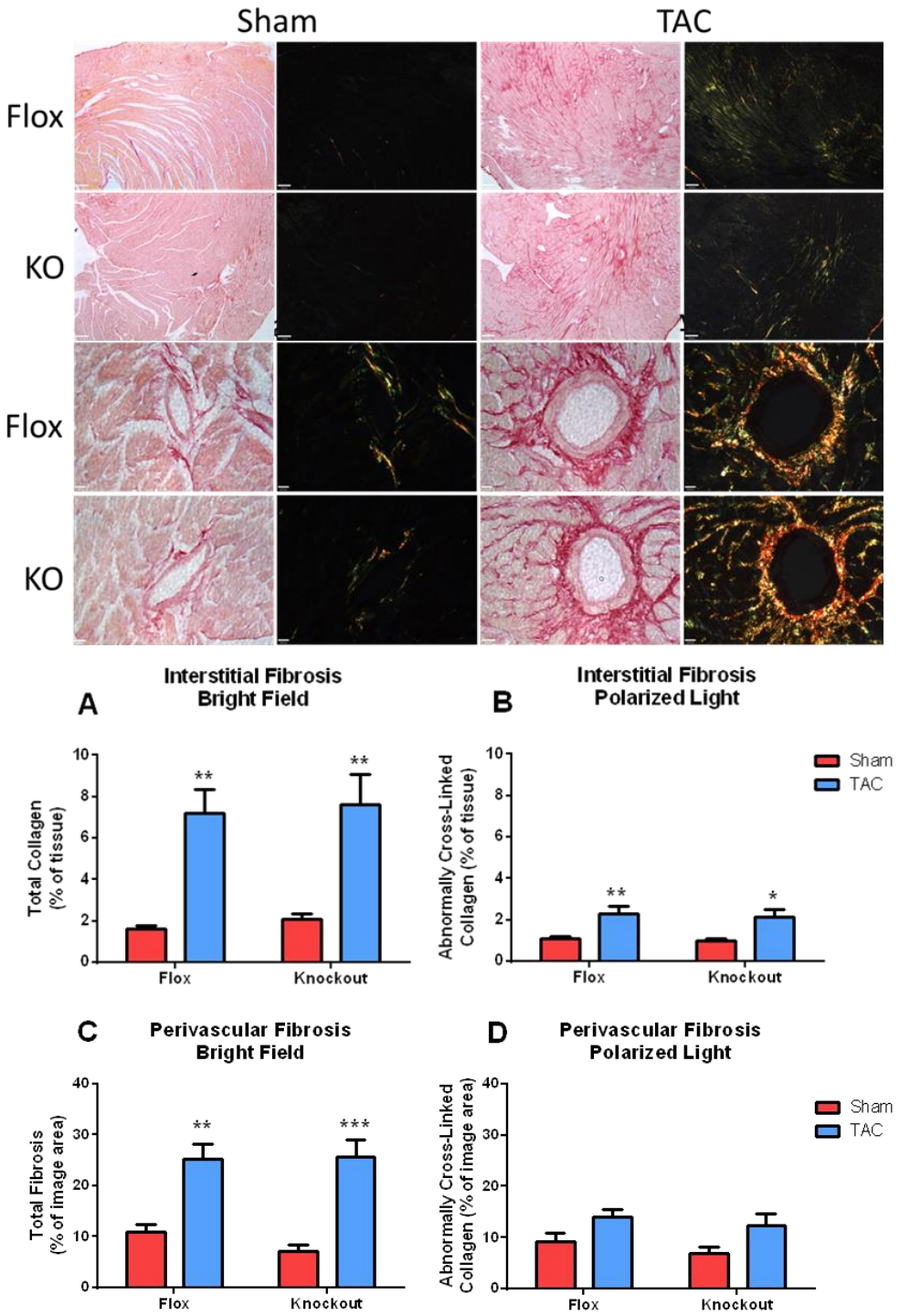

Figure 4-4: Cardiac interstitial and perivascular fibrosis in mice 14 days after TAC surgery. Upper 2 rows: representative images for interstitial fibrosis (scale 300µm) and quantification (A and B). **Bottom 2 rows:** representative images for perivascular fibrosis (scale 100µm) and quantification (C and D). 2way ANOVA shows significant increase vs. sham for both groups.*$P<0.05$, **$P<0.01$ and ***$P<0.001$ vs. respective sham control; 2-way ANOVA with Bonferroni's post-test; n=10, 12, 11, 11.

The observed cardiac fibrosis is supported by gene expression data, showing an increase in fibrotic gene markers in hearts of both flox and KO mice (Figure 4-5). In particular, analysis of collagen 1α1 and collagen 3α1 by qPCR showed an upregulation of between 200% to 300% for both flox and KO mice, however there is no difference between genotypes. Interestingly, in contrast to flox controls, fibronectin expression is not significantly increased in fibroblast NOX2 KO TAC mice, though the interaction is not regarded as statistically significant (Figure 4-5D).

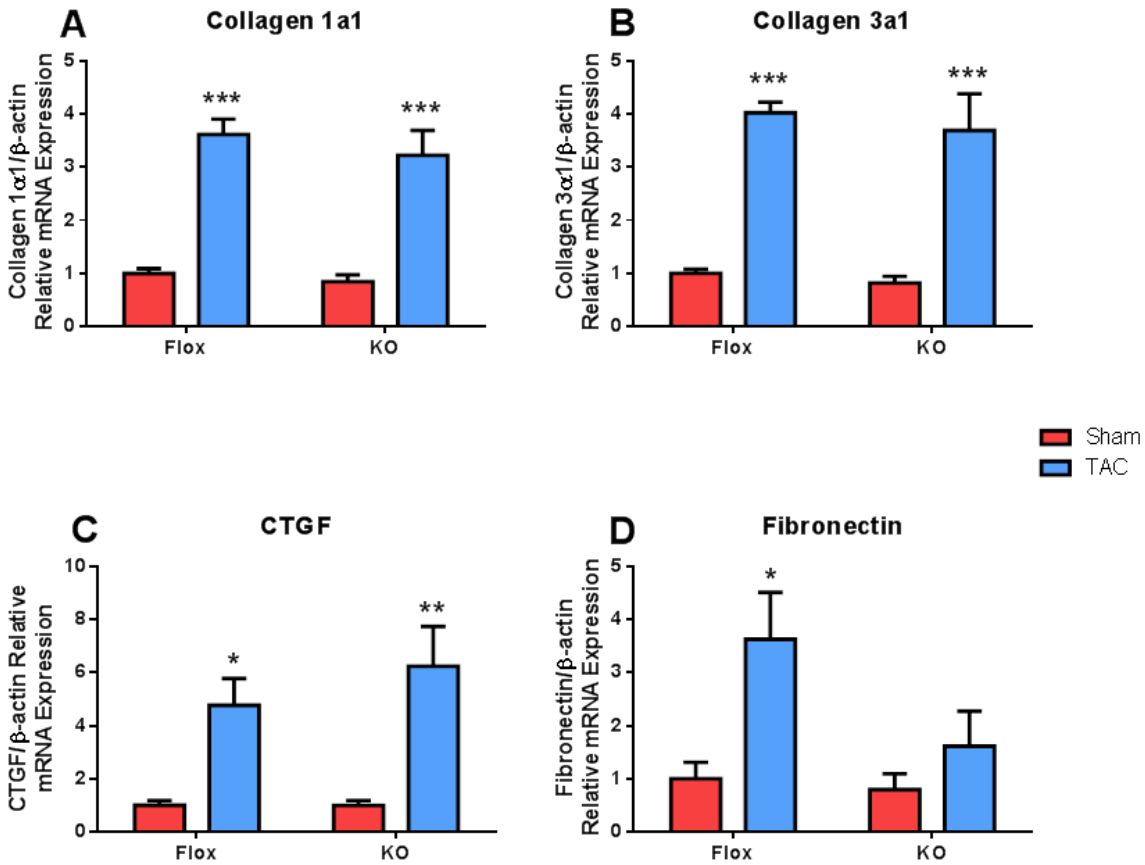

Figure 4-5: Increased expression of fibrotic gene markers in mice 14 days after TAC surgery. **A:** Collagen 1α1, **B:** Collagen 3α1, **C:** connective tissue growth factor (CTGF) and **D:** fibronectin. 2way ANOVA shows significant increase vs. sham for both groups. *$P<0.05$, **$P<0.01$, ***$P<0.001$ vs. respective sham control; 2way ANOVA with Bonferroni post-test; n=6.

In addition to cardiac fibrosis, cardiac hypertrophy was also observed following 2 weeks of TAC (Figure 4-6). Flox and fibroblast NOX2 KO mice responded similarly with approximately 40-50% hypertrophy determined by whole heart weight and individual cardiac chambers.

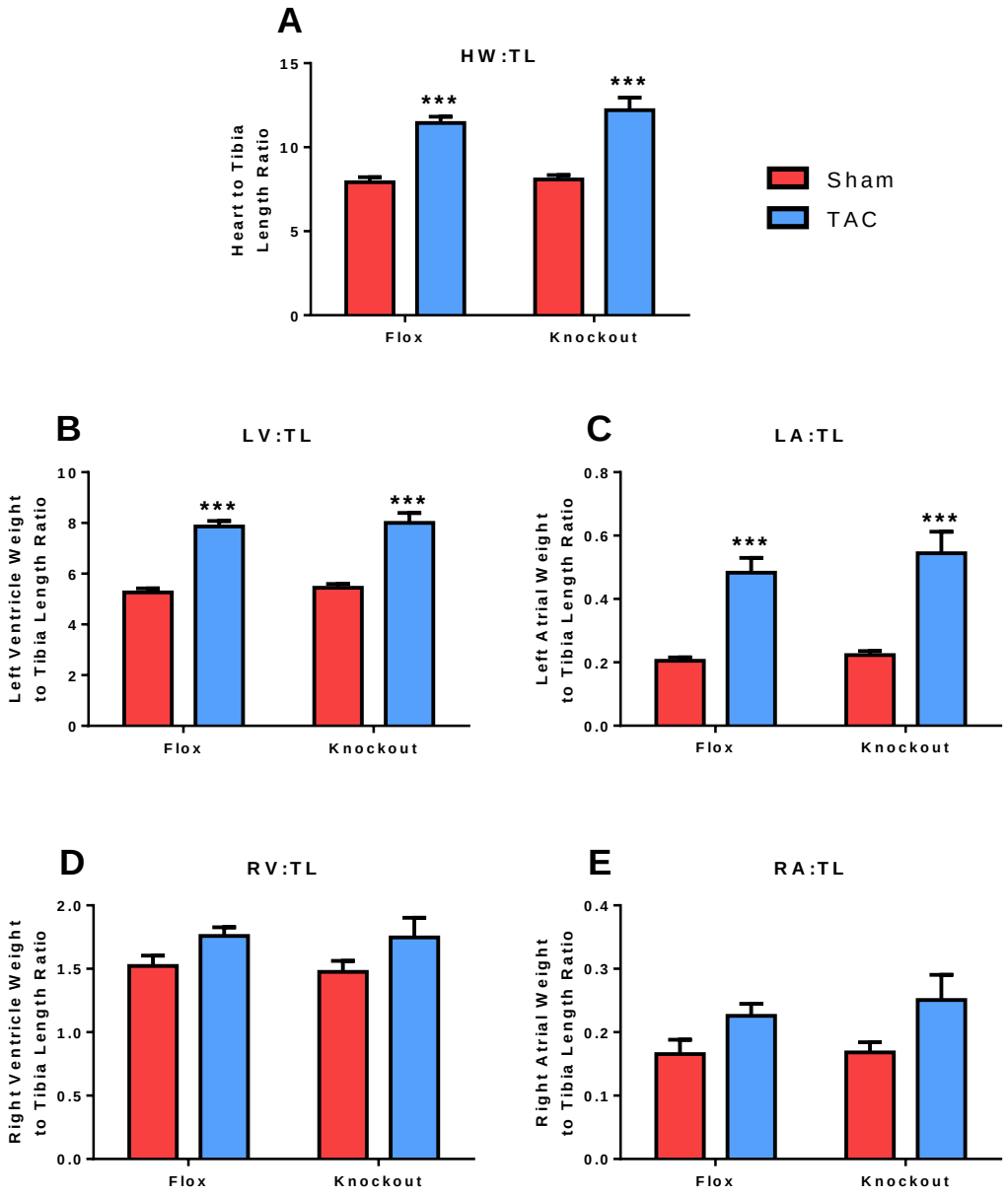

Figure 4-6: Cardiac hypertrophy determined by weight 14 days after TAC surgery. A: Whole heart weight (HW), **B:** left ventricle (LV), **C:** left atrium (LA), **D:** right ventricle (RV) and **E:** right atrium (RA) all normalised to left tibia length. ****P<0.001* vs. respective sham control; n=10, 12, 11, 11, respectively.

In support of cardiac weight analysis, echocardiography-derived cardiac dimensions indicated marked hypertrophy (Figure 4-7), which occurred to a similar extent in flox and fibroblast NOX2 KO TAC mice. In addition to left ventricular posterior and septal wall thickening, increases in left ventricular end systolic volume and internal diameter during systole indicate cardiac dilatation (Figure 4-7A and D).

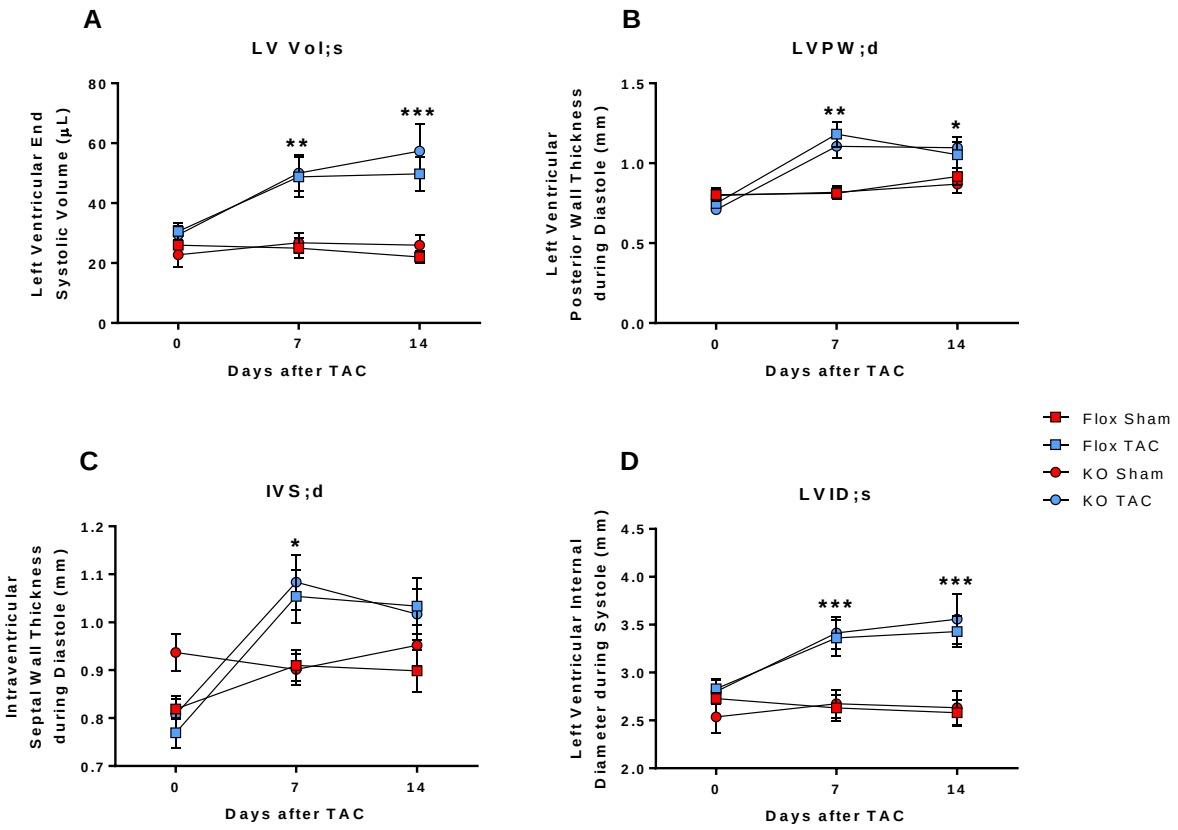

Figure 4-7: Echocardiography-derived cardiac dimensions, indicative of hypertrophy, are increased to the same extent in flox and fibroblast NOX2 KO TAC mice. **A:** left ventricular end systolic volume, **B:** left ventricular posterior wall thickness, **C:** intraventricular septal wall thickness and **D:** left ventricular internal diameter during systole. **P<0.05*, ***P<0.01*, ****P<0.001* vs. respective sham control; 2way ANOVA with repeated measures and Bonferroni post-test; n=10, 12, 11, 11, respectively.

The observed overall cardiac hypertrophy is likely to be a direct effect of cardiomyocyte hypertrophy, as indicated by left ventricular cardiomyocyte cross-sectional area analysis (Figure 4-8). TAC surgery led to a similar increase in average

cardiomyocyte cross-sectional area in flox and KO mice of 43% and 39%, respectively (*P<0.01* vs. respective sham controls).

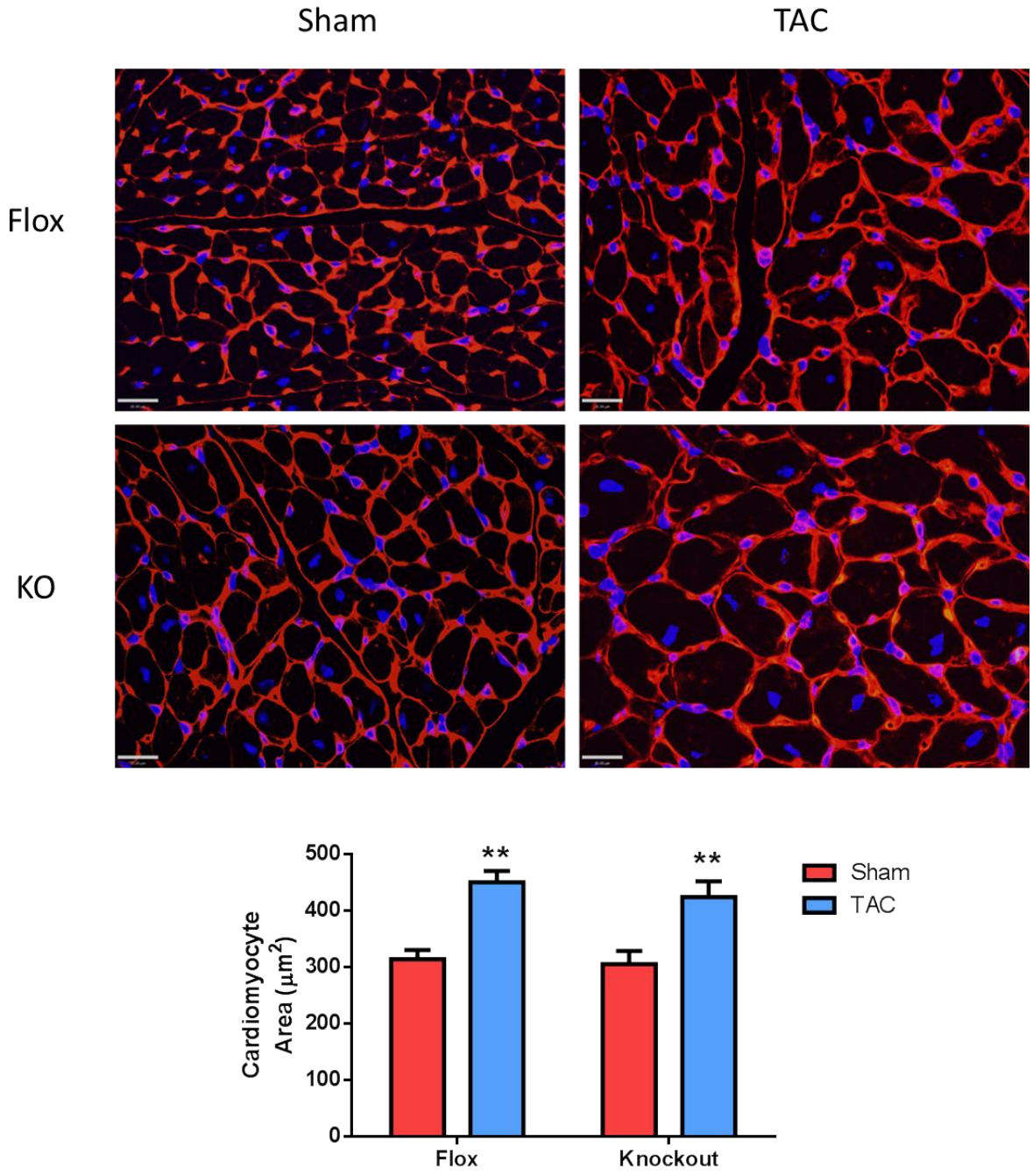

Figure 4-8: Cardiomyocyte hypertrophy determined by cross-sectional area analysis of wheat germ agglutinin- (WGA) stained cardiac tissue sections. Upper panels: representative images for WGA stained cardiac sections in mice 14 days after surgery. **Lower graph:** quantification showing enlarged cardiomyocytes in mice receiving TAC surgery. Data is from an average of ≥100 individual cardiomyocytes per mouse. ***P<0.01* vs. respective sham control; scale 30µm; n=6, 6, 8, 8, respectively.

Taken together, flox and fibroblast NOX2 KO mice both underwent cardiac remodelling following 2 weeks of TAC and, importantly, this occurred to a comparable extent.

4.3.3 Cardiac Function

Chronic pressure overload in mice is known to cause cardiac dysfunction.[29, 175] Echocardiography was used to examine cardiac function both before and 1 and 2 weeks after TAC. Indices of systolic dysfunction including ejection fraction, fractional shortening and cardiac output were significantly reduced in TAC mice at both 1 and 2 week time points (Figure 4-9). The dysfunction was equivalent between flox and fibroblast NOX2 KO mice, with an approximate 33% reduction in ejection fraction in both groups (Figure 4-9A).

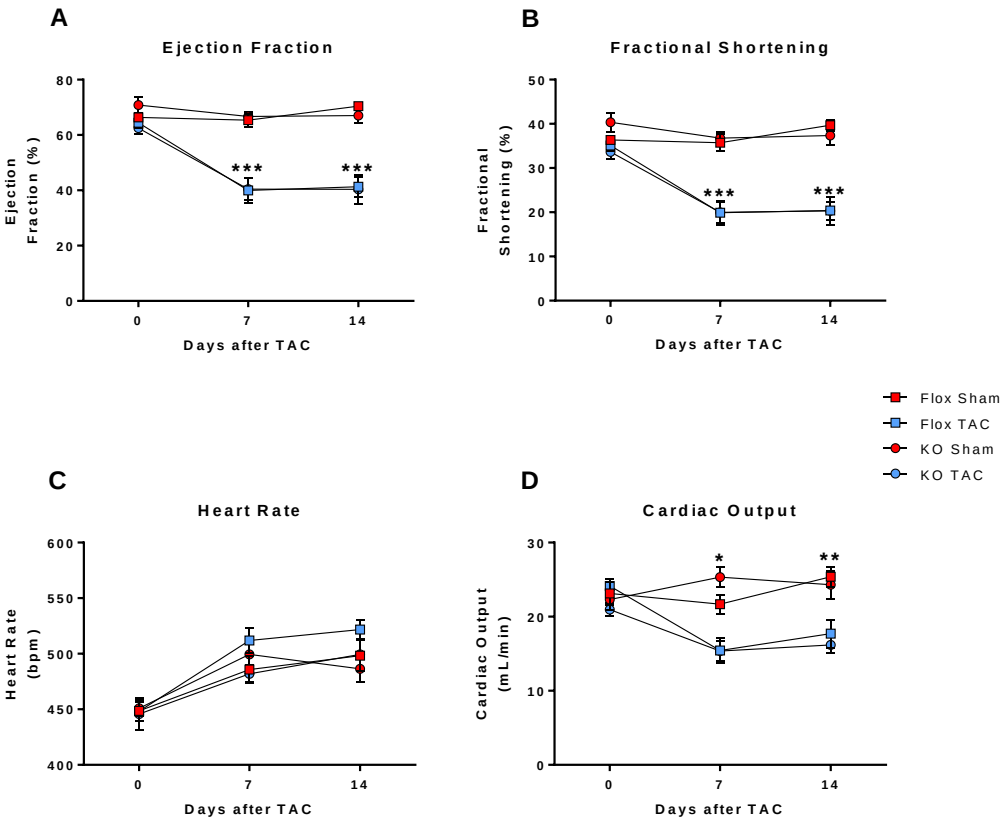

Figure 4-9: Systolic function is reduced to the same extent in flox and fibroblast NOX2 KO TAC mice as determined by echocardiography. A: Ejection fraction, **B:** fractional shortening, **C:** heart rate and **D:** cardiac output. *$P<0.05$, **$P<0.01$, ***$P<0.001$ vs. respective sham control; 2way ANOVA with repeated measures and Bonferroni post-test; n=10, 12, 11, 11, respectively.

Diastolic dysfunction, for example reduced ventricular compliance, is seen on the progression to heart failure and can be caused by cardiac fibrosis.[118, 176] Cardiac diastolic function was assessed by echocardiography, showing a similar extent of dysfunction in flox and fibroblast NOX2 KO mice (Figure 4-10). Here, the mitral valve E-wave deceleration time appears to be a highly sensitive measure in mice, reducing by about 50% with TAC (Figure 4-10D). Left atrial remodelling is also a reflection of left ventricular diastolic dysfunction, since a reduction in left ventricular compliance and relaxation capacity will increase filling pressures and therefore left atrial pressure. A similar ~85% increase in left atrial area was observed in both flox and fibroblast NOX2 KO TAC mice (Figure 4-10B).

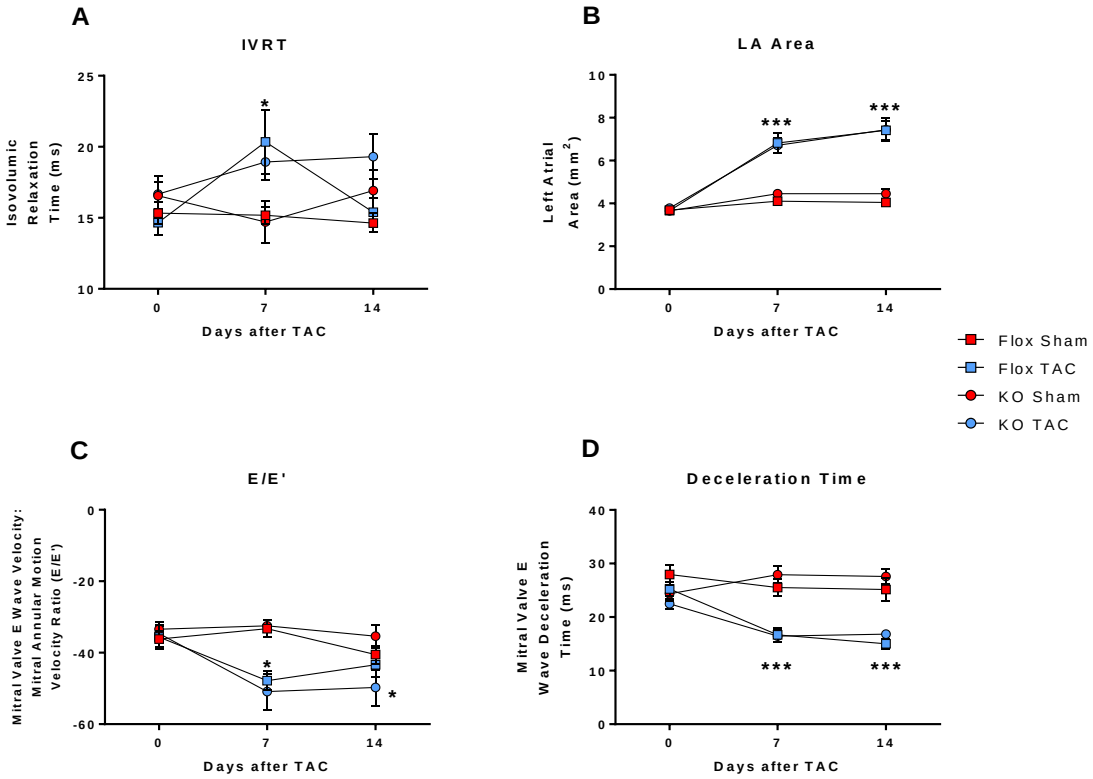

Figure 4-10: Diastolic function was reduced to a similar extent in flox and fibroblast NOX2 KO TAC mice as determined by echocardiography. **A:** Isovolumic relaxation time, **B:** left atrial area, **C:** mitral valve 'E' wave velocity to annular motion ratio (E/E') and **D:** mitral valve 'E' wave deceleration time. *$P<0.05$, ***$P<0.001$ vs. respective sham control; 2way ANOVA with repeated measures and Bonferroni post-test; n=10, 12, 11, 11, respectively.

Sensitive strain and strain rate analysis in TAC mice revealed declines in cardiac function over time from baseline to 14 days after TAC (Figure 4-11). These declines in radial and longitudinal strain and strain rate were comparable between flox and fibroblast NOX2 KO mice, further confirming the lack of difference between genotypes.

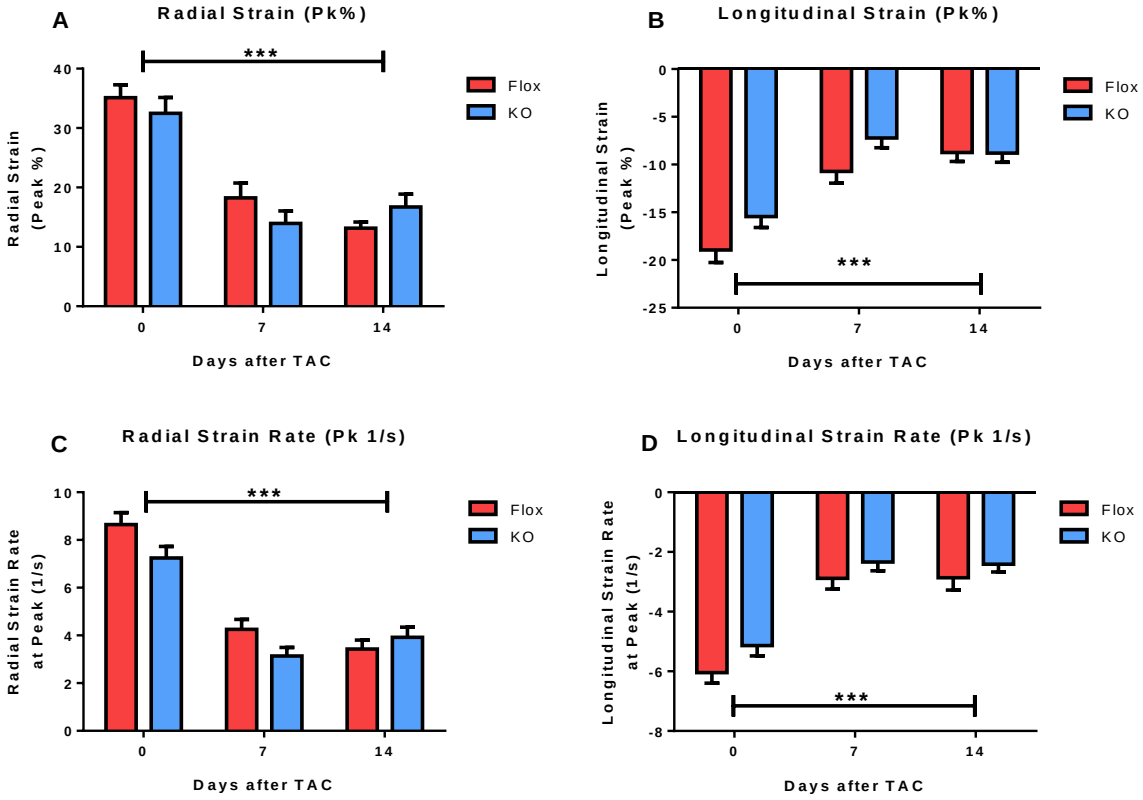

Figure 4-11: Strain and strain rate echocardiography revealed comparable declines in cardiac function for flox and fibroblast NOX2 KO mice. **A:** Average radial strain as percentage of peak, **B:** average longitudinal strain as percentage of peak, **C:** Radial strain rate at peak per second, **D:** Longitudinal strain rate at peak per second. ****P<0.001* from baseline (0) to 14 days after TAC; 2way ANOVA with repeated measures with Bonferroni post-test; n=12 and 11 for flox and KO, respectively.

Taken together, these results indicate that fibroblast NOX2 does not contribute to the development of TAC-induced cardiac fibrosis, hypertrophy or systolic or diastolic dysfunction.

4.4 Discussion

Previous studies have shown the importance of NOX2 in the development of cardiac fibrosis; however the cell-specific contribution remains unclear. In particular, fibroblast NOX2 is thought to be important, owing to the central role in extracellular matrix homeostasis. In the current study, fibroblast NOX2 KO mice subjected to TAC were comparable to flox controls in terms of cardiac fibrosis, remodelling, hypertrophy and systolic and diastolic function. This finding was perhaps unexpected and is in contrast to results obtained from the Ang II model. This suggested stimulus-dependent effects of fibroblast NOX2 as well as a non-critical role for fibroblast NOX2 in the development of cardiac fibrosis in response to TAC.

It is known that NOX2 contributes to both cardiac dysfunction and fibrosis in response to chronic Ang II[35, 62] or pressure overload, but only plays a role in Ang II-induced left ventricular hypertrophy.[31, 174] This showed that NOX2 activation is stimulus dependent and that NOX2 activity may be superseded by other ROS sources or other pathways for certain pressure overload-induced pathological effects. If the contribution of fibroblast NOX2 is also stimulus dependent, further experiments would be needed to confirm this. Since Ang II-treated fibroblast NOX2 KO mice have a delayed hypertensive response (chapter 3), a possible experiment could include the normalisation of blood pressure for both flox and KO mice. However, such an experiment would have to be carefully considered to avoid "preventing" cardiac fibrosis with an anti-hypertensive agent, effects often seen with resveratrol[156] or losartan.[177]

Activation of NOX2 by neurohumoral stimulation such as with Ang II is well characterized, involving Ang II receptor 1 (AT1R) activation, TGFβ signalling and phosphorylation of p47phox.[178] In contrast, mechanical stimulation such as with pressure overload is less understood. What *is* known is that mechanical stretch of cardiomyocytes induces RAAS signalling and NOX2 activation[179] and that stretched cardiac fibroblasts *in vitro* results in increased collagen deposition.[180] ROS production in fibroblasts has also been reported in response to osmotic swelling, though this was deemed to be NOX4 mediated.[181] Echocardiography data from this chapter showed development of cardiac strain and so stretch-induced activation of cardiac fibroblasts

is to be expected, but the extent, if any, of NOX2 activation in fibroblasts by this mechanism is unknown. As shown, in contrast to Ang II-stimulation, fibroblast NOX2 deletion was unable to prevent cardiac fibrosis in TAC. This hints towards fibroblast NOX2 activation being most important in Ang II-mediated fibrosis and dispensable in TAC. It is also worth noting that TAC is expected to cause less RAAS activation than AAB[173] and as such, the loss of fibroblast NOX2 may be of little consequence in a system less reliant on Ang II-mediated signalling.

Regardless, the absence of a reduction in cardiac fibrosis in fibroblast NOX2 KO mice suggested that NOX2 in non-fibroblasts is of greater importance in TAC. For example, it is known that inflammation occurs during TAC, leading to the recruitment of circulating leukocytes. These leukocytes are high expressers of NOX2 and rapidly increase their cardiac cell numbers after TAC, peaking at 3-7 days followed by a slow decline over time.[182] Recent reports suggest some dependence on infiltrating leukocytes for the development of cardiac fibrosis in TAC. Phosphoinositide 3-kinase γ (PI3Kγ) is known to be essential for leukocyte recruitment during inflammation and kinase-dead mutant mice have been shown not to develop cardiac fibrosis following TAC.[183] Similar results were obtained using a selective PI3Kγ inhibitor, but treatment had no effect when started 1 week after TAC, indicating that the initial leukocyte infiltration was most important.[183] It is possible that a mechanical stimulus such as TAC is more dependent on leukocyte recruitment and leukocyte NOX2 activation for the development of cardiac fibrosis, since deletion of fibroblast NOX2 had no effect.

Interestingly, this increase in leukocyte recruitment is also documented in response to chronic Ang II. Surprisingly however, it was shown that NOX2 from inflammatory cells was not essential for Ang II-induced cardiac fibrosis,[53] highlighting both a stimulus and cell dependent effect.

4.4.1 Transverse Aortic Constriction Model

Transverse aortic constriction is a well-established murine model, repeatedly shown to induce cardiac hypertrophy and fibrosis.[29, 118, 141] A major consideration for TAC studies is the degree of aortic constriction and the pressure differential generated as a result. It has been described that invasively measured trans-TAC pressure gradients correlate with TAC severity and left ventricular hypertrophy after 21 days.[141]

Importantly, non-invasively measured transverse aortic Doppler flow correlates with these invasive measures, providing an opportunity to prospectively assess TAC severity non-terminally.

Here we measured blood pressure from the left and right foreleg immediately after TAC using non-invasive plethysmography. This method makes the assumption that the pressure measured peripherally in the right and left foreleg, is reflective of the pressures occurring proximal (transverse aorta) and distal (descending aorta) to the TAC site, respectively. We show an average 26mmHg pressure differential by plethysmography and close to 41mmHg measured by pulsed-wave Doppler echocardiography, the latter of which is comparable to catheter and Doppler-derived values previously reported.[141] Given the vast variability in the TAC model, it is surprising that an indication of TAC severity or success is not included in many publications.[29, 118, 184-186] In addition to a Doppler-based approach we present a plethysmography-based, and to our knowledge previously unreported, method for assessing TAC severity immediately post-surgery, which could be used in the absence of echocardiographic equipment.

Taken together we can be confident in the TAC model effectiveness and reproducibility in our hands, giving strength to the conclusion that fibroblast NOX2 is dispensable in the development of TAC-induced cardiac fibrosis.

4.4.2 Echocardiography and TAC

In contrast to chronic Ang II models, TAC was capable of inducing significant systolic and diastolic dysfunction, as well as more profound cardiac fibrosis. As such, TAC provides a wider window through which to investigate subtle functional effects of gene deletion *in vivo*.

Clinical echocardiography suggests that the E/A ratio is a very reliable and predictive index of diastolic function, however this is difficult to measure in mice due to higher heart rates. With a high heart rate, the mitral E and A waves can become fused, making it impossible to accurately distinguish the two components (Figure 4-12). This is a commonly reported problem in murine models and can be overcome either by

lowering heart rates artificially with increased isoflurane or by simply measuring alternative indices.

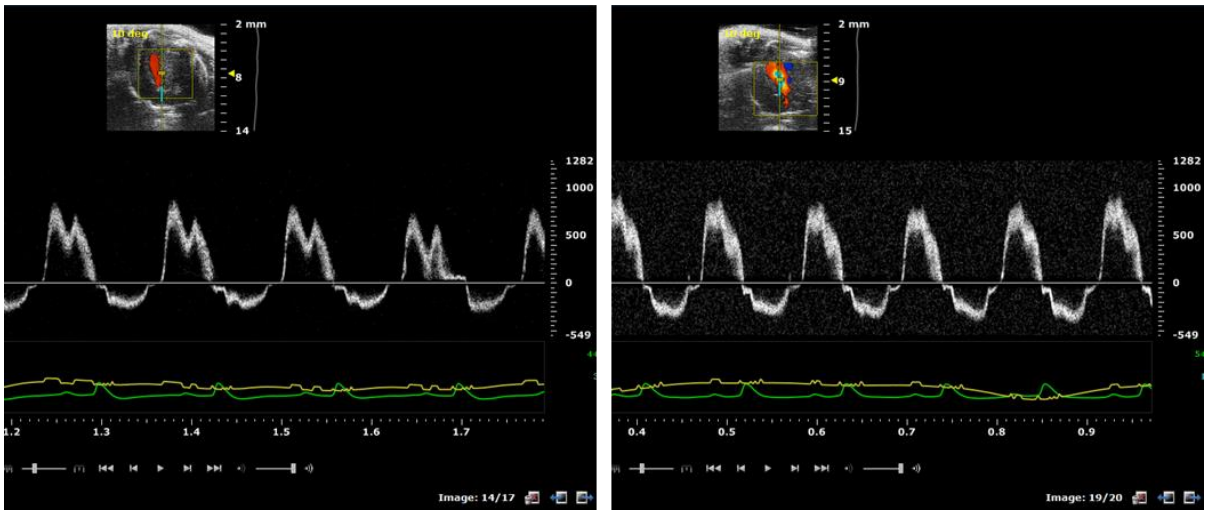

Figure 4-12: Lower heart rates increase the probability of separate, measureable E and A waves. Left: Heart rate of 447 bpm compared to **Right:** heart rate of 540 bpm. Images are representative taken from a single mouse 7 days apart.

Alternative indices include left atrial area and mitral E wave deceleration time, both of which have emerged as robust indicators of diastolic dysfunction by echocardiography, as well as IVRT and E/E'. The left atrium can be observed in an apical 4-chamber view probe orientation, and whilst difficult to achieve, is a way to determine the left atrial area. This index was found to be highly reproducible in TAC mice in this study and is clinically relevant, since it is commonly seen in patients with heart failure and can be an independent risk factor for death.[168] Both the E wave deceleration time and IVRT are associated with left ventricular relaxation, becoming prolonged with impaired relaxation,[153, 187] but also become shortened by increased filling pressures[188] – a seemingly paradoxical event, explained by a U-shaped relationship.[168] In the current study, TAC mice showed signs of impaired relaxation, denoted by an increased IVRT at day 7. However evidence predominantly points towards a more advanced pseudonormal or restrictive ventricular filling pattern due to severely increased atrial pressure (indicated by increased left atrial area), since the E wave deceleration time was reduced and IVRT appeared reduced in some mice. In addition, the E/E' ratio increased (more negative). This occurs as the E wave tends to

increase with increased filling pressures, whereas mitral annular motion (E') is reduced.[168]

Collectively, echocardiography data presented in this chapter provide firm evidence for diastolic dysfunction following 14 days pressure overload by TAC in our own hands and is therefore a powerful tool for functional studies.

4.4.3 Summary

Data presented in this chapter strongly suggest that fibroblast NOX2 is dispensable in the development of TAC-induced cardiac fibrosis. This is in contrast to results from chapter 3 and taken together strongly supports the argument in chapter 3.5 for a pressor-dependent effect of fibroblast NOX2 in the development of cardiac fibrosis. In addition, these data could suggest a stimulus-dependent role for fibroblast NOX2, or a non-critical role in the development of cardiac fibrosis.

CHAPTER 5: Contribution of Endothelial Cell NOX2 to Pressure Overload Remodelling induced by Transverse Aortic Constriction

5.1 Introduction

5.1.1 Endothelial Cells and the Endothelium

The endothelium is a monolayer of cells, lining blood vessels and acting as a barrier between tissues and circulating blood. Endothelial cells are therefore critically positioned to be able to respond to physical and chemical stimuli in order to maintain vascular homeostasis.

The endothelium-derived relaxing factor, identified as nitric oxide, mediates the quiescent state of the endothelium, including relaxation of underlying smooth muscle cells and a reduced tendency towards vascular inflammation, thrombosis and cell recruitment and adhesion.[189] As such, nitric oxide signalling can be regarded as anti-fibrotic. In fact, endothelial nitric oxide synthase KO mice are hypertensive[190] and were more prone to develop cardiac hypertrophy and fibrosis.[191]

Endothelial dysfunction is regarded as the activation of the endothelium coinciding with a switch from nitric oxide signalling towards reactive oxygen species.[192] Activation occurs in response to a range of stimuli, including abnormal shear stress, inflammatory mediators and agonists such as Ang II and results in inflammatory cell recruitment and adhesion, vasoconstriction and thrombosis.[189] Reactive oxygen species, including NOX2-derived superoxide, can react and inactivate nitric oxide, reducing its bioavailability and thereby promoting fibrotic signalling.[193] In addition, reactive oxygen species can directly activate neighbouring endothelial cells, leading to further fibrotic signalling via TGFβ.

5.1.2 Endothelial Cells and Cardiac Fibrosis

A number of studies have investigated the importance of endothelial cell signalling in the development of cardiac fibrosis.

Endothelin-1 is secreted by activated endothelial cells for example during hypertension[95] and is associated with the development of pulmonary and renal fibrosis.[194] A role for endothelial cell endothelin-1 in the development of cardiac fibrosis has also been reported, since Endothelial cell endothelin-1 KO mice (*Tie-2* promoter) develop less interstitial and perivascular cardiac fibrosis following Ang II treatment.[54] In addition, endothelial cell endothelin-1 KO mice had reduced fibrotic

gene expression for collagen 1, collagen 3 and connective tissue growth factor. Importantly, these effects were not due to differences in hypertension, since systolic blood pressure in KO mice was similar to that of wildtype controls.[54] Similar results were found using a streptozotocin-induced model of diabetes in mice, giving further evidence for a pro-fibrotic role of endothelial cell-derived endothelin-1.[52]

The tumour suppressor gene, p53, is elevated in heart failure patient biopsies.[195] Mice with endothelial cell-specific (*Tie2* promoter) deletion of p53 were shown to have significantly lower basal cardiac collagen 1 and CTGF gene expression, suggesting that normal endothelial cell p53 signalling might be pro-fibrotic.[196] Furthermore, when these mice were subjected to TAC, they had greater survival, associated with reduced cardiac fibrosis and hypertrophy and with better cardiac function compared to wildtype controls.[196]

A direct link between endothelial cell NOX2 activation and cardiac fibrosis was found by Murdoch and colleagues using an endothelial cell-specific transgenic NOX2 overexpressing mouse.[53] Transgenic mice had a 2-fold increase in NOX2,[124] accompanied by an approximate 2-fold increase in cardiac fibrosis following chronic angiotensin II treated compared to WT mice.[53] Collagen 1 gene expression, overall NOX activity and diastolic stiffness were all increased in transgenic mice. The Ang II-induced cardiac inflammatory cell infiltration ($CD45^+$ and $MAC3^+$ cells) was significantly increased in transgenic mice compared to wildtype, coinciding with increased endothelial cell expression of vascular cell adhesion molecule-1. It was therefore thought that these pro-fibrotic effects of endothelial NOX2 could be due to increased leukocyte recruitment. Surprisingly, inflammatory cell NOX2 was shown to be dispensable for the augmented cardiac fibrosis, but a role for NOX2-mediated endothelial-mesenchymal transition was reported.[53]

5.1.3 Endothelial-Mesenchymal Transition

Endothelial-mesenchymal transition (EndoMT) is a process by which cells lose their endothelial-specific markers, e.g. CD31 or CD144 and begin to express markers similar to fibroblasts (mesenchymal lineage), e.g. αSMA, vimentin, CD140α and DDR2. Cells will also change phenotype and may become motile and able to differentiate, such as from fibroblasts to myofibroblasts. This phenotypic switch is seen during the

development of the cardiac atrioventricular cushion in embryonic development,[197] but historically has not been documented in adult tissue.

Evidence of EndoMT in cardiac tissue was first reported by Zeisberg and colleagues in 2007, showing that up to 35% of fibroblasts were originally endothelial cells in a mouse model of chronic pressure overload (discussed in detail in chapter 6).[30] Murdoch and colleagues were also able to show that the augmented cardiac fibrosis in endothelial NOX2 transgenic mice coincided with cells undergoing EndoMT, as revealed by co-localisation of CD31 and αSMA markers in immunostained cardiac sections.[53] Moreover, significantly less CD31 and significantly more αSMA and collagen 1 protein was detected in the hearts of Ang II-treated transgenic mice compared to wildtype, indicative of completed EndoMT.[53]

In another experiment, human umbilical vein endothelial cells were stimulated to undergo EndoMT by hypoxia and subsequent re-oxygenation, leading to the loss of CD31 and CD144 markers and upregulation of αSMA.[198] These cells were then assessed for their ability to produce collagen type I, showing only a mild contribution relative to that of either isolated cardiac fibroblasts or H9C2 rat cardiomyoblasts. It was then shown that conditioned medium from these EndoMT-derived cells could induce the transdifferentiation of cardiac fibroblasts into myofibroblasts.[198] These data indicate that rather than just directly contributing to the fibroblast pool, endothelial cells undergoing EndoMT may stimulate resident fibroblasts via a paracrine signalling method, leading to increased collagen deposition and subsequent fibrosis.

In summary, NOX2 overexpression in endothelial cells induces augmented cardiac fibrosis in Ang II-treated mice and increased EndoMT. In addition, the potential paracrine signalling between endothelial cells and fibroblasts further highlights this cell type's importance and warrants further investigation.

5.1.4 Aims

The aim of this chapter was to investigate the contribution of endothelial cell NOX2 in the development of TAC-induced cardiac fibrosis. Based on previous studies, it was anticipated that NOX2 is a key driver of endothelial to mesenchymal cell transition and so specific deletion of NOX2 would reduce the development of cardiac fibrosis.

5.2 Methods

5.2.1 Generation of Experimental Mice

Male Cre-positive *Cdh5*-CreER(T2) mice were crossed with Cre-negative female NOX2$^{flox/flox}$ mice to generate *Cdh5*-CreER(T2)/NOX2$^{flox/y}$ male or *Cdh5*-CreER(T2)/NOX2$^{flox/flox}$ female mice respectively, or Cre-negative littermates. Cre-positive progeny are deficient in endothelial cell NOX2 following daily *i.p.* injection with 1mg tamoxifen in peanut oil for 3 days.[130]

As with the fibroblast NOX2 KO experiments, all experimental mice were NOX2 floxed and Cre-negative male littermates were used as flox controls. Recombination of disrupted NOX2 in heart tissue (following 3-day 1mg *i.p.* tamoxifen injections) was confirmed by the presence of a smaller PCR product (lower band, Figure 5-1). Mice with recombined NOX2 are referred to as endothelial cell NOX2 KO and those without are flox controls.

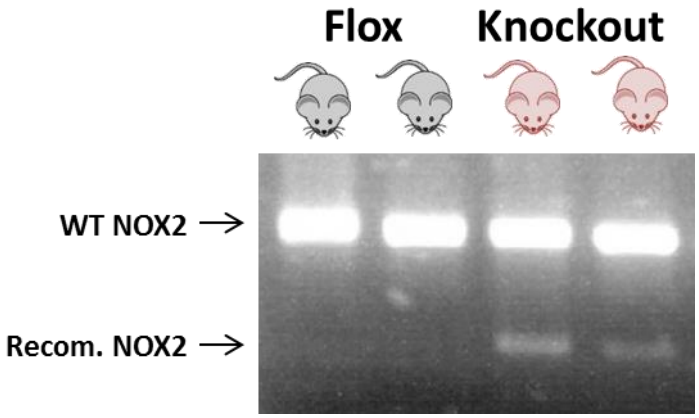

Figure 5-1: PCR-based genotyping of mice using DNA gel analysis. Primers recognise WT NOX2 or recombined NOX2 in heart tissue following tamoxifen treatment. The upper band indicated WT NOX2, whereas the lower band indicated the presence of a disrupted (non-functional) NOX2 gene, so-called knockout. Recom. = recombined.

Expression of NOX2 protein was significantly reduced by approximately 50-60% in aortae of endothelial cell NOX2 KO mice following three days tamoxifen treatment (Figure 5-2). Protein expression in aorta was analysed owing to the predicted low number of cardiac endothelial cells (<10%).[172, 199] As such, any reduction in cardiac endothelial cell NOX2 protein might be masked by the contribution of cardiomyocyte and cardiac fibroblast NOX2.

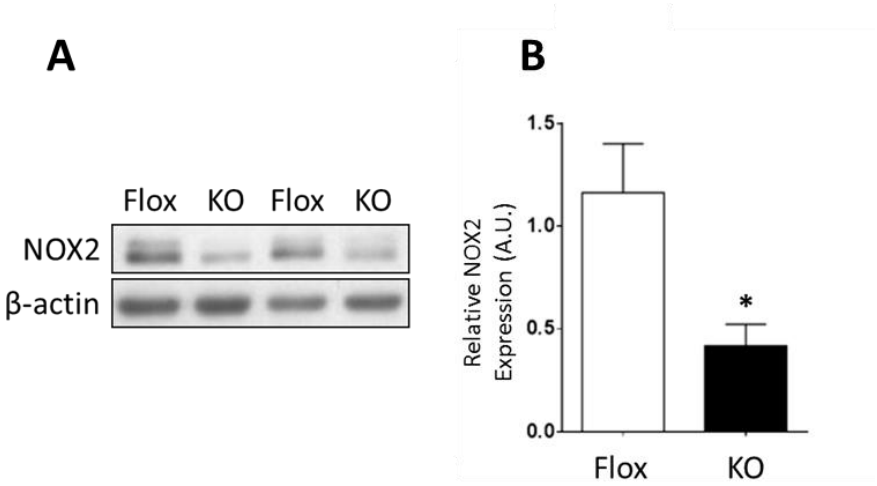

Figure 5-2: NOX2 protein expression in aorta following mouse treatment with tamoxifen. A: Western blot for NOX2, with β-actin for normalisation, representative image. **B:** Quantification of western blot protein expression relative to flox controls. n=5; *P<0.05*; student's t-test. Reproduced from Sag CM et al., 2016; manuscript submitted to Circulation Journal.

Flox and KO mice were viable, had normal life expectancy, bred normally and did not show any obvious basal phenotype.

5.2.2 Experimental Methods

All other experiments were conducted exactly as for those described in chapter 4, excluding the estimation of adequate TAC gradient by forepaw blood pressure assessment, which was deemed extraneous owing to the accuracy and consistency of Doppler-derived TAC-gradients.

5.3 Results

5.3.1 Survival

Mice subjected to TAC surgery had estimated trans-TAC gradients of between 40-50mmHg, significantly higher than that of sham-operated mice (Figure 5-3). Importantly, there was no difference between flox and endothelial cell NOX2 KO mice.

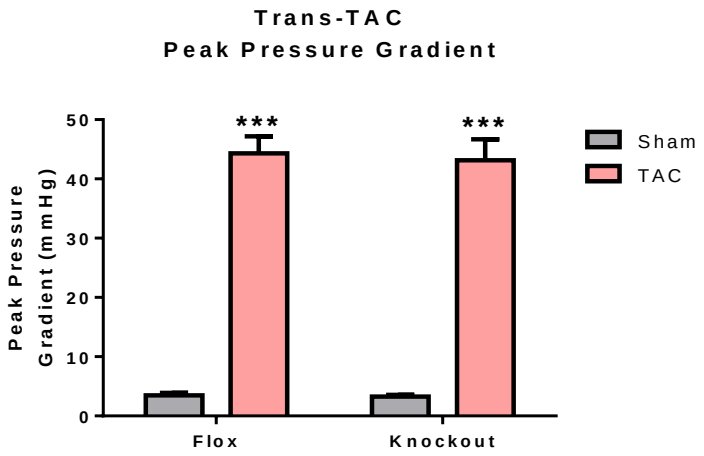

Figure 5-3: Estimation of trans-TAC gradient by Doppler echocardiography performed 24 hours after surgery. Gradients are significantly increased after TAC surgery compared to sham ****P<0.001*; n=8, 10, 8, 8, respectively; 2-way ANOVA with Tukey post-test.

Deletion of NOX2 in endothelial cells had no effect on survival and all mice surviving the perioperative 24 hours went on to survive for the complete 2 week study duration (Figure 5-4).

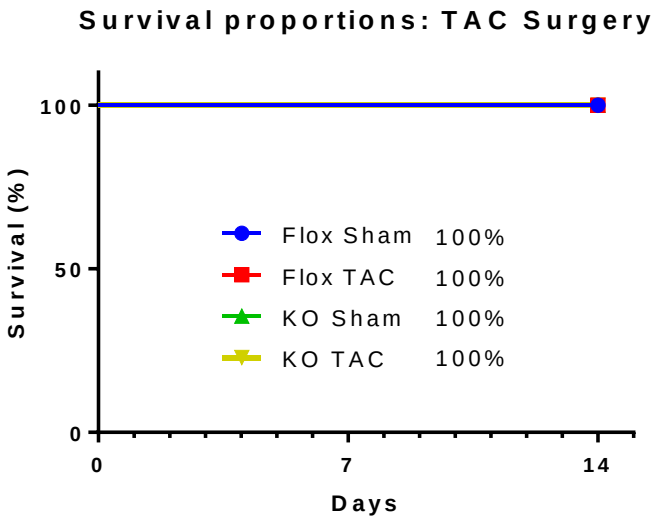

Figure 5-4: Kaplan Meier survival curves for mice from 24 hours after surgery. Survival proportions are listed within, with no significant differences between surgery and genotype groups; *P>0.05*; n=8, 10, 8, 8, respectively.

5.3.2 Cardiac Fibrosis and Hypertrophy

Chronic transverse aortic constriction led to the development of significant interstitial and perivascular fibrosis in flox and endothelial cell NOX2 KO mice compared to sham-operated controls (Figure 5-5). Bright field analysis of cardiac sections stained with Picrosirius red revealed an increase in interstitial fibrosis of 7.72% and 9.83% for flox and endothelial cell NOX2 KO TAC mice, respectively (*P<0.01*), with similar values for perivascular fibrosis analysis (Figure 5-5A and C). Importantly, there was no difference in the extent of cardiac fibrosis for flox and endothelial cell NOX2 KO TAC mice, even with the more sensitive polarised light analysis method (Figure 5-5B and D).

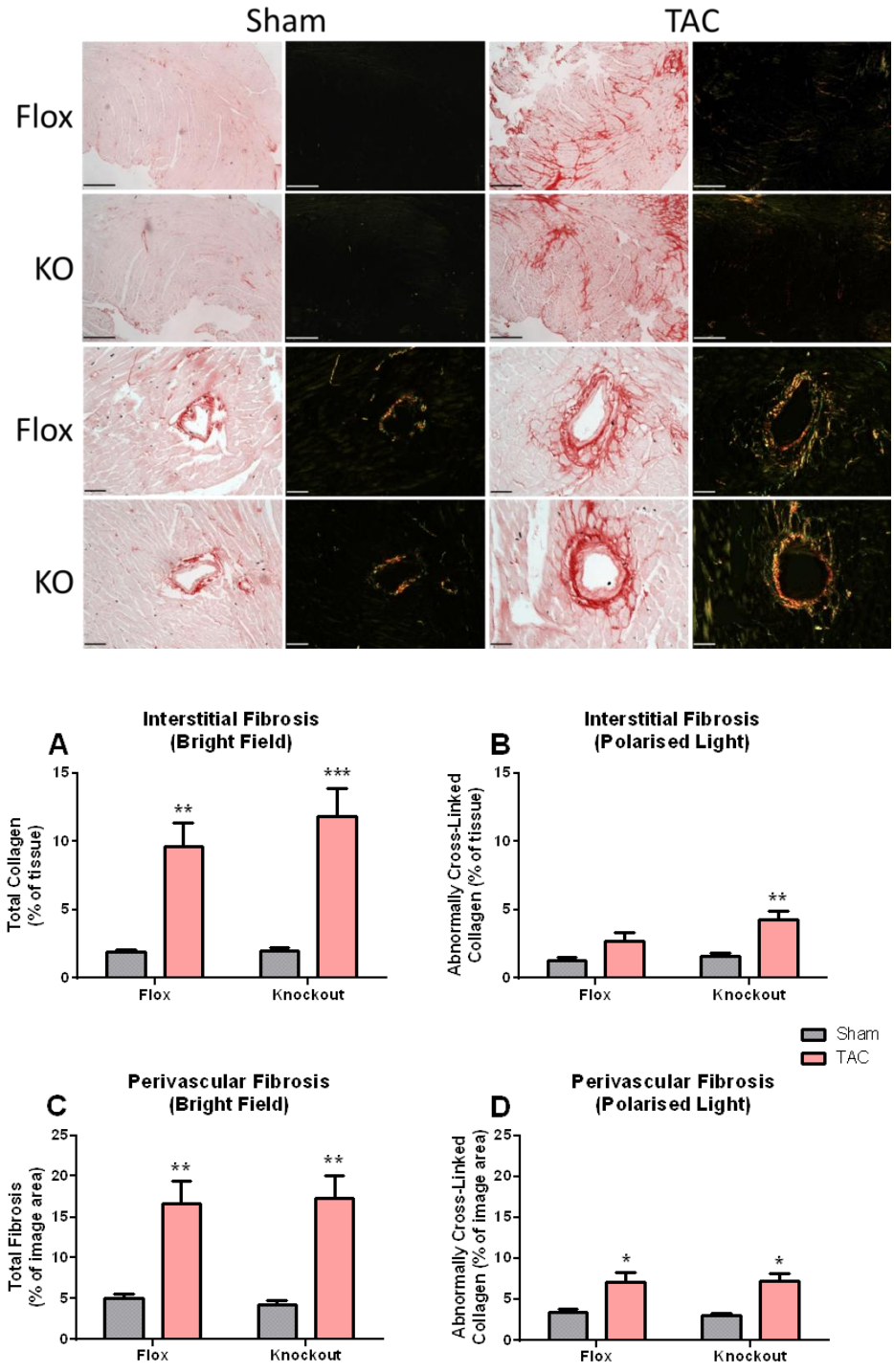

Figure 5-5: TAC induced comparable cardiac interstitial and perivascular fibrosis in flox and endothelial NOX2 KO mice 14 days after surgery. Upper 2 rows: representative images for interstitial fibrosis (scale 300µm) and quantification **(A and B)**. **Bottom 2 rows:** representative images for perivascular fibrosis (scale 100µm) and quantification **(C and D)**. 2way ANOVA shows significant increase vs. sham for both groups. **P<0.05*, ***P<0.01* and ****P<0.001* vs. respective sham control with Bonferroni's post-test; n=8, 10, 8, 8, respectively.

The observed cardiac fibrosis was supported by gene expression by qPCR, showing a marked upregulation of the fibrotic gene markers collagen 1 and 3α1, connective tissue growth factor and fibronectin (Figure 5-6). Endothelial NOX2 KO mice had a similar or greater upregulation of fibrotic genes compared to flox controls. A significant interaction was observed for collagen 3α1 gene expression, with endothelial cell NOX2 KO mice having higher expression than floxed controls (Figure 5-6B). This indicated a possible exacerbation of cardiac fibrosis signalling in these mice and is in agreement with the trend observed in Figure 5-5.

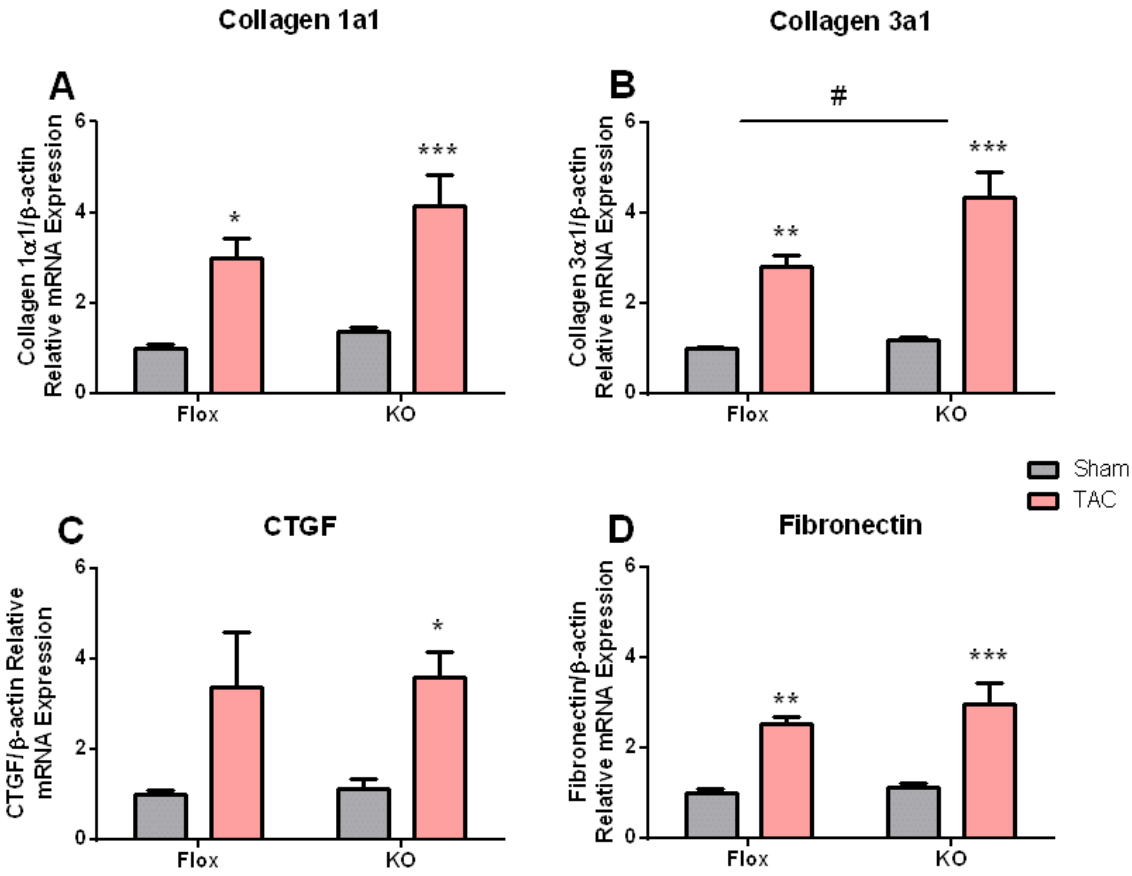

Figure 5-6: Increased expression of fibrotic gene markers in mice 14 days after TAC surgery. **A:** Collagen 1α1, **B:** Collagen 3α1, **C:** connective tissue growth factor (CTGF) and **D:** fibronectin. $^{\#}P<0.05$ for interaction between flox and endothelial cell NOX2 KO mice; $^{*}P<0.05$, $^{**}P<0.01$, $^{***}P<0.001$ vs. respective sham control; 2-way ANOVA with Bonferroni post-test; n=6, 5, 6, 6, respectively.

Reports suggest that endothelial cell undergoing EndoMT lose their specific markers such as CD31. Analysis of cardiac CD31 mRNA revealed that total CD31 expression levels were not changed by TAC, nor did they differ between flox and endothelial NOX2 KO mice (Figure 5-7). Any reduction in CD31 mRNA would have indicated evidence for EndoMT, especially in light of increased collagen 1α1 and collagen 3α1 mRNA.

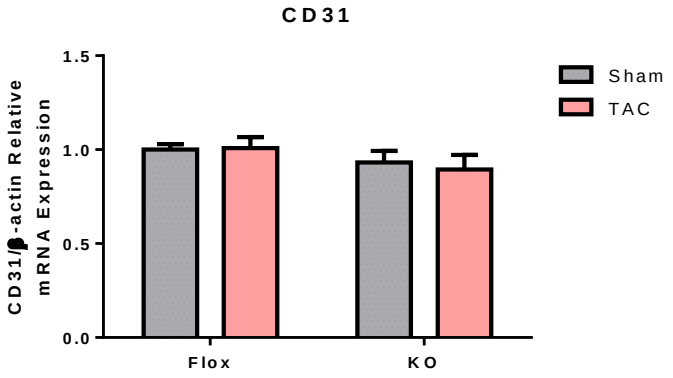

Figure 5-7: Unaltered cardiac CD31 gene expression in mice 14 days after TAC surgery. *P>0.05*; 2-way ANOVA with Bonferroni post-test; n=6, 5, 6, 6, respectively.

An increase in whole heart weight: tibia length ratio was observed in both flox and endothelial cell NOX2 KO TAC mice (27.2% and 49.2% respectively; *P>0.05*; Figure 5-8). This trend was also seen for left ventricular and left atrial weight: tibia length ratio (Figure 5-8B and C). Interestingly, cardiac hypertrophy in the current study did not extend to the right side of the heart, since right ventricular and right atrial weight: tibia length ratios were not increased in flox or endothelial cell NOX2 KO mice following TAC (Figure 5-8D and E). This is in contrast to results obtained in chapter 4, and possibly reflects a lower TAC severity in this chapter, since right ventricular remodelling and even dysfunction can be dependent on TAC severity.[200]

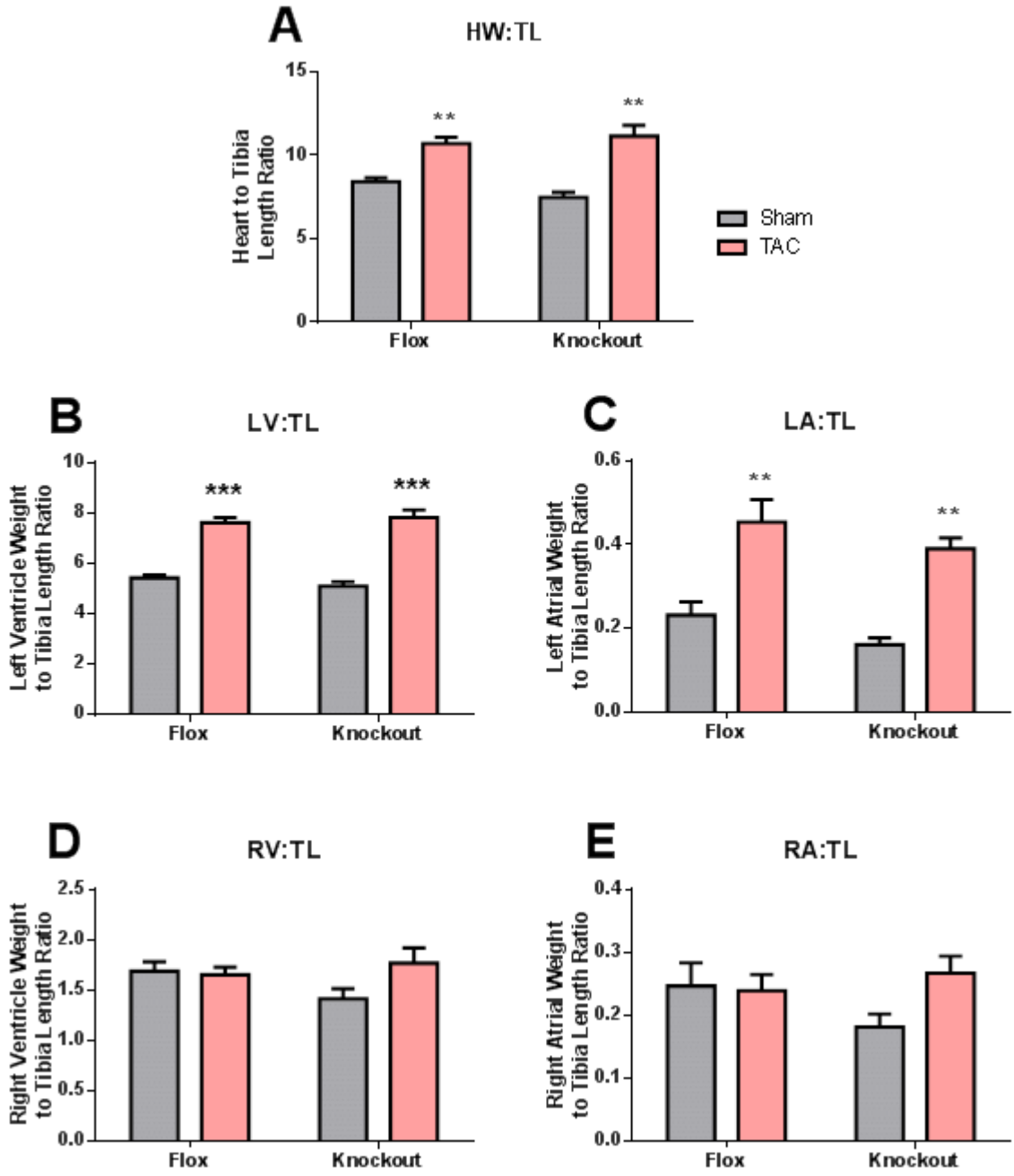

Figure 5-8: Comparable cardiac hypertrophy determined by weight 14 days after TAC surgery. A: Whole heart weight (HW), **B:** left ventricle (LV), **C:** left atrium (LA), **D:** right ventricle (RV) and **E:** right atrium (RA) all normalised to left tibia length (TL). ***P<0.01* and ****P<0.001* vs. respective sham control; n=8, 10, 8, 8.

In agreement with cardiac tissue weight analysis, echocardiography-derived cardiac dimensions indicated marked hypertrophy, which was to a similar extent in both flox and endothelial cell NOX2 KO TAC mice (Figure 5-9). Of particular note, both flox and endothelial cell NOX2 KO mice had approximately 50% hypertrophy, as determined

by echocardiography-derived LV mass (Figure 5-9D). Differences in left ventricular end diastolic volume were only detected between flox sham and endothelial cell NOX2 KO sham mice after 14 days; however this likely represents a sampling error, since all mice have much greater variability than for other parameters (Figure 5-9A).

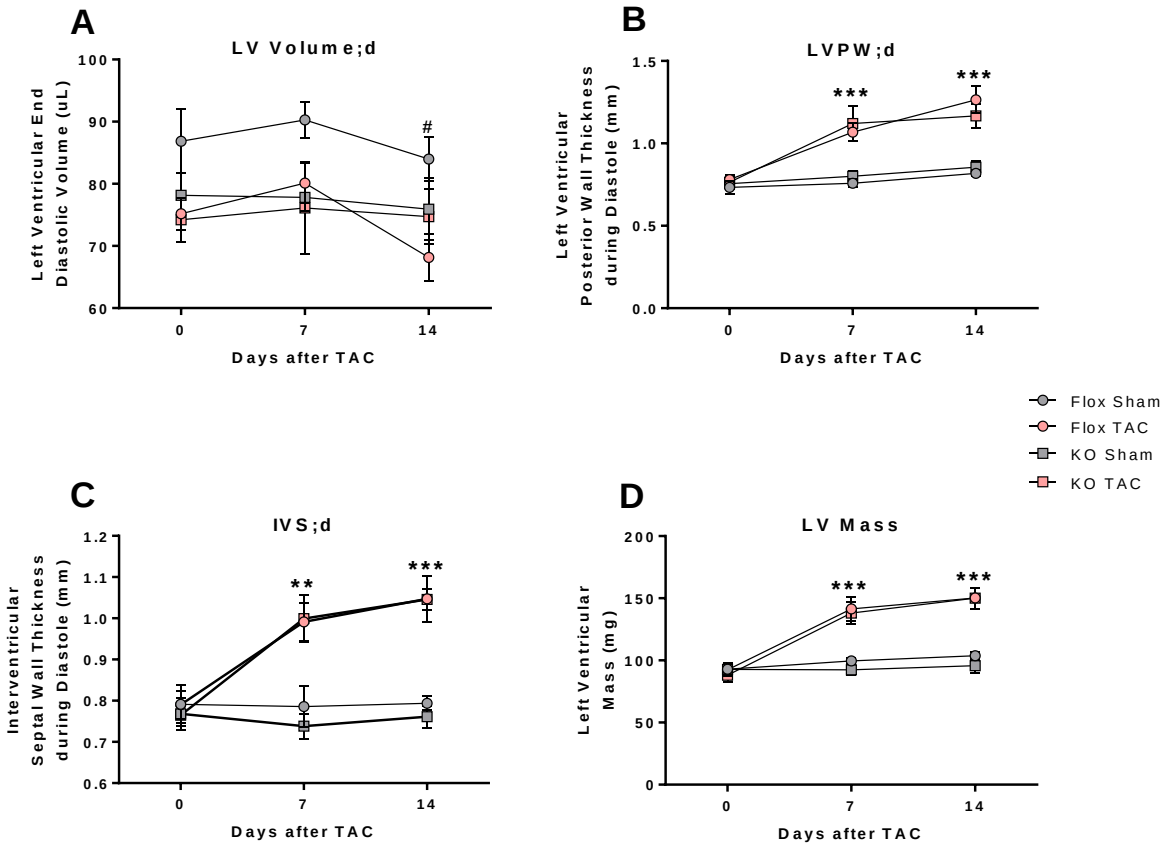

<u>Figure 5-9: Echocardiography-derived cardiac dimensions, indicative of hypertrophy, were increased to the same extent in flox and endothelial cell NOX2 KO TAC mice.</u> **<u>A:</u>** left ventricular end systolic volume, **<u>B:</u>** left ventricular posterior wall thickness during diastole, **<u>C:</u>** intraventricular septal wall thickness during diastole and **<u>D:</u>** left ventricular mass. ***P<0.01*, ****P<0.001* minimum vs. respective sham control for both groups; $^{\#}$*P<0.05* for flox sham vs. endothelial cell NOX2 KO sham after 14 days only; 2way ANOVA with repeated measures and Bonferroni post-test; n=8, 10, 8, 8, respectively.

5.3.3 Cardiac Function

TAC led to profound and sustained cardiac systolic dysfunction in both endothelial cell NOX2 KO mice and their controls, with no change or difference between groups in heart rate (Figure 5-10). Similar to that observed for fibroblast NOX2 flox and KO mice, an approximate 33% reduction in ejection fraction was observed here in TAC mice, mirroring changes in fractional shortening.

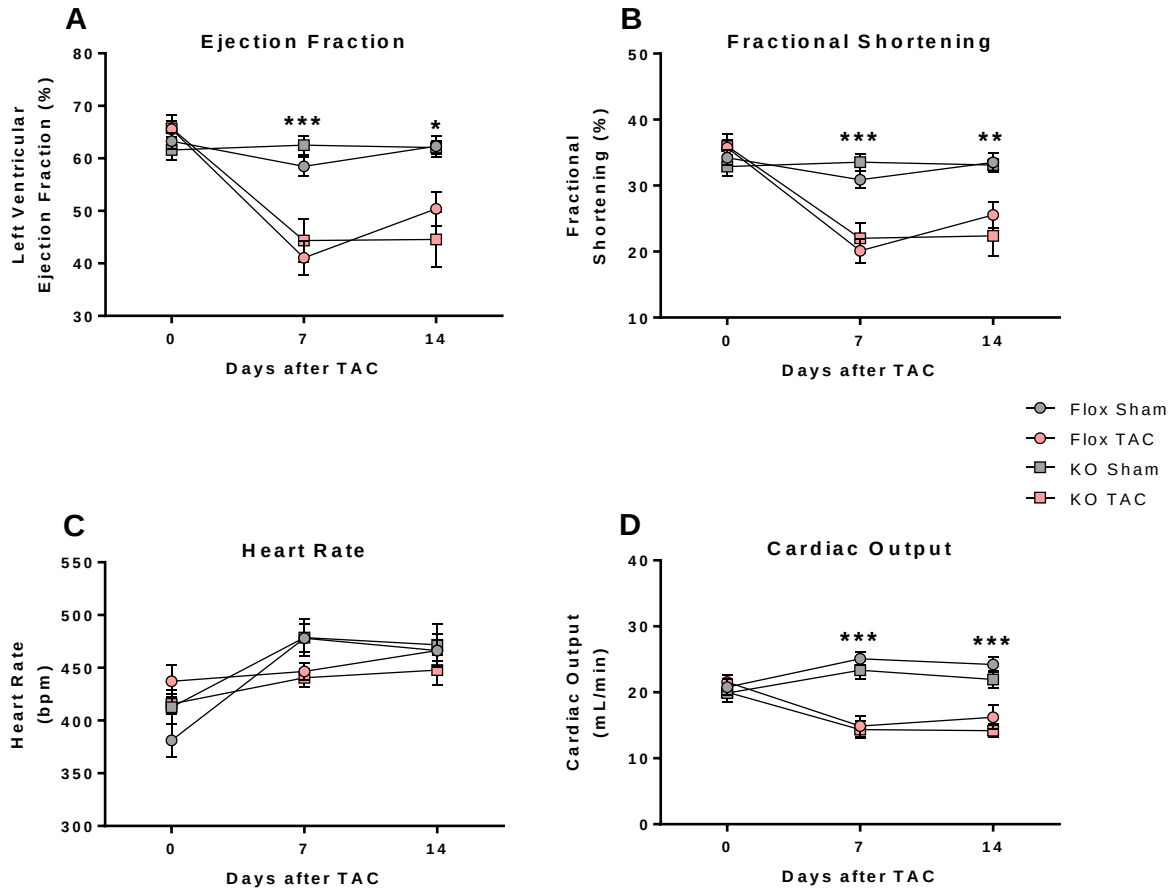

Figure 5-10: Systolic function was reduced to the same extent in flox and endothelial cell NOX2 KO TAC mice as determined by echocardiography. A: Ejection fraction, **B:** fractional shortening, **C:** heart rate and **D:** cardiac output. *$P<0.05$, **$P<0.01$, ***$P<0.001$ minimum vs. respective sham control for both flox and endothelial NOX2 KO TAC mice; 2way ANOVA with repeated measures and Bonferroni post-test; n=8, 10, 8, 8, respectively.

Diastolic dysfunction was evident in both flox and endothelial cell NOX2 KO TAC mice, as determined by echocardiography-derived left atrial area and mitral valve

deceleration time which increase and decrease, respectively (*P<0.05*; Figure 5-11). Isovolumic relaxation time tended to increase in both TAC groups; however this was statistically insignificant (Figure 5-11A). Similar to data obtained in the fibroblast TAC study, E/E' generally decreased in TAC mice, however statistical significance was only obtained for flox TAC mice.

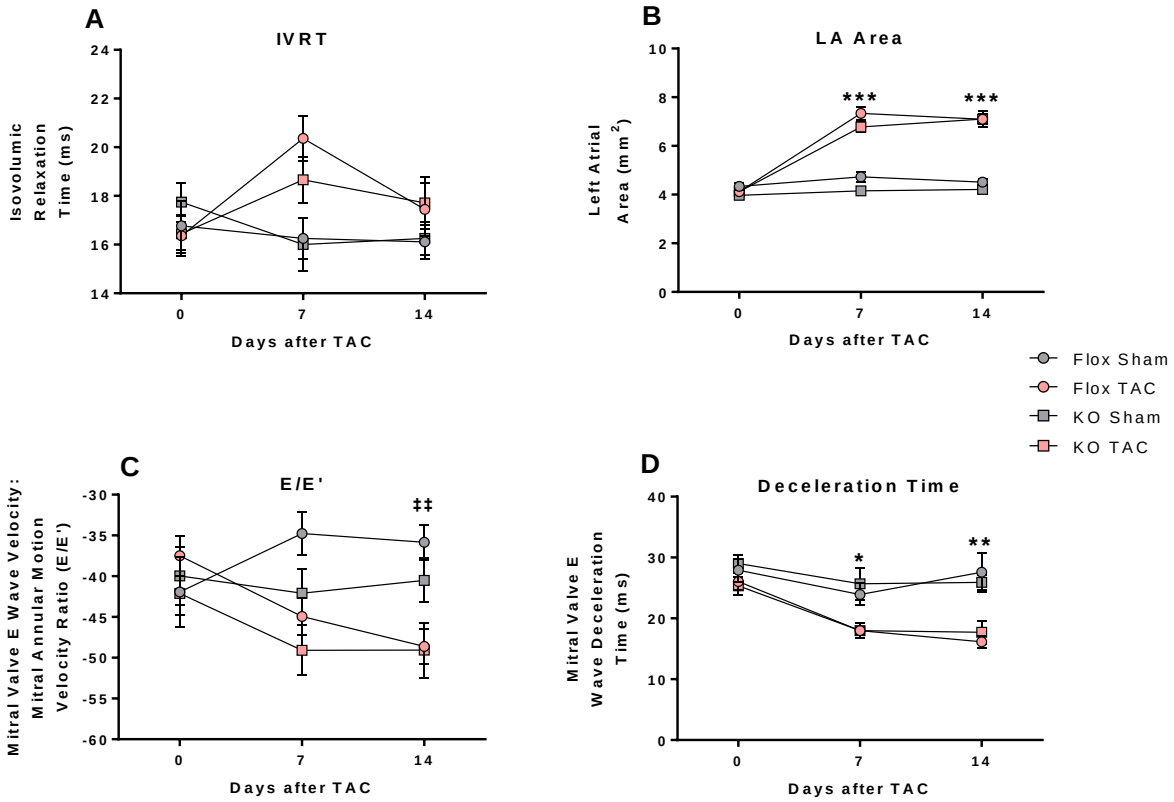

Figure 5-11: Diastolic function was reduced in both flox and endothelial cell NOX2 KO TAC mice as determined by echocardiography. **A:** Isovolumic relaxation time (IVRT), **B:** left atrial (LA) area, **C:** mitral valve 'E' wave velocity to annular motion ratio (E/E') and **D:** mitral valve 'E' wave deceleration time. **P<0.05*, ***P<0.01* and ****P<0.001* minimum vs. respective sham control; ‡‡*P<0.01* vs. respective control for flox only; 2way ANOVA with repeated measures and Bonferroni post-test; n=8, 10, 8, 8.

Echocardiography-derived strain analysis showed profound cardiac dysfunction in TAC mice after surgery (Figure 5-12). Importantly, flox and endothelial NOX2 KO mice have almost identical function, both showed an approximate 40-50% decline in radial

and longitudinal strain and strain rate indices from baseline (day 0) to 14 days after TAC.

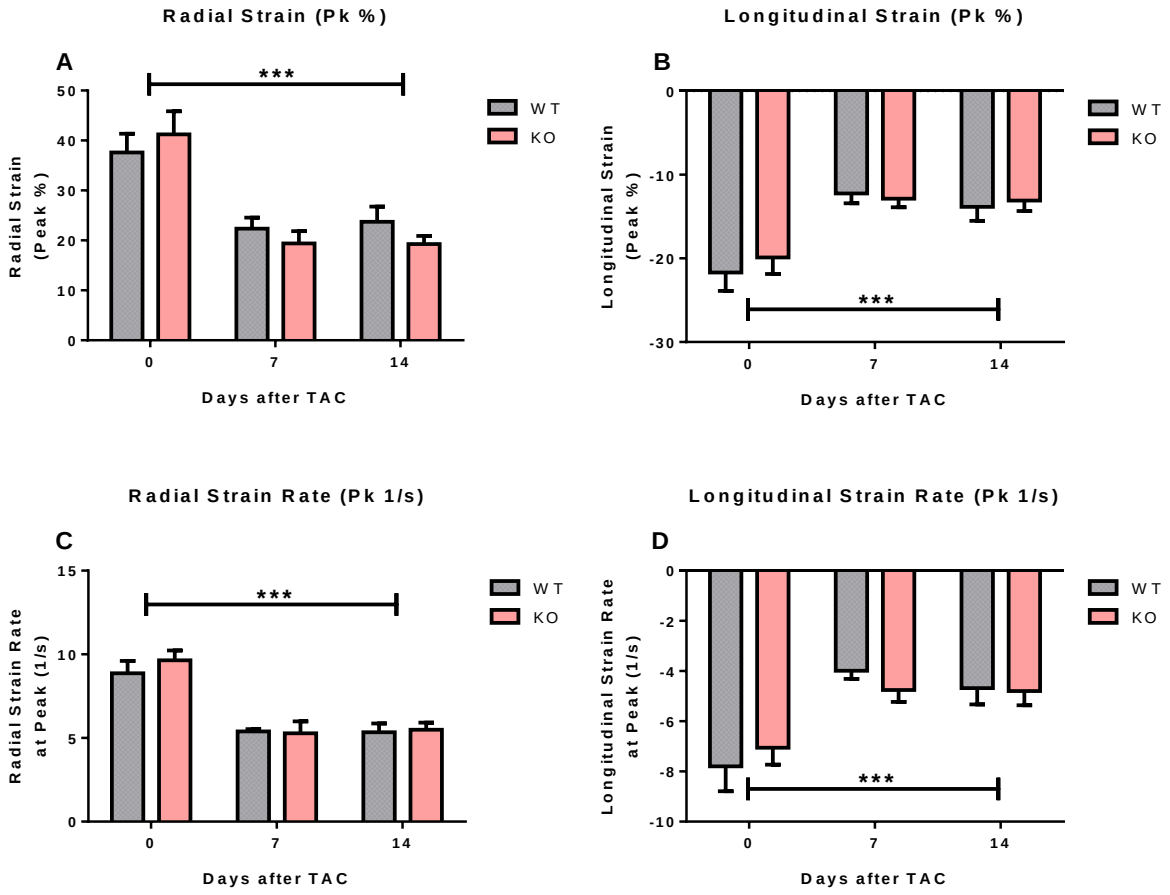

Figure 5-12: Strain and strain rate echocardiography revealed comparable declines in cardiac function for flox and endothelial cell NOX2 KO mice. **A:** Average radial strain as percentage of peak, **B:** average longitudinal strain as percentage of peak, **C:** Radial strain rate at peak per second, **D:** Longitudinal strain rate at peak per second. ****P<0.001* from baseline (0) to 14 days after TAC; 2way ANOVA with repeated measures with Bonferroni post-test; n=6.

Overall these data suggest that endothelial NOX2 does not play a role in the development of cardiac fibrosis, hypertrophy or systolic or diastolic dysfunction after chronic pressure overload due to TAC.

5.4 Discussion

Endothelial cell ROS signalling is implicated in cardiac pathogenesis. As well as inducing endothelial cell activation, endothelial cell NOX2-derived ROS can react with nitric oxide (NO), causing NO inactivation and a reduction in bioavailability.[201] This is important since endothelial-derived NO from endothelial nitric oxide synthase (eNOS) has paracrine actions on cardiomyocytes, limiting deleterious effects during pathology.[193] In particular, eNOS KO mice were shown to have exacerbated left ventricular wall thickening, cardiac dysfunction and fibrosis following pressure overload compared to wildtype mice.[202] Endothelial cell activation is also shown to upregulate vascular cell adhesion modelcule-1 expression,[53] facilitating the attachment and infiltration of circulating leukocytes.

In a previous study from our lab, the overexpression of endothelial cell NOX2 led to augmented cardiac fibrosis in mice subjected to chronic Ang II.[53] With this in mind, it was expected that deletion of endothelial cell NOX2 would lead to a reduction in the development of cardiac fibrosis. In this chapter the TAC model was used to induce cardiac fibrosis, however it is indicated that endothelial cell NOX2 may be dispensable for the development of cardiac fibrosis in this model.

One major consideration is the choice of mouse model. A direct comparison study has not yet been reported, however in general the TAC model might be considered as more severe than chronic Ang II. Chronic Ang II has been reported to cause mixed pressure and volume overload, with mild or negligible cardiac dysfunction,[203] whereas the TAC model is acute onset and one of pressure overload, resulting in profound cardiac dysfunction as observed in the current study. Even so, both models would be expected to induce endothelial cell activation: TAC due to abnormal shear stress, particularly of coronary vessels, and Ang II due to direct endothelial cell activation and progressive hypertension. It is possible however, that the acute onset of pressure overload in the TAC model bypasses the need for endothelial cell NOX2 signalling for the development of cardiac fibrosis. This explanation could also apply to data obtained in chapter 4 for fibroblast NOX2 KO mice subjected to TAC.

Interestingly, data presented here suggested an exacerbation of pro-fibrotic signalling in endothelial cell NOX2 KO mice compared to flox controls subjected to TAC. The

significant increase in collagen 3α1 gene expression is supported by trends towards collagen 1α1 and fibronectin expression, as well as overall fibrotic staining in cardiac section. This upregulation in fibrotic signalling appears to be in the absence of any systolic or diastolic functional consequences, but could nonetheless suggest a role for endothelial cell NOX2 in TAC. Whether this effect suggests a slight protective role for endothelial cell NOX2 or is just a consequence of greater overall hypertrophic remodelling in KO mice is difficult to say.

5.4.1 Cardiac Cell Crosstalk

Cardiac cells are in close proximity to each other and emerging evidence suggests that this enables crosstalk by paracrine actions.[204] Whilst the role of endothelial-cardiomyocyte crosstalk has been investigated, less is known about the role of endothelial-fibroblast signalling. In preliminary experiments using fibroblast and endothelial cell co-cultures, it was surprising that viral overexpression of endothelial cell NOX2 did not seem to increase collagen expression in fibroblasts, nor did it induce fibroblast-myofibroblast trans-differentiation, even with Ang II stimulation.[53]

Further to paracrine effects of endothelial cell signalling, is the ability to change into fibroblasts through the process of EndoMT. This process was first reported in cardiac tissue by Zeisberg and colleagues, [30] showing up to 35% of fibroblasts as having endothelial cell origins in response to pressure overload. The net result is direct contribution of endothelial cells to the fibroblast pool[30] and the promotion of fibroblast-myofibroblast trans-differentiation.[198] Lee et al., showed that CTGF released from EndoMT-derived cells had paracrine actions on fibroblasts, leading to trans-differentiation to myofibroblasts *in vitro*.[198]

Murdoch and colleagues indicated that the augmented fibrotic response to chronic Ang II corresponded to increased EndoMT in endothelial cell NOX2 overexpressing mice.[53] The process of EndoMT was not measured directly in the current study; however an increase in collagen 1α1 and collagen 3α1 mRNA was observed, likely corresponding to increased fibroblast numbers and/or activity. In addition, quantified CD31 mRNA, used as a marker for endothelial cells, was unchanged after TAC for both genotypes, which suggested that total endothelial cell numbers are not altered by TAC after 14 days. This points towards a lack of EndoMT, though it is a weak method

and firm conclusions cannot be drawn. Another consideration is the time frame of EndoMT; a detailed study showed that endothelial cell numbers are only decreased in the initial 2-3 days following TAC, returning to baseline levels by 7 days.[172] If this study is correct, then a 14 day snapshot would not be expected to provide evidence of EndoMT.

5.4.2 *Tie2* vs. *Cdh5*

Both tunica intima endothelial kinase 2 (*Tie2*) and VE-cadherin (*Cdh5*) Cre-recombinase promoters have been used for endothelial cell-specific recombination. The endothelial NOX2 overexpression study by Murdoch[53] took advantage of the *Tie2* promoter, whereas the *Cdh5* promoter was used in the current study. Recently, it has been described that *Tie2* will also target cells of haematopoietic origin, such as leukocyte subsets.[205] In contrast, the *Cdh5*-CreER(T2) construct is reported to have minimal leakage into the haematopoietic lineage, labelling less than 1% of bone marrow cells.[130] Considering this difference, it is possible that NOX2 overexpression using the *Tie2* promoter[53, 124] may, in addition to endothelial cells, target leukocytes which are known to infiltrate during chronic Ang II stimulation. As such, in the case of augmented cardiac fibrosis, leukocyte-specific effects could be mistaken for endothelial-specific effects. This is an important consideration, though the dependence on bone marrow-derived cells for the development of cardiac fibrosis was ruled out using a global NOX2 KO bone marrow transplant approach.[53]

5.4.3 Future Directions

As discussed, endothelial cell NOX2 KO mice were not protected from developing cardiac fibrosis, dysfunction or any other deleterious effect of TAC, similar to results obtained for fibroblast NOX2 KO mice. Taking these two studies together, one conclusion is that in TAC, NOX2 from a range of cellular sources combine to produce fibrosis and dysfunction and as such, single cell-specific NOX2 deletion may not lead to noticeable protective effects. This would be technically challenging to determine, since a combination of double and possibly triple cell-specific knockouts would be required.

A key experiment would be to investigate the effects of endothelial NOX2 deletion in a chronic Ang II model. Fibroblast NOX2 was shown as important in the development

of Ang II-induced hypertension and cardiac fibrosis and it would be interesting to see if endothelial cell NOX2 KO mice respond in the same way. If endothelial cell NOX2 KO mice were protected from Ang II-induced fibrosis and hypertension, this would add further strength to the idea of stimulus-dependent NOX2 activity.

5.4.4 Summary

Data presented in this chapter strongly suggest that endothelial cell NOX2 is dispensable in the development of TAC-induced cardiac fibrosis. This is somewhat unexpected owing to the reported effects of endothelial cell NOX2 overexpression in Ang II-treated mice; however the stimulus difference is likely to be a determining factor. Studies are ongoing to determine the effect of endothelial cell NOX2 deletion in mice in response to chronic Ang II.

CHAPTER 6: Endothelial-Mesenchymal Transition (EndoMT) in Cardiac Fibrosis

6.1 Introduction

Fibroblasts play a key role in extracellular matrix homeostasis and as such, are thought to be responsible for the generation of fibrosis. The exact origin of these fibroblasts remains disputed, however, with some evidence suggesting that endothelial-mesenchymal transition (EndoMT) gives rise to a large proportion of proliferative and fibrosis-inducing fibroblasts, mediated by TGFβ.[5, 30] As discussed in chapter 5, EndoMT is a process by which cells lose their endothelial-specific markers, e.g. CD31, in favour of mesenchymal markers similar to fibroblasts, e.g. alpha smooth muscle actin. EndoMT-derived cells appear spindle-shaped, similar to that of fibroblasts, and also express collagen 1 and fibronectin.[30]

This phenotypic switch has recently become an area of research interest with a number of reports across a variety of tissues and disease models, including renal fibrosis,[206] liver fibrosis,[207] pulmonary fibrosis[208] and cardiac fibrosis induced by experimental hypoxia,[209] diabetes,[52] chronic neurohumoral stimulation,[53] pressure overload[30] and myocardial infarction.[210]

6.1.1 EndoMT in Cardiac Fibrosis

In a landmark study by Zeisberg and colleagues in 2007 it was found that up to 35% of fibroblasts in fibrotic myocardium were of endothelial origin in mice subjected to chronic pressure overload.[30] In this study, the authors performed lineage tracing of mouse endothelial cells by labelling them with LacZ via a *Tie1*-promoted Cre recombinase. The authors claim that these mice permanently express LacZ specifically in endothelial cells, such that LacZ will still persist following subsequent proliferation, transition or differentiation. Following TAC pressure overload, LacZ expressing endothelial cells were found distributed throughout the fibrotic regions of the myocardium and also stained positive for fibroblast-specific marker-1 (FSP-1), in contrast to sham-operated mice. Flow cytometry of cardiac single cell suspensions revealed a reduction in $LacZ^{+}CD31^{+}$ cells in favour of $LacZ^{+}CD31^{-}$ cells. Furthermore these $LacZ^{+}CD31^{-}$ cells had greater expression of αSMA, FSP-1, DDR2 and collagen 1α1 fibroblast markers, indicating endothelial cells were losing their specific markers in favour of mesenchymal markers.[30] Importantly, the authors were able to show a dependence on TGFβ1 signalling via Smad3, both *in vitro* and *in vivo*.

6.1.2 Involvement of Reactive Oxygen Species

Owing to the ROS-dependent activation of TGFβ, it is logical to suggest that NOX2 activation may contribute to EndoMT and subsequent cardiac fibrosis. In a transgenic endothelial cell-specific NOX2 overexpression model, mice were found to have increased cardiac fibrosis vs. wildtype following chronic treatment with pressor Ang II.[53] In addition, transgenic hearts also had increased αSMA and collagen 1 protein expression, as well as reduced CD31 expression vs. wildtype. There was also enhanced co-localisation of endothelial and mesenchymal markers in transgenic heart sections compared to wildtype and similar results were found using cultured human aortic endothelial cells.[53] These data suggest an increase in EndoMT as a direct result of enhanced endothelial cell NOX2 activation following chronic Ang II stimulation.[53]

6.1.3 Lineage Tracing

In the absence of a truly fibroblast-specific marker, many previous reports have identified fibroblasts using αSMA,[30, 53] FSP-1,[30, 53] DDR2[30] and vimentin,[211] all of which have now been shown to label other lineages, in particular endothelial cells ($CD31^+$),[5, 197, 212] smooth muscle cells ($SM22^+$) and leukocytes ($CD45^+$).[212] Cellular co-expression of a fibroblast and an endothelial cell marker indicated evidence of ongoing EndoMT; however the lack of marker specificity will have no doubt clouded conclusions, since these so-called fibroblast markers were in fact already labelling endothelial cells.

A better approach is to use lineage-specific reporter mice to permanently label cells of interest, prior to applying a disease model. For example, endothelial cells can be tagged with a fluorescent protein using the Cre-LoxP system and then subjected to pressure overload.[213] The behaviour of so-called lineage traced cells can be tracked across its lifetime, including gene expression patterns, tissue location and distribution patterns, morphology, activity and in addition, cells will pass on the fluorescent label to all progeny following proliferation.[133] In the context of EndoMT, lineage traced endothelial cells can be examined for evidence of phenotype switching, i.e. the expression of fibroblast markers and morphological changes, making this a very powerful tool.

A further advantage of permanently tagging cells is to give an indirect measure of Cre-recombinase efficiency, or in other words, how effective the extent of knockout

is.[205] This can be estimated by crossing an established Cre-recombinase mouse line with a STOP-floxed reporter line. A common reporter is LacZ (β-galactosidase/X-gal reaction to produce 5,5'-dibromo-4,4'-dichloro-indigo), used in the characterization of both *Col1α2*[132] and *Cdh5*[130] Cre-recombinase mice, but simpler reporters are now used, including green fluorescent protein (GFP) and tdTomato.[134, 135, 213] Upon tamoxifen induction, the percentage of lineage marker$^+$ cells also expressing the reporter protein gives an estimation of Cre-recombinase efficiency. This approach can be applied to flow cytometry, giving a quantitative readout of estimated Cre-recombinase efficiency. This data is useful when considering the magnitude of effect of gene deletion in Cre-LoxP gene knockout studies.

6.1.4 EndoMT in Cardiac Fibrosis or Myth?

Despite evidence in support of EndoMT, recent and thorough research from Moore-Morris and colleagues suggested that EndoMT did not occur in the context of pressure overload-induced cardiac fibrosis.[213] Instead, the authors propose that fibroblasts arise from resident fibroblast lineages. Collagen 1α1 (*Col1α1*)-GFP reporter mice were characterized for their ability to identify cardiac fibroblasts, showing strong co-localisation of GFP$^+$ cells with the fibroblast markers CD140α and vimentin. These fibroblast reporter mice were then crossed with *Tie2* or *VE-Cadherin* Cre-tdTomato reporter mice, meaning that fibroblasts were tagged green and endothelial cells were tagged red. Small subsets of fibroblasts were found to be of endothelial origin in naive mice, thought to represent EndoMT-driven atrioventricular cushion development. Importantly, when these mice were subjected to TAC, the authors showed no evidence for EndoMT, since the proportion of lineage traced *Tie2*-tdTomato$^+$*Col1α2*-GFP$^+$ cells did not increase and GFP$^+$ *VE-Cadherin* lineage traced cells were extremely rare in cardiac tissue devoid of developmental EndoMT-derived cells.[213]

This work has been supported by another laboratory, who concluded that cardiac myofibroblasts arise from tissue-resident fibroblasts following acute myocardial infarction.[129] In this study Kanisicak and colleagues linage traced myofibroblasts (eGFP$^+$) using the periostin (*Postn*) Cre, showing that these cells did not arise from endothelial lineages.[129] To further complicate matters, there is recent evidence in

support of mesenchymal-endothelial cell transition following ischaemia-reperfusion cardiac injury, the reverse process of EndoMT, although this is the only report of its kind so far.[135]

In light of recent lineage tracing advances and an increased interest in EndoMT, this chapter describes the establishment, characterization and use of tdTomato-labelled mice in the laboratory.

6.1.5 Aims

The first aim of this chapter was to use tdTomato mice to determine an estimation for the degree of *Col1α2* and *Cdh5* Cre-mediated NOX2 deletion in mice (chapters 3, 4 and 5), so-called Cre efficiency. It is known that low and/or non-specific Cre recombinase activity can explain the absence of a phenotype in KO mice and it was deemed important to rule this out.

The second aim was to quantify the extent of EndoMT in TAC mice, using tdTomato lineage tracing of endothelial cells and flow cytometry. This aim also required the accurate estimation of *Cdh5* Cre efficiency.

6.2 Methods

6.2.1 In Vivo Methods

Generation of Experimental Mice

Male *Cdh5*CreER(T2) or *Col1α2*CreER(T) mice were crossed with female ROSA26R-tdTomato$^{flox/flox}$ mice to generate experimental *Cdh5*CreER(T2):*ROSA26R*-tdTomato$^{flox/flox}$ (EndoTom) or *Col1α2*CreER(T):*ROSA26R*-tdTomato$^{flox/flox}$ (FibroTom) reporter mice, respectively. Cre-positive progeny were expected to have permanent tdTomato-labelled endothelial cells or fibroblasts following daily *i.p.* injection with 1mg tamoxifen in peanut oil for 3 or 10 days, respectively.

Mice were genotyped by ear biopsy as described in chapter 2 and homozygous tdTomato "STOP" floxed mice were used for experiments (Figure 6-1).

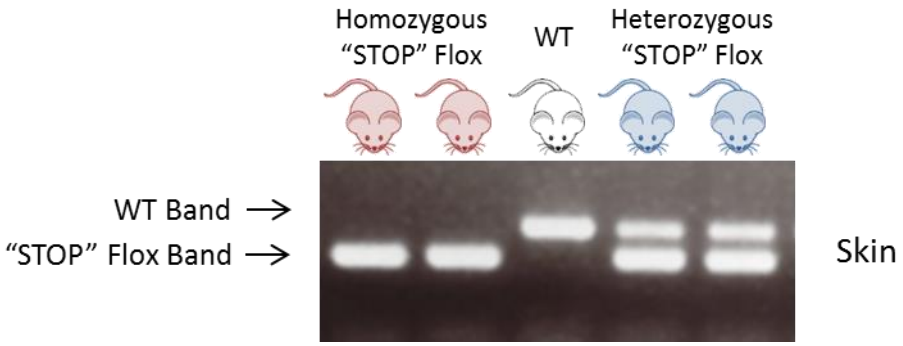

Figure 6-1: PCR-based genotyping of reporter mice using DNA gel analysis. Primers recognised the wildtype (WT) ROSA26 and mutant ROSA26-tdTomato alleles. A single upper band (297 bp) indicated wildtype (WT), a single lower band (196 bp) indicated homozygous "STOP" flox and both bands together (297 bp + 196 bp) indicated heterozygous "STOP" flox mice.

Transverse Aortic Constriction

Transverse aortic constriction (2 weeks) was performed as described in chapter 2, with echocardiography used to determine successful TAC 1 day later as described.

Primary Cardiac Cell Isolation

FibroTom or EndoTom reporter mice were killed by cervical dislocation. An abdominal incision was made and continued up to the thorax to expose the heart. The right atrium was cut and the left ventricle perfused with approximately 1mL saline or PBS to remove circulating blood. The atria were removed and the remaining heart excised

and placed into a pot of ice cold PBS. Heart tissue was disrupted to small (1mm^2) pieces using scissors. Collagenase type II (Worthington Biochemicals; Lakewood, NJ) was reconstituted to 1200 units/mL in pre-warmed serum-free growth medium (Dulbecco's Modified Eagle's Medium (DMEM); Cat# D6546, Sigma, UK). PBS was aspirated from the disrupted tissue and replaced with 1.5mL collagenase media before being incubated with agitation (200rpm) at 37°C for 10 minutes. A further 1.5mL of fresh collagenase was added and tissue chunks were triturated to aid digestion. The suspension was then further incubated for an additional 30 minutes. Enzymatic digestion was arrested by doubling the volume with media containing 10% foetal bovine serum (FBS). Avoiding frothing, cells and remaining tissue chunks were triturated ≥10 times by passing through a 21G needle, followed by a 23G needle to further promote a single cell suspension. Cells were centrifuged at 1200 rpm for 5 minutes, then resuspended in 2mL cold flow cytometry buffer (PBS with 0.4% EDTA and 0.4% FBS) per heart, maintained on ice throughout and protected from light where possible.

Alternatively, cells were resuspended in 5mL fresh warm growth medium with 10% FBS, supplemented with penicillin and streptomycin and transferred to a T25 cell culture flask and incubated at 37°C.

6.2.2 Flow Cytometry

Flow Cytometry Concepts

Flow cytometry is a powerful tool for the quantitative analysis of the optical properties of single cells within a suspension. A flow cytometer can be broken down to 3 essential systems (Figure 6-2). Firstly, the fluidics system uses sheath fluid to hydrodynamically focus the cell suspension into a single cell beam, which is presented to the flow cell. The flow cell is an interrogation point where the optical properties of a cell are analysed. Secondly, the optics system has two components; excitation optics and collection optics. The excitation optics system uses a range of lasers to introduce light to the flow cell and the collection optics systems collects scattered light from the flow cell as a result of light-cell interactions. In addition, the collection optics system uses dichroic mirrors and specific wavelength filters to direct light to specific detectors. Lastly, the electronics system amplifies and converts the optical

signals reaching the detectors into proportional electronic signals, detailing the optical footprint of the cell.

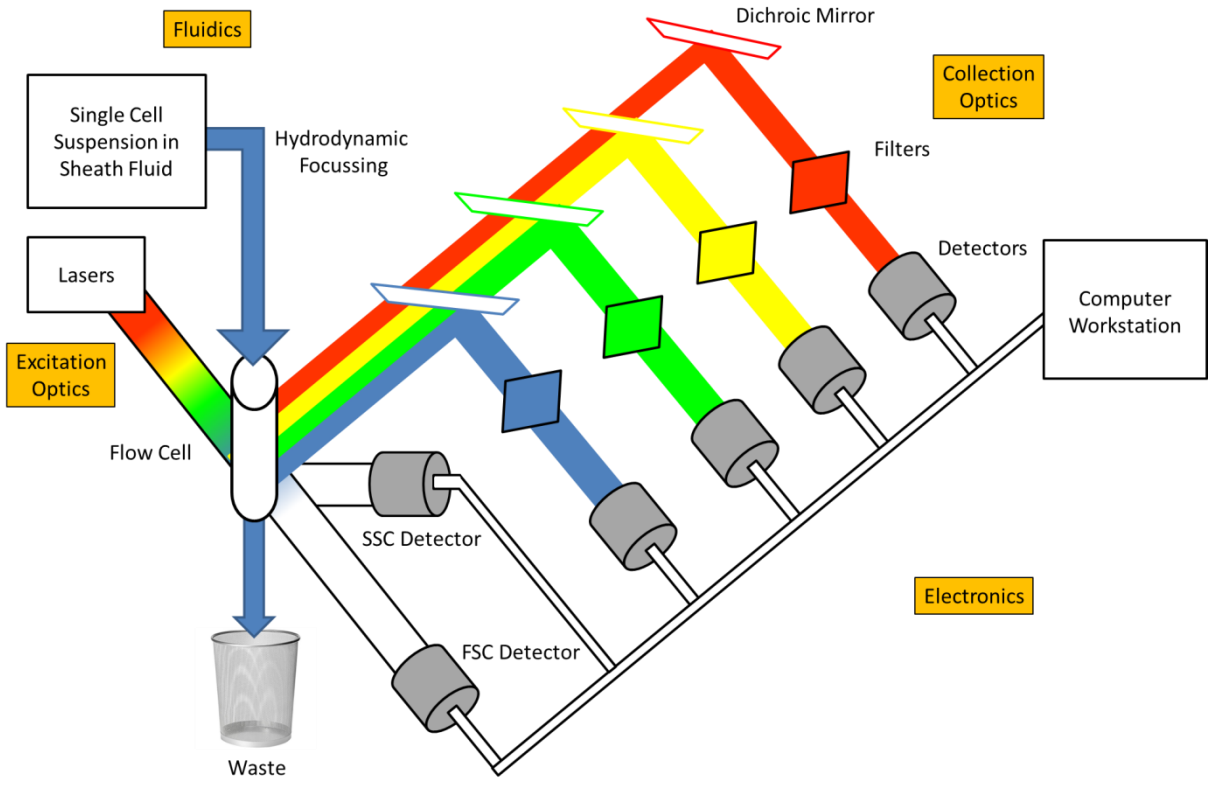

Figure 6-2: Fluidics, optics and electronic components of a typical flow cytometer. The single cell suspension is hydrodynamically focussed and passed through the flow cell via the fluidics system. Scattered light from coloured lasers reaches specific detectors and the information is converted to a digital signal via the electronics. After passing through the flow cell, cells are discarded or can be sorted based on fluorescence for downstream applications. The FSC and SSC detectors report the size and granularity of each cell, respectively.

Scattered light is detected in terms of forward and side scattered light (FSC and SSC, respectively) for size and granularity analysis. In addition, flow cytometers use a range of colour lasers which emit excitation light of a specific wavelength. In a typical flow cytometry experiment, cell suspensions are stained with fluorophore-conjugated antibodies against proteins of interest, which ideally have a distinct, narrow range of excitation/emission wavelength properties. Further to this, optical filters have a specific wavelength median and range for the passage of light, and will absorb or reflect non-suited light. For example a 530/30 filter allows scattered light of

wavelength 515nm-545nm to be detected. As such a 488nm laser used with a 530/30 filter will excite and detect fluorescein isothiocyanate (FITC)-conjugated antibodies, but not allophycocyanin (APC)-conjugated antibodies (Table 6-1). Cells can therefore be stained with multiple conjugated antibodies, enabling multicolour analysis.

Table 6-1: List of conjugated fluorophores used in flow cytometry experiments and the lasers by which they were excited. Note that tdTomato was detected as a phycoerythrin (PE) fluorophore.

Flow Cytometer	Laser (Colour)	Filter/	Fluorophore
BD Accuri C6	488nm (Blue)	533/30	FITC
		585/40	PE
	640nm (Red)	675/25	APC
BD FACSCanto II	488nm (Blue)	530/30	FITC
		585/42	PE
	633nm (Red)	660/20	APC
BD LSR Fortessa	488nm (Blue)	530/30	FITC
	561nm (Yellow/Green)	585/15	PE
	633nm (Red)	670/30	APC

Cell Staining

Flow cytometry was performed in round-bottomed flow cytometry tubes (Falcon, Corning, UK) on a 200µL aliquot of cells per sample, including an unstained control. Cells were incubated with primary antibody (see Table 6-2) for 30 minutes. Non-specific staining was removed by washing via the addition of 2mL cold flow cytometry buffer and centrifugation at 1200 rpm. Cells were then resuspended in 200µL cold flow cytometry buffer before running samples on the flow cytometer (BD Accuri C6, BD FACSCanto II, or BD Fortessa, BD Biosciences). Note that for DDR2 staining, cells underwent a second incubation with Alexa Fluor® 488-conjugated anti-goat

secondary antibody (A-11078, ThermoFisher Scientific, UK; excitation/emission max 495/519nm).

Samples were run initially at slow speed (14µL/minute) using a maximum threshold of 1,000,000 cells. Data was analysed and presented using FlowJo software (FlowJo LLC, OR, USA).

Table 6-2: List of primary conjugated antibodies and their dilutions used in flow cytometry experiments. All antibodies are anti-mouse and developed in rat, except where stated*. Additionally, the reporter, tdTomato, is similar to PE and discosoma sp. red (DsRed) and has maximum excitation at 554nm and maximum emission at 581nm. No staining was required as the reporter is expressed by cells *in vivo*.

Primary Antibody	Conjugated Fluorophore (Ex/Em Max.)	Source (Catalogue number)	Clone	Dilution
CD140α (PDGFRα)	FITC (494/520nm)	eBioscience (11-1401-80)	APA5	1:40
CD31 (PECAM-1)	FITC (494/520nm)	eBioscience (11-0311-81)	390	1:40
CD144 (VE Cadherin)	APC (650/660nm)	eBioscience (17-1441-80)	eBioBV13	1:40
CD90.2 (Thy-1.2)	FITC (494/520nm)	eBioscience (11-0903-81)	30-H12	1:40
CD31 (PECAM-1)	APC (650/660nm)	eBioscience (17-0311-82)	390	1:80
CD201 (EPCR)	APC (650/660nm)	BioLegend (141505)	RCR-16	1:40
CD167b (DDR2) *goat	N/A	Santa Cruz (sc-7555)	N-20	1:20

Voltage Setting

Detected cells are recorded as voltages in flow cytometry. When using the BD FACSCanto or BD Fortessa, an unstained control sample was used to adjust cellular event voltages on FSC-A and SSC-A and for each colour channel used. This was to optimise the signal to noise ratio for recorded events, meaning that negative populations were recorded on the far left of the graph, allowing easy detection of positive populations. A single stained control was then used to further optimise the detection of positive populations. Voltages were then kept constant for each experiment.

Voltage setting was not necessary on the BD Accuri C6 and negative events usually arose before the third log decade.

Flow Cytometry Compensation

Although flow cytometry detectors are aligned to detect specific wavelengths, it is common for fluorescence emitted from a single fluorophore to spill over into another detectors channel. This is known as spectral overlap and leads to false positives in multicolour experiments. The effect of spectral overlap can be eliminated by using appropriate compensation controls in every experiment.[214] Compensation was performed manually using single-stained control samples on the BD Accuri C6, an example compensation matrix is detailed in Table 6-3 (note that channel 3 is not used owing to high spectral overlap between channel 2 and 3). Compensation was applied automatically using single-stained controls on the BD FACSCanto or BD Fortessa via the BD FACSDiva™ acquisition software (BD Biosciences, v8).

Table 6-3: Commonly used compensation matrix for BD Accuri C6 flow cytometer.

Values represent the percentage spectral overlap from channel to channel, e.g. channel 2 spills into channel 4 by 5%. Note that the compensation matrix changed slightly for each experiment.

	Channel 1-A	Channel 2-A	Channel 4-A
Channel 1-A	100%	7%	0.4%
Channel 2-A	7%	100%	5%
Channel 4-A	0%	0%	100%

Flow Cytometry Gating and Analysis of Cardiac Cells

All flow cytometry events were registered on FSC-A and SSC-A for x- and y-axis, respectively. Cardiac cells were gated according to the schematic shown in Figure 6-3. For each round of gating, the main populations of events were manually selected and taken forward. For round one, cells were gated on FSC-A and SSC-A (Figure 6-3A – "cells") for debris exclusion. For round two, cells were gated on FSC-A and FSC-H (Figure 6-3B – "single cells") for doublet exclusion. For the final round, cells were gated on SSC-A and SSC-H (Figure 6-3C) – "single cells") for a second doublet exclusion. Lastly, positive/negative gates were placed on histograms for each fluorescence channel, ensuring less than 1% positivity on an unstained sample (Figure 6-3D-F). This gating strategy was then applied to all samples in the experiment and further adjusted if needed for analysis.

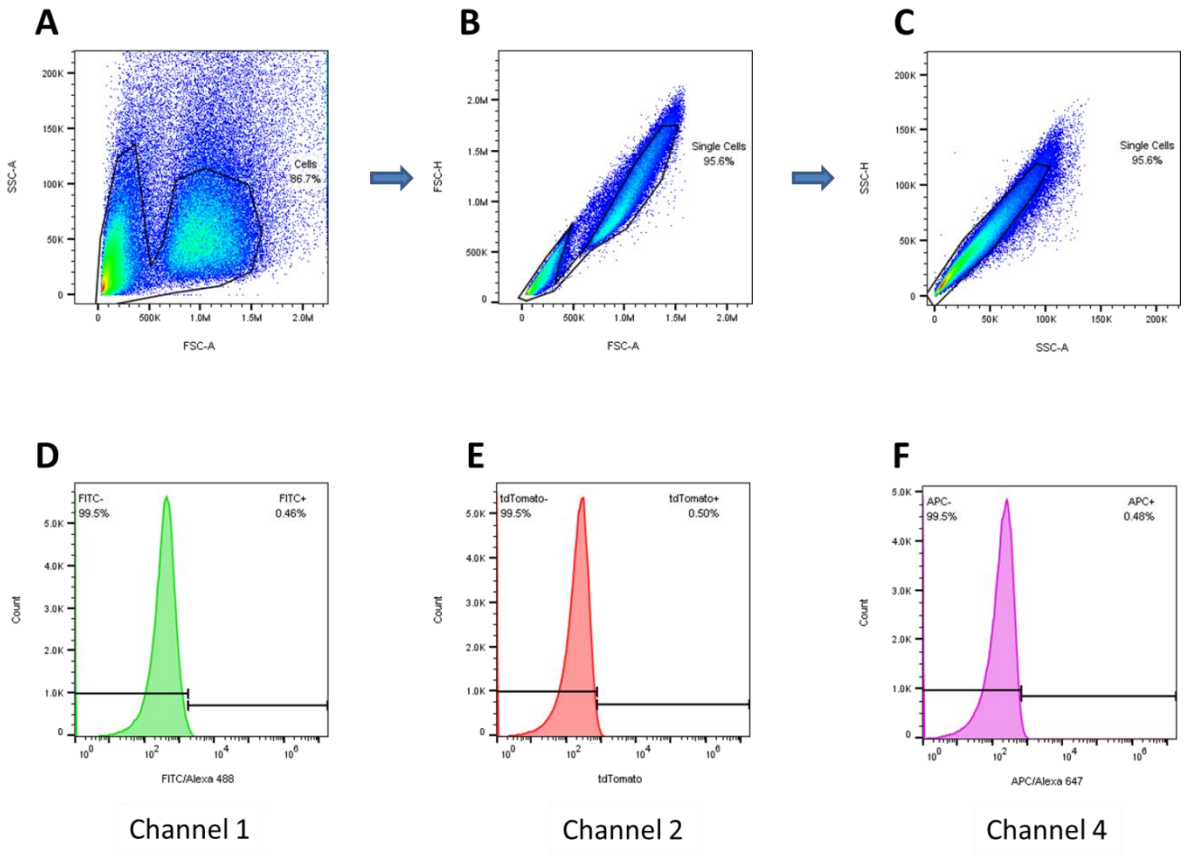

Figure 6-3: Basic flow cytometry gating strategy for cardiac cells. Main populations of cells are selected and taken forward on FSC-A vs. SSC-A **(A)**, FSC-A vs. FSC-H **(B)** and SSC-A vs. SSC-H **(C)**. Positive/negative gates were then placed on fluorescence-specific channel histograms for FITC/Alexa 488 **(D)**, tdTomato **(E)** and APC/Alexa 647 **(F)**.

During cell isolation and staining steps, some cells may die and begin to take up fluorescent dye non-specifically. This skews data and gives false positives. Dead cells were excluded from initial experiments using the dead cell stain 7AAD in fluorescence channel 3 (Figure 6-4). Analysis showed that there was generally less than 1% dead cells on average. Dead cell exclusion was not performed in subsequent experiments, owing to the high spectral overlap between channels 2 and 3, as discussed above.

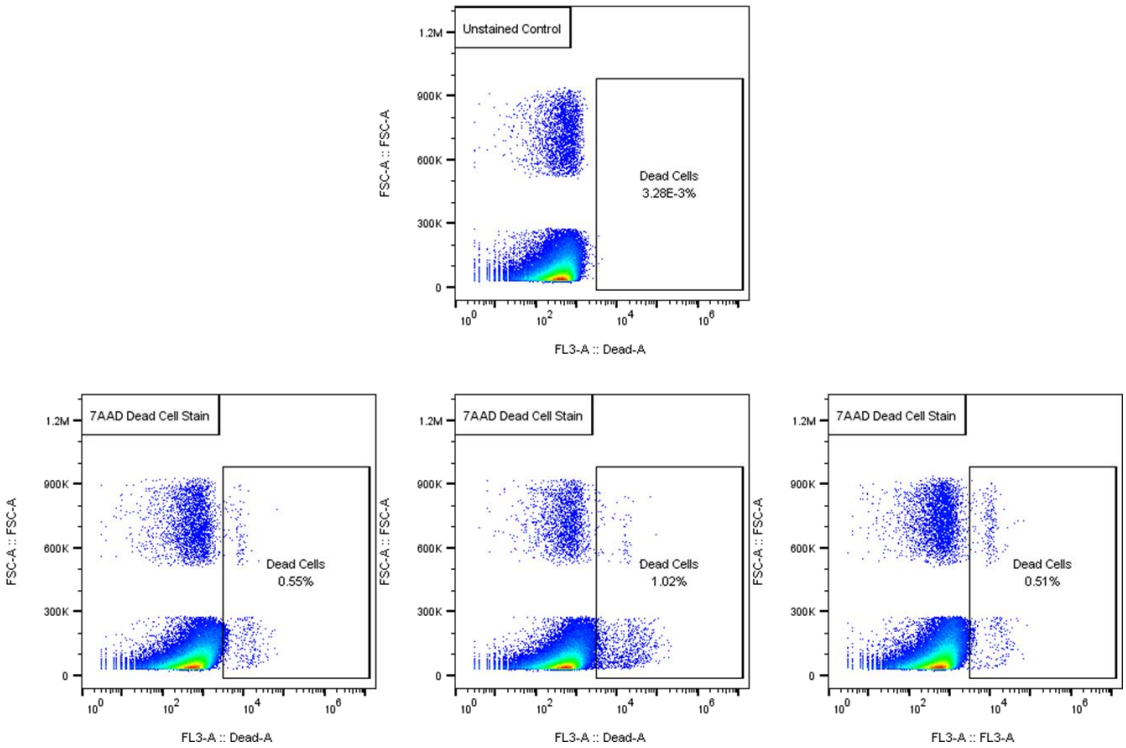

Figure 6-4: Dead cell exclusion using the dead cell marker 7AAD. An unstained control (upper panel) was used to set a positive gate for 7AAD+ (dead) cells (lower panels) showing an average of less than 1% dead cells. Data is taken from 3 separate experiments.

For experiments involving multiple fluorophores, fluorescence minus one (FMO) control samples were used to set positive and negative gates. Essentially, these controls contain all experimental fluorophores except for the named fluorophore. For example, positive and negative gates will be set for the FITC channel using a FITC FMO sample (containing FITC and APC). Using such controls is more accurate, since the presence of multiple fluorophores in one sample can artificially augment the fluorescence signal.

Col1α2 Cre-recombinase Efficiency

Cell suspensions from FibroTom reporter mice were single stained with a fibroblast antibody: CD140α-FITC or CD90-FITC.

Alternatively, freshly isolated cardiac cells from FibroTom reporter mice were seeded onto a T25 flask and allowed to adhere for up to 72 hours. The flask was washed with PBS and non-adherent cells discarded. Remaining cells were detached using trypsin (ThermoFisher Scientific, UK) and washed in growth medium, before being centrifuged and re-suspended as above. Flow cytometry was then performed on these cells as described.

The *Col1α2* Cre-recombinase efficiency was defined as the percentage of fibroblast marker$^+$ cells also expressing tdTomato fluorescence (e.g. CD140α$^+$tdTomato$^+$).

Cdh5 Cre-recombinase Efficiency

Cell suspensions from EndoTom reporter mice were stained with an endothelial cell antibody: CD31-APC, CD31-FITC, CD201-APC or CD144-APC. Flow cytometry was performed and analysed as described. The *Cdh5* Cre-recombinase efficiency was defined as the percentage of endothelial cell marker$^+$ cells also expressing tdTomato fluorescence (e.g. CD31$^+$tdTomato$^+$). Cre-recombinase specificity was defined as the percentage of tdTomato$^+$ cells also expressing an endothelial cell marker (e.g. tdTomato$^+$CD31$^+$). This measure reflects how specific the *Cdh5*-driven Cre-recombinase is at targeting tdTomato expression to endothelial cells.

Determination of Endothelial-Mesenchymal Transition

Male EndoTom reporter mice subjected to 14 days TAC were killed by cervical dislocation and cardiac cells isolated as described. Cardiac cells were stained with CD31-APC and CD140α-FITC or CD201-APC and CD90-FITC antibodies, followed by flow cytometry and analysis as described. The experimental overview and possible outcomes are detailed in Figure 6-5. In brief, tdTomato$^+$ cells from TAC mice were assessed for their expression of fibroblast markers. The percentage of tdTomato$^+$ fibroblast marker$^+$ cells was compared to EndoTom reporter sham controls. In addition, lungs were excised and processed as described for cardiac tissue, including isolation of lung cells, staining and flow cytometry.

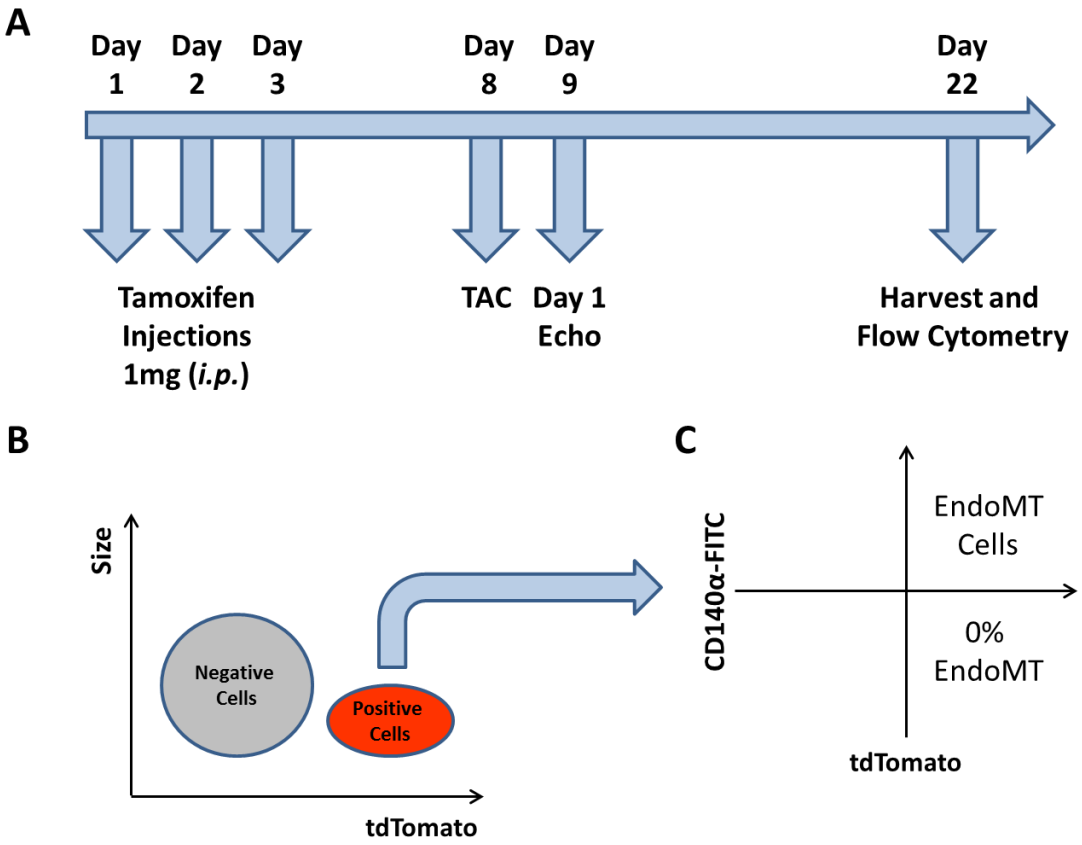

Figure 6-5: Experimental plan to determine the extent of endothelial-mesenchymal transition in EndoTom reporter mice subjected to TAC. **A:** Experimental timeline, including day 1 echocardiography for the estimation of TAC gradient. **B:** tdTomato^{+} cells are identified and **C:** examined for expression of the fibroblast marker CD140α. Cells falling into the upper right quadrant would be regarded as fibroblasts with endothelial cell origins i.e. EndoMT cells.

6.3 Results

6.3.1 FibroTom Reporter Mice

Further Characterization

Following tamoxifen treatment for 10 days, exposed skin of FibroTom reporter mice was visibly pink/red and with quantitatively higher tdTomato fluorescence compared to Cre-negative controls when placed in a bioluminescence scanner (Figure 6-6). This indicated successful Cre-recombinase activity and recombination in skin fibroblasts.

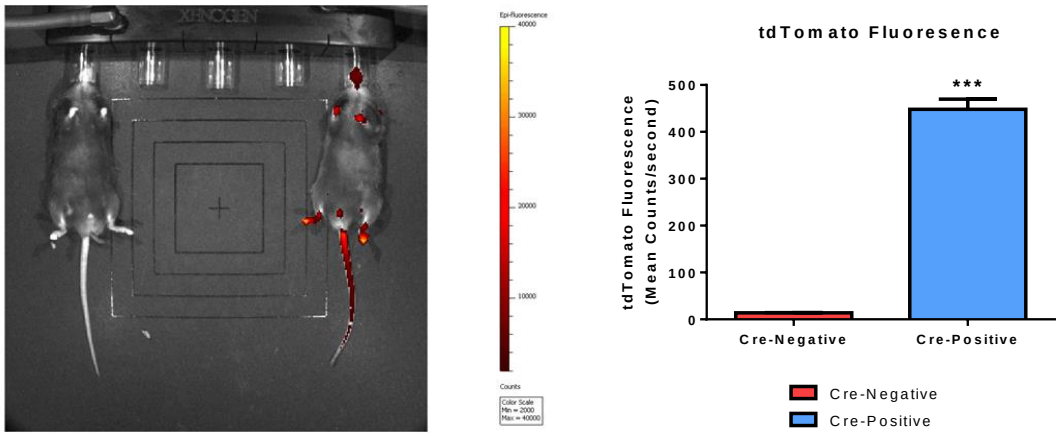

Figure 6-6: Successful Cre-recombinase activity in *Col1α2*CreER(T):ROSA26-tdTomatoflox/flox (FibroTom) mouse skin fibroblasts. Left: Cre-negative and **right:** Cre-positive mice were scanned in a bioluminescence scanner set to detect tdTomato fluorescence. Fluorescence counts were quantified and are shown on the right-hand bar chart. Data represents mean counts of tdTomato fluorescence in 1 second; ***$P<0.001$ vs. Cre-negative control by t-test; n=3.

Successful recombination in heart and lung tissue was shown qualitatively by the detection of tdTomato fluorescence in excised FibroTom heart and lungs using fluorescence microscopy (Figure 6-7). Importantly, this highlighted sustained expression, as heart and lung tissues were excised approximately 12 weeks following cessation of tamoxifen treatment. Additionally, tdTomato fluorescence was not detected in Cre-negative mice.

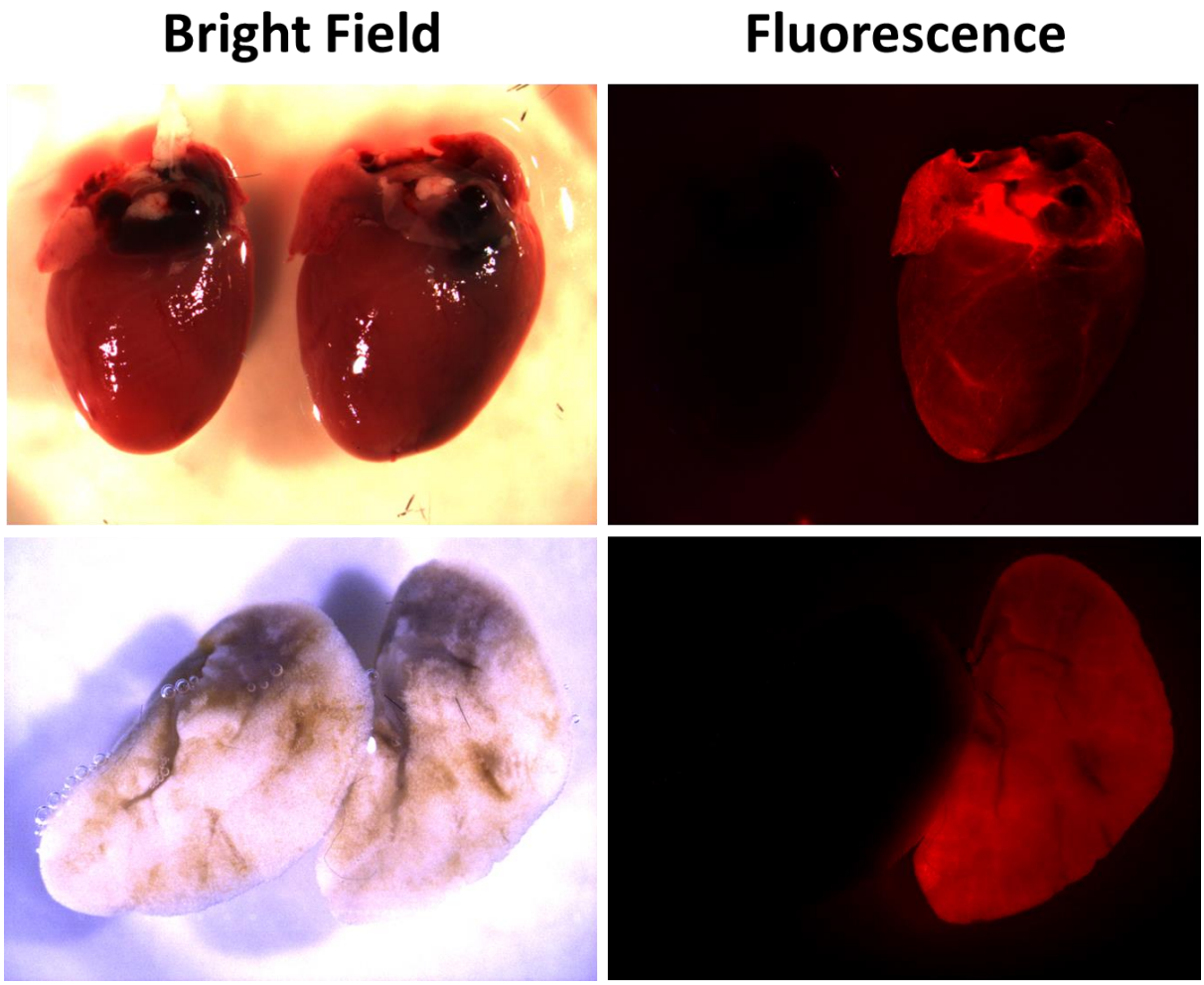

Figure 6-7: Successful recombination in heart and lungs of FibroTom reporter mice. Representative bright-field and fluorescence microscopy images of whole excised heart **(upper images)** and lung **(lower images)** in a FibroTom reporter mouse 12 weeks after cessation of tamoxifen (right on each image) and Cre-negative control (left on each image).

Furthermore, florescence microscopy of cardiac sections from FibroTom reporter mice showed diffuse tdTomato fluorescence throughout heart tissue (Figure 6-8B). In contrast, Cre-negative hearts did not have any tdTomato fluorescence (Figure 6-8A).

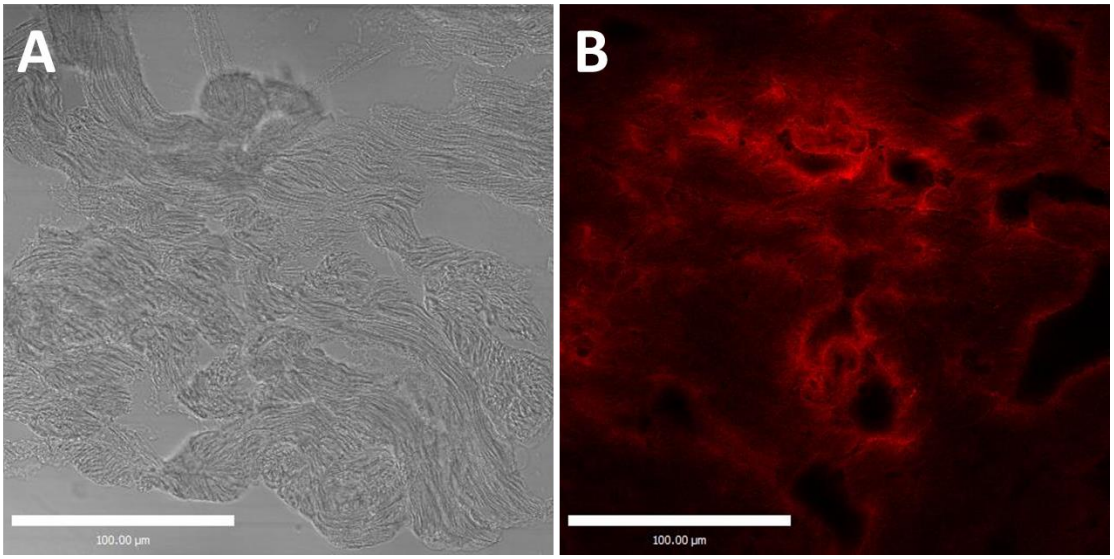

Figure 6-8: Diffuse tdTomato fluorescence throughout cardiac sections of FibroTom reporter mice. A: Cre-negative control as seen using transmitted light. **B:** Diffuse tdTomato fluorescence in Cre-positive cardiac section. Scale bars 100µm. Images captured on a Leica TCS SP5 Confocal Microscope (Leica Microsystems LTD, UK).

Cardiac sections were fixed and prepared for staining with DDR2 or vimentin fibroblast-specific antibodies, however processing led to the rapid loss of tdTomato fluorescence. This included fixation with 4% PFA or acetone, as well as the application of cover slips with commercial mounting media.

Regardless, taken together tdTomato is expressed in fibroblasts in a range of tissues, indicating *Col1α2* Cre-recombinase activity.

Cardiac Fibroblast Labelling and *Col1α2* Cre Efficiency

Despite qualitative evidence to suggest successful expression of tdTomato in fibroblasts, cardiac cell suspensions from FibroTom mice frequently yielded a very low percentage (<2%) of tdTomato^{+} cells (Figure 6-9 and 6-10). This could suggest an effect of the collagenase digestion enzyme used, which may affect the fluorescence of fibroblast-derived tdTomato. It is worth noting that collagenase digestion may also affect the binding of fibroblast markers used here. In contrast, fibroblasts were found to represent up to 27% of total cardiac cells, as determined by CD140α, CD90 or DDR2 antibody staining (Figure 6-10). There was a significant difference in the proportion of cells indicated to be fibroblasts depending on the antibody used. In addition to CD140α and DDR2, CD90 was used since it is a surface marker, shown to be expressed

by the majority of cardiac fibroblasts.[215, 216] CD140α, CD90 and DDR2 stained on average 6%, 15% and 27% respectively, indicating that these antibodies were unlikely to be labelling all fibroblasts.

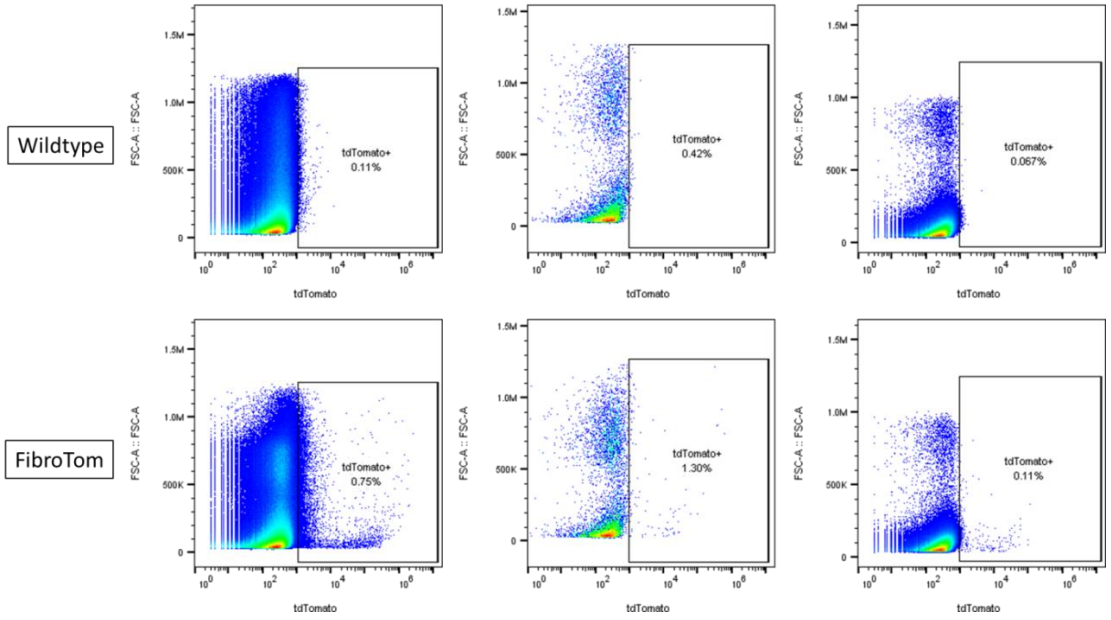

Figure 6-9: Flow cytometry of FibroTom cardiac cells yielded a very low percentage of tdTomato$^+$ cells. Plots are from 3 separate experiments comparing Cre-negative (wildtype) and Cre-positive (FibroTom) mice treated with tamoxifen. Positive percentages are shown inside gates, ranging from 0.11% to 0.75%.

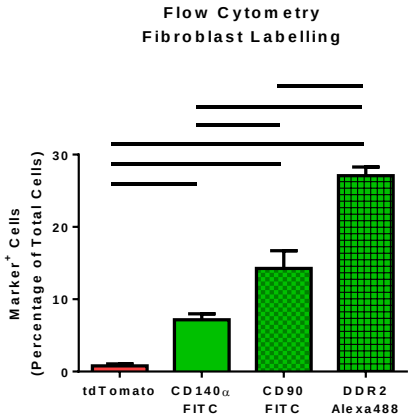

Figure 6-10: Flow cytometry of cardiac cells revealed differential labelling of fibroblasts with CD140α, CD90 or DDR2 antibodies. Antibody targets and conjugated fluorophores are shown. Horizontal lines represent significant differences in staining proportions by flow cytometry *P<0.05*; 1way ANOVA with Tukey's post-test for multiple comparison; n=6, 8, 7, 2, respectively.

Taken together, a low percentage of tdTomato$^+$ cells would indicate a very low Cre-recombinase efficiency; however this was unlikely to be true (e.g. based on assessment of whole heart or heart sections). For further investigation, flow cytometry experiments were then performed on adhered cardiac fibroblasts. Firstly, isolated cardiac cells seeded in T25 flasks attached and grew to confluency. Fibroblasts were identified by their elongated morphology, whereas contaminating cardiomyocytes and other cells were identified as weakly auto-fluorescent, rounded shapes. Fluorescence microscopy of cardiac cells from FibroTom mice showed tdTomato florescence in the majority of fibroblasts (Figure 6-11). In contrast, tdTomato fluorescence was absent in cardiac cells isolated from Cre negative mice, confirming Cre-recombinase dependency.

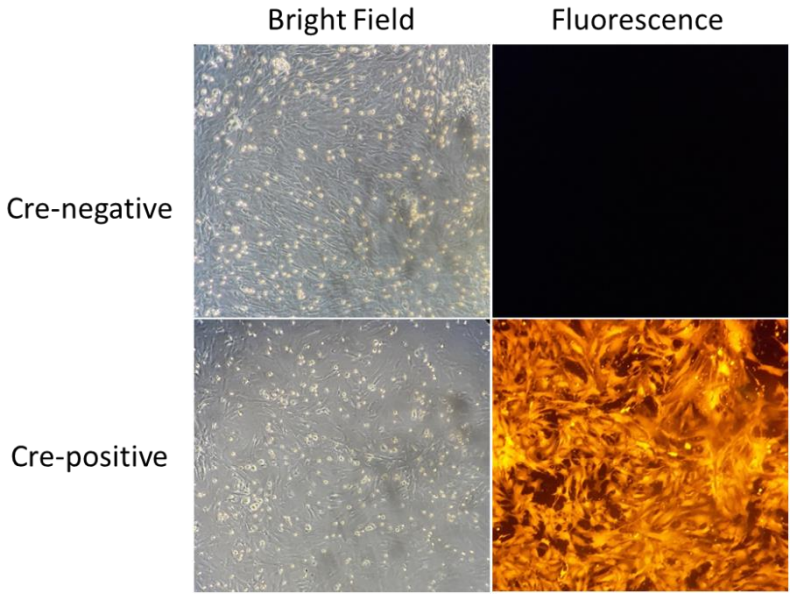

Figure 6-11: tdTomato fluorescence in seeded fibroblasts isolated from FibroTom mouse cardiac tissue. Bright field **(left)** and fluorescence **(right)** images from cardiac cells in culture. Fibroblasts were identified by morphology. Representative images using 20x objective.

Adhered cells were detached, stained and subjected to flow cytometry and showed that 30-40% of adhered cardiac cells were tdTomato$^+$ (Figure 6-12). Additionally, on average 44% of cells were CD140α$^+$, of which nearly 70% were also tdTomato$^+$ in FibroTom-derived cells (Figure 6-13).

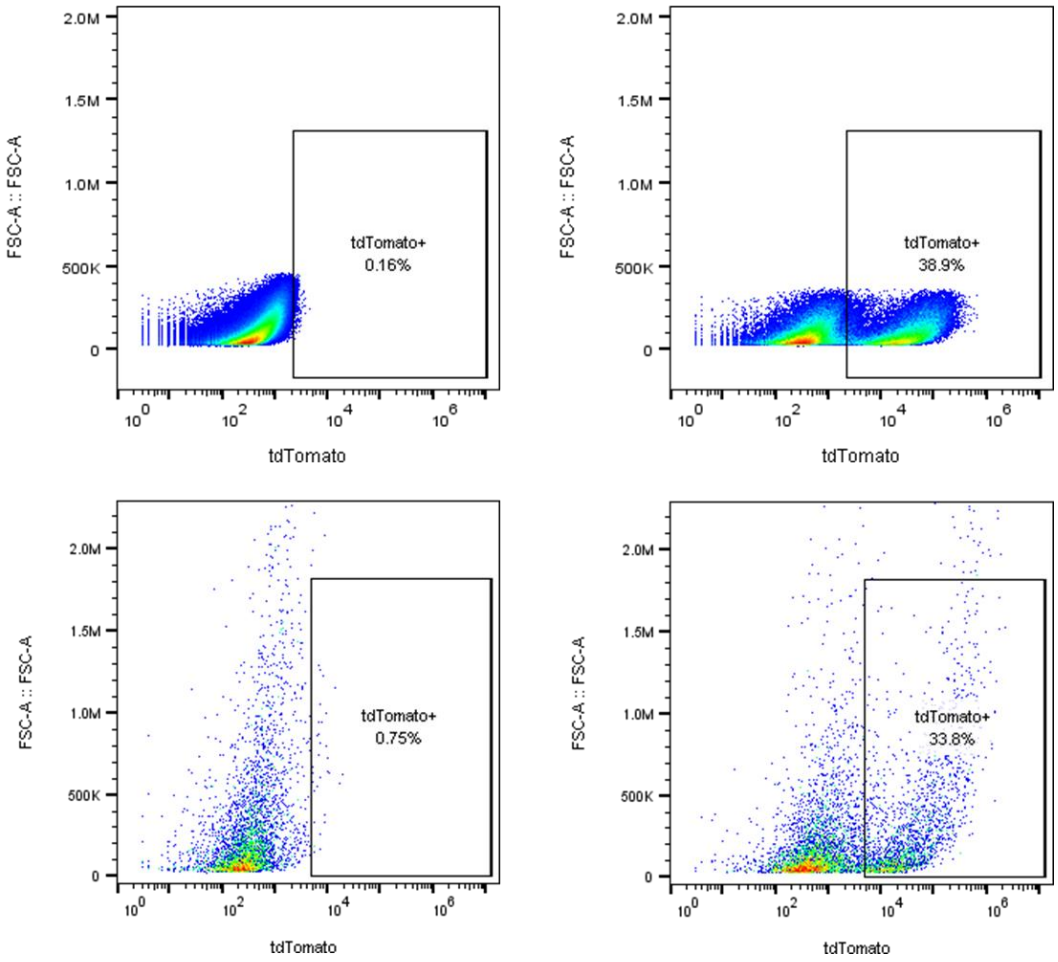

Figure 6-12: Adhered cardiac cells subjected to flow cytometry. Two separate experimental cultures are shown, with FibroTom cells shown on the right and Cre-negative control cells on the left.

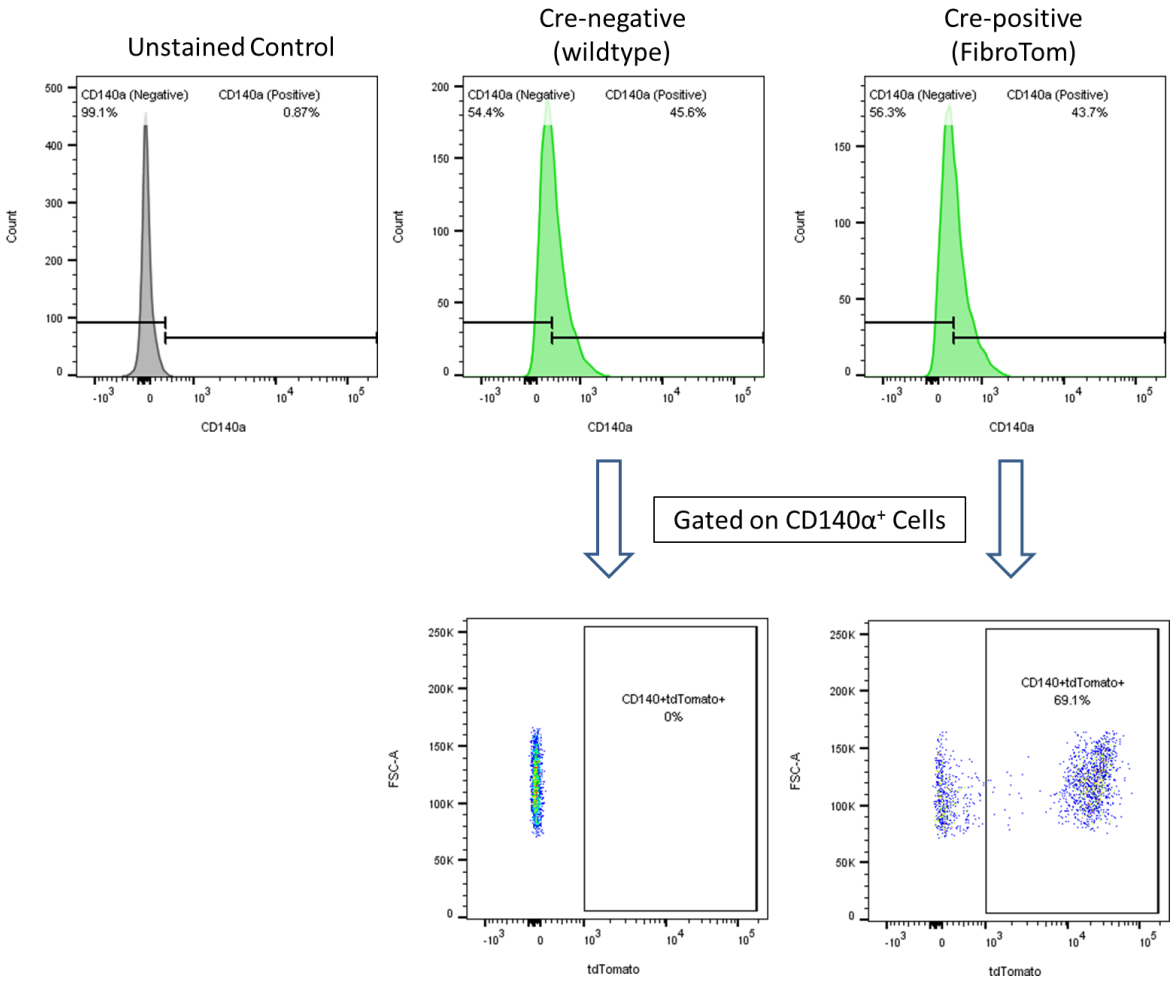

Figure 6-13: Flow cytometry of adhered cardiac cells from FibroTom and Cre-negative mice. CD140α^{+} cells represent approximately 44% of adhered cells and nearly 70% of CD140α^{+} cells were also tdTomato^{+}.

Assuming similar *Col1α2* Cre-recombinase activity in fibroblast NOX2 KO mice, these data suggest that the Cre-recombinase efficiency was up to approximately 70%. It was therefore inferred that the lack of phenotype in fibroblast NOX2 KO mice in response to TAC was not due to inadequate knockdown.

6.3.2 EndoTom Reporter Mice

Further Characterization

Following tamoxifen treatment for 3 days, EndoTom mice had tdTomato fluorescence in cardiac sections (Figure 6-14). Fluorescence microscopy at low magnification showed a speckled tdTomato fluorescence appearance throughout the heart (Figure 6-14B). Higher magnification showed that tdTomato fluorescence was found in between cardiomyocytes at cell junctions, suggestive of small capillaries (6.14C). In

addition, larger coronary vessels were tdTomato-positive in areas corresponding to the vessel wall (6.14D). Lastly, Cre-negative controls did not express tdTomato and are only visible using transmitted light (6.14A).

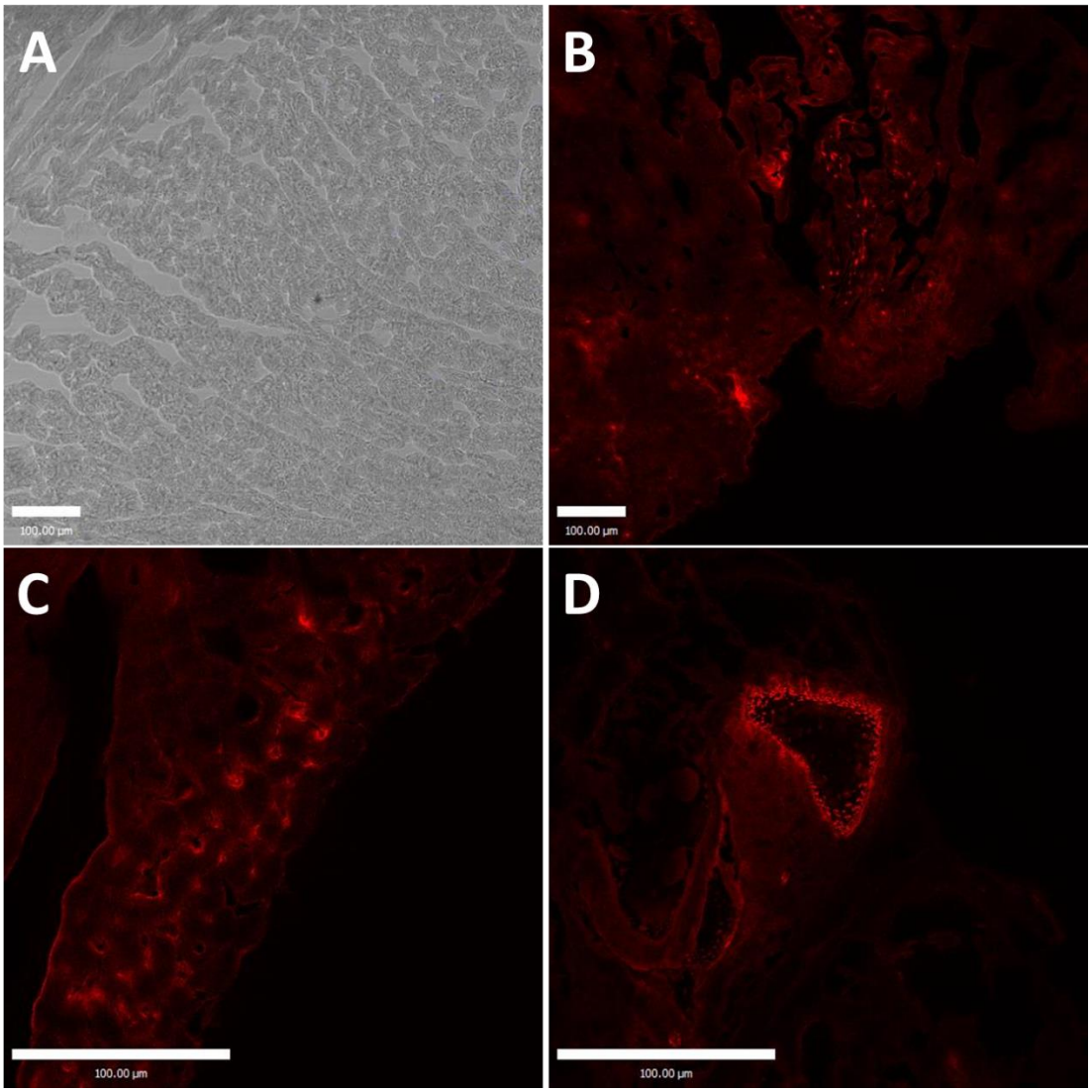

Figure 6-14: Fluorescence microscopy of cardiac sections from EndoTom reporter mice show tdTomato fluorescence in areas corresponding to cardiac endothelial cells. **A:** Cre-negative control as seen using transmitted light. **B:** Low magnification (20x objective) of Cre-positive cardiac section showing speckled tdTomato fluorescence. **C:** High magnification (63x objective) showing tdTomato cells in between cardiomyocytes, with a tube-like appearance similar to that of small capillaries. **D:** Large coronary vessel (63x objective) with tdTomato fluorescence in the luminal lining. Scale bars 100µm. Images captured on a Leica TCS SP5 Confocal Microscope (Leica Microsystems LTD, UK).

Cardiac sections were fixed and prepared for staining with CD31 antibody, however processing led to the rapid loss of tdTomato fluorescence. This included fixation with 4% PFA or acetone, as well as the application of cover slips with commercial mounting media.

Cardiac Endothelial Cell Labelling and *Cdh5* Cre Efficiency

Results show that tdTomato$^+$ cells represented approximately 6-7% of total cardiac cells from EndoTom mice. From this, it was anticipated that endothelial cell markers would provide a similar proportion, assuming high Cre recombinase efficiency.

In contrast to tdTomato, the proportion of endothelial cell marker$^+$ cells was higher and varied significantly depending on the antibody and fluorophore used (Figure 6-15). 13% of total cardiac cells stained positive for the commonly used endothelial cell marker, CD31. 20% of total cardiac cells stained positive for CD144, another commonly used endothelial cell marker. CD201 is suggested to play a key role in the prevention of thrombosis by interaction with Protein C[217] and is expressed by endothelial cells in the heart and lungs and in large vessels.[218] Furthermore, CD201 was shown not to be expressed in fibroblast cultures in vitro.[219] Here, CD201 was similar to CD31-FITC, staining approximately 11% of total cardiac cells.

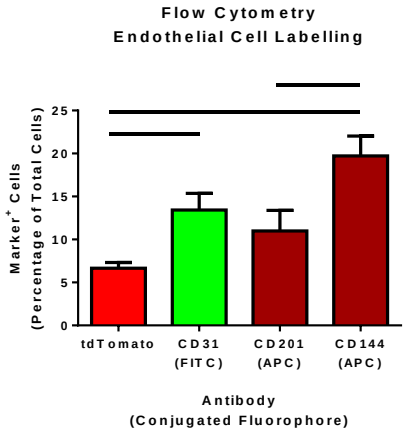

Figure 6-15: Flow cytometry of cardiac cells reveals differential labelling with endothelial cell specific markers. Antibody targets and conjugated fluorophores are shown. Horizontal lines above bars represent significant differences in staining proportions by flow cytometry *P<0.05*; 1way ANOVA with Tukey's post-test for multiple comparison; n=13 for tdTomato and n=6, 3, 6, respectively for conjugated antibodies.

The majority (approximately 85%) of tdTomato$^+$ cells also expressed CD31 (Figure 6-16), which indicated highly specific targeting of the *Cdh5*-driven Cre recombinase to endothelial cells. In contrast, of the CD31$^+$ cells, only 15-40% were also tdTomato$^+$, suggestive of low *Cdh5* Cre-recombinase efficiency. This, however, most likely reflects non-endothelial cell staining by CD31, since endothelial cells are reported to only account for approximately 5-10% of all cardiac cells and CD31 is also expressed by other cells including leukocytes and platelets. The CD144 and CD201 antibodies also estimated a low Cre-recombinase efficiency, however in contrast to CD31, very few tdTomato$^+$ cells were positive for these markers (approximately 17-28%; Figure 6-16). Since the majority of tdTomato *Cdh5*-derived "endothelial cells" in cardiac tissue do not express CD144 and CD201 in the current study, these markers might not be best suited to determine *Cdh5* Cre-recombinase efficiency.

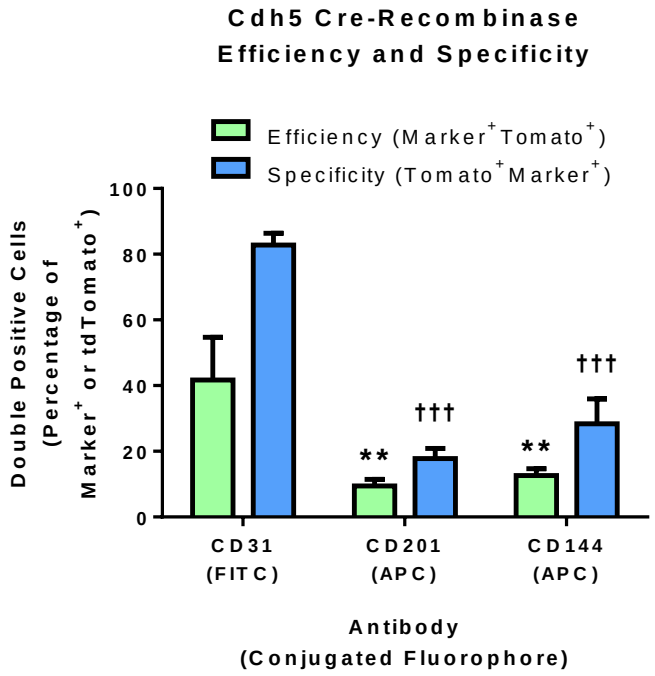

Figure 6-16: *Cdh5* Cre-recombinase efficiency and specificity varies depending on the endothelial cell-specific marker used. The percentage of endothelial cell marker positive cells also expressing tdTomato (efficiency) or tdTomato positive cells also expressing an endothelial cell marker (specificity) is shown. ***P<0.01* vs. CD31 (FITC) efficiency; †††*P<0.001* vs. CD31 (FITC) specificity; 2way ANOVA with Tukey's post-test for multiple comparison; n=3.

Since CD31 is also expressed by non-endothelial cells, it is difficult to accurately determine the *Cdh5* Cre-recombinase efficiency in this experiment. However, more than 80% of tdTomato$^+$ cells express CD31, suggesting high Cre specificity for targeting endothelial cells.

Endothelial-Mesenchymal Transition in TAC

Male EndoTom mice subjected to TAC developed trans-TAC pressure gradients of greater than 40mmHg, similar to those generated in chapters 4 and 5 (Figure 6-17).

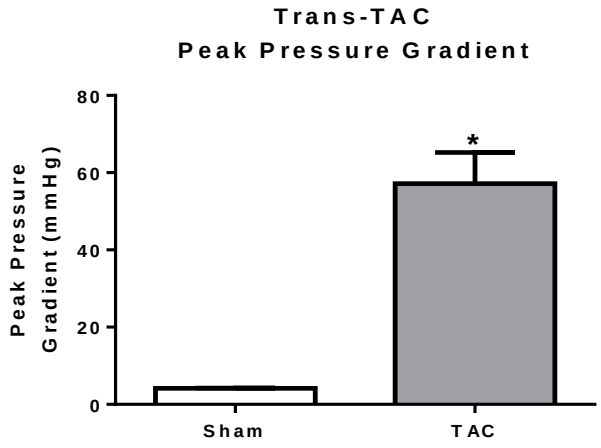

Figure 6-17: EndoTom mice developed significant echocardiography-derived trans-TAC pressure gradients of between 50-60mmHg, indicative of successful TAC surgery. Student's t-test; **P<0.05* vs. sham control; n=3.

Flow cytometry of sham operated EndoTom mouse hearts suggested a basal population of fibroblasts with endothelial origin, since approximately 21% of tdTomato$^+$ cells also express the fibroblast marker CD140α (Figure 6-18). It is possible that CD140α might have labelled endothelial cells, giving rise to this subpopulation of fibroblasts with endothelial origin. Most importantly, TAC did not significantly augment this percentage, with approximately 26% of tdTomato$^+$ cells also CD140α$^+$ cells (*P=0.34*), suggesting an absence of TAC-induced EndoMT.

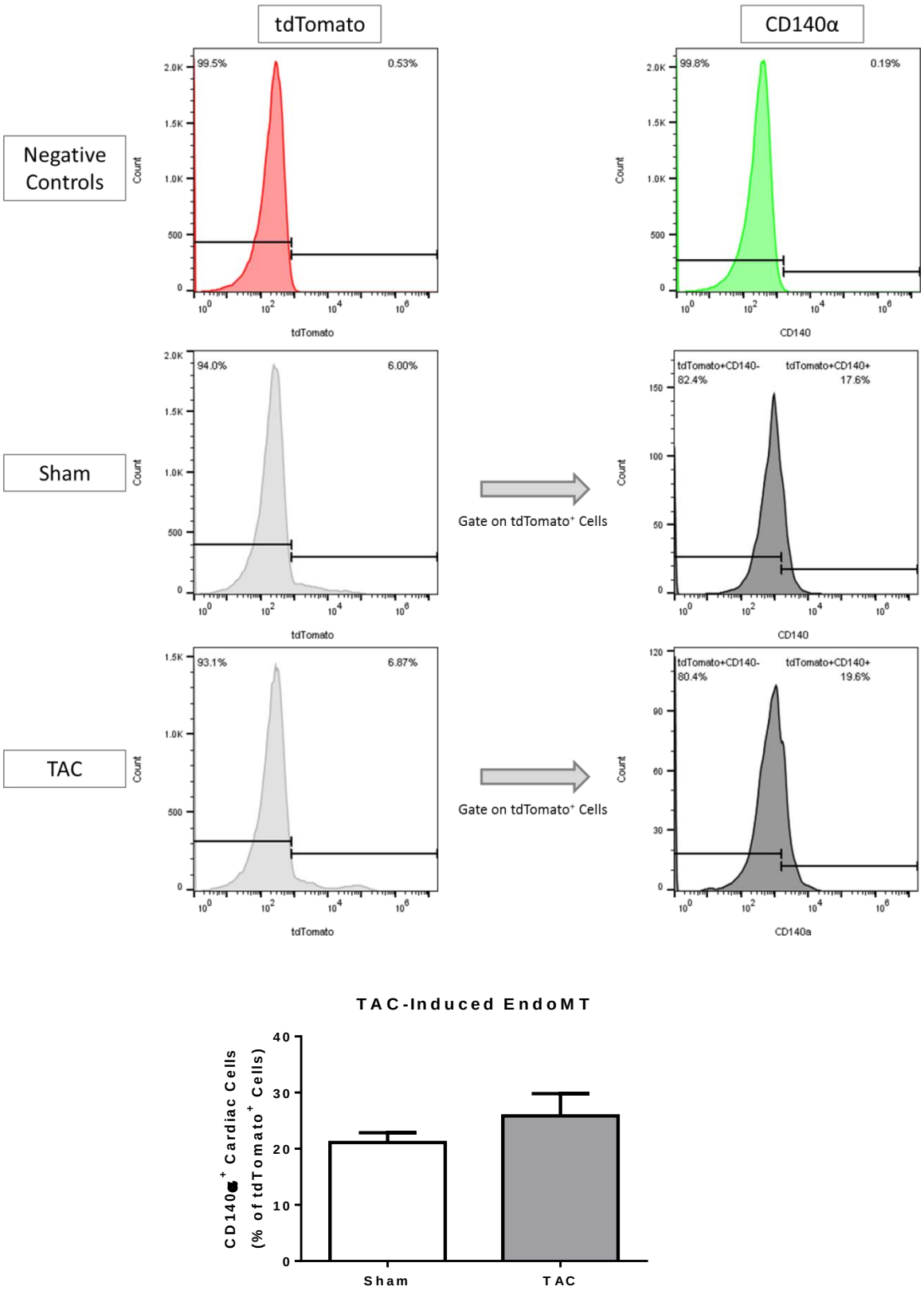

Figure 6-18: TAC did not lead to an increase in cardiac tdTomato$^+$ cells expressing the fibroblast marker CD140α. Representative plots from flow cytometry of EndoTom mouse hearts. *P=0.34* vs. sham; student's t-test; n=3.

Similar to cardiac tissue, the lungs also contain endothelial cells and fibroblasts, and evidence suggested that EndoMT may contribute towards the development of pulmonary fibrosis.[208] In parallel experiments, lung tissue was collected and processed for flow cytometry following TAC. Virtually all lung tdTomato$^+$ cells expressed CD31 (92-96%). Importantly, 35% of tdTomato cells expressed CD140α, which was not augmented by TAC (*P=0.95*; Figure 6-19). This is again suggestive of a lack of EndoMT following TAC and a possible lack of fibroblast specificity for CD140α.

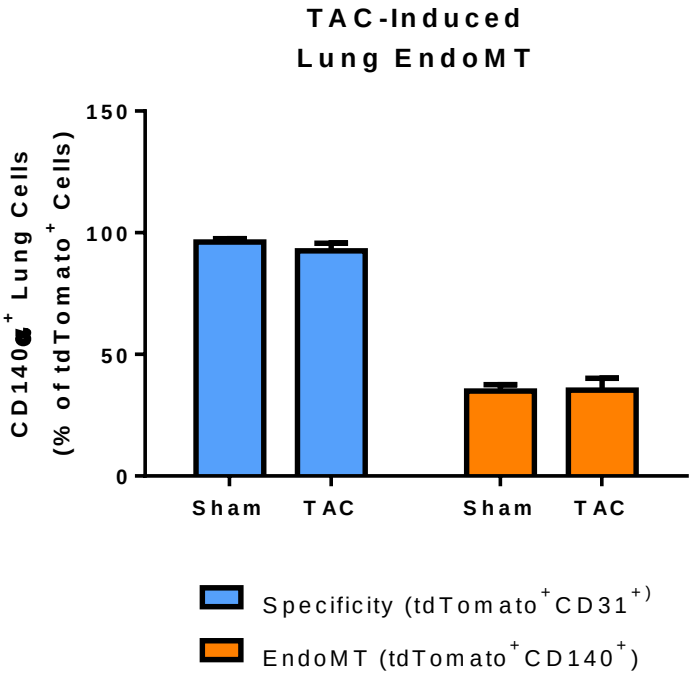

Figure 6-19: TAC did not lead to an increase in lung tdTomato$^+$ cells expressing the fibroblast marker CD140α. Flow cytometry of lung tissue from EndoTom mice. Approximately 92-96% of tdTomato$^+$ cells were positive for CD31. Approximately 35% of tdTomato$^+$ cells express CD140α, both prior to and after TAC. *P=0.95* vs. sham; student's t-test; n=3.

6.4 Discussion

A key report regarding cardiac EndoMT in 2007 provided a potentially new and exciting target for preventing the development of cardiac fibrosis.[30] There is now a larger body of evidence supporting the process of EndoMT in cardiac fibrosis from a range of stimuli.[52, 53, 198, 211] This is alongside reports detailing a reduction in endothelial cells and an increase in fibroblast numbers following pressure overload.[172, 212] Despite this, emerging research disputes these claims, suggesting that EndoMT does not occur.[129, 213, 216] The data presented in this chapter, although preliminary, are in support of the recent and thorough report by Moore-Morris and colleagues,[213] showing no evidence of cardiac EndoMT in mice subjected to chronic pressure overload.

6.4.1 Fibroblast-Specific Markers?

A truly fibroblast-specific marker has yet to be identified. FSP-1 appears to be a misnomer, since up to 45% of FSP-1$^+$ cells also express CD31, indicating that FSP-1 antibodies label endothelial cells and leukocytes.[212] Furthermore, FSP-1$^+$ cells were not detected during neonatal cardiac remodelling in mice, a process involving the proliferation of fibroblasts, further limiting the credibility of FSP-1.[212] αSMA is also often used in the detection of fibroblasts or myofibroblasts,[30, 53] but is actually a smooth muscle cell marker, with very little fibroblasts labelled in healthy cardiac tissue.[213]

Other fibroblast markers include CD140α, CD90, DDR2 and vimentin, all of which are reported to be expressed by other cell types.[213] Further difficulty arises since fibroblasts have varied origins and form subsets between different tissues and even within tissues. For example, a thorough examination of CD90$^+$ fibroblasts showed different marker profiles between mouse tail skin and cardiac populations.[215] There is also low co-expression of multiple fibroblast markers, including CD140α and CD90 which are only co-expressed by approximately 28% of cardiac fibroblasts.[215] As such, it can be now accepted that not all fibroblasts express all fibroblast markers, however in non-haematopoietic CD90$^+$ cardiac cells, up to 80% expressed collagen 1, DDR2 or CD140α, suggesting that populations can be enriched prior to analysis.[216] In this

chapter, CD140α was selected, since it is regarded as the most robust cardiac fibroblast marker and its surface location allows for easy antibody staining.[220]

Regardless of the antibody used, it seems that the use of αSMA and FSP-1 as fibroblast markers is now ill-suited. Unfortunately, many of the earlier studies on EndoMT were based on the use of these markers.[30, 52, 53]

6.4.2 Fibroblast Origins and Changes during Pressure Overload

Interestingly, data in this chapter showed that under basal conditions, up to 20% of CD140α^{+} cardiac cells (fibroblasts) were of endothelial origin. This percentage is in agreement with a previous study using double transgenic mice with *Tie2*-tdTomato lineage traced endothelial cells and *Col1α1*-GFP lineage traced fibroblasts.[213] The report concluded that up to 19% of fibroblasts had endothelial cell origins in naïve mice. In the current study however, tdTomato expression was induced during adulthood in mice. This would suggest that tdTomato^{+}CD140α^{+} cells only became fibroblasts following induction at between 6-8 weeks of age, an unlikely occurrence. Alternatively, data presented here suggested that CD140α was also expressed on a subset of mature endothelial cells. This may also be true for CD90, another fibroblast marker. In a study using tamoxifen-induced *Tie2*-GFP lineage traced endothelial cells and CD90 as a fibroblast marker, approximately 20% of cardiac fibroblasts were shown to be of endothelial origin in naive mice. Importantly, this percentage did not change following TAC-induced fibroblast proliferation and fibrosis, similar to results obtained here.[216] Data in this chapter suggested a lack of EndoMT in chronic pressure overload, supported by reports using two different approaches. Furthermore, CD140α and CD90, similar to FSP-1 and αSMA, might not be best suited for the study of EndoMT.

6.4.3 Determination of Cre-Recombinase Efficiency

A significant phenotype of delayed Ang II-induced hypertension was observed in fibroblast NOX2 KO mice in chapter 3. As such, and considering the previous characterization of the *Col1α2* promoter,[132, 136, 162] the Cre efficiency was never called into question. Using an indirect reporter mouse cross approach on isolated cells, it was estimated here that the *Col1α2* Cre-recombinase efficiency was approximately 70% in cardiac tissue following 10 consecutive days of tamoxifen.

In EndoTom reporter mice, the Cre efficiency could not be accurately estimated, owing to predicted non-endothelial targeting by the CD31 antibody. Encouragingly, tdTomato$^+$ cells represented 6-7% of all cardiac cells, similar to that reported by two reports using CD31 as a marker.[172, 199] Although care was taken to remove blood from excised hearts, contamination by platelets in particular may be responsible for the increased CD31$^+$ proportions. With this in mind, the percentage of tdTomato$^+$CD31$^+$ (rather than CD31$^+$tdTomato$^+$) cells may provide a better efficiency estimate. A high efficiency is therefore predicted, since up to 90% of tdTomato$^+$ cells also expressed CD31, with a higher percentage (close to 100%) in lung tissue.

6.4.4 Study Limitations

As discussed, the lack of a specific fibroblast marker has hampered research into this cell type for decades. Previous studies have highlighted the use of CD140α as a robust fibroblast marker, despite it being known to be expressed by endothelial cells.[213] Here it was found that CD140α might be expressed by approximately 20% of endothelial cells, which potentially makes it difficult to detect low levels of EndoMT. In fact, EndoTom mice which underwent TAC appeared to have a modest increase in cardiac tdTomato$^+$CD140α$^+$ cells compared to sham (26% vs 21%). Therefore statistical analysis could represent a type II error, though the number of replicates used here is in line with previous reports of this type.[30, 213] Regardless, despite emerging strategies for identifying fibroblasts, a more robust and specific marker is desperately needed.

In addition, experiments carried out in this chapter were not without further challenges and limitations.

In initial stages, tdTomato was selected owing to its superior brightness, stability and fluorescence persistence following various processing steps including fixation.[133, 221] In contrast to reports, tdTomato fluorescence was almost immediately lost from cardiac sections following fixation with 4% PFA or acetone. Even the application of commercial DAPI mounting medium led to the loss of tdTomato fluorescence. This led to difficulty in characterising FibroTom and EndoTom reporter mice by immunohistochemistry. Antibodies directed to tdTomato are available; however this avenue was not pursued.

In determining the *Col1α2* Cre-recombinase efficiency, FibroTom hearts yielded very low proportions of tdTomato^{+} cells. This was despite up to 27% of cells being labelled as fibroblasts with DDR2, in agreement with current literature for mouse cardiac fibroblasts.[199] As a consequence, the *Col1α2* Cre-recombinase efficiency was determined using adhered cardiac cells in culture. This may have led to inaccuracies, since it is feasible that tdTomato fibroblasts may have different proliferation rates to that of non-reporter fibroblasts, thereby increasing or decreasing the relative numbers and therefore estimated efficiency. Culture time was limited to 72 hours in an attempt to limit this, whilst allowing adequate time for adhesion. It is possible that the loss of tdTomato fluorescence following collagenase digestion may be due to enzymatic modification of the fluorophore.

6.4.5 Summary

In summary, this chapter provides more evidence against the process of cardiac EndoMT in response to chronic pressure overload, in agreement with other recent reports.

CHAPTER 7: General Discussion

7.1 Cardiac Fibrosis and Cardiac Dysfunction

Cardiac fibrosis leads to cardiac dysfunction via mechanical and electrical defects. This is exemplified by heart failure with preserved ejection fraction (HFpEF), which represents around half of all heart failure cases.[12] There is currently no specific therapy for cardiac fibrosis and the best commonly used treatments target signalling pathways relating to the renin angiotensin system, such as Ang II receptor blockers, angiotensin converting enzyme inhibitors and beta blockers, all of which take an indirect approach. [10]

Since cardiac fibrosis is central to the development and persistence of diastolic dysfunction and therefore HFpEF, anti-fibrotic therapies are highly desirable. Clinical trials involving MMP inhibition have been largely unsuccessful, likely owing to off-target systemic effects and a possible dependence on duration of use.[24, 222] Recent work indicates that serelaxin, a recombinant form of the human hormone relaxin-2, is an effective anti-fibrotic agent in experimental models of heart failure.[223] It has also been shown to provide positive benefits in clinical trials, including reduction of hemodynamic load, dyspnoea and death after 180 days,[224, 225] though questions over efficacy have halted progression to approval. Resveratrol is another drug which has gained much attention in recent years for its combined anti-hypertensive and antioxidant properties in mouse studies, shown to improve cardiac fibrosis.[156, 226] Unfortunately such studies have not been successfully translated to the clinical setting and an anti-cardiac fibrosis therapy still seems a long way off. It is common for promising pre-clinical candidates to fail in clinical trials, highlighting the need for more basic research. Furthermore, owing to an aging population, the burden of heart failure with preserved ejection fraction is expected to rise in the near future, since cardiac aging is associated with pathological stiffening and dysfunction.[16]

NOX2 is expressed in a range of tissues and cell types, including cardiac fibroblasts, endothelial cells, cardiomyocytes and inflammatory cells. It has been repeatedly shown to play a key role in mediating cardiac remodelling and dysfunction in response to pathological stimuli such as infarction,[32] chronic neurohumoral[35, 62] or mechanical stimulation.[118] Global NOX2 KO mice were shown to be resistant to hypertrophy and cardiac fibrosis, making it an attractive target for clinical research;

however the pleiotropic role of NOX2, not just as a pathological signalling molecule, makes it unsuitable to target indiscriminately. With this in mind, research has shifted towards trying to elucidate the cell-specific contribution of NOX2 to the development of these pathologies, yielding largely positive results. Fibroblasts are central to the production of cardiac fibrosis, and preliminary data suggested that fibroblast NOX2 is essential in a rat model of ethanol-induced fibrosis, though the lack of a fibroblast-specific deletion approach makes it difficult to attribute NOX2 activity to fibroblasts specifically.[227] In another recent report, NOX2 was overexpressed in mouse endothelial cells, showing an augmentation of cardiac fibrosis in response to chronic Ang II *in vivo*.[53] This, along with other evidence, suggested that disrupting fibroblast or endothelial cell NOX2 activity may prevent the development of cardiac fibrosis.

7.2 Thesis Summary

The studies described in this thesis used novel NOX2 floxed mice to develop cell-specific NOX2 KO mice and in particular, sought to determine the role of fibroblast and endothelial cell NOX2 in the development of cardiac fibrosis. The NOX2 floxed mice have essential regions of exons 1 and 2 flanked by LoxP sites, rendering NOX2 dysfunctional upon Cre recombinase-mediated excision. Both cell-specific Cre recombinase promoters have been previously used and characterized[130, 132] and the Cre recombinase efficiency was further investigated in chapter 6. Additional characterisation in terms of ROS production was not performed in the current study, but could have provided greater reassurance regarding NOX2 gene deletion. Although basal levels of superoxide production would not be expected to differ, since a lucigenin chemiluminescence-based approach in global NOX2 KO mouse heart homogenates showed similar production to that of wildtype mice,[62] analysis following angiotensin II or pressure overload may have been beneficial. Other methods include spin trapping and dihydroethidium staining coupled with high performance liquid chromatography.[228]

The possibility that deletion of NOX2 in fibroblasts or endothelial cells could be compensated for by upregulation of other NOX isoforms was not investigated in the current study, however our lab has previously shown that global NOX2 KO mice have unaltered NOX4 expression levels compared to wildtype.[32] Similarly, in NOX4 KO mice

the expression of NOX2 was unaltered, suggesting that NOX2 and NOX4 can be deleted without affecting the expression of each other.[34] In addition, the expression of p22phox and p47phox were unaltered in KO mice compared to flox. While this provides some support, if the loss fibroblast NOX2 is indeed compensated for by NOX4, then any effects on cardiac fibrosis would be masked.

In chapter 3 it was found that NOX2 in fibroblasts is essential in the proper development of hypertension in response to chronic Ang II *in vivo*. Further to this, the development of cardiac fibrosis was found to be blunted in fibroblast NOX2 KO mice, supporting the hypothesis that fibroblast NOX2 plays a key, pathological role.

It is known that hypertension in isolation promotes the development of cardiac fibrosis and as such, the delayed hypertensive response in fibroblast NOX2 KO mice could contribute towards the decreased development of cardiac fibrosis in these mice. The blood pressure component of chronic angiotensin II was therefore removed by the use of a chronic subpressor dose in mice, however this coincided with an absence of cardiac fibrosis and other cardiac pathology even in wild-type mice. A thorough review of current literature revealed a range of conflicting data with subpressor Ang II, most likely reflecting different routes of administration, strain differences and other variables. Taken together, chapter 3 suggested a possible indirect, pressor-dependent effect on the development of cardiac fibrosis in fibroblast NOX2 KO mice. In support of this, A novel potential mechanism for fibroblast NOX2-mediated hypertension and vascular remodelling in response to chronic Ang II has been elucidated (Harrison et al., 2017; manuscript in preparation).

Investigations were then focussed on determining this using a non-RAAS, blood pressure-independent model of fibrosis.

Chapter 4 sought to determine the role of fibroblast NOX2 in a relatively blood pressure-independent mouse model of pressure overload induced by transverse aortic constriction. Curiously and in contrast to chronic Ang II, it was found that deletion of NOX2 in fibroblasts was not cardioprotective in terms of cardiac fibrosis following TAC. There was also no prevention of other cardiac remodelling and cardiac dysfunction. It was concluded that fibroblast NOX2 was either dispensable in the development of TAC-induced cardiac fibrosis – suggesting stimulus dependent NOX2

effects, or that there is a general non-essential role for fibroblast NOX2 in isolation. Taken together, chapters 3 and 4 suggested that fibroblast NOX2 led to cardiac fibrosis via a blood-pressure dependent mechanism. Experiments then moved towards investigating NOX2 derived from another cell type, namely endothelial cells.

The role of endothelial cell NOX2 was investigated in chapter 5, again using TAC. Work from our own lab inferred that deletion of endothelial cell NOX2 would be beneficial, leading to a reduction in cardiac fibrosis and dysfunction. This was not the case, and endothelial cell NOX2 also seemed to be dispensable in the development of TAC-induced cardiac fibrosis. One obvious question remains unanswered and as such work is ongoing to determine the effect of endothelial cell NOX2 deletion in Ang II-induced cardiac fibrosis, which would greatly compliment the experiments in chapter 3. Such a study would also compliment work published by Murdoch et al., in 2014, which showed augmented cardiac fibrosis in Ang II-treated transgenic mice overexpressing endothelial cell NOX2. Interestingly, similar to fibroblast NOX2, the role of endothelial cell NOX2 appears to also be stimulus dependent. Very recent research from our laboratory has shown that transgenic mice overexpressing NOX2 in endothelial cells do not have augmented cardiac fibrosis in response to acute myocardial infarction.[123] In addition, infarct sizes, survival and cardiac function is comparable to wildtype controls in these transgenic mice. These findings could have implications regarding how NOX2 might be targeted in both different cell types and different pathologies; however it must be considered that transgenic and knockout mouse model approaches might not always be comparable.

Since endothelial cells have been repeatedly shown to be involved in the development of cardiac fibrosis, experiments were designed to investigate EndoMT as a possible mechanism.

Recent research suggested a role for EndoMT in the development of cardiac fibrosis by contributing to the fibroblast pool and or promoting the conversion of resident fibroblasts to myofibroblasts.[30, 52, 198] To test this, reporter mice were generated in which endothelial cells could be lineage traced with tdTomato. Reporter mice subjected to TAC showed no evidence of cardiac or lung EndoMT, since the proportion of fibroblasts with endothelial (tdTomato) origins was similar in TAC and

sham-operated mice. This was in agreement with more recent reports.[213, 216] Evidence of EndoMT using the tdTomato reporter system would have allowed further investigation into the possible role of NOX2 in this process. For example, the effect of global NOX2 deletion on the extent of EndoMT could be investigated. Further still, the effect of fibroblast or endothelial cell-specific NOX2 deletion could then be investigated. Such experiments were not deemed necessary owing to the lack of evidence for EndoMT in standard reporter mice following TAC.

7.3 Clinical Implications

The clinical impact of cardiac fibrosis is well described, involving diastolic dysfunction and an eventual progression to systolic dysfunction and death. As discussed above, both cardiac fibrosis and diastolic dysfunction lack specific treatments, though there are a number of promising pre-clinical agents.[10]

Various signalling pathways have been targeted in an attempt to attenuate the pathological development of cardiac fibrosis, discussed in chapter 1.5. In addition, there is a role for natriuretic peptides in the development of cardiac fibrosis. Secreted by ventricles, B-type natriuretic peptide is increased during cardiac stress and appears to be anti-fibrotic. B-type natriuretic peptide KO mice were shown to have significant basal fibrotic lesions compared to wildtype, and an exacerbation following pressure overload.[229, 230]

The involvement of NOX2 in these pathologies provides an additional target, however a universal NOX2 blocker is anticipated to have severe detrimental effects in terms of leukocyte host defence. In addition, general antioxidant clinical studies have been largely unsuccessful. Whilst NOX2 activity is often regarded as pathological, other ROS sources can be beneficial. An example of this includes NOX4 signalling in cardiomyocytes, which is shown to limit adverse cardiac remodelling and fibrosis in response to pressure overload, as well as promoting angiogenesis.[34] This offered some explanation as to why many antioxidant therapies failed to show significant benefits.

Selective inhibition of NOX2 over NOX4 is therefore of interest. A small peptide, PR-39, was shown to prevent transient cardiac dysfunction in a rat model of ischaemia-

reperfusion.[231] This peptide binds to p47phox, thereby preventing its interaction with p22phox and subsequent NOX2 enzyme assembly. Selectivity is a problem however, since the SH3 binding domain required for inhibition is also present in other proteins.[232]

In contrast, the peptide inhibitor NOX2ds-tat is currently regarded as being NOX2 isoform specific. The *in vivo* Inhibition of NOX2 by NOX2ds-tat was shown as beneficial in mice receiving chronic Ang II, leading to reduced superoxide production and systolic blood pressure.[233] The extent of cardiac fibrosis was not reported, though a reduction in systolic blood pressure would be expected to alleviate its development. Furthermore, assays designed to monitor the interaction of p22phox and p47phox for NOX2 assembly have highlighted a number of opportunities for small molecule inhibition. *In vitro* experiments identified ebselen and a range of its analogues as selective inhibitors of NOX2 over NOX4, though these small molecules were also shown to target NOX1.[234]

Despite these advances, it is known that not only is the ROS producing NOX isoform important, but also the cell type on which NOX is active. For example NOX2 activity in endothelial cells is detrimental in chronic Ang II, but appears to be merely coincidental in inflammatory cells.[53]

Data in this thesis adds another layer of complexity, since NOX2 signalling is essential in fibroblasts for Ang II-induced hypertension and subsequent cardiac fibrosis, but is dispensable in TAC-induced adverse remodelling and dysfunction. This potential stimulus-dependent effect of cell-specific NOX2 activation requires further investigation.

7.4 Study Limitations and Considerations

The experiments presented in this thesis were conducted on mice and used mouse tissue in hopes of translation to human disease. Using mice has some drawbacks owing to species differences. In particular, cellular composition of cardiac tissue may differ significantly. There are a few reports stating that fibroblasts represent up to 30% of the total cells in mouse cardiac tissue,[172, 199] whereas this figure is estimated to be closer to 60% in rat hearts.[199] This highlights significant species variation and

similar differences may exist between mouse and human hearts. Differing fibroblast proportions between species may alter the relative dependence on cell-specific ROS signalling or even the extent of EndoMT. This study used single cell suspensions from mouse hearts and estimated cardiac fibroblast proportions to be up to 27%. A comparable study in humans and especially one encompassing lineage tracing, is not feasible, making it difficult to bridge the gap between pre-clinical and clinical settings. Careful consideration is therefore required when attempting to conduct translational research.

In the studies outlined here, the TAC model was extensively used in mice. TAC is a crude model of aortic stenosis, which simulates common clinical symptoms, including systolic and diastolic cardiac dysfunction, as well as severe cardiac fibrosis and hypertrophy. Despite this, owing to the rapid onset of stenosis and subsequent dysfunction, the TAC model is often regarded as lacking direct clinical relevance.[170] A number of other mouse models leading to the development of cardiac fibrosis with slower onset are routinely used, such as chronic drug administration (e.g. Ang II or doxorubicin).[35, 235] However, as seen in the experiments performed here, it is possible for cell-specific NOX2 to have stimulus dependent effects, requiring consideration of the mechanism of fibrosis development in these models.

A final consideration is the fact that the development of cardiac fibrosis is complex and involves a range of cell types. Here, efforts were towards elucidating the role of fibroblast and endothelial cell NOX2, owing to their involvement in extracellular matrix production or EndoMT. It must be considered however, that a concerted activation of NOX2 from a range of cell types might be at play in response to chronic pressure overload. As such, whilst fibroblast and endothelial cell NOX2 will be activated following TAC, NOX2 from infiltrating inflammatory cells and even cardiomyocytes is also important, as well as cell-cell communication and cross activation. To investigate further, challenging double and or triple cell-specific knockout mice would have to be generated, as discussed in chapter 5.

7.5 Future Work

Experiments to investigate the effect of endothelial cell NOX2 deletion on Ang II-induced cardiac fibrosis would greatly compliment the studies described in this thesis. Work is already ongoing in the lab to determine this, though preliminary data suggests that endothelial NOX2 KO mice have a blunted hypertensive response, similar to that observed in fibroblast NOX2 KO mice. The extent of cardiac interstitial and perivascular fibrosis was determined using both brightfield and polarized light microscopy for most studies detailed in this thesis. The exception is for experiments in chapter 3.3.1, at which time a reproducible method was still under development. Thorough analysis is ongoing to make these data consistent with those reported in chapters 4.3.2 and 5.3.2 for use in publication.

Collagen 1α2-promoted Cre recombinase was used in the current study to confer fibroblast specificity, but this promoter will target all fibroblasts, not just cardiac. Periostin is expressed by cardiac fibroblasts during development and in adult tissue in response to pressure overload.[184] As such it identifies activated fibroblasts and is a useful tool for the study of cardiac fibrosis development. Deletion of NOX2 in activated fibroblasts using a periostin-driven Cre recombinase might provide more specific insights, especially considering that collagen 1α2 is expressed by cells other than fibroblasts.[129]

7.6 Final Summary

In summary, this thesis has built on knowledge of NOX2 in cardiac remodelling. Here, a role for fibroblast NOX2 specifically has been described in the development of angiotensin II-induced hypertension and cardiac fibrosis. The importance of fibroblast NOX2 may also be stimulus dependent, since mechanically-induced pressure overload did not require NOX2 in this cell type for detrimental cardiac effects. There is also a non-essential role for endothelial cell NOX2 in TAC and contrary to early reports, EndoMT is shown not to occur in cardiac or lung tissue in response to TAC.

References

1. Bernardo BC, Weeks KL, Pretorius L and McMullen JR. Molecular distinction between physiological and pathological cardiac hypertrophy: experimental findings and therapeutic strategies. *Pharmacol Ther*. 2010;128:191-227.

2. Leask A. Getting to the heart of the matter: new insights into cardiac fibrosis. *Circ Res*. 2015;116:1269-76.

3. Asbun J and Villarreal FJ. The pathogenesis of myocardial fibrosis in the setting of diabetic cardiomyopathy. *J Am Coll Cardiol*. 2006;47:693-700.

4. Ambale-Venkatesh B and Lima JA. Cardiac MRI: a central prognostic tool in myocardial fibrosis. *Nat Rev Cardiol*. 2015;12:18-29.

5. Krenning G, Zeisberg EM and Kalluri R. The origin of fibroblasts and mechanism of cardiac fibrosis. *J Cell Physiol*. 2010;225:631-7.

6. Flett AS, Sado DM, Quarta G, Mirabel M, Pellerin D, Herrey AS, Hausenloy DJ, Ariti C, Yap J, Kolvekar S, Taylor AM and Moon JC. Diffuse myocardial fibrosis in severe aortic stenosis: an equilibrium contrast cardiovascular magnetic resonance study. *Eur Heart J Cardiovasc Imaging*. 2012;13:819-26.

7. Creemers EE and Pinto YM. Molecular mechanisms that control interstitial fibrosis in the pressure-overloaded heart. *Cardiovasc Res*. 2011;89:265-72.

8. Celermajer DS, Chow CK, Marijon E, Anstey NM and Woo KS. Cardiovascular disease in the developing world: prevalences, patterns, and the potential of early disease detection. *J Am Coll Cardiol*. 2012;60:1207-16.

9. North BJ and Sinclair DA. The intersection between aging and cardiovascular disease. *Circ Res*. 2012;110:1097-108.

10. Gourdie RG, Dimmeler S and Kohl P. Novel therapeutic strategies targeting fibroblasts and fibrosis in heart disease. *Nat Rev Drug Discov*. 2016.

11. Kearney PM, Whelton M, Reynolds K, Muntner P, Whelton PK and He J. Global burden of hypertension: analysis of worldwide data. *Lancet*. 2005;365:217-23.

12. Butler J, Fonarow GC, Zile MR, Lam CS, Roessig L, Schelbert EB, Shah SJ, Ahmed A, Bonow RO, Cleland JG, Cody RJ, Chioncel O, Collins SP, Dunnmon P, Filippatos G, Lefkowitz MP, Marti CN, McMurray JJ, Misselwitz F, Nodari S, O'Connor C, Pfeffer MA, Pieske B, Pitt B, Rosano G, Sabbah HN, Senni M, Solomon SD, Stockbridge N, Teerlink JR, Georgiopoulou VV and Gheorghiade M. Developing therapies for heart failure with preserved ejection fraction: current state and future directions. *JACC Heart Fail*. 2014;2:97-112.

13. Yamamoto K, Masuyama T, Sakata Y, Nishikawa N, Mano T, Yoshida J, Miwa T, Sugawara M, Yamaguchi Y, Ookawara T, Suzuki K and Hori M. Myocardial stiffness is determined by ventricular fibrosis, but not by compensatory or excessive hypertrophy in hypertensive heart. *Cardiovasc Res*. 2002;55:76-82.

14. Loffredo FS, Nikolova AP, Pancoast JR and Lee RT. Heart failure with preserved ejection fraction: molecular pathways of the aging myocardium. *Circ Res*. 2014;115:97-107.

15. van Heerebeek L and Paulus WJ. Understanding heart failure with preserved ejection fraction: where are we today? *Neth Heart J*. 2016;24:227-36.

16. Borlaug BA. The pathophysiology of heart failure with preserved ejection fraction. *Nat Rev Cardiol*. 2014;11:507-15.

17. Olson TP, Johnson BD and Borlaug BA. Impaired Pulmonary Diffusion in Heart Failure With Preserved Ejection Fraction. *JACC Heart Fail*. 2016;4:490-8.

18. Borlaug BA, Kane GC, Melenovsky V and Olson TP. Abnormal right ventricular-pulmonary artery coupling with exercise in heart failure with preserved ejection fraction. *Eur Heart J*. 2016.

19. de Jong S, van Veen TA, van Rijen HV and de Bakker JM. Fibrosis and cardiac arrhythmias. *J Cardiovasc Pharmacol*. 2011;57:630-8.

20. Lin LY, Wu CK, Juang JM, Wang YC, Su MY, Lai LP, Hwang JJ, Chiang FT, Tseng WY and Lin JL. Myocardial Regional Interstitial Fibrosis is Associated With Left Intra-Ventricular Dyssynchrony in Patients With Heart Failure: A Cardiovascular Magnetic Resonance Study. *Sci Rep*. 2016;6:20711.

21. Basaran Y, Tigen K, Karaahmet T, Isiklar I, Cevik C, Gurel E, Dundar C, Pala S, Mahmutyazicioglu K and Basaran O. Fragmented QRS complexes are associated with cardiac fibrosis and significant intraventricular systolic dyssynchrony in nonischemic dilated cardiomyopathy patients with a narrow QRS interval. *Echocardiography*. 2011;28:62-8.

22. Assayag P, Carre F, Chevalier B, Delcayre C, Mansier P and Swynghedauw B. Compensated cardiac hypertrophy: arrhythmogenicity and the new myocardial phenotype. I. Fibrosis. *Cardiovasc Res*. 1997;34:439-44.

23. Rienks M, Papageorgiou AP, Frangogiannis NG and Heymans S. Myocardial extracellular matrix: an ever-changing and diverse entity. *Circ Res*. 2014;114:872-88.

24. Takawale A, Sakamuri SS and Kassiri Z. Extracellular matrix communication and turnover in cardiac physiology and pathology. *Compr Physiol*. 2015;5:687-719.

25. Weiner RB, DeLuca JR, Wang F, Lin J, Wasfy MM, Berkstresser B, Stohr E, Shave R, Lewis GD, Hutter AM, Jr., Picard MH and Baggish AL. Exercise-Induced Left Ventricular Remodeling Among Competitive Athletes: A Phasic Phenomenon. *Circ Cardiovasc Imaging*. 2015;8.

26. Wilson MG, Ellison GM and Cable NT. Basic science behind the cardiovascular benefits of exercise. *Heart*. 2015;101:758-65.

27. Zamilpa R and Lindsey ML. Extracellular matrix turnover and signaling during cardiac remodeling following MI: causes and consequences. *J Mol Cell Cardiol*. 2010;48:558-63.

28. Kong P, Christia P and Frangogiannis NG. The pathogenesis of cardiac fibrosis. *Cell Mol Life Sci*. 2014;71:549-74.

29. Richards DA, Bao W, Rambo MV, Burgert M, Jucker BM and Lenhard SC. Examining the relationship between exercise tolerance and isoproterenol-based cardiac reserve in murine models of heart failure. *J Appl Physiol*. 2013;114:1202-10.

30. Zeisberg EM, Tarnavski O, Zeisberg M, Dorfman AL, McMullen JR, Gustafsson E, Chandraker A, Yuan X, Pu WT, Roberts AB, Neilson EG, Sayegh MH, Izumo S and Kalluri R. Endothelial-to-mesenchymal transition contributes to cardiac fibrosis. *Nat Med*. 2007;13:952-61.

31. Grieve DJ, Byrne JA, Siva A, Layland J, Johar S, Cave AC and Shah AM. Involvement of the nicotinamide adenosine dinucleotide phosphate oxidase isoform Nox2 in cardiac contractile dysfunction occurring in response to pressure overload. *J Am Coll Cardiol*. 2006;47:817-26.

32. Looi YH, Grieve DJ, Siva A, Walker SJ, Anilkumar N, Cave AC, Marber M, Monaghan MJ and Shah AM. Involvement of Nox2 NADPH oxidase in adverse cardiac remodeling after myocardial infarction. *Hypertension*. 2008;51:319-25.

33. Li YQ, Li XB, Guo SJ, Chu SL, Gao PJ, Zhu DL, Niu WQ and Jia N. Apocynin attenuates oxidative stress and cardiac fibrosis in angiotensin II-induced cardiac diastolic dysfunction in mice. *Acta Pharmacol Sin*. 2013;34:352-9.

34. Zhang M, Brewer AC, Schroder K, Santos CX, Grieve DJ, Wang M, Anilkumar N, Yu B, Dong X, Walker SJ, Brandes RP and Shah AM. NADPH oxidase-4 mediates protection against chronic load-induced stress in mouse hearts by enhancing angiogenesis. *Proc Natl Acad Sci U S A*. 2010;107:18121-6.

35. Johar S, Cave AC, Narayanapanicker A, Grieve DJ and Shah AM. Aldosterone mediates angiotensin II-induced interstitial cardiac fibrosis via a Nox2-containing NADPH oxidase. *FASEB J*. 2006;20:1546-8.

36. Halper J and Kjaer M. Basic components of connective tissues and extracellular matrix: elastin, fibrillin, fibulins, fibrinogen, fibronectin, laminin, tenascins and thrombospondins. *Adv Exp Med Biol*. 2014;802:31-47.

37. Wagenseil JE, Ciliberto CH, Knutsen RH, Levy MA, Kovacs A and Mecham RP. Reduced vessel elasticity alters cardiovascular structure and function in newborn mice. *Circ Res*. 2009;104:1217-24.

38. Mizuno T, Yau TM, Weisel RD, Kiani CG and Li RK. Elastin stabilizes an infarct and preserves ventricular function. *Circulation*. 2005;112:I81-8.

39. Henderson BC, Sen U, Reynolds C, Moshal KS, Ovechkin A, Tyagi N, Kartha GK, Rodriguez WE and Tyagi SC. Reversal of systemic hypertension-associated cardiac remodeling in chronic pressure overload myocardium by ciglitazone. *Int J Biol Sci*. 2007;3:385-92.

40. Picard F, Brehm M, Fassbach M, Pelzer B, Scheuring S, Kury P, Strauer BE and Schwartzkopff B. Increased cardiac mRNA expression of matrix metalloproteinase-1 (MMP-1) and its inhibitor (TIMP-1) in DCM patients. *Clin Res Cardiol*. 2006;95:261-9.

41. Hoegy SE, Oh HR, Corcoran ML and Stetler-Stevenson WG. Tissue inhibitor of metalloproteinases-2 (TIMP-2) suppresses TKR-growth factor signaling independent of metalloproteinase inhibition. *J Biol Chem*. 2001;276:3203-14.

42. Okamoto H and Imanaka-Yoshida K. Matricellular proteins: new molecular targets to prevent heart failure. *Cardiovasc Ther*. 2012;30:e198-209.

43. Schellings MW, Vanhoutte D, van Almen GC, Swinnen M, Leenders JJ, Kubben N, van Leeuwen RE, Hofstra L, Heymans S and Pinto YM. Syndecan-1 amplifies angiotensin II-induced cardiac fibrosis. *Hypertension*. 2010;55:249-56.

44. Bradshaw AD, Baicu CF, Rentz TJ, Van Laer AO, Boggs J, Lacy JM and Zile MR. Pressure overload-induced alterations in fibrillar collagen content and myocardial diastolic function: role of secreted protein acidic and rich in cysteine (SPARC) in post-synthetic procollagen processing. *Circulation*. 2009;119:269-80.

45. Xie Z, Singh M and Singh K. Osteopontin modulates myocardial hypertrophy in response to chronic pressure overload in mice. *Hypertension*. 2004;44:826-31.

46. Souders CA, Bowers SL and Baudino TA. Cardiac fibroblast: the renaissance cell. *Circ Res*. 2009;105:1164-76.

47. Pellman J, Zhang J and Sheikh F. Myocyte-fibroblast communication in cardiac fibrosis and arrhythmias: Mechanisms and model systems. *J Mol Cell Cardiol*. 2016;94:22-31.

48. Koitabashi N, Danner T, Zaiman AL, Pinto YM, Rowell J, Mankowski J, Zhang D, Nakamura T, Takimoto E and Kass DA. Pivotal role of cardiomyocyte TGF-beta signaling in the murine pathological response to sustained pressure overload. *J Clin Invest*. 2011;121:2301-12.

49. Lauriol J, Keith K, Jaffre F, Couvillon A, Saci A, Goonasekera SA, McCarthy JR, Kessinger CW, Wang J, Ke Q, Kang PM, Molkentin JD, Carpenter C and Kontaridis MI. RhoA signaling in cardiomyocytes protects against stress-induced heart failure but facilitates cardiac fibrosis. *Sci Signal*. 2014;7:ra100.

50. Zhang D, Gaussin V, Taffet GE, Belaguli NS, Yamada M, Schwartz RJ, Michael LH, Overbeek PA and Schneider MD. TAK1 is activated in the myocardium after pressure overload and is sufficient to provoke heart failure in transgenic mice. *Nat Med*. 2000;6:556-63.

51. Kovacic JC, Mercader N, Torres M, Boehm M and Fuster V. Epithelial-to-mesenchymal and endothelial-to-mesenchymal transition: from cardiovascular development to disease. *Circulation*. 2012;125:1795-808.

52. Widyantoro B, Emoto N, Nakayama K, Anggrahini DW, Adiarto S, Iwasa N, Yagi K, Miyagawa K, Rikitake Y, Suzuki T, Kisanuki YY, Yanagisawa M and Hirata K. Endothelial cell-derived endothelin-1 promotes cardiac fibrosis in diabetic hearts through stimulation of endothelial-to-mesenchymal transition. *Circulation*. 2010;121:2407-18.

53. Murdoch CE, Chaubey S, Zeng L, Yu B, Ivetic A, Walker SJ, Vanhoutte D, Heymans S, Grieve DJ, Cave AC, Brewer AC, Zhang M and Shah AM. Endothelial NADPH oxidase-2 promotes interstitial cardiac fibrosis and diastolic dysfunction through proinflammatory effects and endothelial-mesenchymal transition. *J Am Coll Cardiol*. 2014;63:2734-41.

54. Adiarto S, Heiden S, Vignon-Zellweger N, Nakayama K, Yagi K, Yanagisawa M and Emoto N. ET-1 from endothelial cells is required for complete angiotensin II-induced cardiac fibrosis and hypertrophy. *Life Sci*. 2012;91:651-7.

55. Swirski FK and Nahrendorf M. Leukocyte behavior in atherosclerosis, myocardial infarction, and heart failure. *Science*. 2013;339:161-6.

56. Benigni A, Cassis P and Remuzzi G. Angiotensin II revisited: new roles in inflammation, immunology and aging. *EMBO Mol Med*. 2010;2:247-57.

57. Frieler RA and Mortensen RM. Immune cell and other noncardiomyocyte regulation of cardiac hypertrophy and remodeling. *Circulation*. 2015;131:1019-30.

58. Gonzalez GE, Rhaleb NE, D'Ambrosio MA, Nakagawa P, Liu Y, Leung P, Dai X, Yang XP, Peterson EL and Carretero OA. Deletion of interleukin-6 prevents cardiac inflammation, fibrosis and dysfunction without affecting blood pressure in angiotensin II-high salt-induced hypertension. *J Hypertens*. 2015;33:144-52.

59. Lin RJ, Su ZZ, Liang SM, Chen YY, Shu XR, Nie RQ, Wang JF and Xie SL. Role of Circulating Fibrocytes in Cardiac Fibrosis. *Chin Med J (Engl)*. 2016;129:326-31.

60. Keeley EC, Mehrad B and Strieter RM. The role of fibrocytes in fibrotic diseases of the lungs and heart. *Fibrogenesis Tissue Repair*. 2011;4:2.

61. Brilla CG and Weber KT. Reactive and reparative myocardial fibrosis in arterial hypertension in the rat. *Cardiovasc Res*. 1992;26:671-7.

62. Bendall JK, Cave AC, Heymes C, Gall N and Shah AM. Pivotal role of a gp91(phox)-containing NADPH oxidase in angiotensin II-induced cardiac hypertrophy in mice. *Circulation*. 2002;105:293-6.

63. Gonzalez A, Lopez B and Diez J. Fibrosis in hypertensive heart disease: role of the renin-angiotensin-aldosterone system. *Med Clin North Am*. 2004;88:83-97.

64. Rickard AJ, Morgan J, Bienvenu LA, Fletcher EK, Cranston GA, Shen JZ, Reichelt ME, Delbridge LM and Young MJ. Cardiomyocyte mineralocorticoid receptors are essential for deoxycorticosterone/salt-mediated inflammation and cardiac fibrosis. *Hypertension*. 2012;60:1443-50.

65. Chan V, Fenning A, Iyer A, Hoey A and Brown L. Resveratrol improves cardiovascular function in DOCA-salt hypertensive rats. *Curr Pharm Biotechnol*. 2011;12:429-36.

66. Kapur NK. Transforming growth factor-beta: governing the transition from inflammation to fibrosis in heart failure with preserved left ventricular function. *Circ Heart Fail*. 2011;4:5-7.

67. Li Q, Xu Y, Li X, Guo Y and Liu G. Inhibition of Rho-kinase ameliorates myocardial remodeling and fibrosis in pressure overload and myocardial infarction: role of TGF-beta1-TAK1. *Toxicol Lett*. 2012;211:91-7.

68. Kolwicz SC, Jr., Olson DP, Marney LC, Garcia-Menendez L, Synovec RE and Tian R. Cardiac-specific deletion of acetyl CoA carboxylase 2 prevents metabolic remodeling during pressure-overload hypertrophy. *Circ Res*. 2012;111:728-38.

69. Meems LM, Cannon MV, Mahmud H, Voors AA, van Gilst WH, Sillje HH, Ruifrok WP and de Boer RA. The vitamin D receptor activator paricalcitol prevents fibrosis and diastolic dysfunction in a murine model of pressure overload. *J Steroid Biochem Mol Biol*. 2012;132:282-9.

70. Morgan LA, Olzinski AR, Upson JJ, Zhao S, Wang T, Eisennagel SH, Hoang B, Tunstead JR, Marino JP, Jr., Willette RN, Jucker BM and Behm DJ. Soluble epoxide hydrolase inhibition does not prevent cardiac remodeling and dysfunction after aortic constriction in rats and mice. *J Cardiovasc Pharmacol*. 2013;61:291-301.

71. Chen Y, Guo H, Xu D, Xu X, Wang H, Hu X, Lu Z, Kwak D, Xu Y, Gunther R, Huo Y and Weir EK. Left ventricular failure produces profound lung remodeling and pulmonary hypertension in mice: heart failure causes severe lung disease. *Hypertension*. 2012;59:1170-8.

72. Toischer K, Rokita AG, Unsold B, Zhu W, Kararigas G, Sossalla S, Reuter SP, Becker A, Teucher N, Seidler T, Grebe C, Preuss L, Gupta SN, Schmidt K, Lehnart SE, Kruger M, Linke WA, Backs J, Regitz-Zagrosek V, Schafer K, Field LJ, Maier LS and Hasenfuss G. Differential cardiac remodeling in preload versus afterload. *Circulation*. 2010;122:993-1003.

73. Kong P, Christia P and Frangogiannis NG. The pathogenesis of cardiac fibrosis. *Cell Mol Life Sci*. 2013.

74. Sutton MG and Sharpe N. Left ventricular remodeling after myocardial infarction: pathophysiology and therapy. *Circulation*. 2000;101:2981-8.

75. Wenk JF, Klepach D, Lee LC, Zhang Z, Ge L, Tseng EE, Martin A, Kozerke S, Gorman JH, 3rd, Gorman RC and Guccione JM. First evidence of depressed contractility in the border zone of a human myocardial infarction. *Ann Thorac Surg*. 2012;93:1188-93.

76. Tang RN, Lv LL, Zhang JD, Dai HY, Li Q, Zheng M, Ni J, Ma KL and Liu BC. Effects of angiotensin II receptor blocker on myocardial endothelial-to-mesenchymal transition in diabetic rats. *Int J Cardiol*. 2013;162:92-9.

77. Stein M, Boulaksil M, Jansen JA, Herold E, Noorman M, Joles JA, van Veen TA, Houtman MJ, Engelen MA, Hauer RN, de Bakker JM and van Rijen HV. Reduction of fibrosis-related arrhythmias by chronic renin-angiotensin-aldosterone system inhibitors in an aged mouse model. *Am J Physiol Heart Circ Physiol*. 2010;299:H310-21.

78. Tachikawa H, Kodama M, Hui L, Yoshida T, Hayashi M, Abe S, Kashimura T, Kato K, Hanawa H, Watanabe K, Nakazawa M and Aizawa Y. Angiotensin II type 1 receptor blocker, valsartan, prevented cardiac fibrosis in rat cardiomyopathy after autoimmune myocarditis. *J Cardiovasc Pharmacol*. 2003;41 Suppl 1:S105-10.

79. Takeda Y, Yoneda T, Demura M, Usukura M and Mabuchi H. Calcineurin inhibition attenuates mineralocorticoid-induced cardiac hypertrophy. *Circulation*. 2002;105:677-9.

80. Milliez P, Deangelis N, Rucker-Martin C, Leenhardt A, Vicaut E, Robidel E, Beaufils P, Delcayre C and Hatem SN. Spironolactone reduces fibrosis of dilated atria during heart failure in rats with myocardial infarction. *Eur Heart J*. 2005;26:2193-9.

81. Okada H, Takemura G, Kosai K, Li Y, Takahashi T, Esaki M, Yuge K, Miyata S, Maruyama R, Mikami A, Minatoguchi S, Fujiwara T and Fujiwara H. Postinfarction gene therapy against transforming growth factor-beta signal modulates infarct tissue dynamics and attenuates left ventricular remodeling and heart failure. *Circulation*. 2005;111:2430-7.

82. Kuwahara F, Kai H, Tokuda K, Kai M, Takeshita A, Egashira K and Imaizumi T. Transforming growth factor-beta function blocking prevents myocardial fibrosis and diastolic dysfunction in pressure-overloaded rats. *Circulation*. 2002;106:130-5.

83. Wang X, Guo Z, Ding Z, Khaidakov M, Lin J, Xu Z, Sharma SG, Jiwani S and Mehta JL. Endothelin-1 upregulation mediates aging-related cardiac fibrosis. *J Mol Cell Cardiol*. 2015;80:101-9.

84. Yang B, Li M, Shi ZG and Feng QZ. Bosentan ameliorates the expression of fibrotic related growth factors and collagen-1 in diabetic mice. *Anadolu Kardiyol Derg*. 2012;12:621-7.

85. Yu M, Zheng Y, Sun HX and Yu DJ. Inhibitory effects of enalaprilat on rat cardiac fibroblast proliferation via ROS/P38MAPK/TGF-beta1 signaling pathway. *Molecules*. 2012;17:2738-51.

86. Liu RM and Gaston Pravia KA. Oxidative stress and glutathione in TGF-beta-mediated fibrogenesis. *Free Radic Biol Med*. 2010;48:1-15.

87. Fyhrquist F and Saijonmaa O. Renin-angiotensin system revisited. *J Intern Med*. 2008;264:224-36.

88. Atlas SA. The renin-angiotensin aldosterone system: pathophysiological role and pharmacologic inhibition. *J Manag Care Pharm*. 2007;13:9-20.

89. Te Riet L, van Esch JH, Roks AJ, van den Meiracker AH and Danser AH. Hypertension: renin-angiotensin-aldosterone system alterations. *Circ Res*. 2015;116:960-75.

90. Flores M, Graham D, Dominiczak AF, Milligan G, Baker AH and Nicklin SA. Abstract 231: Angiotensin-(1-9) Antagonises Cardiac Remodelling in a Mouse Model of Angiotensin Ii-induced Hypertension. *Hypertension*. 2012;60:A231-A231.

91. Dobaczewski M, Chen W and Frangogiannis NG. Transforming growth factor (TGF)-beta signaling in cardiac remodeling. *J Mol Cell Cardiol*. 2011;51:600-6.

92. Hein S, Arnon E, Kostin S, Schonburg M, Elsasser A, Polyakova V, Bauer EP, Klovekorn WP and Schaper J. Progression from compensated hypertrophy to failure in the pressure-overloaded human heart: structural deterioration and compensatory mechanisms. *Circulation*. 2003;107:984-91.

93. Teekakirikul P, Eminaga S, Toka O, Alcalai R, Wang L, Wakimoto H, Nayor M, Konno T, Gorham JM, Wolf CM, Kim JB, Schmitt JP, Molkentin JD, Norris RA, Tager AM, Hoffman SR, Markwald RR, Seidman CE and Seidman JG. Cardiac fibrosis in mice with hypertrophic cardiomyopathy is mediated by non-myocyte proliferation and requires Tgf-beta. *J Clin Invest*. 2010;120:3520-9.

94. Kitao A, Sato Y, Sawada-Kitamura S, Harada K, Sasaki M, Morikawa H, Shiomi S, Honda M, Matsui O and Nakanuma Y. Endothelial to mesenchymal transition via transforming growth factor-beta1/Smad activation is associated with portal venous stenosis in idiopathic portal hypertension. *Am J Pathol*. 2009;175:616-26.

95. Leask A. Potential therapeutic targets for cardiac fibrosis: TGFbeta, angiotensin, endothelin, CCN2, and PDGF, partners in fibroblast activation. *Circ Res*. 2010;106:1675-80.

96. Cheng TH, Shih NL, Chen SY, Wang DL and Chen JJ. Reactive oxygen species modulate endothelin-I-induced c-fos gene expression in cardiomyocytes. *Cardiovasc Res*. 1999;41:654-62.

97. Lund AK, Peterson SL, Timmins GS and Walker MK. Endothelin-1-mediated increase in reactive oxygen species and NADPH Oxidase activity in hearts of aryl hydrocarbon receptor (AhR) null mice. *Toxicol Sci*. 2005;88:265-73.

98. Thannickal VJ and Fanburg BL. Reactive oxygen species in cell signaling. *Am J Physiol Lung Cell Mol Physiol*. 2000;279:L1005-28.

99. Cave A, Grieve D, Johar S, Zhang M and Shah AM. NADPH oxidase-derived reactive oxygen species in cardiac pathophysiology. *Philos Trans R Soc Lond B Biol Sci*. 2005;360:2327-34.

100. Irani K, Xia Y, Zweier JL, Sollott SJ, Der CJ, Fearon ER, Sundaresan M, Finkel T and Goldschmidt-Clermont PJ. Mitogenic signaling mediated by oxidants in Ras-transformed fibroblasts. *Science*. 1997;275:1649-52.

101. Zhao W, Zhao T, Chen Y, Ahokas RA and Sun Y. Oxidative stress mediates cardiac fibrosis by enhancing transforming growth factor-beta1 in hypertensive rats. *Mol Cell Biochem*. 2008;317:43-50.

102. Nabeebaccus A, Zhang M and Shah AM. NADPH oxidases and cardiac remodelling. *Heart Fail Rev*. 2011;16:5-12.

103. Burgoyne JR, Mongue-Din H, Eaton P and Shah AM. Redox signaling in cardiac physiology and pathology. *Circ Res*. 2012;111:1091-106.

104. Slupphaug G, Kavli B and Krokan HE. The interacting pathways for prevention and repair of oxidative DNA damage. *Mutat Res*. 2003;531:231-51.

105. D'Autreaux B and Toledano MB. ROS as signalling molecules: mechanisms that generate specificity in ROS homeostasis. *Nat Rev Mol Cell Biol*. 2007;8:813-24.

106. Paravicini TM and Touyz RM. NADPH oxidases, reactive oxygen species, and hypertension: clinical implications and therapeutic possibilities. *Diabetes Care*. 2008;31 Suppl 2:S170-80.

107. Kalyanaraman B. Teaching the basics of redox biology to medical and graduate students: Oxidants, antioxidants and disease mechanisms. *Redox Biol*. 2013;1:244-57.

108. Seddon M, Looi YH and Shah AM. Oxidative stress and redox signalling in cardiac hypertrophy and heart failure. *Heart*. 2007;93:903-7.

109. Matsushima S, Ide T, Yamato M, Matsusaka H, Hattori F, Ikeuchi M, Kubota T, Sunagawa K, Hasegawa Y, Kurihara T, Oikawa S, Kinugawa S and Tsutsui H. Overexpression of mitochondrial peroxiredoxin-3 prevents left ventricular remodeling and failure after myocardial infarction in mice. *Circulation*. 2006;113:1779-86.

110. Marian AJ, Senthil V, Chen SN and Lombardi R. Antifibrotic effects of antioxidant N-acetylcysteine in a mouse model of human hypertrophic cardiomyopathy mutation. *J Am Coll Cardiol*. 2006;47:827-34.

111. Tsujimoto I, Hikoso S, Yamaguchi O, Kashiwase K, Nakai A, Takeda T, Watanabe T, Taniike M, Matsumura Y, Nishida K, Hori M, Kogo M and Otsu K. The antioxidant edaravone attenuates pressure overload-induced left ventricular hypertrophy. *Hypertension*. 2005;45:921-6.

112. Lombardi R, Rodriguez G, Chen SN, Ripplinger CM, Li W, Chen J, Willerson JT, Betocchi S, Wickline SA, Efimov IR and Marian AJ. Resolution of established cardiac hypertrophy and fibrosis and prevention of systolic dysfunction in a transgenic rabbit model of human cardiomyopathy through thiol-sensitive mechanisms. *Circulation*. 2009;119:1398-407.

113. Hill MF. Emerging role for antioxidant therapy in protection against diabetic cardiac complications: experimental and clinical evidence for utilization of classic and new antioxidants. *Curr Cardiol Rev*. 2008;4:259-68.

114. Bedard K and Krause KH. The NOX family of ROS-generating NADPH oxidases: physiology and pathophysiology. *Physiol Rev*. 2007;87:245-313.

115. Lassegue B, San Martin A and Griendling KK. Biochemistry, physiology, and pathophysiology of NADPH oxidases in the cardiovascular system. *Circ Res*. 2012;110:1364-90.

116. Martyn KD, Frederick LM, von Loehneysen K, Dinauer MC and Knaus UG. Functional analysis of Nox4 reveals unique characteristics compared to other NADPH oxidases. *Cell Signal*. 2006;18:69-82.

117. Touyz RM, Mercure C, He Y, Javeshghani D, Yao G, Callera GE, Yogi A, Lochard N and Reudelhuber TL. Angiotensin II-dependent chronic hypertension and cardiac hypertrophy are unaffected by gp91phox-containing NADPH oxidase. *Hypertension*. 2005;45:530-7.

118. Parajuli N, Patel VB, Wang W, Basu R and Oudit GY. Loss of NOX2 (gp91phox) prevents oxidative stress and progression to advanced heart failure. *Clin Sci (Lond)*. 2014;127:331-40.

119. Doerries C, Grote K, Hilfiker-Kleiner D, Luchtefeld M, Schaefer A, Holland SM, Sorrentino S, Manes C, Schieffer B, Drexler H and Landmesser U. Critical role of the NAD(P)H oxidase subunit p47phox for left ventricular remodeling/dysfunction and survival after myocardial infarction. *Circ Res*. 2007;100:894-903.

120. Heymes C, Bendall JK, Ratajczak P, Cave AC, Samuel JL, Hasenfuss G and Shah AM. Increased myocardial NADPH oxidase activity in human heart failure. *J Am Coll Cardiol*. 2003;41:2164-71.

121. Krijnen PA, Meischl C, Hack CE, Meijer CJ, Visser CA, Roos D and Niessen HW. Increased Nox2 expression in human cardiomyocytes after acute myocardial infarction. *J Clin Pathol*. 2003;56:194-9.

122. Meischl C, Krijnen PA, Sipkens JA, Cillessen SA, Munoz IG, Okroj M, Ramska M, Muller A, Visser CA, Musters RJ, Simonides WS, Hack CE, Roos D and Niessen HW. Ischemia induces nuclear NOX2 expression in cardiomyocytes and subsequently activates apoptosis. *Apoptosis*. 2006;11:913-21.

123. Sirker A, Murdoch CE, Protti A, Sawyer GJ, Santos CX, Martin D, Zhang X, Brewer AC, Zhang M and Shah AM. Cell-specific effects of Nox2 on the acute and chronic response to myocardial infarction. *J Mol Cell Cardiol*. 2016;98:11-17.

124. Murdoch CE, Alom-Ruiz SP, Wang M, Zhang M, Walker S, Yu B, Brewer A and Shah AM. Role of endothelial Nox2 NADPH oxidase in angiotensin II-induced hypertension and vasomotor dysfunction. *Basic Res Cardiol*. 2011;106:527-38.

125. Hayashi S and McMahon AP. Efficient recombination in diverse tissues by a tamoxifen-inducible form of Cre: a tool for temporally regulated gene activation/inactivation in the mouse. *Dev Biol*. 2002;244:305-18.

126. Bouabe H and Okkenhaug K. Gene targeting in mice: a review. *Methods Mol Biol*. 2013;1064:315-36.

127. Feil R, Wagner J, Metzger D and Chambon P. Regulation of Cre recombinase activity by mutated estrogen receptor ligand-binding domains. *Biochem Biophys Res Commun*. 1997;237:752-7.

128. Mattioni T, Louvion JF and Picard D. Regulation of protein activities by fusion to steroid binding domains. *Methods Cell Biol*. 1994;43 Pt A:335-52.

129. Kanisicak O, Khalil H, Ivey MJ, Karch J, Maliken BD, Correll RN, Brody MJ, SC JL, Aronow BJ, Tallquist MD and Molkentin JD. Genetic lineage tracing defines myofibroblast origin and function in the injured heart. *Nat Commun*. 2016;7:12260.

130. Monvoisin A, Alva JA, Hofmann JJ, Zovein AC, Lane TF and Iruela-Arispe ML. VE-cadherin-CreERT2 transgenic mouse: a model for inducible recombination in the endothelium. *Dev Dyn*. 2006;235:3413-22.

131. Fioret BA, Heimfeld JD, Paik DT and Hatzopoulos AK. Endothelial cells contribute to generation of adult ventricular myocytes during cardiac homeostasis. *Cell Rep*. 2014;8:229-41.

132. Zheng B, Zhang Z, Black CM, de Crombrugghe B and Denton CP. Ligand-dependent genetic recombination in fibroblasts : a potentially powerful technique for investigating gene function in fibrosis. *Am J Pathol*. 2002;160:1609-17.

133. Kretzschmar K and Watt FM. Lineage tracing. *Cell*. 2012;148:33-45.

134. Driskell RR, Lichtenberger BM, Hoste E, Kretzschmar K, Simons BD, Charalambous M, Ferron SR, Herault Y, Pavlovic G, Ferguson-Smith AC and Watt FM. Distinct fibroblast lineages determine dermal architecture in skin development and repair. *Nature*. 2013;504:277-81.

135. Ubil E, Duan J, Pillai IC, Rosa-Garrido M, Wu Y, Bargiacchi F, Lu Y, Stanbouly S, Huang J, Rojas M, Vondriska TM, Stefani E and Deb A. Mesenchymal-endothelial transition contributes to cardiac neovascularization. *Nature*. 2014;514:585-90.

136. Duan J, Gherghe C, Liu D, Hamlett E, Srikantha L, Rodgers L, Regan JN, Rojas M, Willis M, Leask A, Majesky M and Deb A. Wnt1/betacatenin injury response activates the epicardium and cardiac fibroblasts to promote cardiac repair. *EMBO J*. 2012;31:429-42.

137. Ponticos M, Abraham D, Alexakis C, Lu QL, Black C, Partridge T and Bou-Gharios G. Col1a2 enhancer regulates collagen activity during development and in adult tissue repair. *Matrix biology : journal of the International Society for Matrix Biology*. 2004;22:619-28.

138. Kapoor M, Liu S, Shi-wen X, Huh K, McCann M, Denton CP, Woodgett JR, Abraham DJ and Leask A. GSK-3beta in mouse fibroblasts controls wound healing and fibrosis through an endothelin-1-dependent mechanism. *J Clin Invest*. 2008;118:3279-90.

139. Van Handel B, Montel-Hagen A, Sasidharan R, Nakano H, Ferrari R, Boogerd CJ, Schredelseker J, Wang Y, Hunter S, Org T, Zhou J, Li X, Pellegrini M, Chen JN, Orkin SH, Kurdistani SK, Evans SM, Nakano A and Mikkola HK. Scl represses cardiomyogenesis in prospective hemogenic endothelium and endocardium. *Cell*. 2012;150:590-605.

140. Martin TP, Robinson E, Harvey AP, MacDonald M, Grieve DJ, Paul A and Currie S. Surgical optimization and characterization of a minimally invasive aortic banding procedure to induce cardiac hypertrophy in mice. *Exp Physiol*. 2012;97:822-32.

141. Mohammed SF, Storlie JR, Oehler EA, Bowen LA, Korinek J, Lam CS, Simari RD, Burnett JC, Jr. and Redfield MM. Variable phenotype in murine transverse aortic constriction. *Cardiovasc Pathol*. 2012;21:188-98.

142. Bhan A, Sirker A, Zhang J, Protti A, Catibog N, Driver W, Botnar R, Monaghan MJ and Shah AM. High-frequency speckle tracking echocardiography in the assessment of left ventricular function and remodeling after murine myocardial infarction. *Am J Physiol Heart Circ Physiol*. 2014;306:H1371-83.

143. de Jong S, van Veen TA, de Bakker JM and van Rijen HV. Monitoring cardiac fibrosis: a technical challenge. *Neth Heart J*. 2012;20:44-8.

144. Kawano S, Kubota T, Monden Y, Kawamura N, Tsutsui H, Takeshita A and Sunagawa K. Blockade of NF-kappaB ameliorates myocardial hypertrophy in response to chronic infusion of angiotensin II. *Cardiovasc Res*. 2005;67:689-98.

145. Ichihara S, Senbonmatsu T, Price E, Jr., Ichiki T, Gaffney FA and Inagami T. Angiotensin II type 2 receptor is essential for left ventricular hypertrophy and cardiac fibrosis in chronic angiotensin II-induced hypertension. *Circulation*. 2001;104:346-51.

146. Rocic P and Lucchesi PA. NAD(P)H oxidases and TGF-beta-induced cardiac fibroblast differentiation: Nox-4 gets Smad. *Circ Res*. 2005;97:850-2.

147. Bondi CD, Manickam N, Lee DY, Block K, Gorin Y, Abboud HE and Barnes JL. NAD(P)H oxidase mediates TGF-beta1-induced activation of kidney myofibroblasts. *J Am Soc Nephrol*. 2010;21:93-102.

148. Djamali A, Vidyasagar A, Adulla M, Hullett D and Reese S. Nox-2 is a modulator of fibrogenesis in kidney allografts. *Am J Transplant*. 2009;9:74-82.

149. Bataller R, Schwabe RF, Choi YH, Yang L, Paik YH, Lindquist J, Qian T, Schoonhoven R, Hagedorn CH, Lemasters JJ and Brenner DA. NADPH oxidase signal transduces angiotensin II in hepatic stellate cells and is critical in hepatic fibrosis. *J Clin Invest*. 2003;112:1383-94.

150. Amara N, Goven D, Prost F, Muloway R, Crestani B and Boczkowski J. NOX4/NADPH oxidase expression is increased in pulmonary fibroblasts from patients with idiopathic pulmonary fibrosis and mediates TGFbeta1-induced fibroblast differentiation into myofibroblasts. *Thorax*. 2010;65:733-8.

151. Kuroda J, Ago T, Matsushima S, Zhai P, Schneider MD and Sadoshima J. NADPH oxidase 4 (Nox4) is a major source of oxidative stress in the failing heart. *Proc Natl Acad Sci U S A*. 2010;107:15565-70.

152. Byrne JA, Grieve DJ, Bendall JK, Li JM, Gove C, Lambeth JD, Cave AC and Shah AM. Contrasting roles of NADPH oxidase isoforms in pressure-overload versus angiotensin II-induced cardiac hypertrophy. *Circ Res*. 2003;93:802-5.

153. Ram R, Mickelsen DM, Theodoropoulos C and Blaxall BC. New approaches in small animal echocardiography: imaging the sounds of silence. *Am J Physiol Heart Circ Physiol*. 2011;301:H1765-80.

154. Harada K, Komuro I, Shiojima I, Hayashi D, Kudoh S, Mizuno T, Kijima K, Matsubara H, Sugaya T, Murakami K and Yazaki Y. Pressure overload induces cardiac hypertrophy in angiotensin II type 1A receptor knockout mice. *Circulation*. 1998;97:1952-9.

155. Kim S and Iwao H. Molecular and cellular mechanisms of angiotensin II-mediated cardiovascular and renal diseases. *Pharmacol Rev*. 2000;52:11-34.

156. Inanaga K, Ichiki T, Matsuura H, Miyazaki R, Hashimoto T, Takeda K and Sunagawa K. Resveratrol attenuates angiotensin II-induced interleukin-6 expression and perivascular fibrosis. *Hypertens Res*. 2009;32:466-71.

157. Kawada N, Imai E, Karber A, Welch WJ and Wilcox CS. A mouse model of angiotensin II slow pressor response: role of oxidative stress. *Journal of the American Society of Nephrology : JASN*. 2002;13:2860-8.

158. Schultz Jel J, Witt SA, Glascock BJ, Nieman ML, Reiser PJ, Nix SL, Kimball TR and Doetschman T. TGF-beta1 mediates the hypertrophic cardiomyocyte growth induced by angiotensin II. *J Clin Invest*. 2002;109:787-96.

159. Venegas-Pont M, Sartori-Valinotti JC, Glover PH, Reckelhoff JF and Ryan MJ. Sexual dimorphism in the blood pressure response to angiotensin II in mice after angiotensin-converting enzyme blockade. *American journal of hypertension*. 2010;23:92-6.

160. Danser AHJ. Cardiac angiotensin II: does it have a function? *American Journal of Physiology - Heart and Circulatory Physiology*. 2010;299:H1304-H1306.

161. Xu J, Carretero OA, Liao T-D, Peng H, Shesely EG, Xu J, Liu TS, Yang JJ, Reudelhuber TL and Yang X-P. Local angiotensin II aggravates cardiac remodeling in hypertension. *American Journal of Physiology - Heart and Circulatory Physiology*. 2010;299:H1328-H1338.

162. Florin L, Alter H, Grone HJ, Szabowski A, Schutz G and Angel P. Cre recombinase-mediated gene targeting of mesenchymal cells. *Genesis*. 2004;38:139-44.

163. Junqueira LC, Bignolas G and Brentani RR. Picrosirius staining plus polarization microscopy, a specific method for collagen detection in tissue sections. *Histochem J*. 1979;11:447-55.

164. Whittaker P, Kloner RA, Boughner DR and Pickering JG. Quantitative assessment of myocardial collagen with picrosirius red staining and circularly polarized light. *Basic Res Cardiol*. 1994;89:397-410.

165. Lattouf R, Younes R, Lutomski D, Naaman N, Godeau G, Senni K and Changotade S. Picrosirius red staining: a useful tool to appraise collagen networks in normal and pathological tissues. *J Histochem Cytochem*. 2014;62:751-8.

166. Rich L and Whittaker P. Collagen and picrosirius red staining: a polarized light assessment of fibrillar hue and spatial distribution. *Braz J Morphol Sci*. 2005;22:97–104.

167. Martino TA, Tata N, Simpson JA, Vanderlaan R, Dawood F, Kabir MG, Khaper N, Cifelli C, Podobed P, Liu PP, Husain M, Heximer S, Backx PH and Sole MJ. The primary benefits of angiotensin-converting enzyme inhibition on cardiac remodeling occur during sleep time in murine pressure overload hypertrophy. *J Am Coll Cardiol*. 2011;57:2020-8.

168. Nagueh SF, Appleton CP, Gillebert TC, Marino PN, Oh JK, Smiseth OA, Waggoner AD, Flachskampf FA, Pellikka PA and Evangelista A. Recommendations for the evaluation of left ventricular diastolic function by echocardiography. *J Am Soc Echocardiogr*. 2009;22:107-33.

169. Liao R, Jain M, Cui L, D'Agostino J, Aiello F, Luptak I, Ngoy S, Mortensen RM and Tian R. Cardiac-specific overexpression of GLUT1 prevents the development of heart failure attributable to pressure overload in mice. *Circulation*. 2002;106:2125-31.

170. Patten RD and Hall-Porter MR. Small animal models of heart failure: development of novel therapies, past and present. *Circ Heart Fail*. 2009;2:138-44.

171. deAlmeida AC, van Oort RJ and Wehrens XH. Transverse aortic constriction in mice. *J Vis Exp*. 2010.

172. Souders CA, Borg TK, Banerjee I and Baudino TA. Pressure overload induces early morphological changes in the heart. *Am J Pathol*. 2012;181:1226-35.

173. Akishita M, Iwai M, Wu L, Zhang L, Ouchi Y, Dzau VJ and Horiuchi M. Inhibitory effect of angiotensin II type 2 receptor on coronary arterial remodeling after aortic banding in mice. *Circulation*. 2000;102:1684-9.

174. Maytin M, Siwik DA, Ito M, Xiao L, Sawyer DB, Liao R and Colucci WS. Pressure overload-induced myocardial hypertrophy in mice does not require gp91phox. *Circulation*. 2004;109:1168-71.

175. Kandalam V, Basu R, Moore L, Fan D, Wang X, Jaworski DM, Oudit GY and Kassiri Z. Lack of tissue inhibitor of metalloproteinases 2 leads to exacerbated left ventricular dysfunction and adverse extracellular matrix remodeling in response to biomechanical stress. *Circulation*. 2011;124:2094-105.

176. Lakatta EG and Levy D. Arterial and cardiac aging: major shareholders in cardiovascular disease enterprises: Part II: the aging heart in health: links to heart disease. *Circulation*. 2003;107:346-54.

177. Sopel MJ, Rosin NL, Lee TD and Legare JF. Myocardial fibrosis in response to Angiotensin II is preceded by the recruitment of mesenchymal progenitor cells. *Lab Invest*. 2011;91:565-78.

178. Brandes RP, Weissmann N and Schroder K. Nox family NADPH oxidases: Molecular mechanisms of activation. *Free Radic Biol Med*. 2014;76:208-26.

179. Prosser BL, Ward CW and Lederer WJ. X-ROS signalling is enhanced and graded by cyclic cardiomyocyte stretch. *Cardiovasc Res*. 2013;98:307-14.

180. Carver W, Nagpal ML, Nachtigal M, Borg TK and Terracio L. Collagen expression in mechanically stimulated cardiac fibroblasts. *Circ Res*. 1991;69:116-22.

181. Friis MB, Vorum KG and Lambert IH. Volume-sensitive NADPH oxidase activity and taurine efflux in NIH3T3 mouse fibroblasts. *Am J Physiol Cell Physiol*. 2008;294:C1552-65.

182. Xia Y, Lee K, Li N, Corbett D, Mendoza L and Frangogiannis NG. Characterization of the inflammatory and fibrotic response in a mouse model of cardiac pressure overload. *Histochem Cell Biol*. 2009;131:471-81.

183. Damilano F, Franco I, Perrino C, Schaefer K, Azzolino O, Carnevale D, Cifelli G, Carullo P, Ragona R, Ghigo A, Perino A, Lembo G and Hirsch E. Distinct effects of leukocyte and cardiac phosphoinositide 3-kinase gamma activity in pressure overload-induced cardiac failure. *Circulation*. 2011;123:391-9.

184. Takeda N, Manabe I, Uchino Y, Eguchi K, Matsumoto S, Nishimura S, Shindo T, Sano M, Otsu K, Snider P, Conway SJ and Nagai R. Cardiac fibroblasts are essential for the adaptive response of the murine heart to pressure overload. *J Clin Invest*. 2010;120:254-65.

185. Bernardo BC, Nguyen SS, Gao XM, Tham YK, Ooi JY, Patterson NL, Kiriazis H, Su Y, Thomas CJ, Lin RC, Du XJ and McMullen JR. Inhibition of miR-154 Protects Against Cardiac Dysfunction and Fibrosis in a Mouse Model of Pressure Overload. *Sci Rep*. 2016;6:22442.

186. Balasubramanian S, Pleasant DL, Kasiganesan H, Quinones L, Zhang Y, Sundararaj KP, Roche S, O'Connor R, Bradshaw AD and Kuppuswamy D. Dasatinib Attenuates Pressure Overload Induced Cardiac Fibrosis in a Murine Transverse Aortic Constriction Model. *PLoS One*. 2015;10:e0140273.

187. Collins KA, Korcarz CE and Lang RM. Use of echocardiography for the phenotypic assessment of genetically altered mice. *Physiol Genomics*. 2003;13:227-39.

188. Garcia MJ, Thomas JD and Klein AL. New Doppler echocardiographic applications for the study of diastolic function. *J Am Coll Cardiol*. 1998;32:865-75.

189. Versari D, Daghini E, Virdis A, Ghiadoni L and Taddei S. Endothelial dysfunction as a target for prevention of cardiovascular disease. *Diabetes Care*. 2009;32 Suppl 2:S314-21.

190. Shesely EG, Maeda N, Kim HS, Desai KM, Krege JH, Laubach VE, Sherman PA, Sessa WC and Smithies O. Elevated blood pressures in mice lacking endothelial nitric oxide synthase. *Proc Natl Acad Sci U S A*. 1996;93:13176-81.

191. Flaherty MP, Brown M, Grupp IL, Schultz JE, Murphree SS and Jones WK. eNOS deficient mice develop progressive cardiac hypertrophy with altered cytokine and calcium handling protein expression. *Cardiovasc Toxicol*. 2007;7:165-77.

192. Deanfield JE, Halcox JP and Rabelink TJ. Endothelial function and dysfunction: testing and clinical relevance. *Circulation*. 2007;115:1285-95.

193. Zhang M and Shah AM. ROS signalling between endothelial cells and cardiac cells. *Cardiovasc Res*. 2014;102:249-57.

194. Hocher B, Schwarz A, Fagan KA, Thone-Reineke C, El-Hag K, Kusserow H, Elitok S, Bauer C, Neumayer HH, Rodman DM and Theuring F. Pulmonary fibrosis and chronic lung inflammation in ET-1 transgenic mice. *Am J Respir Cell Mol Biol*. 2000;23:19-26.

195. Song H, Conte JV, Jr., Foster AH, McLaughlin JS and Wei C. Increased p53 protein expression in human failing myocardium. *J Heart Lung Transplant*. 1999;18:744-9.

196. Gogiraju R, Xu X, Bochenek ML, Steinbrecher JH, Lehnart SE, Wenzel P, Kessel M, Zeisberg EM, Dobbelstein M and Schafer K. Endothelial p53 deletion improves angiogenesis and prevents cardiac fibrosis and heart failure induced by pressure overload in mice. *J Am Heart Assoc*. 2015;4.

197. Zeisberg EM and Kalluri R. Origins of cardiac fibroblasts. *Circ Res*. 2010;107:1304-12.

198. Lee SW, Won JY, Kim WJ, Lee J, Kim KH, Youn SW, Kim JY, Lee EJ, Kim YJ, Kim KW and Kim HS. Snail as a potential target molecule in cardiac fibrosis: paracrine action of endothelial cells on fibroblasts through snail and CTGF axis. *Mol Ther*. 2013;21:1767-77.

199. Banerjee I, Fuseler JW, Price RL, Borg TK and Baudino TA. Determination of cell types and numbers during cardiac development in the neonatal and adult rat and mouse. *Am J Physiol Heart Circ Physiol*. 2007;293:H1883-91.

200. van Nierop BJ, van Assen HC, van Deel ED, Niesen LB, Duncker DJ, Strijkers GJ and Nicolay K. Phenotyping of left and right ventricular function in mouse models of compensated hypertrophy and heart failure with cardiac MRI. *PLoS One*. 2013;8:e55424.

201. Drummond GR and Sobey CG. Endothelial NADPH oxidases: which NOX to target in vascular disease? *Trends Endocrinol Metab*. 2014;25:452-63.

202. Ruetten H, Dimmeler S, Gehring D, Ihling C and Zeiher AM. Concentric left ventricular remodeling in endothelial nitric oxide synthase knockout mice by chronic pressure overload. *Cardiovasc Res*. 2005;66:444-53.

203. Hermans H, Swinnen M, Pokreisz P, Caluwe E, Dymarkowski S, Herregods MC, Janssens S and Herijgers P. Murine pressure overload models: a 30-MHz look brings a whole new "sound" into data interpretation. *J Appl Physiol (1985)*. 2014;117:563-71.

204. Tirziu D, Giordano FJ and Simons M. Cell communications in the heart. *Circulation*. 2010;122:928-37.

205. Tang Y, Harrington A, Yang X, Friesel RE and Liaw L. The contribution of the Tie2+ lineage to primitive and definitive hematopoietic cells. *Genesis*. 2010;48:563-7.

206. Zeisberg EM, Potenta SE, Sugimoto H, Zeisberg M and Kalluri R. Fibroblasts in kidney fibrosis emerge via endothelial-to-mesenchymal transition. *J Am Soc Nephrol*. 2008;19:2282-7.

207. Li J, Qu X and Bertram JF. Endothelial-myofibroblast transition contributes to the early development of diabetic renal interstitial fibrosis in streptozotocin-induced diabetic mice. *Am J Pathol*. 2009;175:1380-8.

208. Hashimoto N, Phan SH, Imaizumi K, Matsuo M, Nakashima H, Kawabe T, Shimokata K and Hasegawa Y. Endothelial-mesenchymal transition in bleomycin-induced pulmonary fibrosis. *Am J Respir Cell Mol Biol*. 2010;43:161-72.

209. Xu X, Tan X, Tampe B, Sanchez E, Zeisberg M and Zeisberg EM. Snail Is a Direct Target of Hypoxia-inducible Factor 1alpha (HIF1alpha) in Hypoxia-induced Endothelial to Mesenchymal Transition of Human Coronary Endothelial Cells. *J Biol Chem*. 2015;290:16653-64.

210. Zhaocai Z and Jianan W. MENSTRUAL BLOOD STEM CELLS ATTENUATE POST-INFARCTION MYOCARDIAL FIBROSIS VIA INHIBITING ENDOTHELIAL TO MESENCHYMAL TRANSITION (ENDMT). *Heart*. 2012;98:E36.

211. Zhou X, Chen X, Cai JJ, Chen LZ, Gong YS, Wang LX, Gao Z, Zhang HQ, Huang WJ and Zhou H. Relaxin inhibits cardiac fibrosis and endothelial-mesenchymal transition via the Notch pathway. *Drug Des Devel Ther*. 2015;9:4599-611.

212. Kong P, Christia P, Saxena A, Su Y and Frangogiannis NG. Lack of specificity of fibroblast-specific protein 1 in cardiac remodeling and fibrosis. *Am J Physiol Heart Circ Physiol*. 2013;305:H1363-72.

213. Moore-Morris T, Guimaraes-Camboa N, Banerjee I, Zambon AC, Kisseleva T, Velayoudon A, Stallcup WB, Gu Y, Dalton ND, Cedenilla M, Gomez-Amaro R, Zhou B, Brenner DA, Peterson KL, Chen J and Evans SM. Resident fibroblast lineages mediate pressure overload-induced cardiac fibrosis. *J Clin Invest*. 2014;124:2921-34.

214. Maecker HT and Trotter J. Flow cytometry controls, instrument setup, and the determination of positivity. *Cytometry A*. 2006;69:1037-42.

215. Furtado MB, Costa MW, Pranoto EA, Salimova E, Pinto AR, Lam NT, Park A, Snider P, Chandran A, Harvey RP, Boyd R, Conway SJ, Pearson J, Kaye DM and Rosenthal NA. Cardiogenic genes expressed in cardiac fibroblasts contribute to heart development and repair. *Circ Res*. 2014;114:1422-34.

216. Ali SR, Ranjbarvaziri S, Talkhabi M, Zhao P, Subat A, Hojjat A, Kamran P, Muller AM, Volz KS, Tang Z, Red-Horse K and Ardehali R. Developmental heterogeneity of cardiac fibroblasts does not predict pathological proliferation and activation. *Circ Res*. 2014;115:625-35.

217. Gu JM, Crawley JT, Ferrell G, Zhang F, Li W, Esmon NL and Esmon CT. Disruption of the endothelial cell protein C receptor gene in mice causes placental thrombosis and early embryonic lethality. *J Biol Chem*. 2002;277:43335-43.

218. Crawley JT, Gu JM, Ferrell G and Esmon CT. Distribution of endothelial cell protein C/activated protein C receptor (EPCR) during mouse embryo development. *Thromb Haemost*. 2002;88:259-66.

219. Fukudome K and Esmon CT. Molecular cloning and expression of murine and bovine endothelial cell protein C/activated protein C receptor (EPCR). The structural and functional conservation in human, bovine, and murine EPCR. *J Biol Chem*. 1995;270:5571-7.

220. Moore-Morris T, Guimaraes-Camboa N, Yutzey KE, Puceat M and Evans SM. Cardiac fibroblasts: from development to heart failure. *J Mol Med (Berl)*. 2015;93:823-30.

221. Morris LM, Klanke CA, Lang SA, Lim FY and Crombleholme TM. TdTomato and EGFP identification in histological sections: insight and alternatives. *Biotech Histochem*. 2010;85:379-87.

222. Spinale FG, Escobar GP, Hendrick JW, Clark LL, Camens SS, Mingoia JP, Squires CG, Stroud RE and Ikonomidis JS. Chronic matrix metalloproteinase inhibition following myocardial infarction in mice: differential effects on short and long-term survival. *J Pharmacol Exp Ther*. 2006;318:966-73.

223. Samuel CS, Bodaragama H, Chew JY, Widdop RE, Royce SG and Hewitson TD. Serelaxin is a more efficacious antifibrotic than enalapril in an experimental model of heart disease. *Hypertension*. 2014;64:315-22.

224. Teerlink JR, Cotter G, Davison BA, Felker GM, Filippatos G, Greenberg BH, Ponikowski P, Unemori E, Voors AA, Adams KF, Jr., Dorobantu MI, Grinfeld LR, Jondeau G, Marmor A, Masip J, Pang PS, Werdan K, Teichman SL, Trapani A, Bush CA, Saini R, Schumacher C, Severin TM, Metra M and Investigators REiAHF. Serelaxin, recombinant human relaxin-2, for treatment of acute heart failure (RELAX-AHF): a randomised, placebo-controlled trial. *Lancet*. 2013;381:29-39.

225. Tietjens J and Teerlink JR. Serelaxin and acute heart failure. *Heart*. 2015.

226. Gupta PK, DiPette DJ and Supowit SC. Protective effect of resveratrol against pressure overload-induced heart failure. *Food Sci Nutr*. 2014;2:218-29.

227. Mouton A, Walker M, El Hajj M, Molina P, Gilpin N and Gardner J. Ethanol-induced cardiac fibrosis is mediated by NADPH oxidase (1152.12). *The FASEB Journal*. 2014;28.

228. Dikalov SI and Harrison DG. Methods for detection of mitochondrial and cellular reactive oxygen species. *Antioxid Redox Signal*. 2014;20:372-82.

229. Tamura N, Ogawa Y, Chusho H, Nakamura K, Nakao K, Suda M, Kasahara M, Hashimoto R, Katsuura G, Mukoyama M, Itoh H, Saito Y, Tanaka I, Otani H and Katsuki M. Cardiac fibrosis in mice lacking brain natriuretic peptide. *Proc Natl Acad Sci U S A*. 2000;97:4239-44.

230. Ogawa Y, Tamura N, Chusho H and Nakao K. Brain natriuretic peptide appears to act locally as an antifibrotic factor in the heart. *Can J Physiol Pharmacol*. 2001;79:723-9.

231. Ikeda Y, Young LH, Scalia R, Ross CR and Lefer AM. PR-39, a proline/arginine-rich antimicrobial peptide, exerts cardioprotective effects in myocardial ischemia-reperfusion. *Cardiovasc Res*. 2001;49:69-77.

232. Cifuentes-Pagano ME, Meijles DN and Pagano PJ. Nox Inhibitors & Therapies: Rational Design of Peptidic and Small Molecule Inhibitors. *Curr Pharm Des*. 2015;21:6023-35.

233. Rey FE, Cifuentes ME, Kiarash A, Quinn MT and Pagano PJ. Novel competitive inhibitor of NAD(P)H oxidase assembly attenuates vascular O(2)(-) and systolic blood pressure in mice. *Circ Res*. 2001;89:408-14.

234. Smith SM, Min J, Ganesh T, Diebold B, Kawahara T, Zhu Y, McCoy J, Sun A, Snyder JP, Fu H, Du Y, Lewis I and Lambeth JD. Ebselen and congeners inhibit NADPH oxidase 2-dependent superoxide generation by interrupting the binding of regulatory subunits. *Chem Biol*. 2012;19:752-63.

235. Zhao Y, McLaughlin D, Robinson E, Harvey AP, Hookham MB, Shah AM, McDermott BJ and Grieve DJ. Nox2 NADPH oxidase promotes pathologic cardiac remodeling associated with Doxorubicin chemotherapy. *Cancer Res*. 2010;70:9287-97.